

Ge162 Seismology (2004)

1. Introduction (2 hours)

- 1.1 Earthquake Phenomena (Frequency Spectrum)
- 1.2 Source of an Earthquake (Fault, Crustal Deformation etc)
- 1.3 Seismic Waves (*P*, *S*, and Surface Waves)
- 1.4 Seismograph

2. Concepts in Classical Seismology (5 hours)

- 2.1 Structure of the Earth
 - 2.1.1 Ray theory and Snell's Law
 - 2.1.2 Seismic Ray
 - 2.1.3 Travel-Time Curve
 - 2.1.4 Gross Structure of the Earth
- 2.2 Location, Magnitude and Mechanism of Earthquakes
(+Practice Session)
- 2.3 Seismicity of the Earth
 - 2.3.1 Global Seismicity (and Earthquake Mechanism),
California Seismicity
 - 2.3.2 Depth Variation of Seismicity
 - 2.3.3 Temporal Variation of Seismicity
 - 2.3.4 Magnitude-Frequency Relationship

3. Seismic Waves (7 hours)

- 3.1 Review of Theory of Elasticity
- 3.2 Wave Equation
- 3.3 Seismic Body Waves
- 3.4 Ray Theory
- 3.5 Reflection and Refraction
- 3.6 Seismic Surface Waves (+Practice Session)
- 3.7 Normal Mode Theory

4. Seismic Tomography (2 hours)

- 4.1 Herglotz-Wiechert (+Practice Session)
- 4.2 General Tomography (+Practice Session)

5. Theory of Seismic Source (4 hours)

5.1 Static Source

- 5.1.1 Single Force
- 5.1.2 Force Couples
- 5.1.3 Elastic Dislocation and Moment Tensor
- 5.1.4 Summary of Seismic Source Representation
- 5.1.5 Stress Relaxation

5.2 Elastodynamic Source

- 5.2.1 Single Force
- 5.2.2 Force Couples
- 5.2.3 Elastic Dislocation and Moment Tensor
- 5.2.4 Stress Relaxation

6. Retrieval of Seismic Source Parameters (+Practice Session) (2 hours)

- 6.1 Body Waves
- 6.2 Long-Period Waves

7. Summary of Seismic Source Parameters (1 hour)

Seismic Moment, Radiation Pattern, Source Finiteness, Rupture Speed, Directivity, Static and Dynamic Stress Drops, Energy

8. Physics of Earthquakes (2.5 hours)

- 8.1 Scaling Relations
- 8.2 Physics of Earthquakes
- 8.3 Earthquake as a Complex System

9. Earthquakes and Plate Motion (0.5 hour)

Primary Text Books

1. Lay, T., and T. C. Wallace, *Modern Global Seismology*, Academic Press, San Diego, 1-517, 1995.
2. Bullen, K. E., and B. A. Bolt, *An Introduction to the Theory of Seismology*, 4 edition, Press Syndicate of the University of Cambridge, Cambridge, 1-499, 1985.
3. Udias, Agustin, *Principles of Seismology*, Cambridge University Press, Cambridge, 1-475, 1999.

Other References

1. Richter, C. F., *Elementary Seismology*, W. H. Freeman, San Francisco, 1-768, 1958.
2. Scholz, C. H., *The Mechanics of Earthquakes and Faulting*, Cambridge University Press, New York, 1-439, 1990.
3. Bullen, K. E., *An Introduction to the Theory of Seismology*, 3 edition, Cambridge Univ. Press, Cambridge, 1-381, 1963.
4. Kasahara, K., *Earthquake Mechanics*, Cambridge University Press, Cambridge, 1-248, 1981.
5. Aki, K., and P. G. Richards, *Quantitative Seismology*, W. H. Freeman, San Francisco, 1-932, 1980.
6. Aki, K., and P.G. Richards, *Quantitative Seismology*, 2nd Edition, 685 pp., University Science Books, Sausalito, 2002.
7. Dahlen, F. A. and Tromp, J., *Theoretical Global Seismology*, Princeton University Press, Princeton, 1025, 1998.

8. Shearer, P., *Introduction to Seismology*, Cambridge University Press, New York, 260, 1999.

9. Stein, S., and M. Wysession, *An Introduction to Seismology, Earthquakes and Earth Structure*, 498 pp., Blackwell, Malden, 2003.

Ge 162 Seismology

1. Introduction

1.1 Frequency Spectrum of Earthquake Phenomena

Phenomena associated with earthquakes occur over a broad frequency range as shown in Figure 1.1.

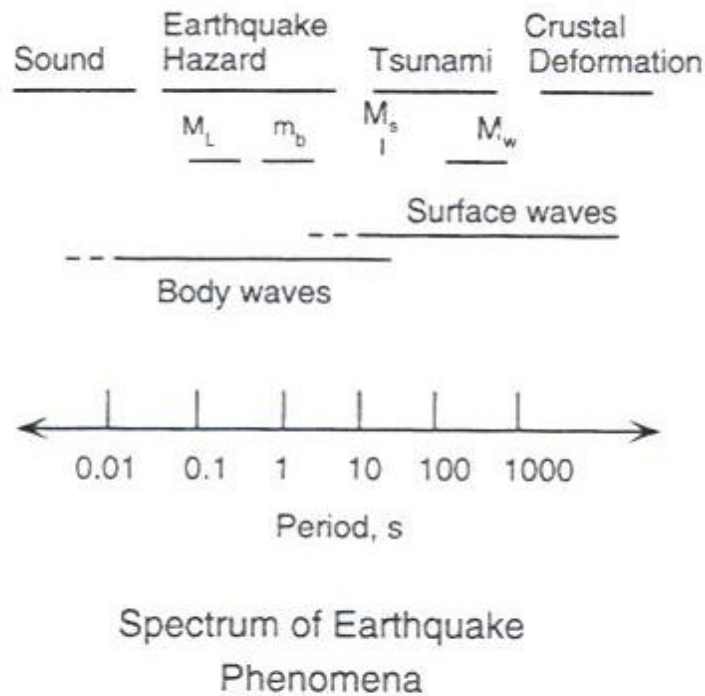


Fig. 1.1

1.2 Source of an Earthquake

Faulting and Crustal Deformation

An earthquake is a failure process in the Earth's crust (sometimes in the mantle, too). As the stress in the crust builds up, it eventually exceeds the strength of crustal rock, and failure occurs. The result is faulting (Figure 1.2), which causes deformation of the crust (Figure 1.3).



Fig. 1.2

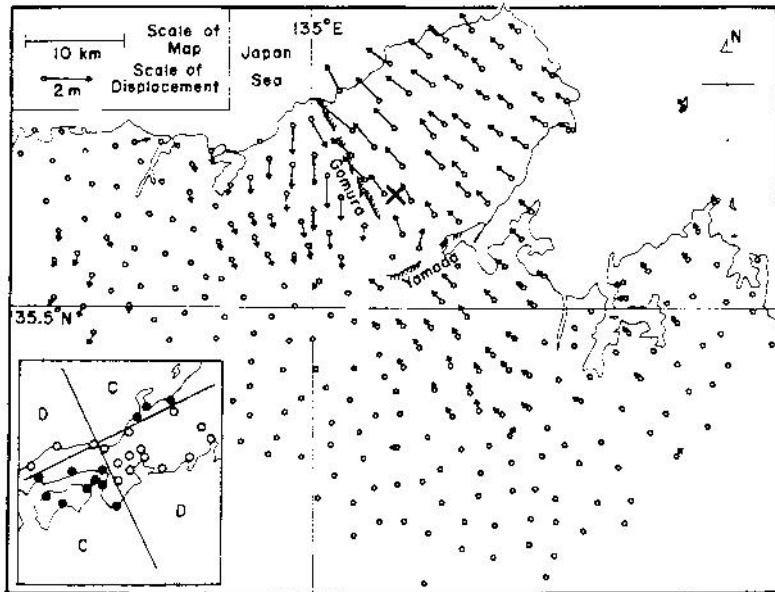


Fig. 1.3

The pattern of crustal deformation can be studied in detail using geodetic methods (traditional ground-based method, GPS, SAR) and seismological methods.

Failure (Fracture vs. Frictional Sliding) (Figure 1.4)

The failure process during an earthquake is often illustrated as fracture of rocks. If a piece of rock is subjected to stress (force), eventually fracture occurs. Although this is qualitatively correct, it is probably more appropriate to view earthquake faulting as frictional sliding. In this case, the sliding surface corresponds to an earthquake fault. A fault is formed by a long-term geological process, and represents a weak zone. In a sense, the major difference between fracture and frictional sliding is whether there is a pre-existing weak zone (plane) or not.

A simple experiment on frictional sliding exhibits many important characteristics of earthquakes; i.e. loading (stress accumulation), sudden slip, repetition of slip events. This general behavior is called stick slip.

Fracture and Frictional Sliding

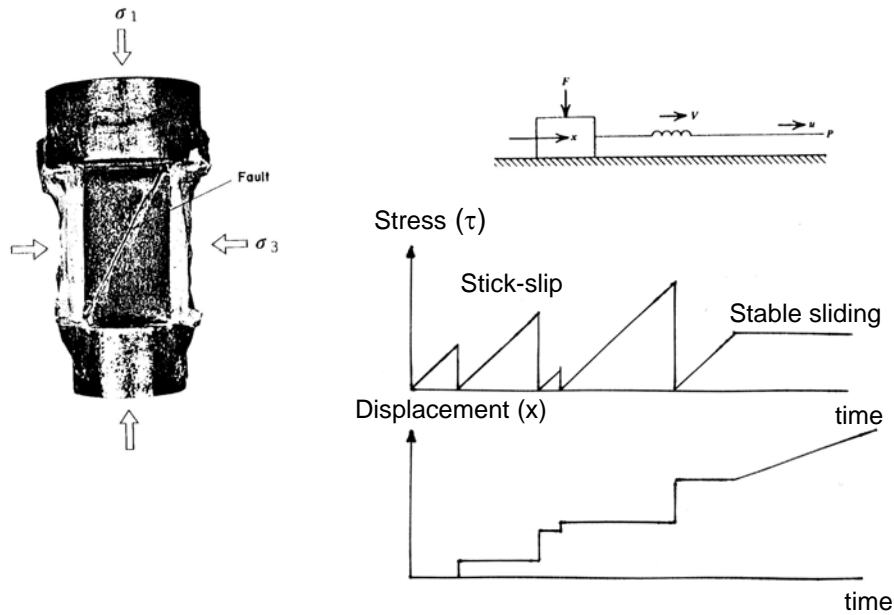


Figure 1.4

Strain, Stress, Stress-Strain Relation (Hooke's law)

Strain is a measure of deformation of a deformable (continuous) medium, and represents displacement per unit length. Stress is a measure of force. It is measured by force per unit area. In seismology, shear strain and shear stress are most important.

The relation between stress (force) and strain (deformation) can be best illustrated by using a spring. (In fact a spring is a very useful analog of Earth's crust, and we can explain many important relationships in seismology using a spring.) Suppose we apply a force F to stretch a spring, and the spring is stretched by Δl . Then F and Δl are related by the Hooke's law,

$$F = k_s \Delta l \quad (1-1)$$

Here k_s is called the spring constant. A similar relation

$$\sigma = \mu \varepsilon \quad (1-2)$$

holds between stress σ and strain ε . Here μ is called the elastic constant. If the rock is harder, then μ is larger. We have different elastic constants for shear deformation and volumetric deformation (volume change). In general, for simple deformable bodies, like rocks, metals etc, we need two elastic constants μ and k , rigidity and incompressibility (also called bulk modulus), for shear and volumetric deformations, respectively. For most seismological problems, these two elastic constants, and the density ρ are most important. For most crustal rocks, the representative values are:

$$\begin{aligned} \mu &= 3 \times 10^{11} \text{ dyne/cm}^2 = 0.3 \text{ Mbars} = 30 \text{ GPa} \\ k &= 5 \times 10^{11} \text{ dyne/cm}^2 = 0.5 \text{ Mbars} = 50 \text{ GPa} \\ \rho &= 2.7 \text{ g/cm}^3 = 2,700 \text{ kg/m}^3 \end{aligned}$$

Critical strain (strength) of Earth's crust

An important question is "How strong is the Earth's crust?". Many geodetic and seismological studies have demonstrated that the change in strain (deformation) associated with an earthquake ranges from 3×10^{-5} to 3×10^{-4} , or, in terms of stress, this corresponds to 10 to 100 bars (i.e., 1 to 10 MPa, or 10 to 100 atmospheric pressure). If we try to break an intact piece of rock, we normally need a few kbar stress. This suggests that an earthquake occurs on a pre-existing weak plane (fault), and frictional sliding appears to be a more appropriate model for an earthquake.

Ground Motion

When an earthquake occurs, the ground shakes. The motion of the ground is given by the displacement $u(t)$ as a function of time, t , in 3 directions, usually, UD, NS, and EW. If we take the time derivative of $u(t)$, we get the velocity of ground motion $v(t) = \dot{u}(t)$, and if we differentiate it again, we get ground-motion acceleration $a(t) = \dot{v}(t) = \ddot{u}(t)$.

The ground motions near the source of an earthquake are measured with geological, geodetic and seismological methods (Figure 1.5).

For large earthquakes,

u is 1 to 20 m

v is 10 cm/sec to 3 m/sec

a is 0.1 to 20 m/sec² (10 m/sec² is about 1 g)

These are useful numbers in seismology to remember.

Near-source Ground Motion (Acceleration, Velocity, Displacement)
1999, Chi-Chi, Taiwan, Earthquake

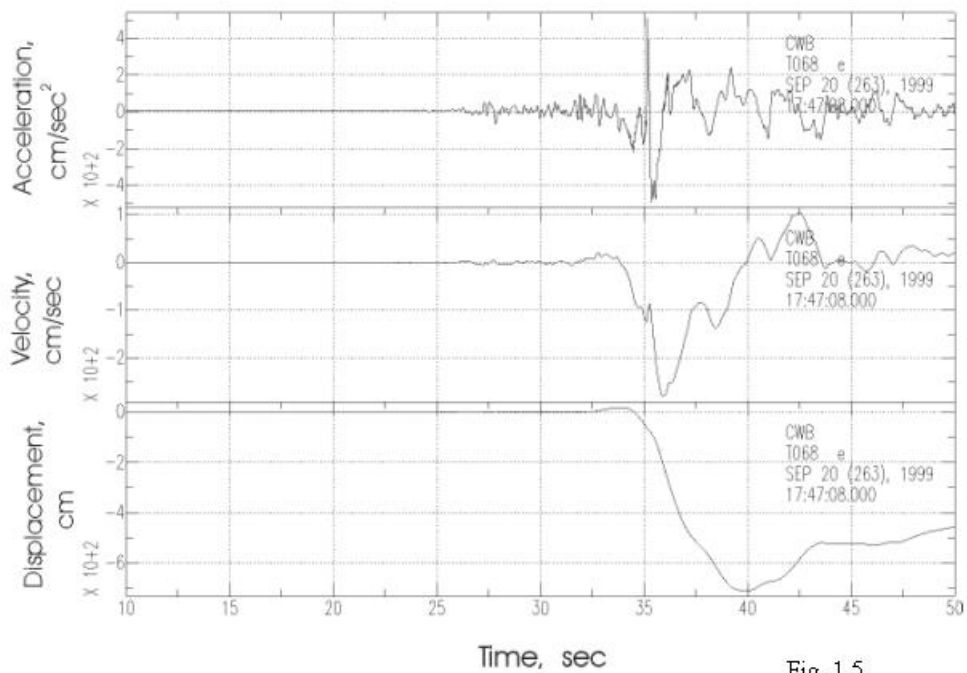


Fig. 1.5

1.3 Seismic Waves

The disturbance caused by a faulting in Earth's crust propagates as elastic waves. These waves are called seismic waves. In a large homogeneous medium without

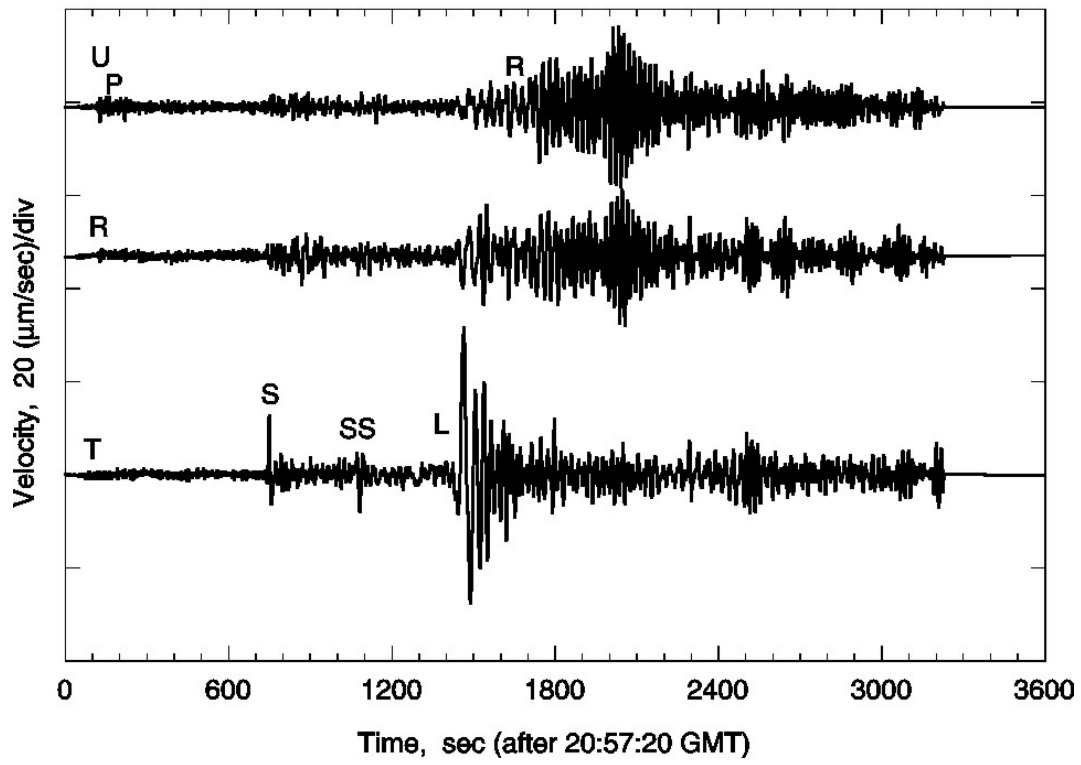
boundary, two types of waves exist. The first wave is mainly due to volume change, and is called compressional wave or P wave, and the second type of wave is caused by shear deformation, and is called shear wave or S wave. The P and S wave velocities, α and β , respectively, are given by

$$\alpha = \sqrt{\frac{k + (4/3)\mu}{\rho}} \quad \text{and} \quad \beta = \sqrt{\frac{\mu}{\rho}} \quad (1-3)$$

For most solids, $k=(5/3)\mu$, so that $\alpha = \sqrt{3}\beta = 1.732\beta$. Although this is an approximate relation, it is a good approximation and useful in observational seismology. In the shallow part of Earth's crust $\alpha=5$ to 6.5 km/sec, and $\beta=3$ to 3.8 km/sec.

In real world, we have the surface of Earth, and also the velocity changes as a function of depth. In general, the velocity increases with depth. When P and S waves propagate in a medium with a free surface and layers of different velocities, complex reflection and refraction occur and P and S waves interact to generate surface waves. This is an interesting mathematical problem, but here we just introduce two types of surface waves, Rayleigh waves and Love waves. These waves primarily propagate along Earth's surface so that the amplitude decays more slowly with distance than P and S waves. Hence, at large distances, surface waves are more dominant on seismograms (recordings of seismic waves). Also, these waves exhibit dispersion (velocity varies with the wave period) so that the appearance of these waves are usually distinct. The particle motion of Rayleigh waves is vertical and in the direction of wave path, and that of Love waves is horizontal and in the direction normal to the path. In the shallow crust, the velocity of Rayleigh waves C_R , ranges approximately from 2.5 to 3.0 km/sec, and that of Love waves, C_L , from 2.8 to 3.5 km/sec. Two examples are shown in Figure 1.6.

1/16/1995 Kobe, Mw=6.9, Pasadena ($\Delta=83$, $\phi=52.9$)



8/17/1999 Turkey, Mw=7.5 Pasadena ($\Delta=99.8, \phi=33.3$)

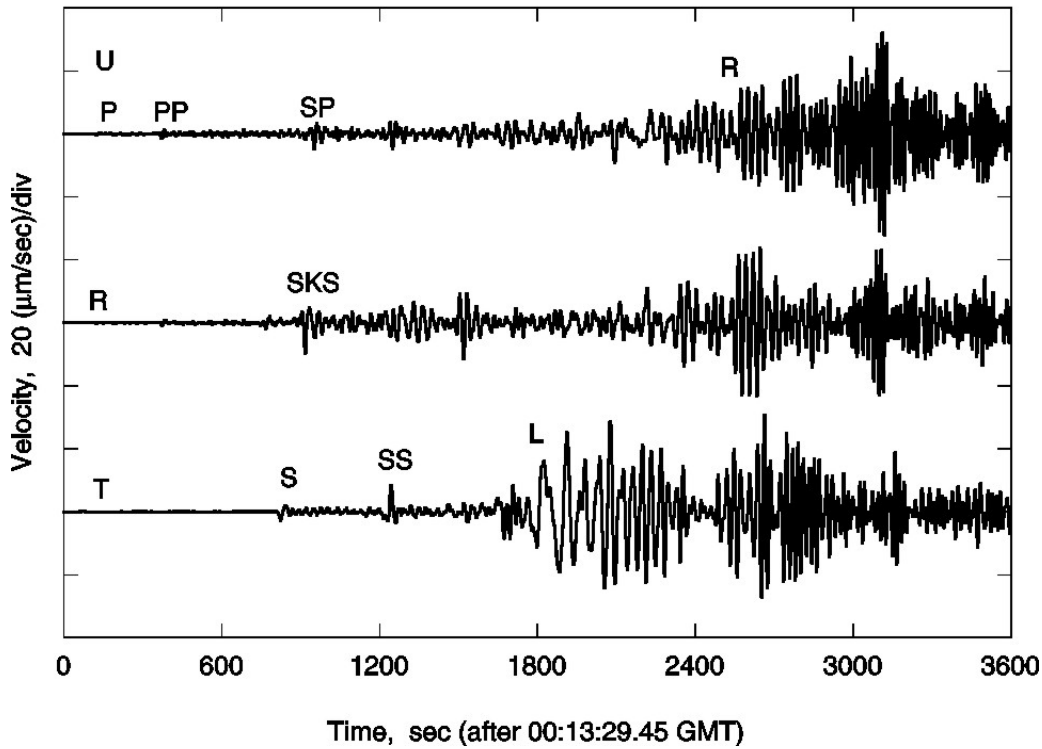


Fig. 1.6 Seismograms of the 1995 Kobe, Japan, and the 1999 Izmit, Turkey, earthquakes.

As shown above, the velocities of these waves are different, i.e., in general $\alpha > \beta > C_L > C_R$. Thus, at a station some distance from the source, the P wave arrives first, which is followed by the S wave. Then the large amplitude Love wave and Rayleigh wave arrive.

Seismologists study these seismic waves in detail to determine the earthquake source parameters (the size, type of faulting etc), and the structure of the Earth.

One useful relation is that between the S - P time, t_{S-P} , (time interval between P and S waves) and the distance, Δ . Since t_{S-P} is given by

$$t_{S-P} = \frac{\Delta}{\beta} - \frac{\Delta}{\alpha} = \frac{\Delta}{\alpha} \left(\frac{\alpha}{\beta} - 1 \right) \quad (1-4)$$

from which

$$\Delta = \frac{\alpha}{\left(\frac{\alpha}{\beta} - 1 \right)} t_{S-P} \quad (1-5)$$

For the shallow part of the crust (i.e., $\Delta < 1000$ km), α is about 6 km/sec, and α / β is 1.732, so that this relation gives

$$\Delta \approx 8t_{S-P} \quad (t_{S-P} \text{ in sec and } \Delta \text{ in km}) \quad (1-6)$$

For example, if t_{S-P} is 50 sec, the distance is about 400 km.

1.4 Seismograph (LW (Lay and Wallace), pp 173-199)

The instrument that measures ground motion caused by an earthquake is a seismometer or a seismograph. During an earthquake, everything moves so that it is difficult to measure the ground motion accurately. We need a reference point from which we can measure the motion of the ground. Seismologists use a pendulum as a reference.

Since most seismographs use a pendulum as a reference of the position, here we briefly discuss the principle (Figure 1.7).

Principle of a Mechanical Seismograph and the Wiechert Seismograph

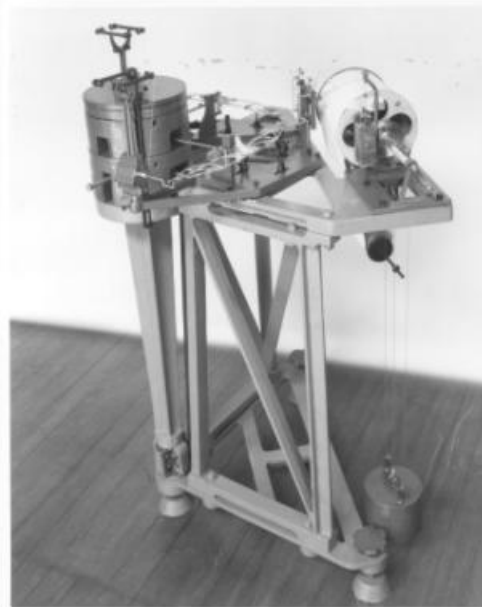
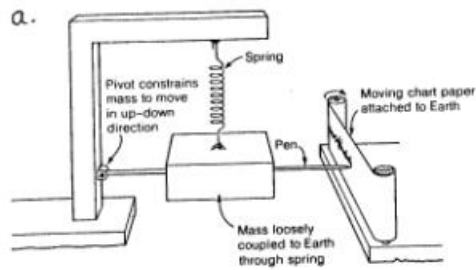


Fig. 1.7

Pendulum and Simple Mechanical Seismograph

Consider a simple pendulum (a string with a small mass hanging from it). Hold one end of the string and let the mass swing in a vertical plane. The natural period of the pendulum, T_0 , is given by,

$$T_0 = 2\pi\sqrt{\frac{l}{g}} \quad (1-7)$$

where g is the acceleration of gravity, 9.8 m/sec^2 . Thus if $l=1 \text{ m}$, then the period is about 2 sec.

Suppose we have an earthquake, and the ground starts shaking horizontally. Since you are standing on the ground (i.e., fixed to the ground), you will be shaken with the ground. If the ground shakes very gradually, say at period $T \gg T_0$, then the mass will move with you so that you cannot use it as a reference point (i.e., everything moves in the same way). In this case, this pendulum is not good as a seismometer. However, if the ground shakes very rapidly, e.g., $T \ll T_0$, then the mass tends to stay at the same place, if not completely. This is the very principle of a horizontal seismometer, a seismometer that measures horizontal motion. You can measure the motion of ground with respect to the mass which is approximately stationary. Thus, if $T \ll T_0$, this pendulum is a good seismometer, and if you record the motion of the ground (i.e., you) with respect to the mass, you can have a seismogram.

If we use a spring with a mass hanging vertically, we can measure the vertical ground motion with the same principle.

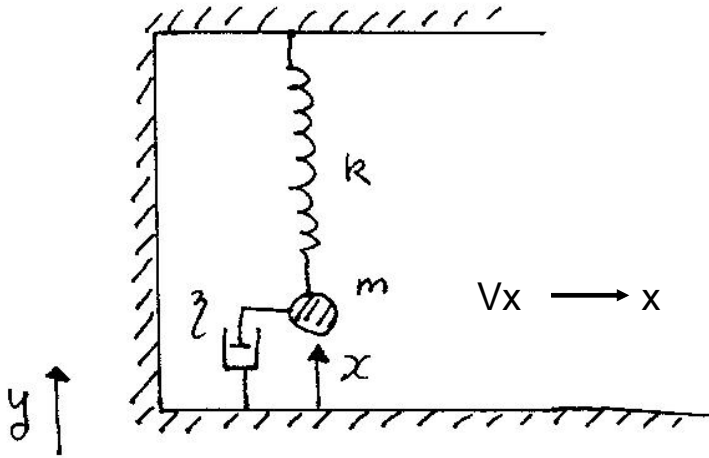
In the real seismometer, we need to attach a device to magnify the motion and damp out the resonance (damper), but the basic principle is the same. The Wiechert seismograph and the Wood-Anderson seismograph used in California are all of this type.

It is difficult to record very long-period ground motions with these simple mechanical seismographs, because it is difficult to build a stable pendulum with a very long natural period.

The response of a mechanical seismograph can be derived from the following equation (see the figure below).

$$\ddot{x} + 2h\omega_0\dot{x} + \omega_0^2x = -V\ddot{y} \quad (1-8)$$

where x is the motion of a reference point (i.e., mass) of the seismograph with respect to the ground, and y is the ground motion displacement. h is the damping constant, $\omega_0 = \sqrt{k/m}$ is the natural angular frequency of the seismograph ($\omega_0 = 2\pi/T_0$, T_0 is the natural period), and V is the static magnification. The response of a mechanical seismograph is completely described by these 3 constants.



For a unit harmonic input

$$y = \exp(i\omega t) \quad (1-9)$$

the output is

$$x = \frac{V\omega^2}{-\omega^2 + 2ih\omega_0\omega + \omega_0^2} \exp(i\omega t) \quad (1-10)$$

then, the response is given by

$$\hat{H}(\omega) = \frac{V\omega^2}{-\omega^2 + 2ih\omega_0\omega + \omega_0^2} \quad (1-11)$$

The amplitude response $|\hat{H}(\omega)|$ is plotted in Figure 1.8.

Other Types of Seismographs

In order to increase the sensitivity of the instrument, and improve the response at long-period, various developments have been made. These seismographs use an electro-magnetic sensor (moving coil etc), and a galvanometer. The examples are: Galitzin, Benioff short-period, Benioff long-period, Press-Ewing, and Benioff strain seismographs (Figure 1.8).

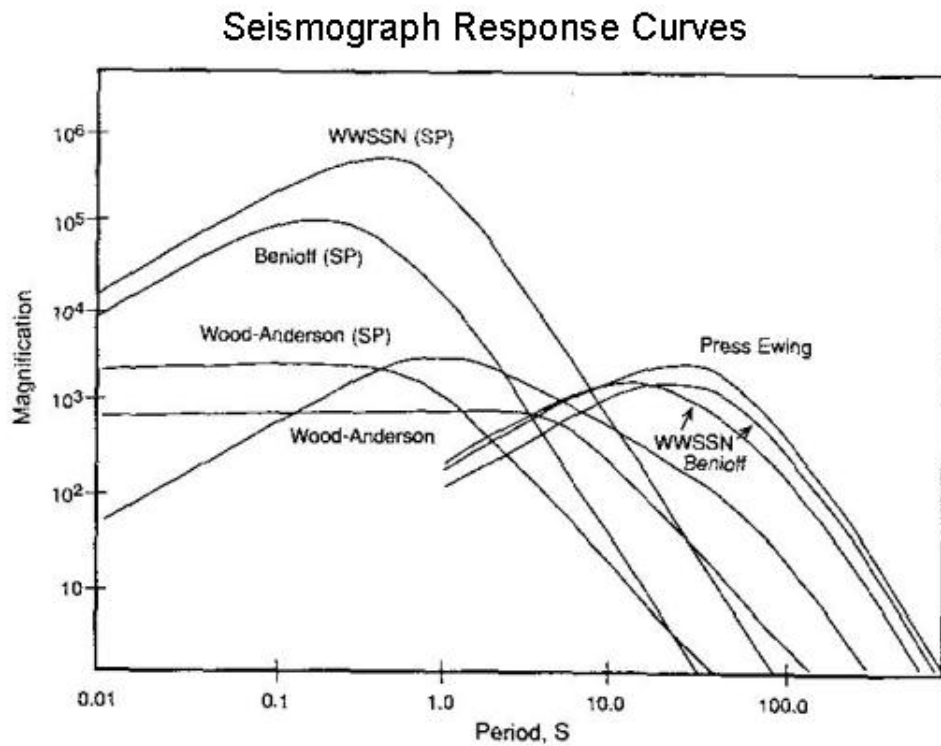


Fig. 1.8

Modern Broad-band Seismograph and Strong-motion Seismograph

Until recently seismograms written on paper were the standard data for most seismological research and routine reporting. While these analog records are still useful for various research purposes, these instruments are limited in two respects. First, since the movement of the pendulum is mechanically limited by the physical size of the instrument, it is not possible to record very large ground motions; *i.e.*, the dynamic range is limited. Second, as long as recordings are made on paper (analog recording), the dynamic range is limited by resolution in visually reading the records, which is normally 1/1000, *i.e.*, 60 db.

To remove these limitations, modern seismographs adopt a force balance mechanism and digital recording system. In the force balance mechanism, the output signal from the transducer is amplified and fed back to a device that holds the mass at the original unperturbed position (Figure 1.9). The strength of the signal (usually measured in voltage) is proportional to ground motion. With some filters in the feedback circuit, it is possible to make the output proportional to acceleration, velocity or displacement of ground motion, at least over a certain frequency band.

In this type of instruments, there is virtually no displacement of the mass, and the dynamic range can be increased. Also, with an appropriate feedback system, the response can be adjusted relatively easily.

Principle of a Force-Balance Seismograph

Streckeisen STS-1 Seismometer

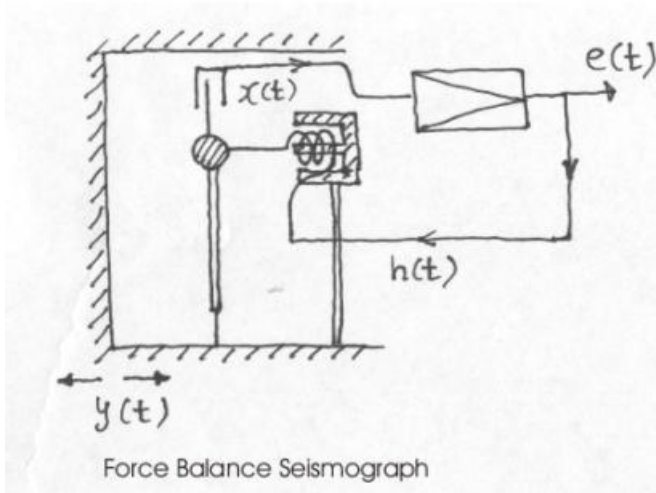


Fig. 1.9

The response of the standard broad-band instruments used in seismology (often called the VBB system) is approximately flat for a ground-motion velocity over a wide frequency band (e.g. 7 Hz to 0.0033 Hz (300 sec)) (Figures 1.10 and 1.11). The broad-band instruments usually have a 140 db (10^7) dynamic range.

Old (Mechanical) and Modern (Force-Balance) Seismograph

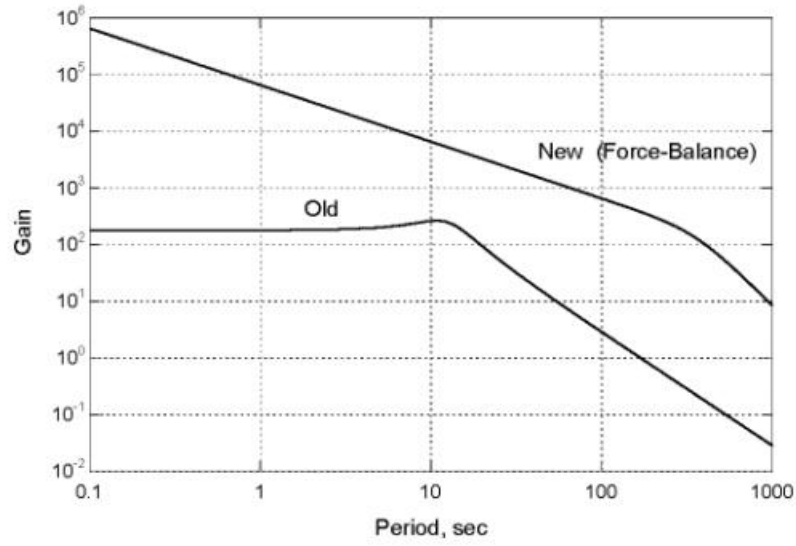


Fig. 1.10

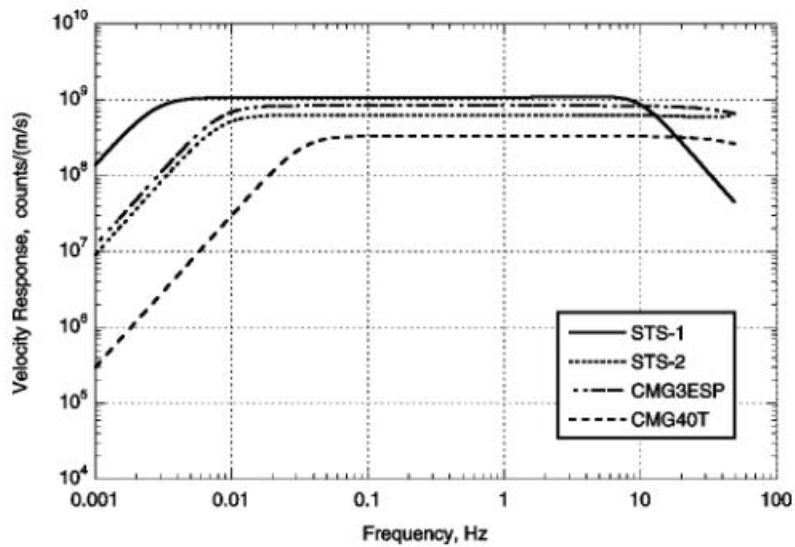


Fig. 1.11

Seismographs designed to record very strong ground motion are called strong-motion seismographs and are used in earthquake engineering. Modern strong-motion seismographs have a force balance mechanism with voltage output proportional to ground-motion acceleration.

Recent developments in solid state electronics made it possible to build stable force balance seismographs; they are now widely used in the world for research and routine monitoring.

Ge 162

2. Concepts in Classical Seismology

2.1 Structure of the Earth

2.1.1 Ray theory and Snell's Law (LW, pp70-91)

In the early days of seismology, the structure of the Earth was determined mainly by using ray theory. When the wavelength of seismic waves is sufficiently short (i.e., if the period is sufficiently short), we can treat seismic waves as a geometrical ray, just as we do in geometrical optics.

In ray theory, the most fundamental is Snell's Law, which is illustrated in Figure 1.

Snell's Law

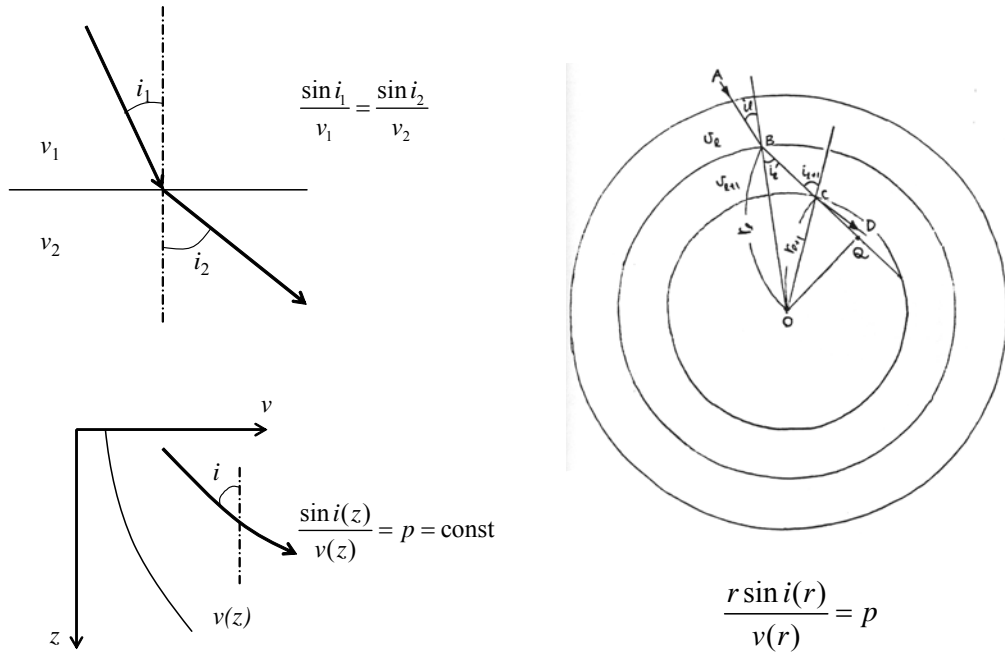
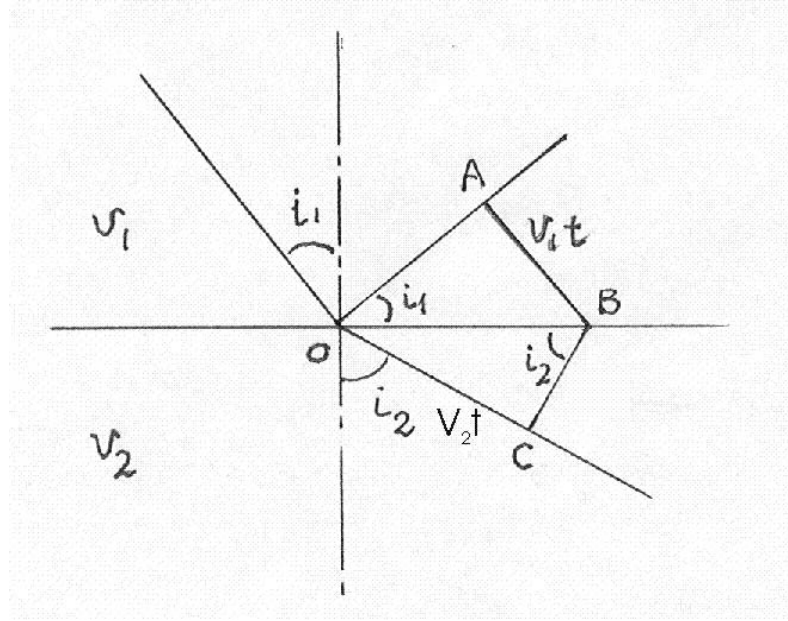


Figure 1

Suppose a ray is incident from a medium with a wave speed v_1 on a medium with a speed v_2 . Let the incident and emergent angles be i_1 and i_2 . Then the Snell's law is given by

$$\frac{\sin i_1}{v_1} = \frac{\sin i_2}{v_2} \quad (1)$$

This can be shown easily from the geometry of the two triangles OAB and OBC shown below.



If the wave speed changes continuously with z (i.e., depth) as $v(z)$, then (1) can be written as

$$\frac{\sin i}{v} = p = \text{constant for a given ray} \quad (2)$$

p is called the ray parameter.

For a spherical geometry as shown in Figure 1, the Snell's law can be written as

$$\frac{r_k \sin i_k}{v_k} = \frac{r_{k+1} \sin i_{k+1}}{v_{k+1}} \quad (3)$$

and

$$\frac{r \sin i(r)}{v(r)} = p \quad (4)$$

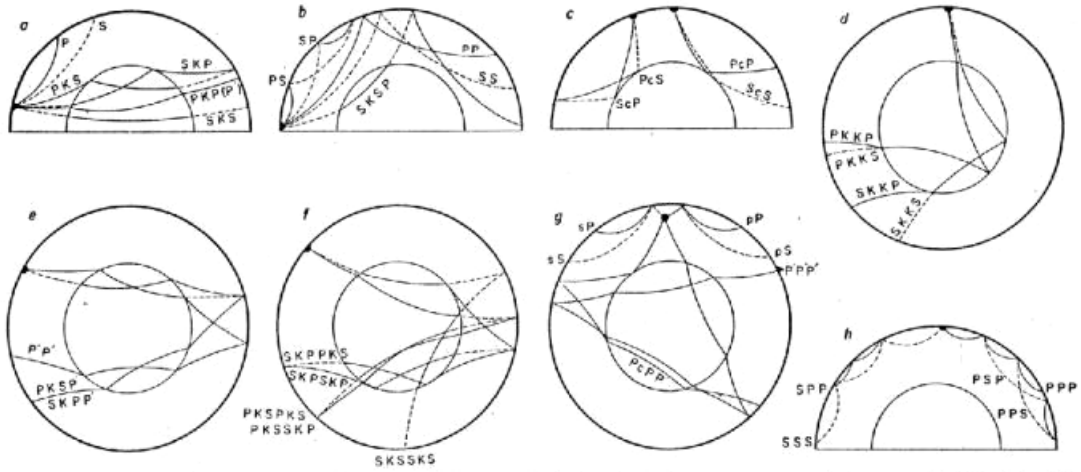
corresponding to (1) and (2), respectively.

2.1.2 Seismic Ray (LW, pp. 200-217)

Figure 2 shows various seismic rays in the Earth's interior. P and S waves are denoted by P and S , respectively. Other symbols are:

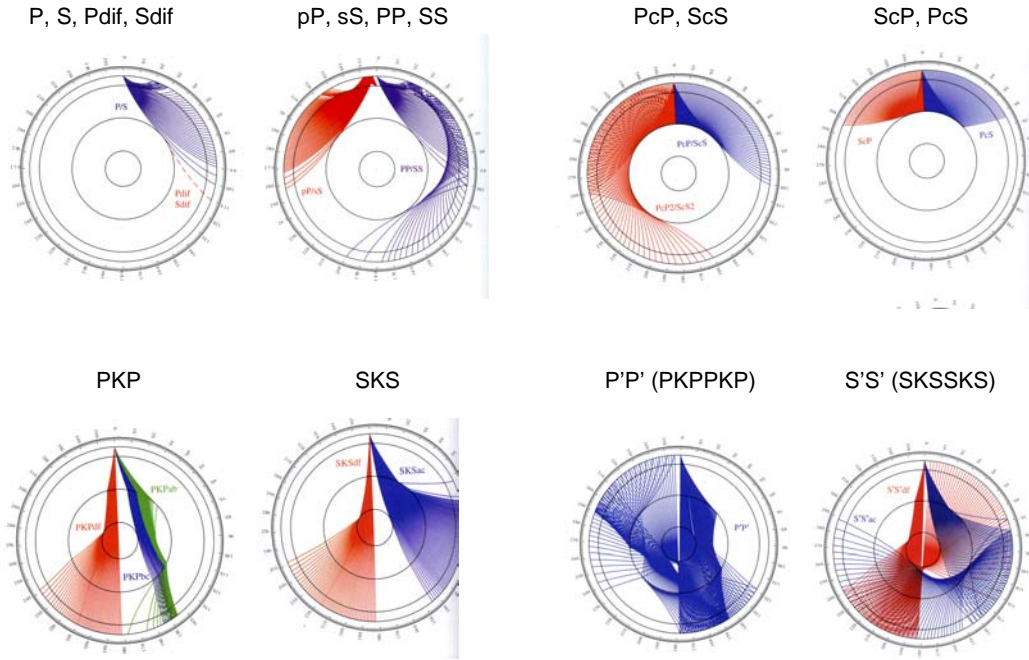
- K: P wave ray in the core
- p : P wave ray before reflection near the source (only for a deep source)
- s : S wave ray before reflection near the source (only for a deep source)
- c: Reflection at the core
- P': PKP

Seismic Rays in Earth



Paths of body waves of teleseisms, with letter symbols. Longitudinal wave ray segments shown as full lines; transverse wave ray segments shown dashed.

Fig. 2



Storchak, D., Schweitzer, J., and Bormann, P., The IASPEI Standard Phase List, *Seismological Research Letters*, 74, 761-772, 2003.

Some Examples

Figure 3 and Figure 4 show some examples.

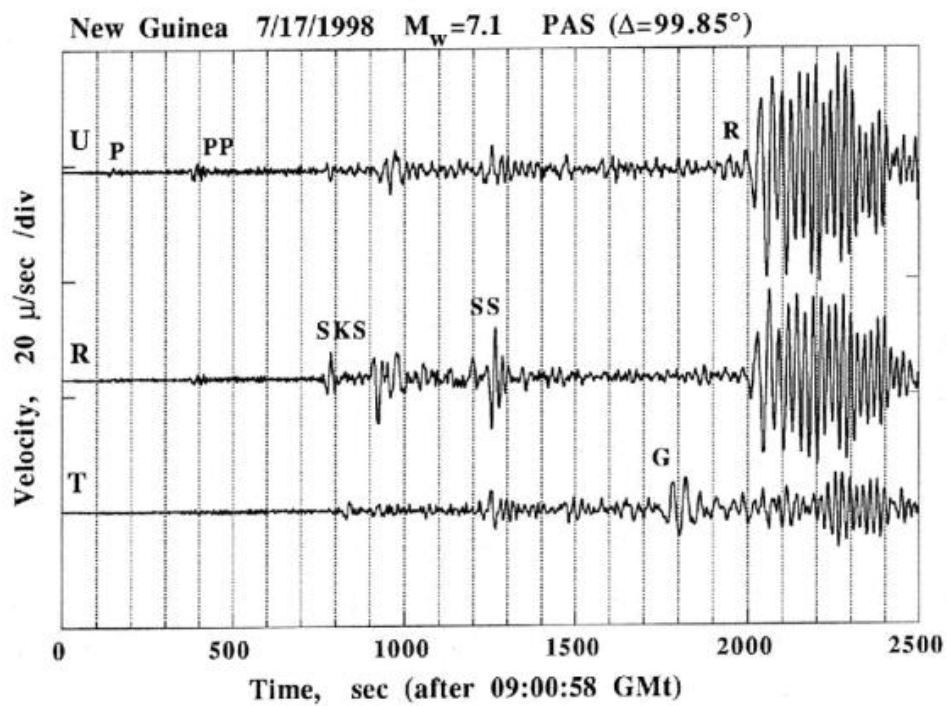


Fig. 3

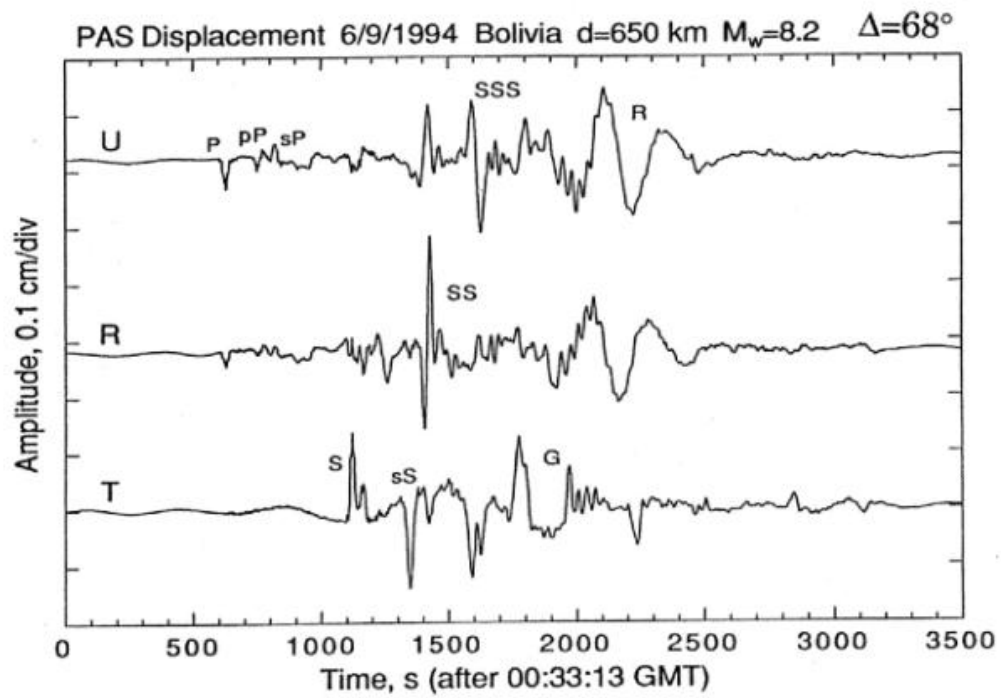


Fig. 4

Figure 5 shows ray paths in the Earth's interior for 3 representative velocity structures, and the corresponding travel time curves.

Velocity Structure and Travel Time Curve

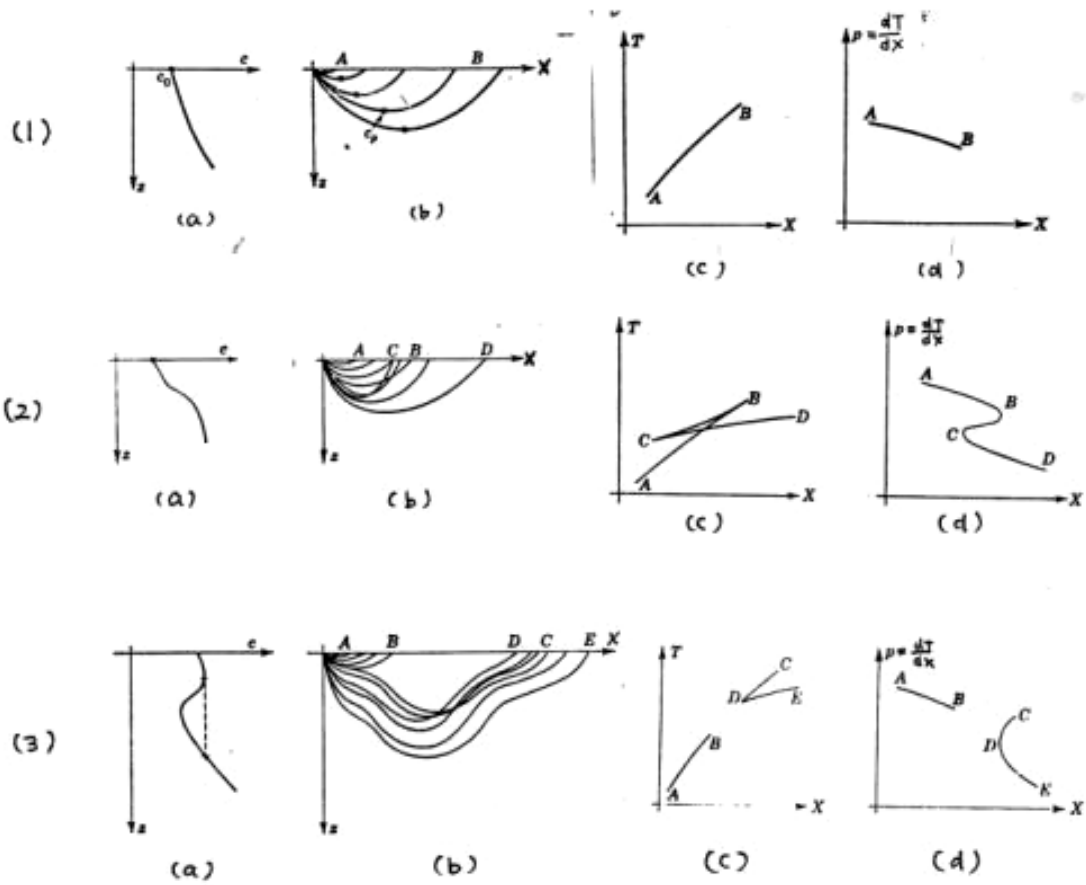


Fig. 5

Figure 6 shows 3 regions in the Earth's interior and the corresponding travel time curves.

Ray Paths in the Earth's Interior and Travel Time Curves

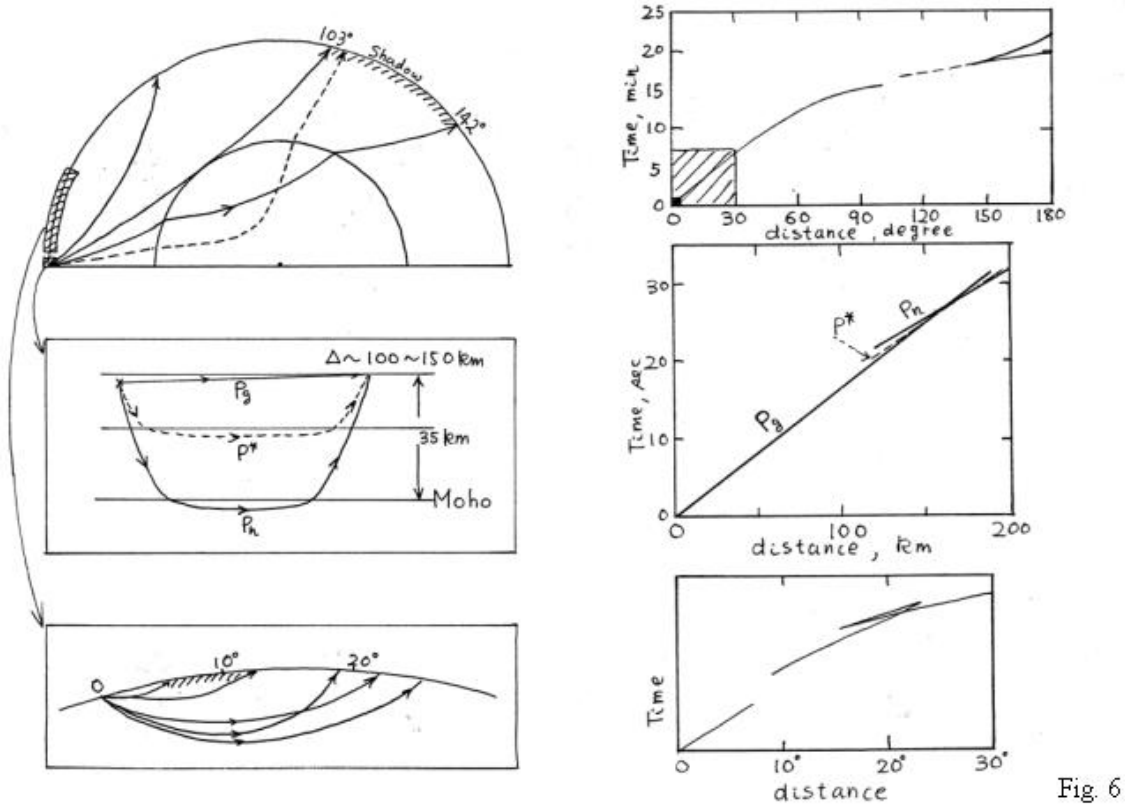


Fig. 6

Figure 7 shows the crustal structure for ocean and continent, and corresponding travel time curves.

Crustal Structure and Travel Time Curves

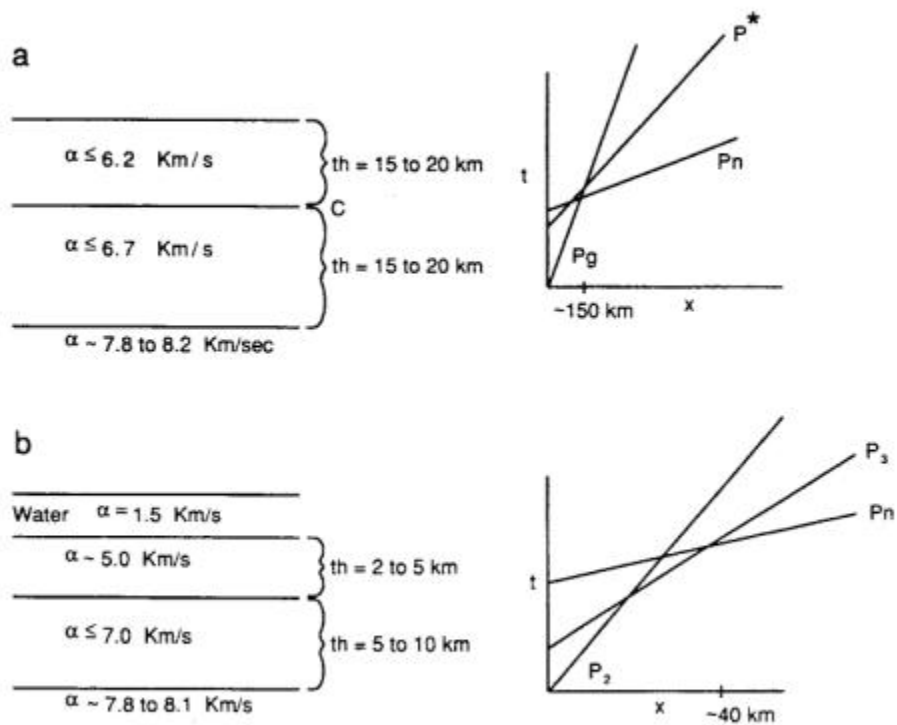


Fig. 7

2.1.3 Travel-Time Curve (LW pp.213-217)

Figure 8 shows the travel times observed at many stations and reported to the International Seismological Center (ISC).

Travel Times of
Seismic Phases
(Observed)

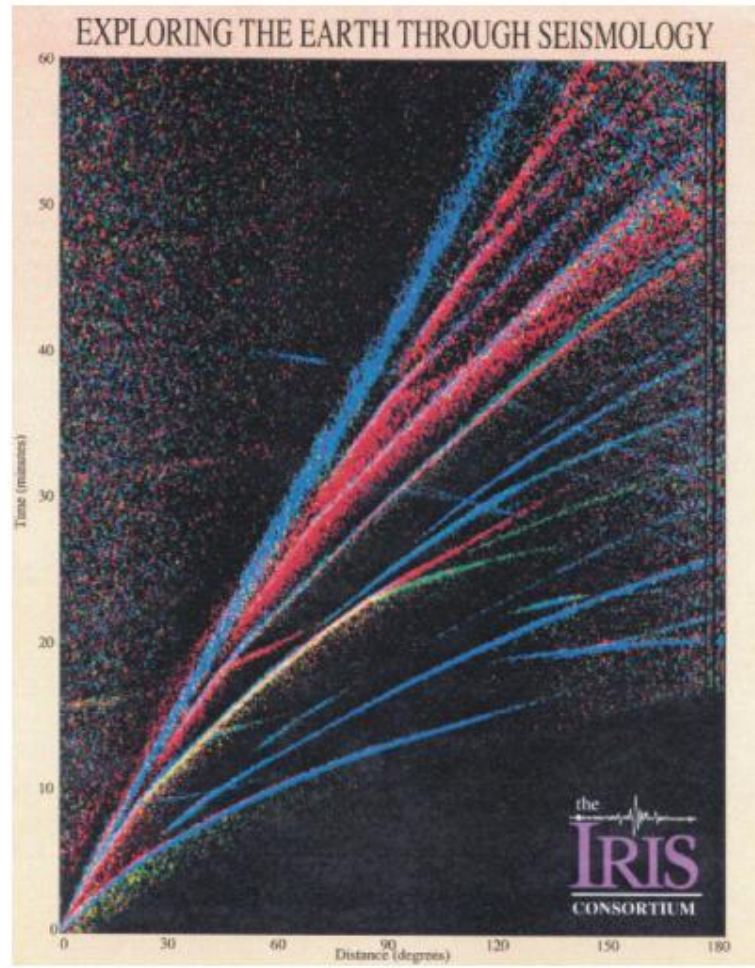


Fig. 8

Figure 9 shows the same with the phase names labeled.

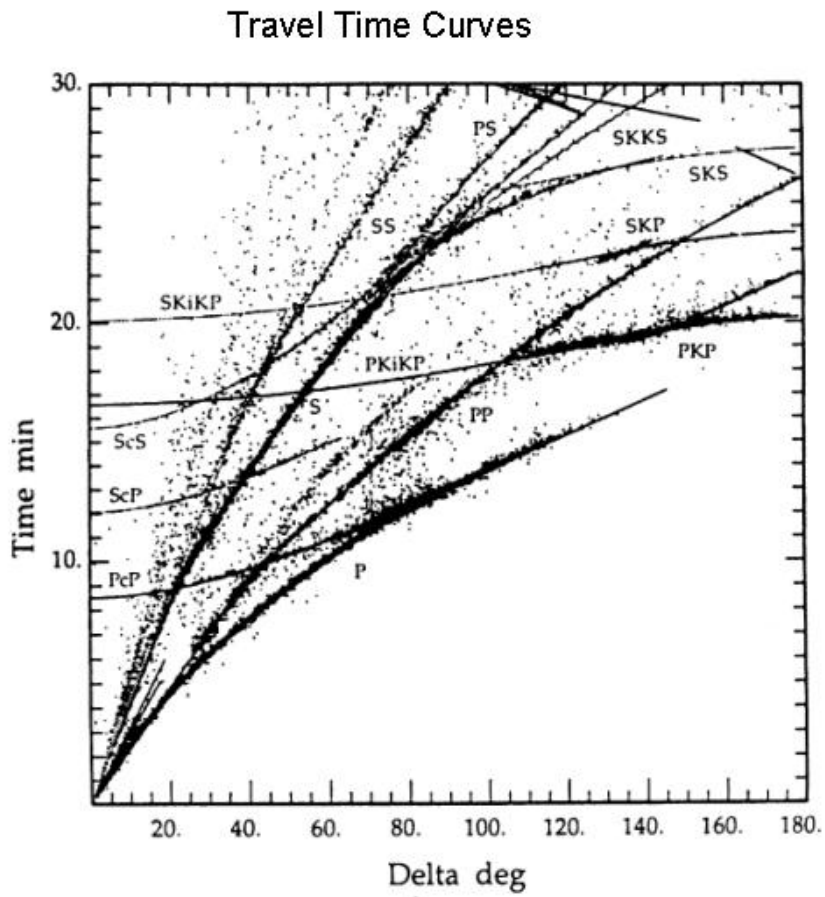
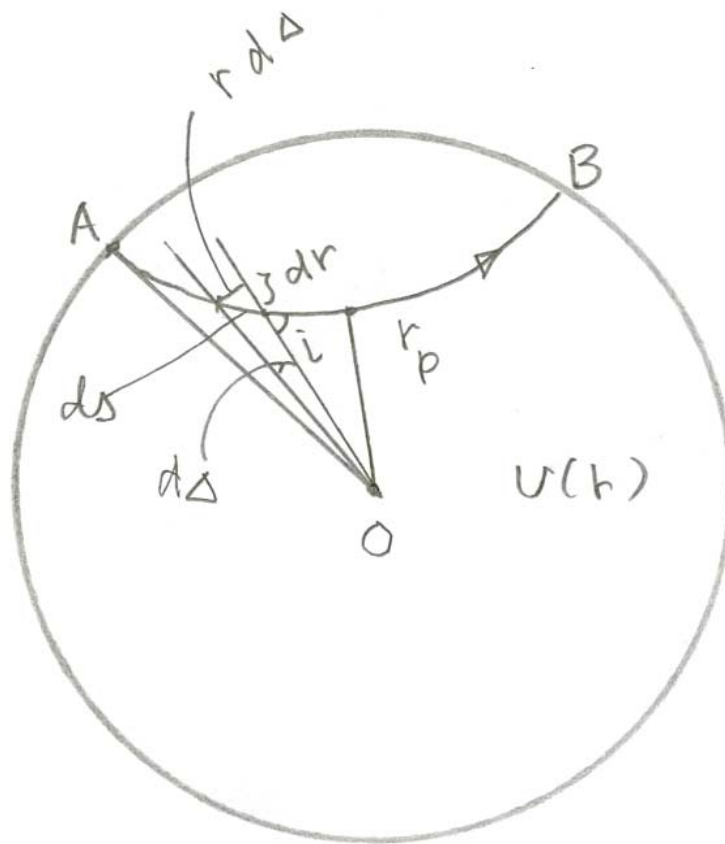


Fig. 9

For a spherically symmetric structure, the distance, Δ , traveled by a seismic ray with a ray parameter p , and the travel times, T , can be computed easily. Referring to the figure below,

$$\frac{dr}{ds} = \cos i = \sqrt{1 - \sin^2 i} = \sqrt{1 - \frac{v^2 p^2}{r^2}} \quad (5)$$

$$d\Delta = \frac{ds \sin i}{r} = \frac{1}{r^2} \frac{vp}{\sqrt{1 - \frac{v^2 p^2}{r^2}}} dr \quad (6)$$



Then,

$$T = 2 \int_{r_p}^{r_0} \frac{r}{v\sqrt{r^2 - v^2 p^2}} dr \quad (7)$$

$$\Delta = 2 \int_{r_p}^{r_0} \frac{vp}{r\sqrt{r^2 - v^2 p^2}} dr \quad (8)$$

where r_0 is the radius of Earth and r_p is the radial distance of the deepest point of the ray. These integrals are fundamental in the seismological ray theory (e.g., Herglotz Wiechert Method).

2.1.4 Gross Structure of the Earth (LW, pp. 26-33)

In the early days of seismology, the structure of the Earth was determined from the travel-time data, as shown in the upper figure of Figure 10. This figure shows one of the standard laterally homogeneous model, which is used for various seismological studies.

The bottom figure in Figure 10 shows an example of 3-D Earth structure determined by more recent studies using seismic body waves, surface waves and normal-mode data (Helffrich and Wood, 2001). Tomographic methods are used for determining these structures.

Structure of the Earth, Old and New

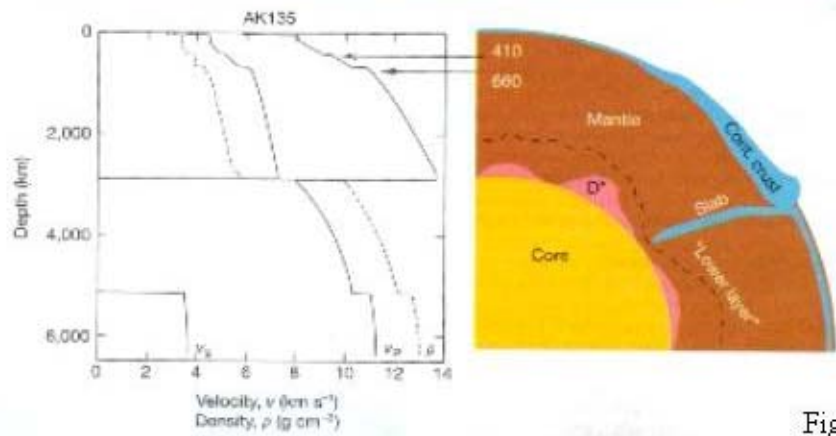
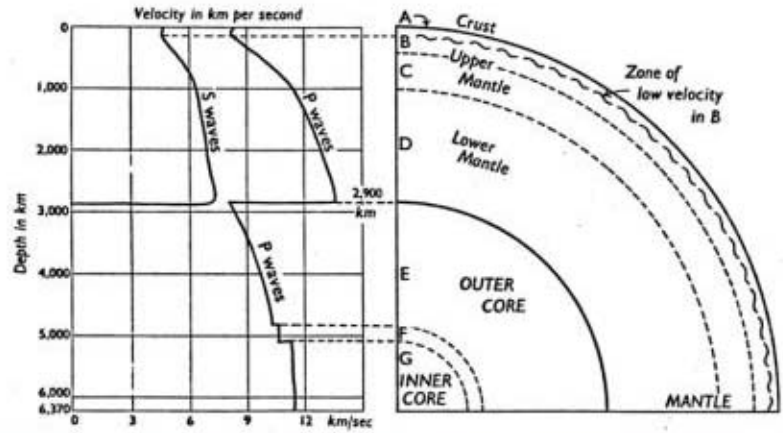


Fig. 10

References

Helfrich, G. R., and B. J. Wood, The earth's mantle, *Nature*, 412, 501-507, 2001.
 Anderson, D. L., Top-down tectonics, *Science*, 293, 2016-2018, 2001.

Ge 162 Plate Motion and Great Earthquakes

Earthquakes occur in the Earth's crust and mantle due to stresses caused by global plate motion. The actual pattern of stress distribution is probably very complex, but we expect that the activities of great and large earthquakes must reflect the global plate motion.

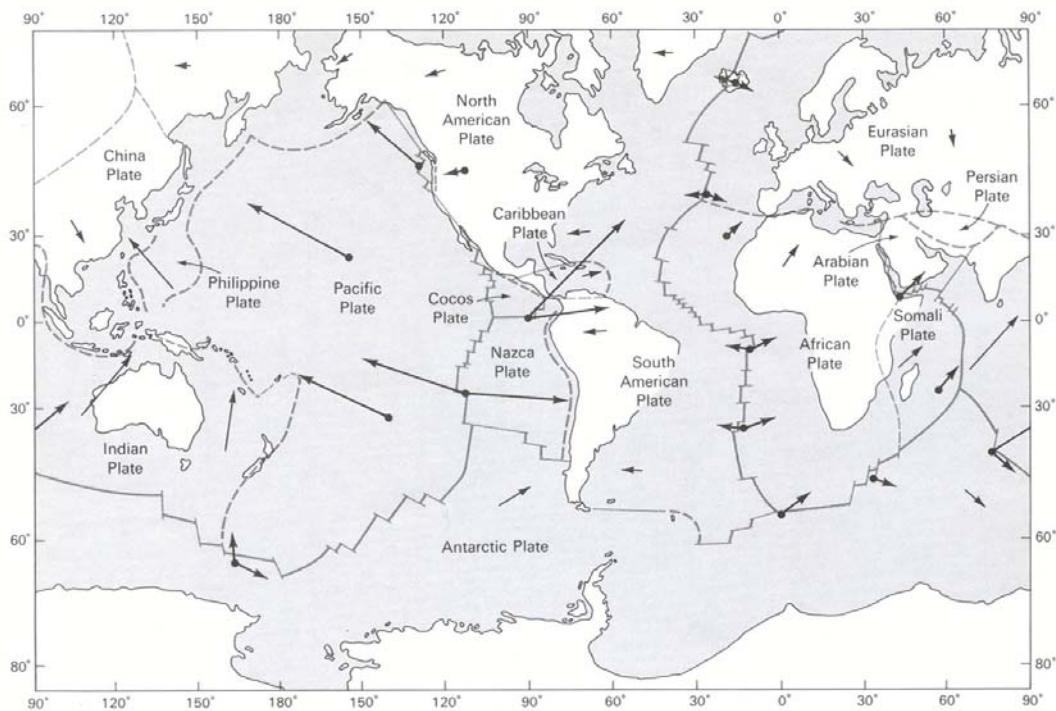
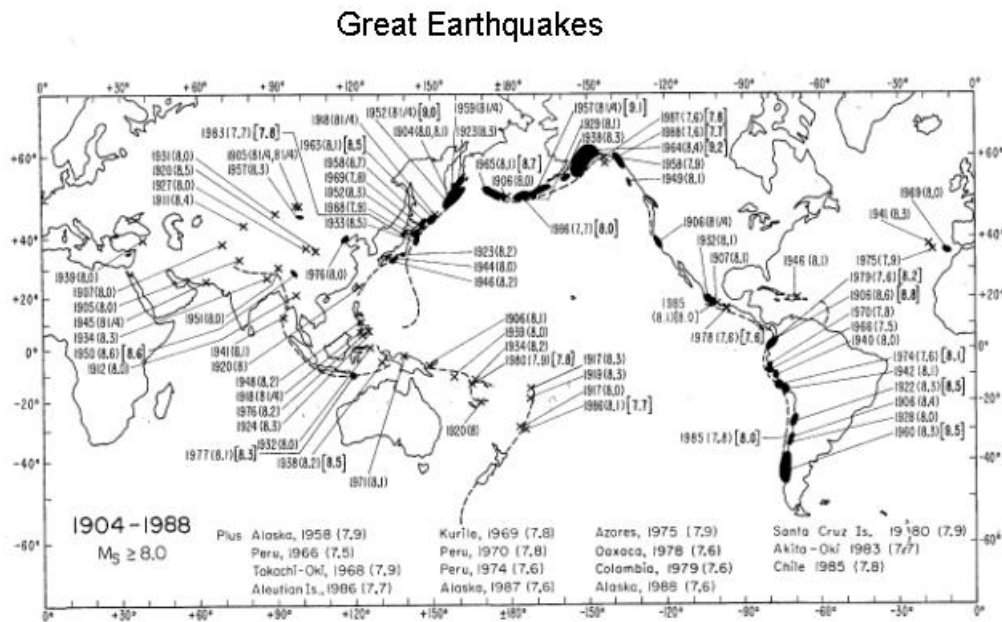


FIGURE 6-8 Present motions of plates over hot spots. The relative motions were determined from fault strikes and spreading rates on rise boundaries; with an appropriate constant rotation added, absolute motion of each plate over the mantle was determined. The lengths of arrows are proportional to the plate speed. [After J. Morgan, "Deep Mantle Convection Plumes and Plate Motions." *Amer. Assoc. Petrol. Geol. Bull.* 56, p. 203, 1972. Redrawn with permission of the author.]

The world greatest earthquakes occur at subduction zones (e.g., 1960 Chilean earthquake, and the 1964 Alaskan earthquake), but not every subduction zone has experienced a great earthquake (e.g., the Marianas, the Tonga-Kermadec). It is possible that the length of earthquake catalog is too short to be representative of long-term



seismicity. With this caveat in mind, we investigate the level of seismic activity and plate motion. Ideally, the seismic activity along a subduction zone should be defined by the energy release per unit length along the subduction zone, and unit time, i.e.,

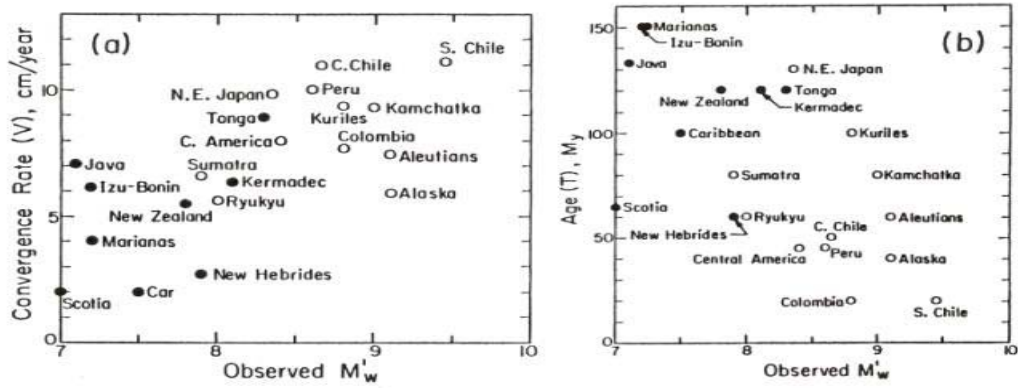
$$\bar{e} = \frac{1}{LT} \int_0^L \int_0^T E_R dldt$$

where L and T are the length of the subduction zone and the time period involved, respectively.

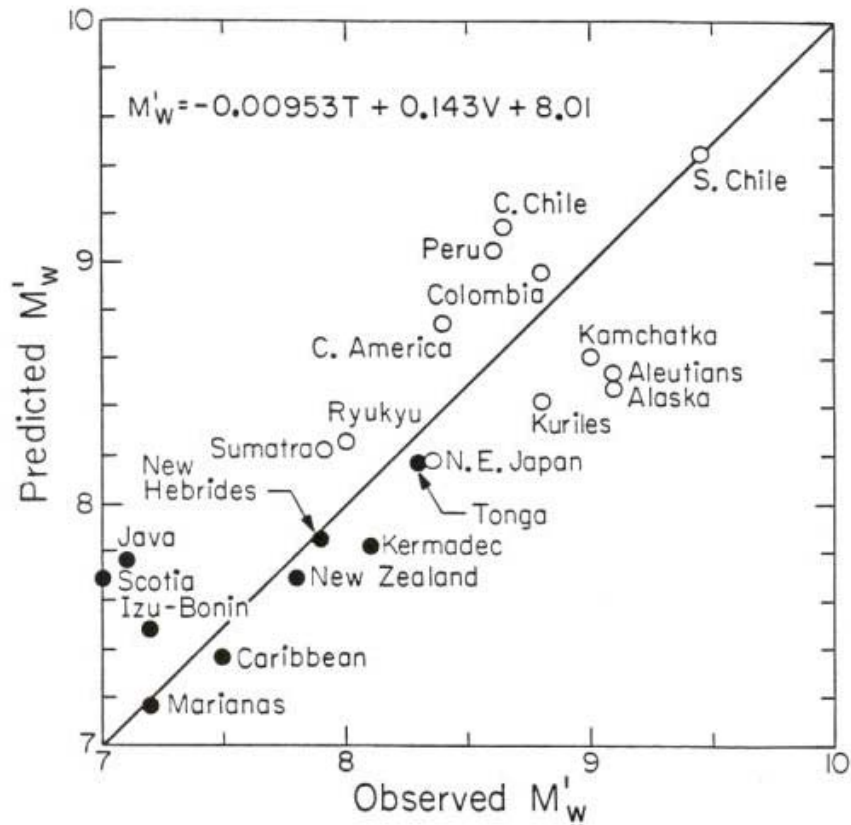
Unfortunately, the available seismic record is too short to compute this. So, we take the magnitude, M_w , of the largest earthquake that occurred in a particular subduction zone as a parameter that represents \bar{e} for that subduction zone. Then, it is reasonable to assume that

$$M_w \propto V$$

where V is the convergence rate. However, the plot of M_w versus V does not show any obvious trend. This suggests that other factors may be controlling seismicity. Another potentially relevant parameter is the age, T , of the subducting plate. However, no obvious negative correlation is seen between M_w and T .



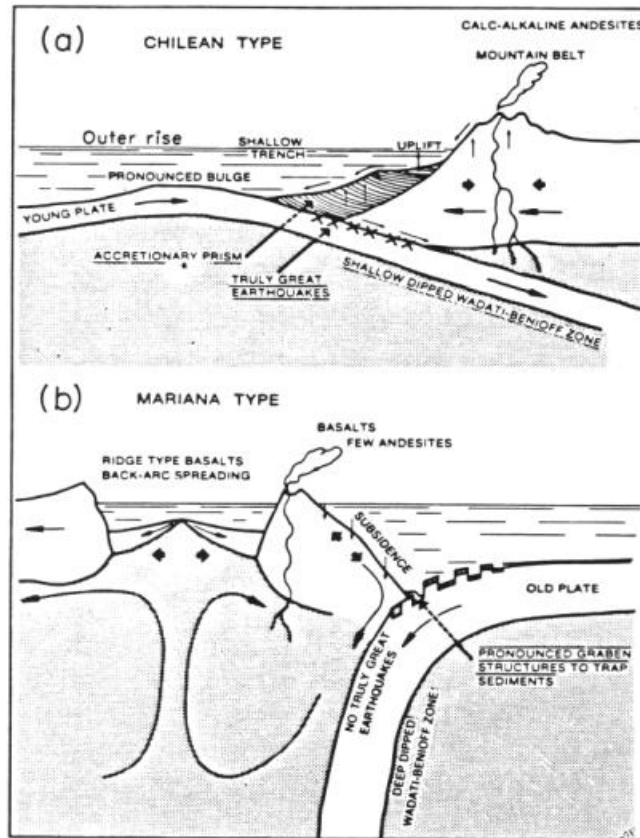
Then, we can try a 3-parameter regression between M_w , V and T . The result is shown in the following figure. The horizontal axis shows the observed M_w and the vertical axis shows M_w predicted by the regression relation.



(Ruff, L., and H. Kanamori, Seismicity and the subduction process, *Phys. Earth Planet. Inter.*, 23, 240-252, 1980)

If this regression is valid, this provides a useful method for assessing the seismic potential of subduction zones for which no great earthquake has occurred. This pattern suggests that the subduction zones where a relatively young plate is subducting at a

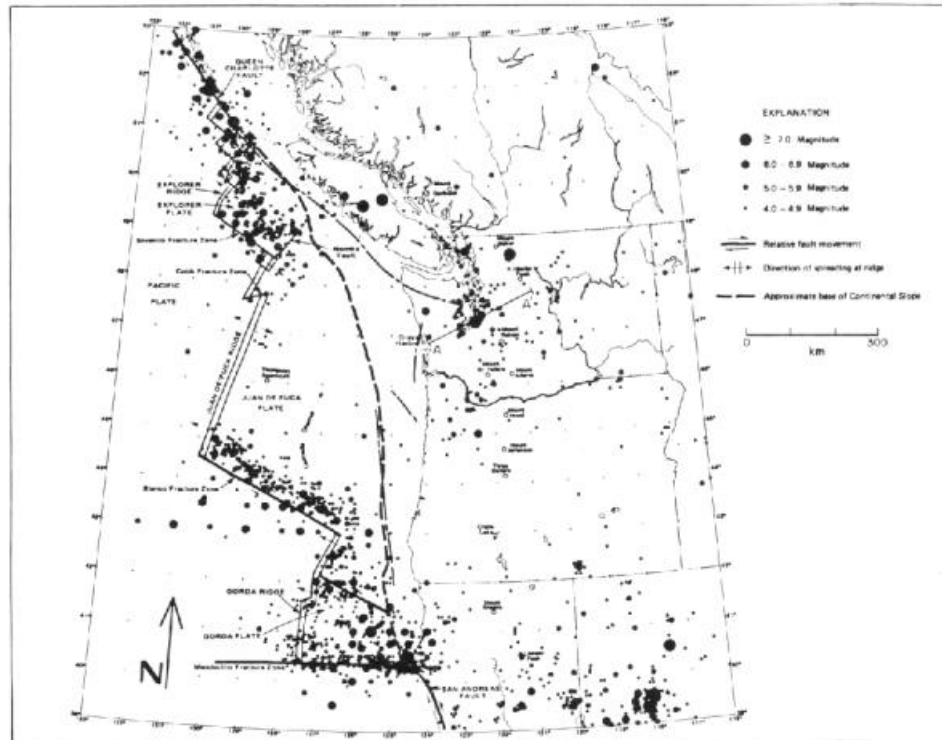
relatively fast rate are more likely to have great earthquakes, and those with an old plate subducting at a moderate rate are less likely to have great earthquakes. The end-member subduction zones are the Chilean type and the Mariana type, shown below.



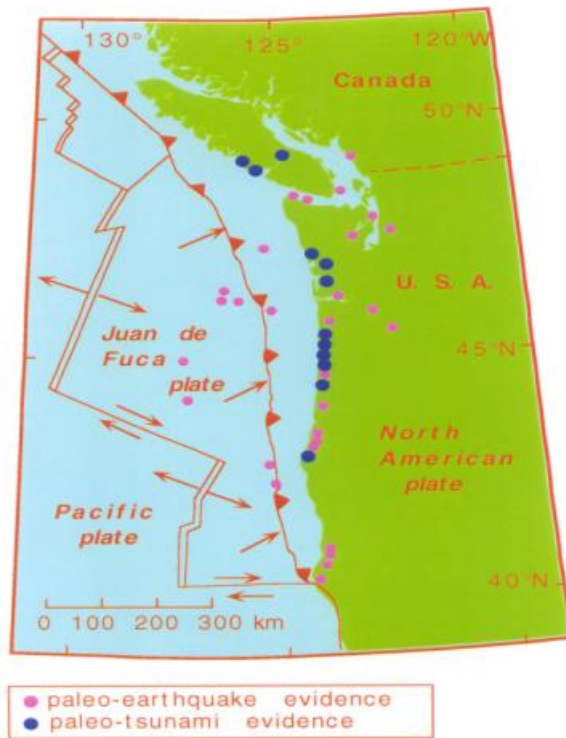
(Uyeda, S., and H. Kanamori, Back-arc opening and the mode of subduction, *J. Geophys. Res.*, 84 (B3), 1049-1061, 1979)

Another interesting implication of this correlation is the seismic potential of the Pacific Northwest (i.e., Oregon-Washington coast). The Juan de Fuca plate is subducting beneath the states of Oregon and Washington. The background seismicity there is very low, as shown below, and until mid 1980's, it was generally believed that the seismic potential in the Pacific Northwest is low (i.e., great earthquakes are unlikely). However, the age of the Juan de Fuca plate is very young, about 10 My, and it is subducting at a rate of 3 cm/year. Thus, in view of the regression relation shown above, one would expect a large, $M_w=8.5$ to 9, earthquake there. This suggestion motivated the interest of geologists who started extensive investigation for finding palaeo-seismological evidence. Geological evidence for regional submergence and evidence for large tsunami which occurred in 1700 [Satake et al., 1996] now seem to have convinced most people, which seems to have led to upgrading of building code in the area. This is a good example in which seismological study, even if it is poorly constrained, can be useful if it is followed up by investigations from different disciplines.

Seismicity in the Pacific Northwest



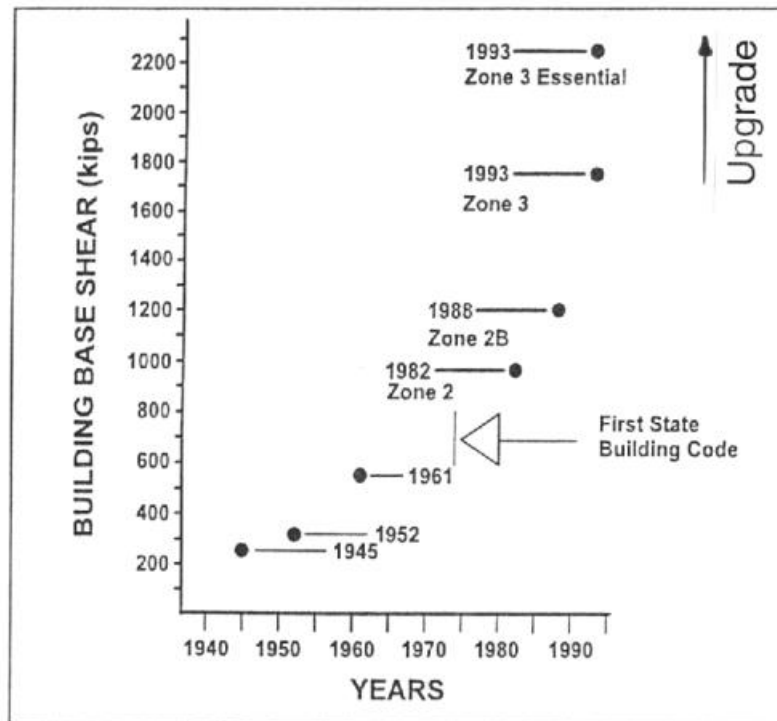
(Heaton, T., and H. Kanamori, Seismic potential associated with subduction in the northwestern United States, *Seismol. Soc. Am. Bull.*, 74 (3), 933-941, 1984)



based on Atwater et al., 1995

(see, Atwater, B. F., and others, Summary of coastal geologic evidence for past great earthquakes at the Cascadia subduction zone, Earthquake Spectra, 11, 1-18, 1995)

Change in Building Codes in Oregon



(R. S. Yeats, *Living with Earthquakes in the Pacific Northwest*, Oregon State University Press, 1998)

References

Brune, J., Seismic moment, seismicity, and rate of slip along major fault zones, *J. Geophys. Res.*, 73, 777-784, 1968.

Satake, K., Shimazaki, K., Tsuji, Y. and Ueda, K., Time and size of a giant earthquake in Cascadia inferred from Japanese tsunami records of January 1700, *Nature*, 379, 246-249, 1996.

Ge 162

2.2 Location, Magnitude, and Mechanism of Earthquakes

Locating Earthquakes (LW, pp. 217-235)

Referring to Figure 1, the arrival time of P wave at station i can be written as,

$$t_i = f(\vec{r}_o, \vec{r}_i, v(\vec{r})) + t_o \quad (1)$$

where the function $f()$ gives the travel time between the source and station i .

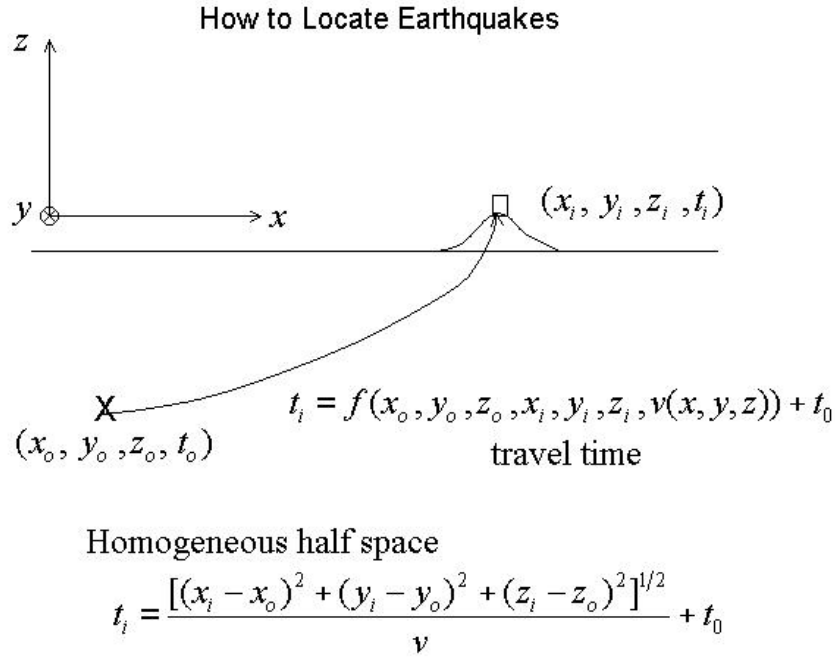


Fig 1

Here, \bar{r}_o is the hypocenter location (i.e., the location of the beginning of an earthquake), \bar{r}_i is the location of the i -th station, $v(\bar{r})$ is the wave speed which is in general a function of the position, and t_o is the origin time. For a homogeneous medium,

$$f(\bar{r}_o, \bar{r}_i, v(\bar{r})) = \frac{[(x_i - x_o)^2 + (y_i - y_o)^2 + (z_i - z_o)^2]^{1/2}}{v} \quad (2)$$

We want to determine 4 unknowns, $\bar{r}_o = (x_o, y_o, z_o)$ and t_o , from N observations, $t_1, t_2, t_3, t_4, \dots, t_N$.

This problem is a nonlinear problem even for the simplest case for a homogeneous medium.

To solve a nonlinear problem like this, we start from a first approximation

$$\bar{r}_o^0 = (x_o^0, y_o^0, z_o^0) \text{ and } t_o^0 \quad (3)$$

Then writing

$$x_o = x_o^0 + \delta x_o \text{ etc, and } t_o = t_o^0 + \delta t_o \quad (4)$$

and taking the first order terms in δx_o etc and δt_o , we set up linear equations for δx_o etc and δt_o as,

$$t_i - t_i^0 = \left. \frac{\partial f(\bar{r}_i)}{\partial x_o} \right|_0 \delta x_o + \left. \frac{\partial f(\bar{r}_i)}{\partial y_o} \right|_0 \delta y_o + \left. \frac{\partial f(\bar{r}_i)}{\partial z_o} \right|_0 \delta z_o + \delta t_o \quad (5)$$

($i=1, 2, 3, \dots, N$), where t_i^0 is the arrival time at station i computed for the first approximation (*i.e.*, $t_i^0 = t_o^0 + (\text{travel time computed for the first approximation})$).

This problem can be solved by the method of least squares. By iterating this, we can determine $\bar{r}_o = (x_o, y_o, z_o)$ and t_o which best fit the observed travel times. More details will be discussed in the practice session.

Traditionally, magnitude scales are used to indicate the size of an earthquake. The magnitude M is determined from the amplitude of the observed seismic waves. In general,

$$M = \log(A) + f(\Delta) \quad (6)$$

where A is the amplitude of the observed seismic waves (body waves, surface waves, or unspecified), and $f(\Delta)$ is an amplitude attenuation curve as a function of distance determined for specific type of waves.

For example, in case of the traditional local magnitude M_L , the amplitude A is the amplitude of the Wood Anderson seismogram in mm, and $f(\Delta)$ is given by a table, or by a nomogram such as that shown in Figure 2.

Local Magnitude (M_L)

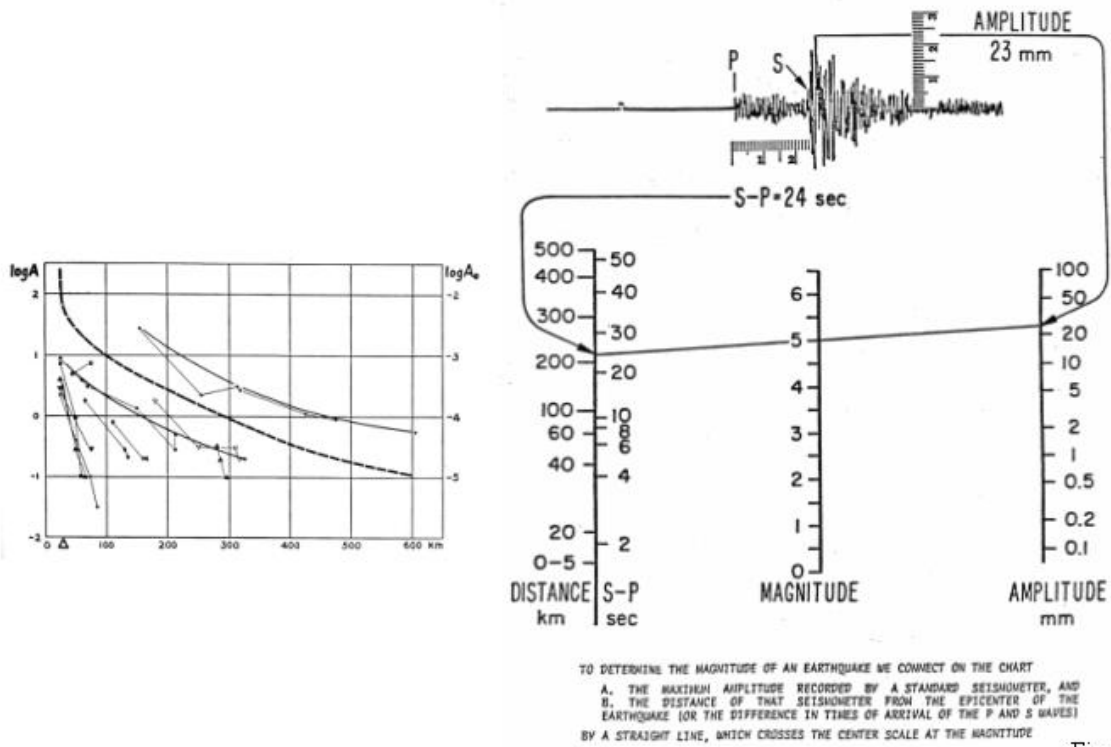


Fig. 2

In case of the surface-wave magnitude, M_S , A is the ground-motion amplitude of 20 sec (period) surface waves in μ observed at a distance of Δ deg. Then,

$$M_S = \log A + 1.656 \log(\Delta) + 1.818 \quad (7)$$

Although the magnitude is a useful parameter, it is difficult to attach some specific physical quantity to it. Empirically, M_S is related to the total wave energy, E_R , radiated from an earthquake by

$$\log E_R = 1.5M_S + 4.8 \text{ (joule)} \quad (8)$$

In more recent studies, we use another scale, M_w , which is determined from seismic moment, M_0 . The seismic moment M_0 is given by

$$M_0 = \mu DS \quad (9)$$

where D is the fault offset, S is the fault area, and μ is the rigidity of the crust surrounding the fault. The unit of M_0 is N-m. Unlike other magnitude scales, M_w represents a specific earthquake source parameter, the overall static size of an earthquake given by M_0 . The relation between M_w and M_0 is given by

$$\log M_0 = 1.5M_w + 9.1 \quad (10)$$

This will be discussed in more detail later.

Earthquake Mechanism (LW, pp.346-356)

As shown in Figure 3, the fault motion on a vertical strike slip fault would produce compressional and dilatational quadrants in the Earth's crust.

P-wave First-motion and Focal Sphere

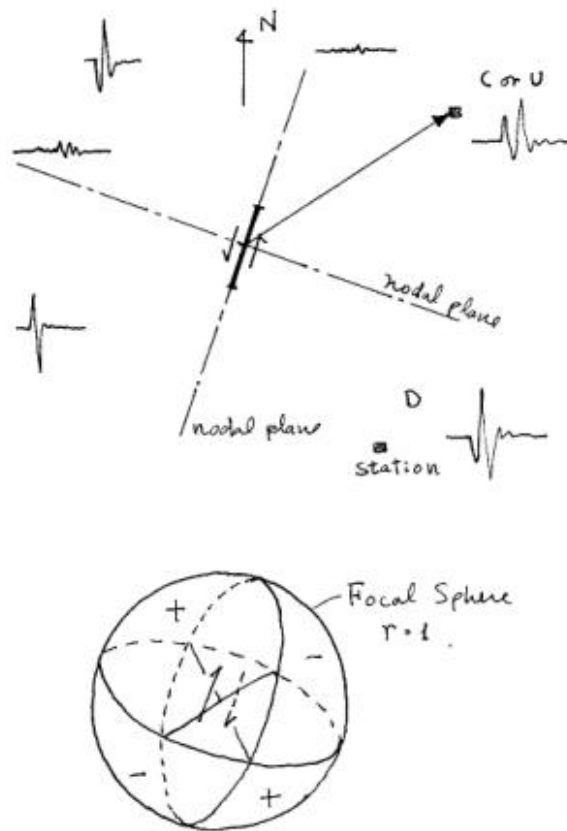


Fig. 3

The pattern of compression and dilatation can be detected by the first motion of P waves. In the compressional quadrant P wave is up and in the dilatational quadrant, it is down. As viewed from above, the sense of the first motion (up or down, or compression or dilatation) alternates in quadrant. The planes separating the compressional quadrant and the dilatational quadrant are called the nodal planes. The fault plane coincides with

one of the nodal planes. The other nodal plane is called the auxiliary plane. With this method alone, we cannot distinguish the fault plane from the nodal plane, i.e., the fault plane can be either one of the nodal planes.

Thus, from the observations of *P* wave first-motion data from many stations surrounding the source we can determine the geometry of the faulting. The pattern thus determined is usually referred to as "Mechanism of Earthquake". Faults with different types (e.g., strike slip fault, thrust fault, and normal fault) produce different radiation patterns of *P* waves. This can be easily seen, if we consider a small sphere surrounding the source. This sphere is called the focal sphere (Figure 3).

The radiation pattern is three dimensional, and the surface of the focal sphere is divided into quadrants of compression and dilatation. (This can be best understood using a worn-out tennis ball with compressional quadrants painted dark.)

We need to show this three-dimensional pattern on the focal sphere on a piece of paper. Since the pattern is point symmetric with respect to the center of the focal sphere, we need to show only the pattern on a hemisphere. It is conventional to show the lower focal hemisphere, but in rare cases, the upper hemisphere or the side hemisphere is shown. We use a standard projection method, most commonly the equal-area stereographic projection, to project the lower hemisphere to a flat horizontal plane (Figure 4).

Stereographic Projection of Focal Sphere

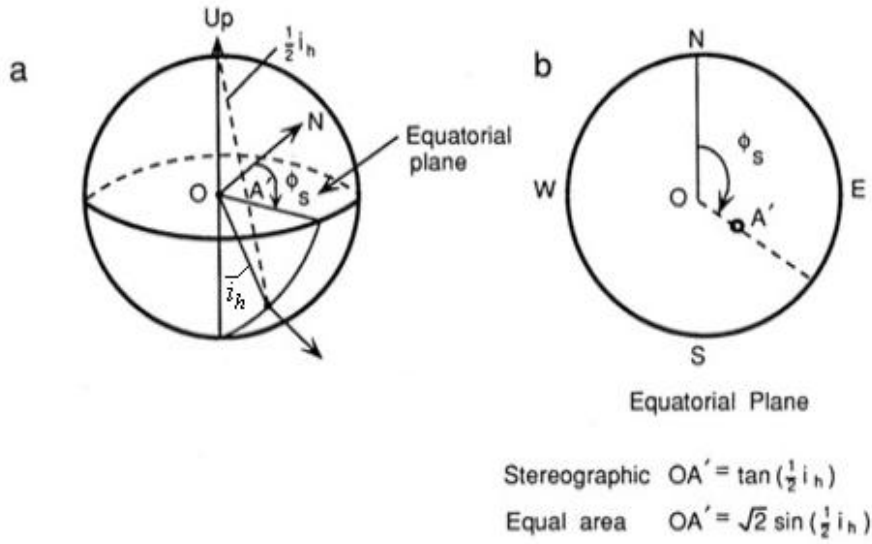


Fig. 4

Some examples are shown in Figure 5. The projected diagram is called the mechanism diagram. As shown in Figure 5, the stereographic mechanism diagram is intuitive for understanding the geometry of faulting (more details in the practice session).

Faulting and Mechanism Diagrams

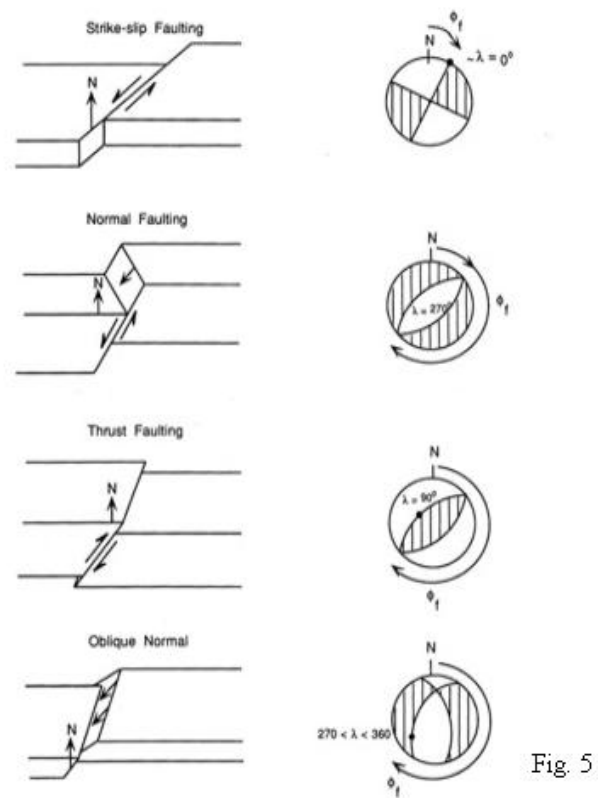


Figure 6 shows the mechanism of large earthquakes along the Circum-Pacific belt. Most of them are low-angle thrust mechanisms which are consistent with subduction of the Nazca and the Pacific plates beneath the South American, the North American, and the Eurasian plates. The normal fault events represents tensional failure within the oceanic plate upon bending caused by subduction.

Mechanism of Great Earthquakes in the Pacific

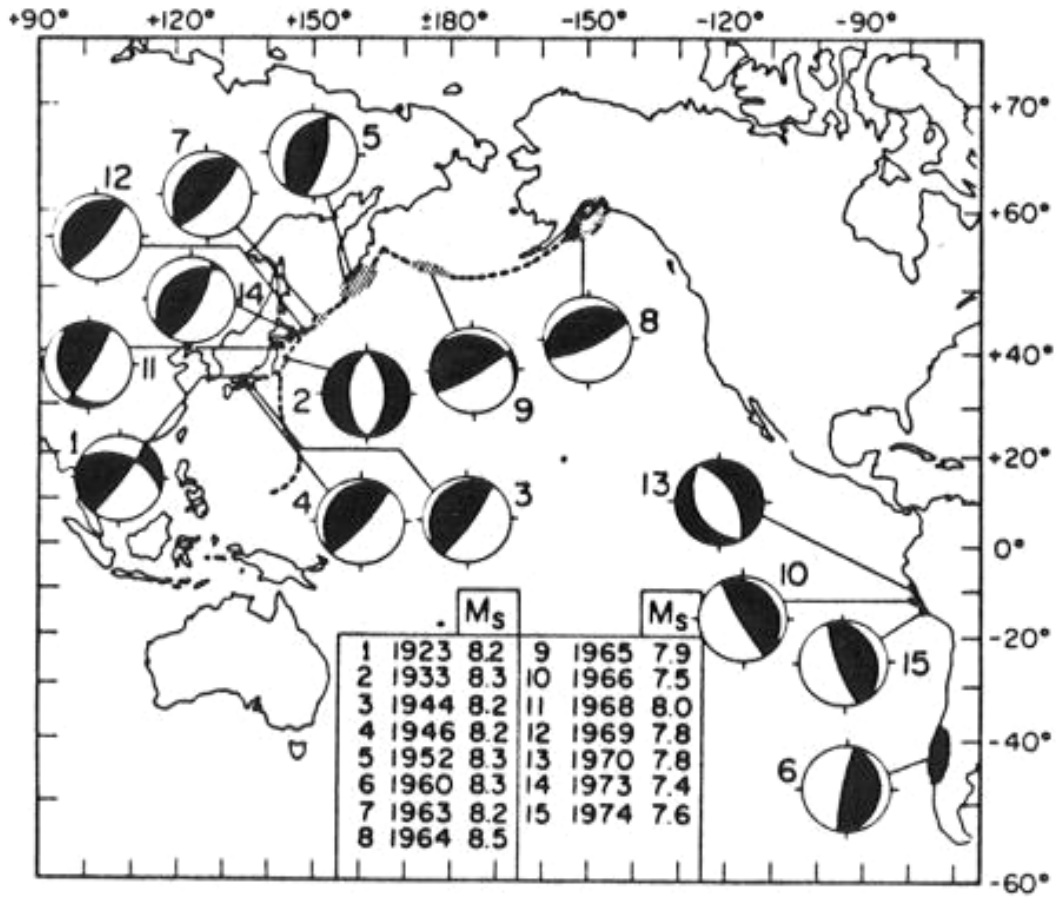


Fig. 6

Ge 162 Practice Session 1 Locating Earthquakes

Data

Table-1 is the travel time data obtained using "STP" which is a SCEC (Southern California Earthquake Center) tool to extract earthquake data (parameter data and waveform data). (For details of STP, see the SCEC Web site). The data are rearranged in (x, y) coordinate (in km) with the Pasadena station (Latitude=34.1484°, Longitude=-118.1711°) as the origin. The origin time of the arrival times is arbitrary. Table-1 gives only the first 10 stations. The actual data are in loc_dat_1 (all the data and program files are in a FTP site on ftp.gps.caltech.edu /home/ftp/pub/hiroo/ge162.dir).

Table 1.

Earthquake-1				Reference Station (Origin of (x,y))		
				PAS	34.1484	-118.1711
Station	Lat.	Long.	Elev.	x(km)	y(km)	arrival t.(sec)
MIK	34.1370	-118.1260	235.0000	4.160	-1.264	1.453
GSA	34.1368	-118.1283	165.0000	3.947	-1.286	1.453
KIK	34.1504	-118.1016	168.0000	6.409	0.224	1.596
PAS	34.1484	-118.1711	257.0000	0.000	0.000	1.615
GVR	34.0497	-118.1200	141.0000	4.718	-10.947	1.620
RUS	34.0505	-118.0799	37.0000	8.420	-10.856	1.753
RIO	34.1047	-117.9796	79.0000	17.670	-4.831	2.778
MWC	34.2237	-118.0529	1696.0000	10.891	8.359	2.731
LGB	33.9756	-118.1491	6.0000	2.033	-19.167	3.417
TCC	33.9947	-118.0140	195.0000	14.514	-17.038	2.731
GR2	34.1183	-118.2994	316.0000	-11.837	-3.331	3.134
.....

Locate the earthquake taking the following steps. Ideally, you should write your own program to carry out 2 to 6, but if you find it difficult to do so, you can use a simple program, eqloc.f. To do 7, you will need to use this program. In case you use this program, try to follow the steps taken in the program.

1. Use the first approximation, (0.0, 0.0, -10.0, 0.0).

2. Compute the travel times and the partial derivatives in a homogeneous medium with $v=6$ km/s which is a good average for the shallow crust. Refer to equation (1) to (5) in class note 2.2.

$$t_i^0, \left. \frac{\partial f(\bar{r}_i)}{\partial x_o} \right|_0, \left. \frac{\partial f(\bar{r}_i)}{\partial y_o} \right|_0 \text{ and } \left. \frac{\partial f(\bar{r}_i)}{\partial z_o} \right|_0 \quad (i=1, 2, 3, \dots, N) \quad (1)$$

3. Set up the equation for the least-square solution.

$$\begin{pmatrix} \left. \frac{\partial f(\bar{r}_1)}{\partial x_o} \right|_0 & \left. \frac{\partial f(\bar{r}_1)}{\partial y_o} \right|_0 & \left. \frac{\partial f(\bar{r}_1)}{\partial z_o} \right|_0 & 1 \\ \left. \frac{\partial f(\bar{r}_2)}{\partial x_o} \right|_0 & \left. \frac{\partial f(\bar{r}_2)}{\partial y_o} \right|_0 & \left. \frac{\partial f(\bar{r}_2)}{\partial z_o} \right|_0 & 1 \\ \left. \frac{\partial f(\bar{r}_3)}{\partial x_o} \right|_0 & \left. \frac{\partial f(\bar{r}_3)}{\partial y_o} \right|_0 & \left. \frac{\partial f(\bar{r}_3)}{\partial z_o} \right|_0 & 1 \\ \cdot & \cdot & \cdot & \cdot \\ \cdot & \cdot & \cdot & \cdot \\ \cdot & \cdot & \cdot & \cdot \\ \left. \frac{\partial f(\bar{r}_N)}{\partial x_o} \right|_0 & \left. \frac{\partial f(\bar{r}_N)}{\partial y_o} \right|_0 & \left. \frac{\partial f(\bar{r}_N)}{\partial z_o} \right|_0 & 1 \end{pmatrix} \begin{pmatrix} \delta x_0 \\ \delta y_0 \\ \delta z_0 \\ \delta t_0 \end{pmatrix} = \begin{pmatrix} t_1 - t_1^0 \\ t_2 - t_2^0 \\ t_3 - t_3^0 \\ \cdot \\ \cdot \\ t_N - t_N^0 \end{pmatrix} \quad (2)$$

which we write as

$$A\bar{m} = \bar{d} \quad (3)$$

where A is an $N \times 4$ matrix

$$A = \begin{pmatrix} \left. \frac{\partial f(\bar{r}_1)}{\partial x_o} \right|_0 & \left. \frac{\partial f(\bar{r}_1)}{\partial y_o} \right|_0 & \left. \frac{\partial f(\bar{r}_1)}{\partial z_o} \right|_0 & 1 \\ \left. \frac{\partial f(\bar{r}_2)}{\partial x_o} \right|_0 & \left. \frac{\partial f(\bar{r}_2)}{\partial y_o} \right|_0 & \left. \frac{\partial f(\bar{r}_2)}{\partial z_o} \right|_0 & 1 \\ \left. \frac{\partial f(\bar{r}_3)}{\partial x_o} \right|_0 & \left. \frac{\partial f(\bar{r}_3)}{\partial y_o} \right|_0 & \left. \frac{\partial f(\bar{r}_3)}{\partial z_o} \right|_0 & 1 \\ \cdot & \cdot & \cdot & \cdot \\ \cdot & \cdot & \cdot & \cdot \\ \cdot & \cdot & \cdot & \cdot \\ \left. \frac{\partial f(\bar{r}_N)}{\partial x_o} \right|_0 & \left. \frac{\partial f(\bar{r}_N)}{\partial y_o} \right|_0 & \left. \frac{\partial f(\bar{r}_N)}{\partial z_o} \right|_0 & 1 \end{pmatrix} \quad (4)$$

and \bar{m} and \bar{d} are column vectors containing the parameters to be determined and the data, respectively, i.e.,

$$\bar{m} = \begin{pmatrix} \delta x_0 \\ \delta y_0 \\ \delta z_0 \\ \delta t_0 \end{pmatrix}, \text{ and } \bar{d} = \begin{pmatrix} t_1 - t_1^0 \\ t_2 - t_2^0 \\ t_3 - t_3^0 \\ \cdot \\ \cdot \\ \cdot \\ t_N - t_N^0 \end{pmatrix} \quad (5)$$

4. Determine \bar{m} .

The normal equation is,

$$A^T A \bar{m} = A^T \bar{d} \quad (6)$$

If $A^T A$ is not singular, the formal solution is given by

$$\bar{m} = (A^T A)^{-1} A^T \bar{d} \quad (7)$$

and the error estimates are determined by the variance of the data and the diagonal elements of the inverse matrix of the normal equation (6). Usually, we write the uncertainty in m_i by Δm_i , and compute it by

$$\Delta m_i = \sqrt{c_{ii}} \sqrt{\sum_{j=1}^N (t_j - t_j^c)^2 / (N - N_p)}, \quad i=1, 2, 3 \quad (8)$$

where N_p is the number of parameters (here 4), c_{ii} are the diagonal elements of $(A^T A)^{-1}$, and t_j^c are the computed arrival times for station j .

5. Obtain the 2nd approximation by:

$$\begin{aligned} x_0 &= 0 + \delta x_0 \\ y_0 &= 0 + \delta y_0 \\ z_0 &= -10. + \delta z_0 \\ t_0 &= 0 + \delta t_0 \end{aligned} \tag{9}$$

6. Iterate 2, 3, 4, 5.

A simple program `eqloc.f` is in `/home/ftp/pub/hiroo`. This program uses 2 input files.

i_eqloc and **c_eqloc**

i_eqloc

```
loc_dat_1          : Name of the travel-time data file
0.0      0.0      -10.0   0.0   : 1st approx.
```

c_eqloc

```
10                : maximum number of iterations
```

half_space

```
                : name of the structure
```

```
s-cal.pvel
```

half_space

```
half_space
```

```

1                               : number of layers
9999.  6.0                       : layer thickness,  $\alpha$ 

```

s-cal.pvel

southern cal. P structure, with a slightly low surface velocity

```

5
1.0      4.0
3.       5.5
23.4     6.3
5.       6.8
9999.0   7.8

```

7. If the second line of `c_eqloc` is replaced by `s-cal.pvel`, it will use a more general subroutine which computes the travel times etc for a layered model given by `s-cal.pvel`. Try `eqloc.f` with `s-cal.pvel`. Output of `eqloc` is in `o_eqloc`.

8. Vary the 1st approximation to see how the solution is affected.

9. Remove the data for which t_i is less than 5 sec, and locate the event.

Example output

o_eqloc

```

10
southern california P structure, with a
  1.000    4.000
  3.000    5.500
 23.400    6.300
  5.000    6.800
 9999.000  7.800
loc_dat_1
  0.000    0.000   -10.000    0.000
Earthquake-1
PAS      34.148  -118.171
x0=      6.778    0.319
y0=     -4.360    0.378

```

```

z0=      -10.676      1.159
th0=       0.017      0.054
  34.148     -118.171     -10.000      0.000
x0=       6.790      0.316
y0=      -4.186      0.381
z0=      -8.184      1.079
th0=       0.027      0.054
  34.109     -118.098     -10.676      0.017
x0=       6.782      0.308
y0=      -4.172      0.367
z0=      -7.645      1.180
th0=       0.030      0.048
  34.111     -118.098      -8.184      0.027
x0=       6.782      0.307
y0=      -4.167      0.365
z0=      -7.533      1.217
th0=       0.032      0.047
  34.111     -118.098     -7.645      0.030

```

.....
station data

Station	Dist. (km)	Azm. (deg)	t_i	t_i (computed)	Res.
MIK	3.911	317.927	1.453	1.552	-0.099
GSA	4.040	315.481	1.453	1.563	-0.110
KIK	4.404	355.193	1.596	1.594	0.002
PAS	7.958	301.591	1.615	1.983	-0.368
GVR	7.088	196.979	1.620	1.876	-0.256
RUS	6.888	166.284	1.753	1.853	-0.100
RIO	10.909	93.540	2.778	2.377	0.401
MWC	13.179	18.203	2.731	2.703	0.028
LGB	15.734	197.612	3.417	3.083	0.334
TCC	15.014	149.045	2.731	2.975	-0.244
GR2	18.637	272.606	3.134	3.525	-0.391
WLT	17.605	129.626	3.714	3.367	0.347
USC	20.145	239.757	3.804	3.756	0.048
WTT	23.123	219.086	4.858	4.218	0.640
PEM	21.884	73.425	3.989	4.026	-0.037

.....
0.3273

RMS of residuals

Ge 162 Practice Session 2 *P*-wave First-Motion Mechanism

Data

Table-1 is the phase data obtained using "STP" which is a SCEC tool to extract earthquake data (parametric data and waveform data). (For details of STP, see the SCEC Web site). The data contain station names, first motion data (C or D), quality (Q, ignore in this problem), azimuth, and take-off angle. The azimuth and take-off angle, i_h , (measured from downward vertical) are computed using a standard southern California structure. Table-1 lists only selected 10 stations. The actual data are in mech_dat_1 in /home/ftp/pub/hiroo/ge162.dir/practice2.dir.

Table 1. *P*-wave first-motion data

station	C or D	Q	Azimuth (°)	i_h (°)
BVH	D	2	340.332	164.798
SMS	D	2	231.855	131.689
DJJ	C	2	310.759	131.679
USC	C	2	114.973	123.098
LAX	D	2	190.413	116.500
HLL	D	2	11.487	115.842
PAS	D	2	63.638	103.096
NOT	C	2	320.286	101.493
MWC	D	2	59.358	96.635
LKL	D	2	39.880	92.397

.....

Determine the mechanism of this earthquake taking the following steps.

1. Compute the radial distance on a mechanism diagram using the equal-area projection,

$$r_i = \sqrt{2} \sin(i_{h_i} / 2) \quad (\text{equal-area projection}) \quad (1)$$

Remember that if i_h is larger than 90° , then 180° must be added to the azimuth (i.e., the station must be plotted in the opposite azimuth.), and i_h must be changed to $180^\circ - i_h$.

2. Plot the first-motion (filled circle for compression and open circle for dilatation) on a mechanism diagram. (Plot the data for the 10 stations listed in Table-1 manually, or with your own program).

3. A program `mplotr_2.f` is provided in `practice_2.dir` to plot the first-motion data on a mechanism diagram. `mplotr_2.f` takes 2 input files, `i_mplotr_2` and `c_mplotr_2`. The output is a postscript file `p_mplotr_2`.

`i_mplotr_2`

```
Earthquake(mech)-1      : Job ID
f                       : fault(f) or moment tensor(m)
85.  180.  350.         : dip, rake, and fault strike
mech_dat_1              : file name of the data
```

(For plotting only the first-motion data, the 2nd and 3rd lines are irrelevant.)

`c_mplotr_2`

```
7.0  0.1  10.  5.0  0  0  1  0      : these parameters control the type and
style of the plot
(change plot_opt parameter (2nd from the last) only. 1 for the first-motion
data only (in this case, the fault parameters are ignored), 3 for the data +
nodal lines)
```

```
(radius, sizef, deltlc, delt2c, shading p, sv or sh, ndens,
plot_opt., projection)
```

4. The final step is to determine the mechanism by drawing two orthogonal nodal planes so that they divide the compressional and dilatational stations. Usually there are always some inconsistent stations, but try to find the best solution. Many methods have been developed, but here try a few mechanisms. `mplotr_2.f` draws 2 nodal lines corresponding to the fault mechanism given by dip, δ , rake, λ , and fault strike, ϕ_f (run `mplotr_2` with `plot_opt=3` in `c_mplotr_2`). These fault parameters are defined in the figure below.

(ξ_1, ξ_2, ξ_3) fault coordinate
(Right-handed)

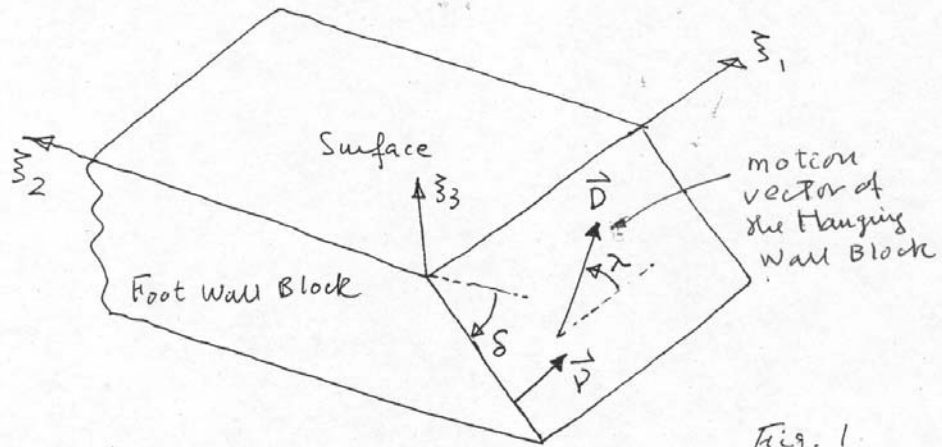


Fig. 1.

Map View

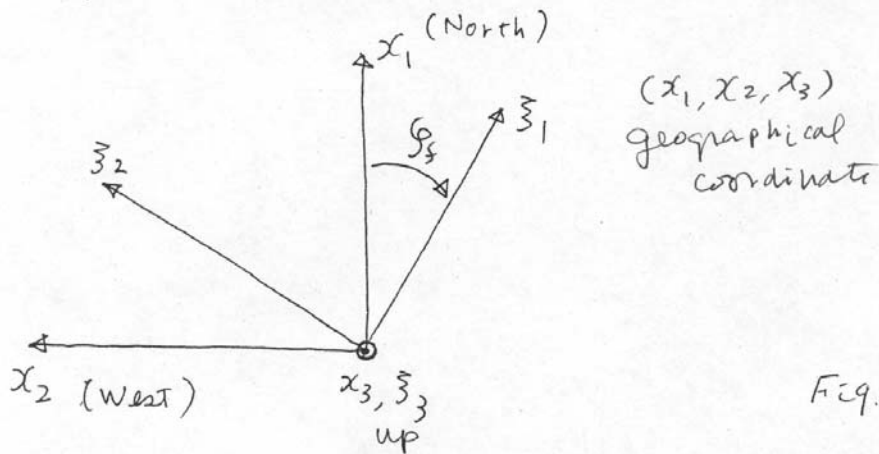


Fig. 2

5. Assume that the fault strike is -45° from N. Plot the mechanism diagrams for (1) right-lateral vertical strike slip, (2) vertical dip slip (north-east side down), (3) thrust fault dipping 20° NE, (4) normal fault dipping 45° NE, and (4) an oblique-slip mechanism (e.g., add some right-lateral component to (3)). (This problem has nothing to do with

the first-motion data given in mech_dat_1. You can just draw a sketch of mechanism diagrams, or run mplotr_2.f with

c_mplotr_2

7.0 0.1 10. 5.0 0 50 4 0

.)

Ge162

2.3. Seismicity of the Earth (LW, pp.434-477)

2.3.1 Global Seismicity

Earthquakes occur mainly:

1. Along trenches (subduction zones),
2. Along ridge-transform systems,
3. In continental interiors.

Figures 1 and 2 show seismicity in the world and California, and Figures 3 and 4 show the mechanisms of large earthquakes in the world and California.

World Seismicity

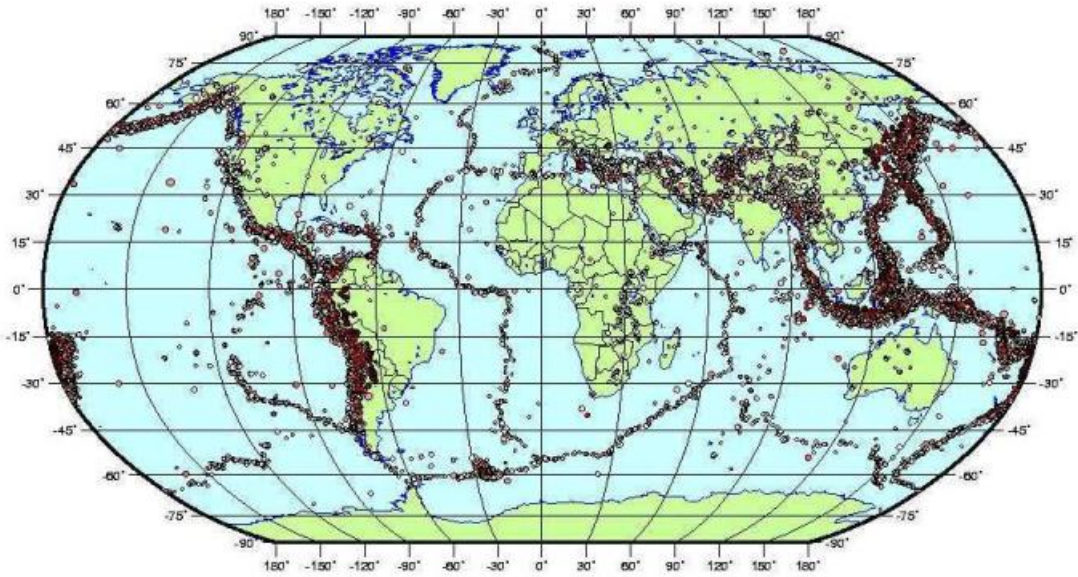


Fig. 1

Seismicity of California
1900-2001, $M_L \geq 3.5$

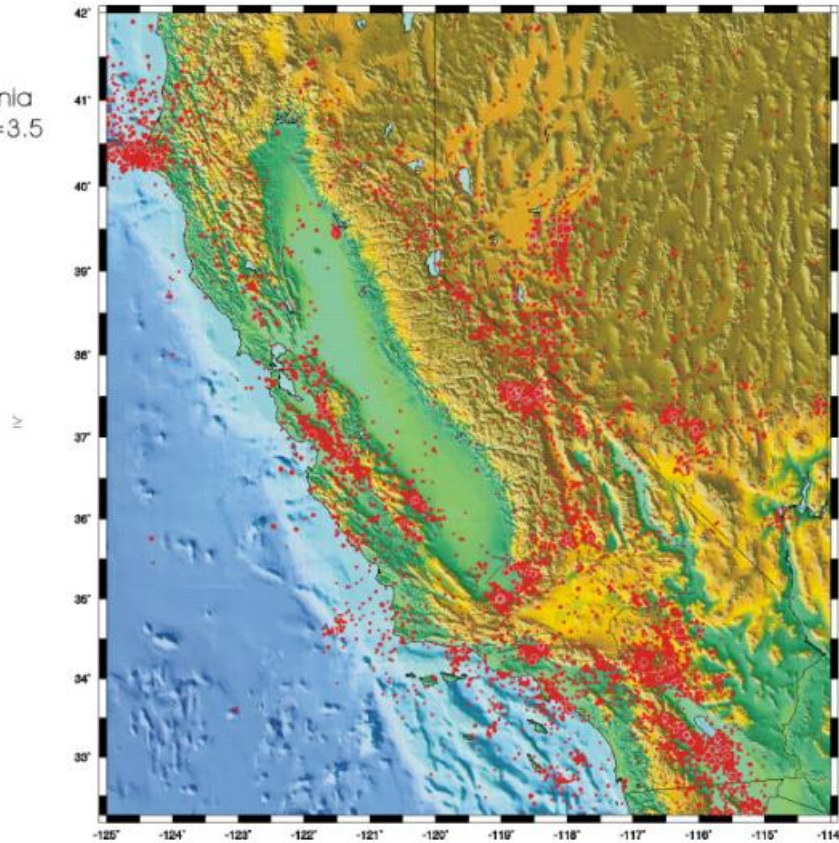


Fig. 2

The world largest earthquakes occur along subduction zones (e.g., the 1960 Chilean earthquake, $M_w=9.5$, the 1964 Alaskan earthquake, $M_w=9.2$). More than 75 % of the seismic energy release takes place there. Most of these events represent slip on the interface between a subducting oceanic plate and an overriding plate (Figure 3). In these zones deep focus earthquakes occur to a depth of about 700 km.

Mechanism of Large Earthquakes in the World ($M_w \geq 7.5$, 1976-2001)

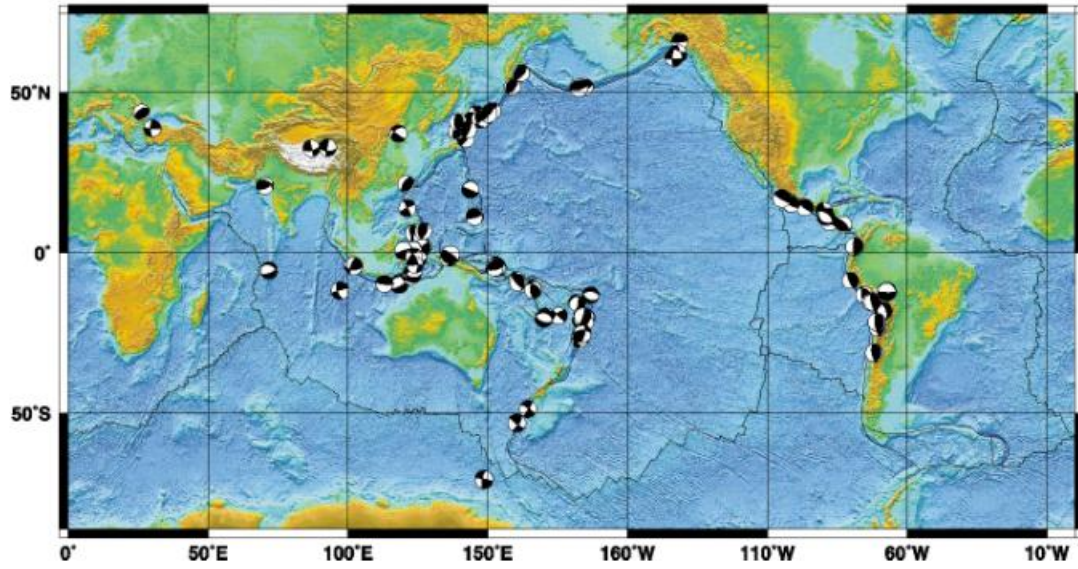


Fig. 3

Mechanism of Large Earthquakes in California ($M_w \geq 6.5$, 1976-2001)

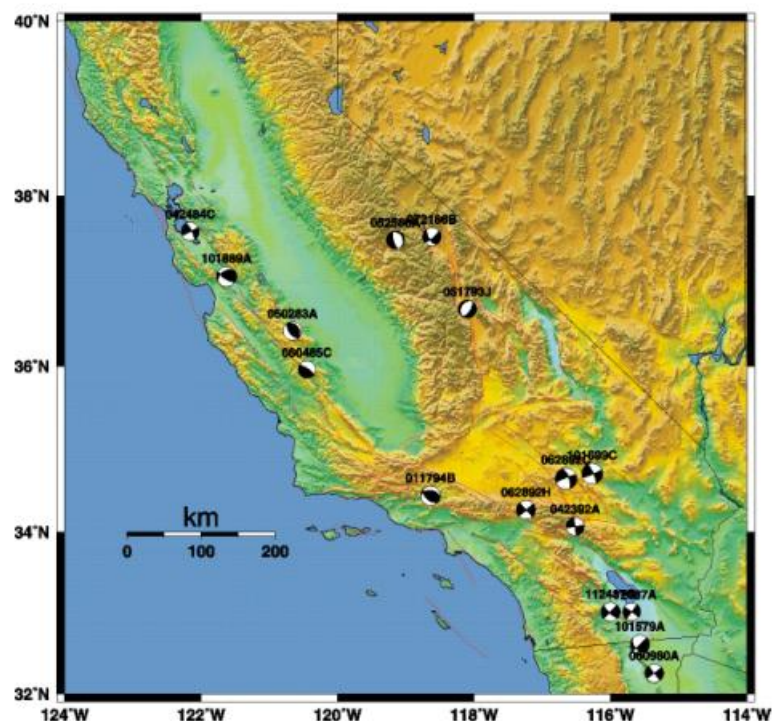


Fig. 4

Most earthquakes along ridge-transform systems are shallow and relatively small (10% in energy release). The events on ridges have normal-fault mechanism, and those along the transform boundaries have strike-slip mechanisms. Transform fault events are generally larger; occasionally the magnitude reaches 8 (e.g., the 1906 San Francisco earthquake, $M_w \approx 8$). No deep focus earthquake has been found beneath ridge-transform systems.

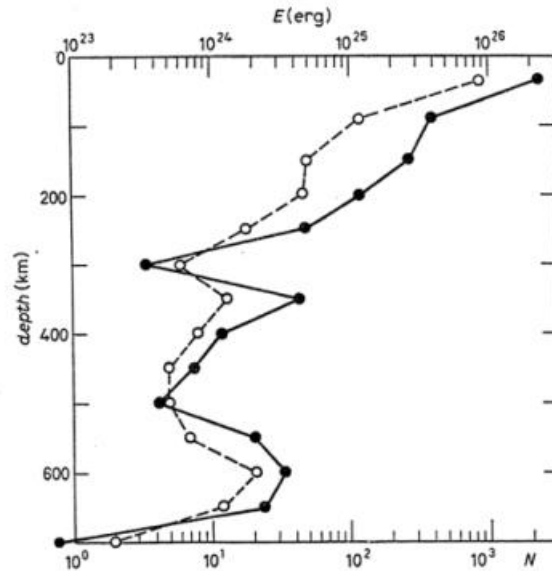
The distribution of the events in continental interiors (15 % in energy release) is very diffuse. Partly because of their proximity to major population centers, large intra-

continental events are often very devastating (e.g., the 1976 Tanshang earthquake, the 1988 Armenian earthquake, the 2001 India earthquake)

2.3.2 Depth Variation (Figure 5)

Most earthquakes occur at depths shallower than 60 km. However, some significant earthquakes occur at depths of as deep as 700 km, especially in subduction zones (e.g. 1970 Colombia, $d=653$ km, $M_w=8.1$; 1954 Spain, $d=640$ km, $M=7.8$, 1994 Bolivia, $d=635$ km, $M_w=8.3$). The largest recorded deep focus earthquake is the 1994 Bolivia earthquake.

Depth Variation of Seismicity



The variation of seismic activity as a function of depth. The solid curve shows the energy and the dashed curve the number of events with $m_B > 7$. The scale at the top indicates the energy (E) and that at the bottom the number (N). Each data point represents the value for a depth range of 50 km centered at the depth of each data point and for the time period of 75 years from 1904 to 1974 [10].

Fig. 5

A pronounced peak in the energy release is seen at a depth of 600 km, just before the seismic activity dies out.

2.3.3 Temporal Variation of Seismicity (Figure 6)

Figure 6 shows the temporal variation of seismicity. The energy release during the period from 1952 to 1965 dominates. This peak is a result of five large subduction-zone earthquakes in the Pacific (1952 Kamchatka, 1957 Aleutian Is., 1960 Chile, 1964 Alaska,

1965 Aleutian Is.). The energy release rate is not uniform in time, and fluctuates on a time scale of at least 100 years.

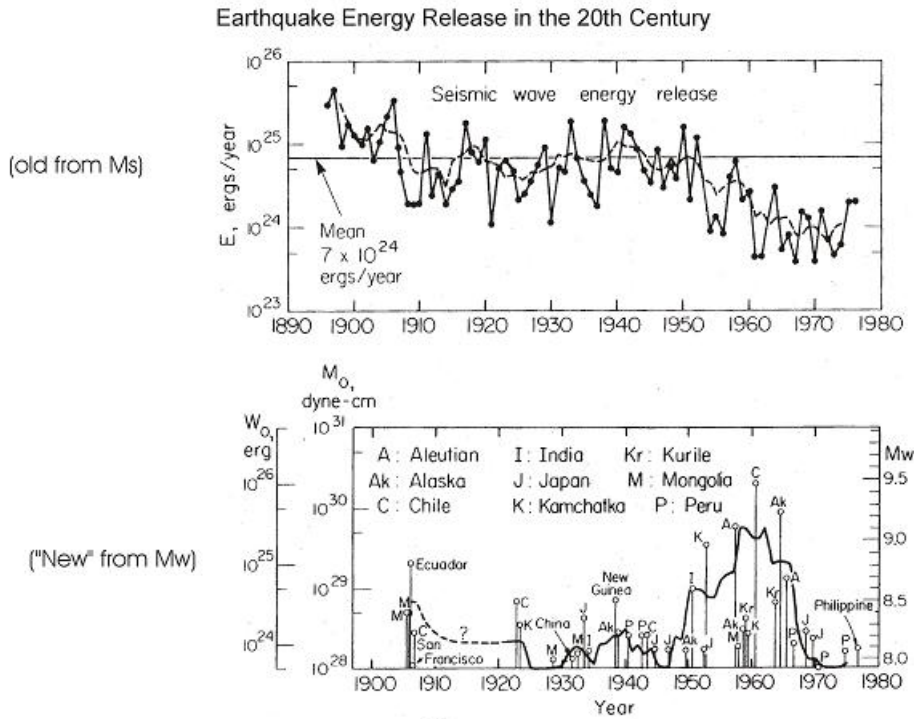


Fig. 6

The average energy release is about 4.5×10^{24} ergs/year, which is approximately 1/4 of the energy released in volcanic eruptions, and 0.05 % of the terrestrial heat flow.

Figures 7, 8, and 9 show the distribution of great earthquakes, the temporal distribution of damaging earthquakes, and the temporal distribution of damaging tsunamis.

Great Earthquakes

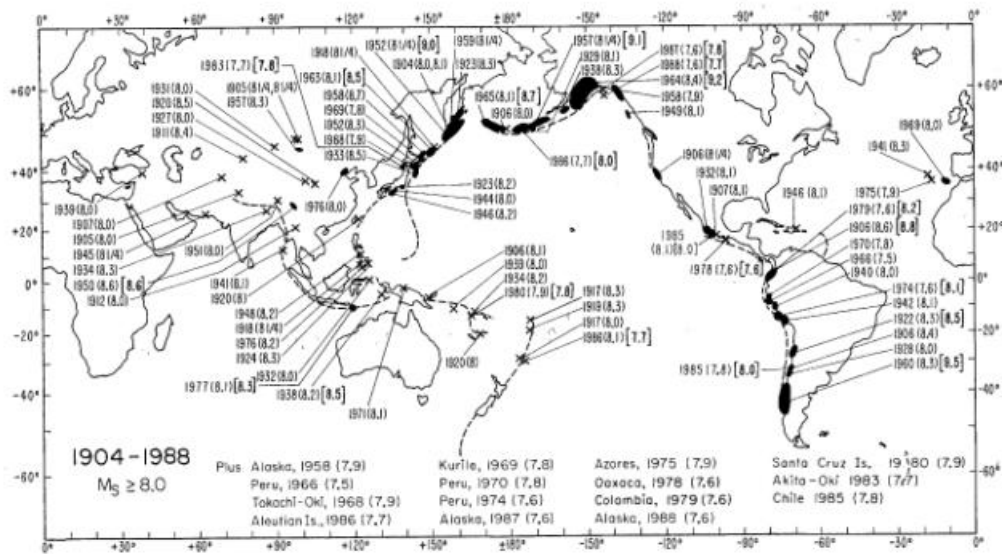


Fig. 7

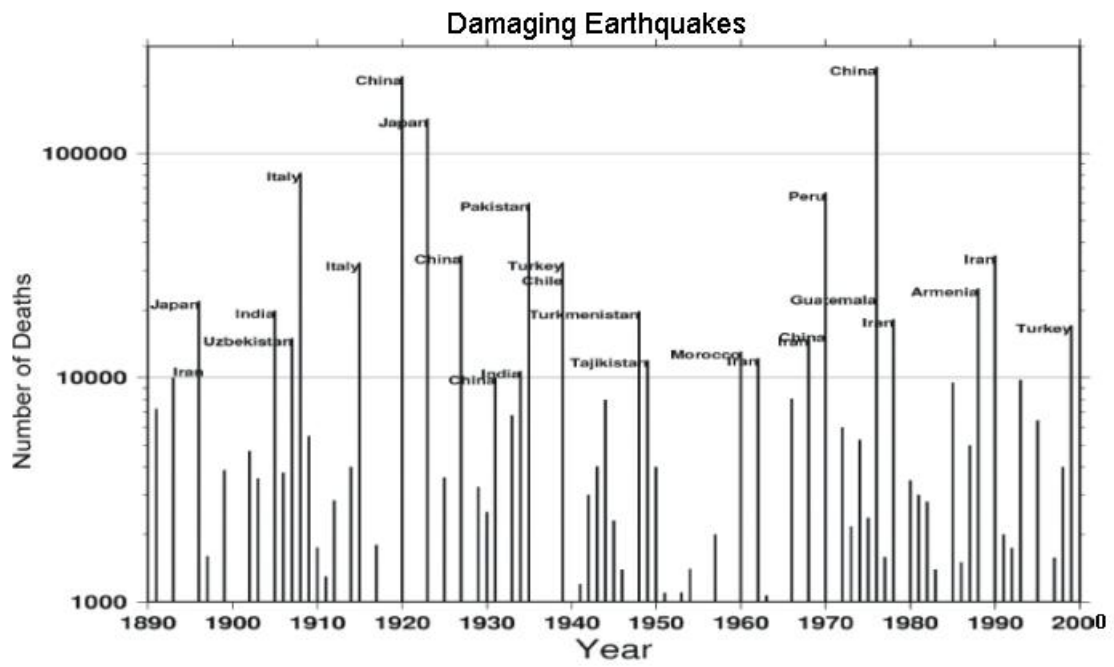
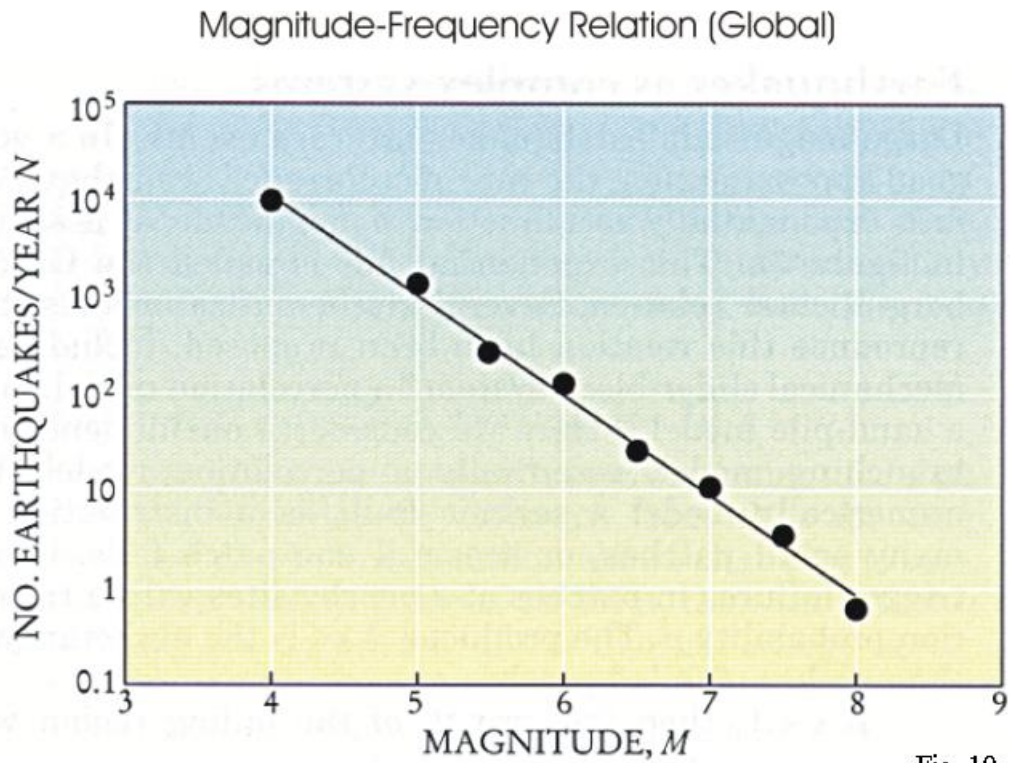


Fig. 8

The results obtained for many regions indicate that the value of b (called b value) is approximately equal to 1.

Figure 9 shows that approximately 1 earthquake with $M \geq 8$ occurs every year.



2.3.5 Aftershocks

After a large earthquake (main shock), many smaller earthquakes occur near the epicenter of the earthquake. The decay of aftershock activity follows the Omori's law given by

$$n(t) = \frac{K}{t+c}$$

where $n(t)$ is the number of aftershocks larger than a given magnitude per unit time. A modified Omori's law is given by

$$n(t) = \frac{K}{(t+c)^p}$$

where p is a constant, which is usually slightly larger than 1.

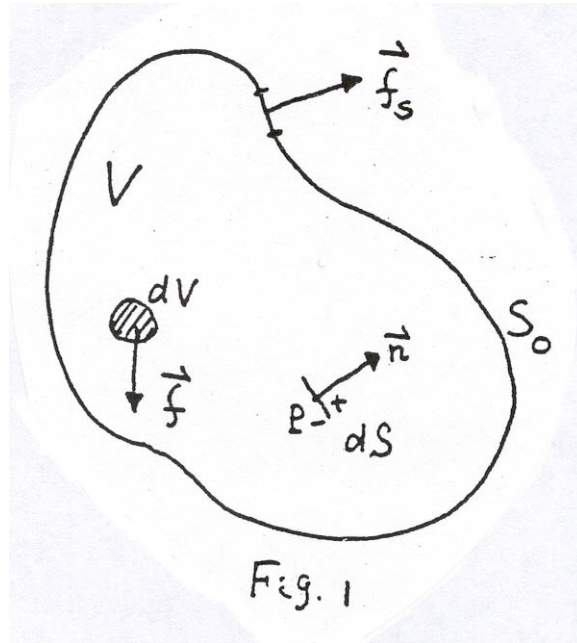
3.1 Review of Elasticity Theory

3.1.1 Stress

In the theory of elasticity we consider two types of forces.

Body Force

The body force \vec{f} is defined by a force per unit mass in a medium (Figure 1). Then, the body force per unit volume is $\rho\vec{f}$ where ρ is the density of the medium.



Then the force acting on a volume element dV is

$$\rho \bar{f} dV$$

which can be integrated over a volume V as

$$\int_V \rho \bar{f} dV$$

e.g. body force due to gravity: $\rho \bar{f} = \rho g$ (downward)

Surface Force

The surface force is the force distributed over a surface of the body, either internal or external. Usually it is defined by the force per unit area, \vec{f}_s . Then the force acting on a surface element dS is $\vec{f}_s dS$.

Stress

Consider a deformed elastic body in equilibrium (see Figure 1). Let dS be a surface element at P which divides the medium on the + side and the - side. A unit normal vector \vec{n} ($|\vec{n}|=1$) is taken from the - side to the + side. In equilibrium, the force, \vec{F}_+ , exerted by the + side on dS should be balanced by the force, \vec{F}_- exerted by the - side on dS , i.e., $\vec{F}_+ + \vec{F}_- = 0$.

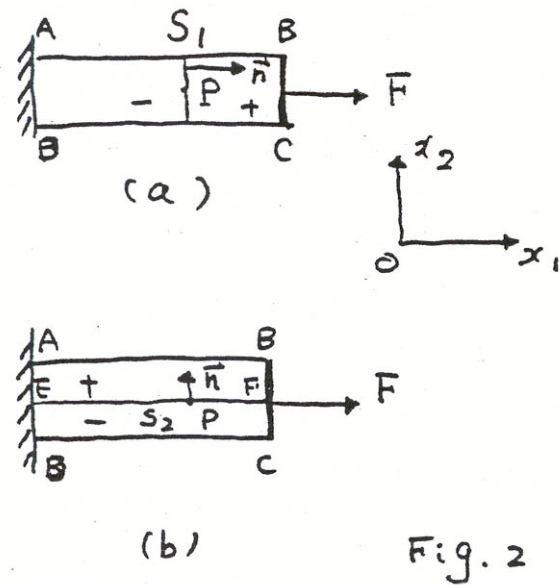
The stress at P acting on dS from the + side is then defined by

$$\vec{f}_n = \lim_{dS \rightarrow 0} \frac{\vec{F}_+}{dS}$$

\vec{f}_n is a vector (often called a stress vector, or traction) and its dimension is force/area.

We take a Cartesian coordinate system (x_1, x_2, x_3) and write $x_1, x_2,$ and x_3 components of \vec{f}_n by (f_{1n}, f_{2n}, f_{3n}) . Note that \vec{f}_n is a function of not only the location of P but also the orientation of \vec{n} . Hence, in order to specify the stress at P uniquely, we need two vectors \vec{n} and \vec{f}_n .

This situation can be understood more easily in the simple example shown in Figure 2.



Consider an elastic beam with one end, AB, clamped at the wall. Then, apply a force F uniformly on the surface S at the other end BC. Let us consider the stress at P. In (a), we consider the stress acting on S_1 that is perpendicular to the axis of the beam. In this case, it is obvious that

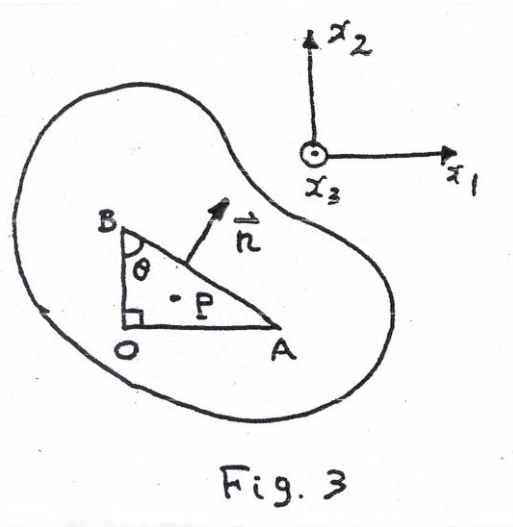
$$(f_{1n}, f_{2n}) = (F / S_1, 0)$$

In (b), we consider S_2 which is parallel to the axis. Suppose we cut the beam in two parts along S_2 . The beam will be still in equilibrium without change in shape. That is, there is no force acting on S_2 . Hence, in this case,

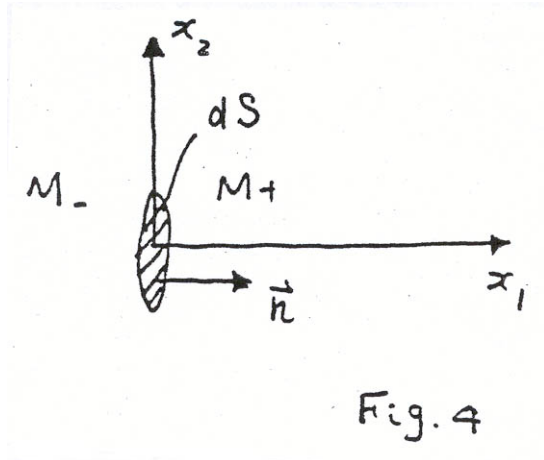
$$(f_{1n}, f_{2n}) = (0, 0)$$

Stress Tensor

For simplicity, we consider a 2-dimensional problem. The section shown in Figure 3 depicts a 2-D medium extending to infinity in x_3 direction (perpendicular to the face of the paper).



Consider a surface element dS_1 normal to the x_1 axis. We call the medium on the $+x_1$ side M+ and that on the $-x_1$ side, M- (Figure 4). Let σ_{11} and σ_{21} be the x_1 and x_2 components of the stress exerted by M+ on dS_1 . Then $-\sigma_{11}$ and $-\sigma_{21}$ are x_1 and x_2 components of stresses exerted by M-, respectively.



Note that the first subscript denotes the component, and the second, the direction of the normal to the surface. σ_{ij} 's with any i and j can be defined similarly.

Consider a triangular beam with an infinitesimally small cross section BOA . Referring to Figure 5, we define the following.

$$n_1: x_1 \text{ component of } \vec{n}, n_1 = \cos \theta$$

$$n_2: x_2 \text{ component of } \vec{n}, n_2 = \sin \theta$$

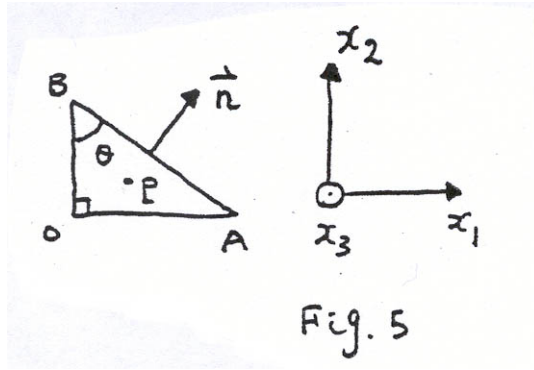
$$\sigma_{1n}: x_1 \text{ component of the stress acting on AB}$$

$$\sigma_{2n}: x_2 \text{ component of the stress acting on AB}$$

$$S: \text{AB} \times \text{unit length in } x_3 \text{ direction}$$

$$S_1: \text{OB} \times \text{unit length in } x_3 \text{ direction}$$

$$S_2: \text{OA} \times \text{unit length in } x_3 \text{ direction}$$



Then the forces acting on BOA are given as follows.

	x_1 component	x_2 component
force on S_1	$-\sigma_{11}S_1$	$-\sigma_{21}S_1$
force on S_2	$-\sigma_{12}S_2$	$-\sigma_{22}S_2$
force on S	$\sigma_{1n}S$	$\sigma_{2n}S$
Total	$-\sigma_{11}S_1 - \sigma_{12}S_2 + \sigma_{1n}S$	$-\sigma_{21}S_1 - \sigma_{22}S_2 + \sigma_{2n}S$

In equilibrium, the total force should vanish. Since $S_1 = S \cos \theta = Sn_1$, and $S_2 = S \sin \theta = Sn_2$, we obtain

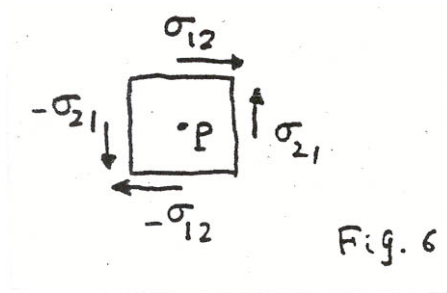
$$\begin{aligned}\sigma_{1n} &= \sigma_{11}n_1 + \sigma_{12}n_2 \\ \sigma_{2n} &= \sigma_{21}n_1 + \sigma_{22}n_2\end{aligned}\tag{1}$$

or, in matrix notation,

$$\begin{pmatrix} \sigma_{1n} \\ \sigma_{2n} \end{pmatrix} = \begin{pmatrix} \sigma_{11} & \sigma_{12} \\ \sigma_{21} & \sigma_{22} \end{pmatrix} \begin{pmatrix} n_1 \\ n_2 \end{pmatrix} \quad (2)$$

Consider an infinitesimally small square around P (Figure 6). In equilibrium, the total moment around P should vanish. This condition leads to

$$\sigma_{12} = \sigma_{21} \quad (3)$$



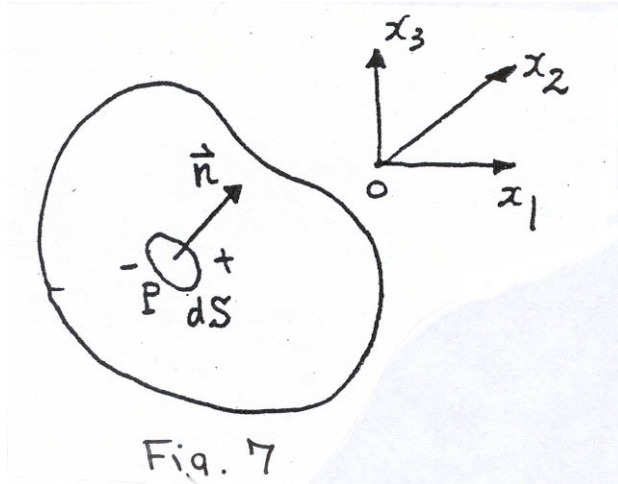
The above analysis can be extended easily to a 3-dimensional problem, and we can derive,

$$\begin{pmatrix} \sigma_{1n} \\ \sigma_{2n} \\ \sigma_{3n} \end{pmatrix} = \begin{pmatrix} \sigma_{11} & \sigma_{12} & \sigma_{13} \\ \sigma_{21} & \sigma_{22} & \sigma_{23} \\ \sigma_{31} & \sigma_{32} & \sigma_{33} \end{pmatrix} \begin{pmatrix} n_1 \\ n_2 \\ n_3 \end{pmatrix} \quad (4)$$

with the symmetry relations $\sigma_{ij} = \sigma_{ji}$. Here, σ_{in} ($i=1,2,3$) are the x_1 , x_2 , and x_3 components of the stress acting on dS (at P) whose unit normal is \vec{n} .

The matrix (σ_{ij}) above is called the stress tensor at P. (It can be shown that (σ_{ij}) is a tensor.) Because of the symmetry $\sigma_{ij} = \sigma_{ji}$, it has only 6 independent elements. Once we

know the stress tensor (σ_{ij}) at P, we can calculate, using (4), the stresses on any surface at P whose unit normal is \bar{n} (Figure 7).



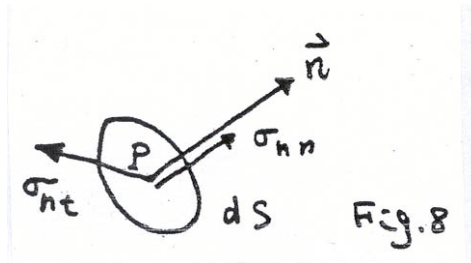
In the above equilibrium analysis, we ignored body forces compared with surface forces. This is justified because if we consider a small volume around P with a linear dimension da , then the total body force is proportional to da^3 while the total surface force is proportional to da^2 . Hence as $da \rightarrow 0$, the body forces can be ignored.

Normal, Shear, Principal Stresses

We resolve the stress acting on dS into two components, one parallel to \bar{n} , σ_{nn} , and the other perpendicular to \bar{n} , σ_{nt} (see Figure 8). σ_{nn} is called the normal stress, and σ_{nt} is the shear stress. In general, $\sigma_{nn} \neq 0$ and $\sigma_{nt} \neq 0$. However, at any point P, it is always possible to choose a Cartesian coordinate system (x'_1, x'_2, x'_3) for which $\sigma_{i'j'} = 0$ ($i' \neq j'$). In other words, for this new coordinate system ($\sigma_{i'j'}$) is a diagonal matrix. The non-zero diagonal components, $\sigma_{1'1'}$, $\sigma_{2'2'}$, and $\sigma_{3'3'}$ are called the principal

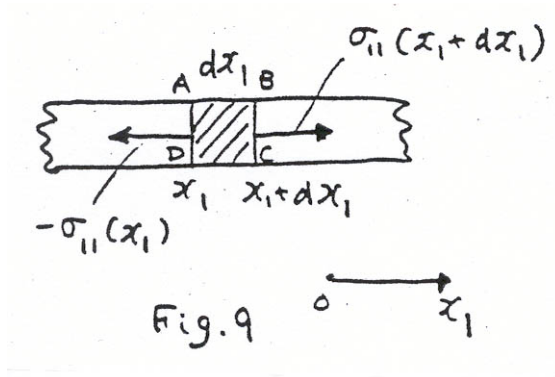
stresses, and x'_1 , x'_2 , and x'_3 axes, the principal axes. It can be shown that

$$\sigma_{1'1'} + \sigma_{2'2'} + \sigma_{3'3'} = \sigma_{11} + \sigma_{22} + \sigma_{33}.$$



Equations of Motion

First, consider a 1-dimensional problem illustrated in Figure 9. Figure 9 shows an elastic rod with cross section S .



The equation of motion for a small part of it, ABCD (length dx_1) is given by,

$$\rho S dx_1 \ddot{u}_1 = \rho f_1 S dx_1 + \sigma_{11}(x_1 + dx_1) S - \sigma_{11}(x_1) S$$

where ρ is the density, u_1 is the displacement, and f_1 is the body force. Expanding $\sigma_{11}(x_1 + dx_1)$ around x_1 , and retaining only the first order terms in dx_1 , we obtain,

$$\rho \ddot{u}_1 = \rho f_1 + \frac{\partial \sigma_{11}}{\partial x_1} \quad (5)$$

This is the equation of motion in 1-dimension.

A similar analysis can be made for a 3-dimensional geometry, and we obtain:

$$\rho \ddot{u}_i = \rho f_i + \sum_{j=1}^3 \frac{\partial \sigma_{ij}}{\partial x_j} \quad (i=1,2,3) \quad (6)$$

These are the equations of motion expressed in terms of the stress components.

Tensor Notation

In tensor notation, if any suffix occurs twice in a single term, it is to be put equal to 1, 2, and 3 in turn and the results are to be added. For example,

$$a_{ii} = a_{11} + a_{22} + a_{33} = \sum_{i=1}^3 a_{ii}$$

$$a_{1j} b_{j3} = a_{11} b_{13} + a_{12} b_{23} + a_{13} b_{33} = a_{1i} b_{i3}$$

$$a_{ip} b_{pj} = \sum_{k=1}^3 a_{ik} b_{kj}$$

Also, we use ∂_j to denote differentiation by x_j . For example,

$$\frac{\partial u_i}{\partial x_j} = u_{i,j}$$

Also note that,

$$u_{1,1} = \frac{\partial u_1}{\partial x_1} = \frac{\partial u_1}{\partial x_1} + \frac{\partial u_2}{\partial x_2} + \frac{\partial u_3}{\partial x_3} = u_{1,1} + u_{2,2} + u_{3,3}$$

We also use the Kronecker's delta

$$\delta_{ij} = \begin{cases} 1 & \text{if } i = j \\ 0 & \text{if } i \neq j \end{cases}$$

Note that $\delta_{ii} = 3$.

In the tensor notation, (6) can be written as

$$\rho \ddot{u}_i = \rho f_i + \sigma_{il,l} \quad (7)$$

Boundary Conditions

From the definition of the stress, it is evident that the normal and the tangential stresses should be continuous across any surface. In particular, at the free surface, there is no force acting on it; hence the normal and the shear stresses should vanish there. If the free surface is perpendicular to x_3 axis,

$$\sigma_{31} = \sigma_{32} = \sigma_{33} = 0$$

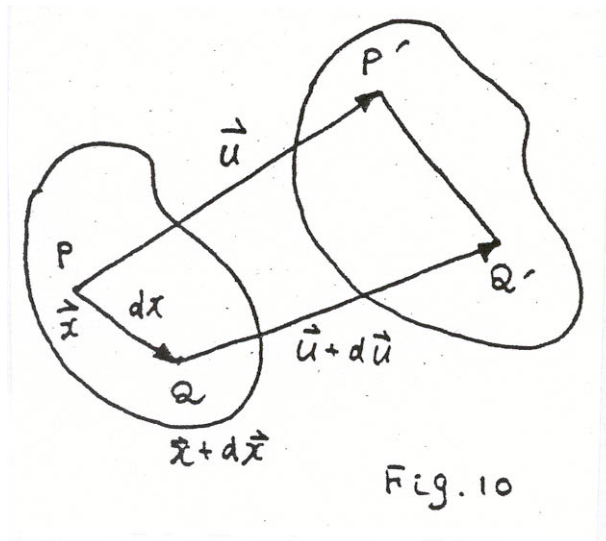
Within the interior of continuum, the displacement u_i should be continuous.

3.1.2 Strain

The displacement in continuum consists of three parts,

1. Translation (rigid body)
2. Rotation (rigid body)
3. Deformation

In the theory of elasticity, we are primarily concerned with “Deformation”.



Referring to Figure 10, let P and Q represent two points $d\vec{x}$ apart in an elastic medium, and \vec{u} and $\vec{u} + d\vec{u}$ be their displacements.

If $\vec{u} = \vec{u} + d\vec{u}$, i.e., $d\vec{u} = 0$, for any pair of points, \vec{u} simply represents

rigid body translation. Thus $d\bar{u}$ is considered to represent rotation and deformation. To the first order,

$$\begin{pmatrix} du_1 \\ du_2 \\ du_3 \end{pmatrix} = \begin{pmatrix} \frac{\partial u_1}{\partial x_1} & \frac{\partial u_1}{\partial x_2} & \frac{\partial u_1}{\partial x_3} \\ \frac{\partial u_2}{\partial x_1} & \frac{\partial u_2}{\partial x_2} & \frac{\partial u_2}{\partial x_3} \\ \frac{\partial u_3}{\partial x_1} & \frac{\partial u_3}{\partial x_2} & \frac{\partial u_3}{\partial x_3} \end{pmatrix} \begin{pmatrix} dx_1 \\ dx_2 \\ dx_3 \end{pmatrix} \quad (8)$$

Denoting the matrix $(u_{i,j})$ by U and $(u_{j,i})$ by U^T (transpose of U), we can write U as

$$U = \frac{1}{2}(U + U^T) + \frac{1}{2}(U - U^T) \quad (9)$$

We denote $\frac{1}{2}(U + U^T)$ by D and $\frac{1}{2}(U - U^T)$ by R . D is symmetric and R is anti-symmetric. We will show that D represents deformation, and R represents rigid-body rotation.

The elements of D , $\frac{1}{2}(u_{i,j} + u_{j,i}) = e_{ij}$ can be interpreted as follows.

If only $e_{11} \neq 0$,

$$\begin{pmatrix} du_1 \\ du_2 \\ du_3 \end{pmatrix} = \begin{pmatrix} e_{11} & 0 & 0 \\ 0 & 0 & 0 \\ 0 & 0 & 0 \end{pmatrix} \begin{pmatrix} dx_1 \\ dx_2 \\ dx_3 \end{pmatrix}$$

We then have, $du_1 = e_{11}dx_1$, $du_2 = 0$, and $du_3 = 0$. This means that the line element dx_1 in

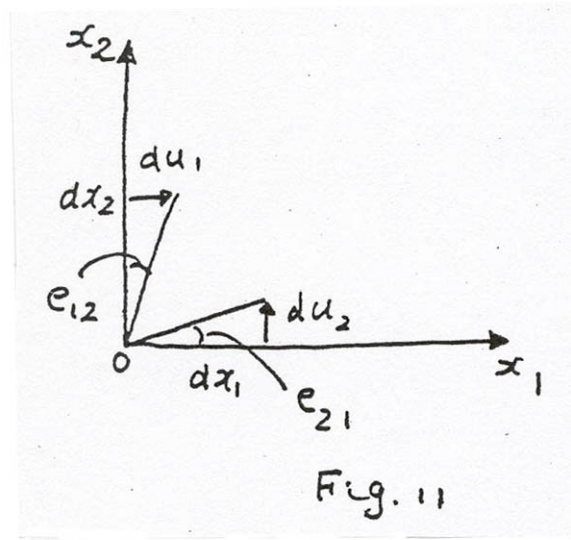
x_1 direction is stretched by $du_1 = e_{11}dx_1$ in x_1 direction. Hence, e_{11} represents extension (or contraction if $e_{11} < 0$) per unit length in x_1 direction. e_{22} and e_{33} can be interpreted similarly.

Next consider e_{12} , and $e_{21} (= e_{12})$.

$$\begin{pmatrix} du_1 \\ du_2 \\ du_3 \end{pmatrix} = \begin{pmatrix} 0 & e_{12} & 0 \\ e_{21} & 0 & 0 \\ 0 & 0 & 0 \end{pmatrix} \begin{pmatrix} dx_1 \\ dx_2 \\ dx_3 \end{pmatrix}$$

i.e., $du_1 = e_{12}dx_2$, $du_2 = e_{21}dx_1$, and $du_3 = 0$. As shown in Figure 11, the angle between x_1 and x_2 axes which is originally $\pi/2$ becomes $\theta = \pi/2 - 2e_{12}$ after the deformation.

Thus, e_{12} is equal to half the angle change between the x_1 axis and x_2 axis, and is called the shear strain. e_{13} and e_{23} can be interpreted similarly.



D is called the strain tensor (it can be shown that (e_{ij}) is a tensor).

e_{11} , e_{22} , and e_{33} represent extension or contraction, and e_{12} , e_{13} , and e_{23} represent shear.

We now show that R represents rigid body rotation. R can be written as

$$R = \begin{pmatrix} 0 & \frac{1}{2}(u_{1,2} - u_{2,1}) & \frac{1}{2}(u_{1,3} - u_{3,1}) \\ \frac{1}{2}(u_{2,1} - u_{1,2}) & 0 & \frac{1}{2}(u_{2,3} - u_{3,2}) \\ \frac{1}{2}(u_{3,1} - u_{1,3}) & \frac{1}{2}(u_{3,2} - u_{2,3}) & 0 \end{pmatrix}$$

Define ω_1 , ω_2 , and ω_3 by

$$\omega_1 = -r_{23} (= r_{32}) = -(1/2)(u_{2,3} - u_{3,2})$$

$$\omega_2 = -r_{31} (= r_{13}) = -(1/2)(u_{3,1} - u_{1,3})$$

$$\omega_3 = -r_{12} (= r_{21}) = -(1/2)(u_{1,2} - u_{2,1})$$

Then,

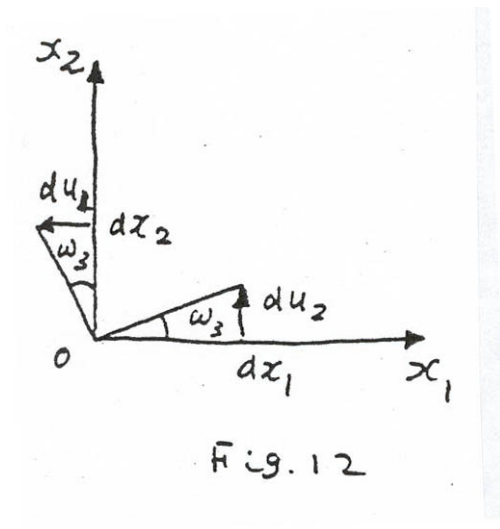
$$R = \begin{pmatrix} 0 & -\omega_3 & \omega_2 \\ \omega_3 & 0 & -\omega_1 \\ -\omega_2 & \omega_1 & 0 \end{pmatrix}$$

Consider the case where $\omega_1 = \omega_2 = 0$ and ω_3 is non-zero.

Then, we have

$$\begin{pmatrix} du_1 \\ du_2 \\ du_3 \end{pmatrix} = \begin{pmatrix} 0 & -\omega_3 & 0 \\ \omega_3 & 0 & 0 \\ 0 & 0 & 0 \end{pmatrix} \begin{pmatrix} dx_1 \\ dx_2 \\ dx_3 \end{pmatrix}$$

i.e., $du_1 = -\omega_3 dx_2$, $du_2 = \omega_3 dx_1$, and $du_3 = 0$. As shown in Figure 12, this displacement represents counter-clockwise rotation by ω_3 around the x_3 axis. ω_1 and ω_2 can be interpreted similarly. Thus R represents rigid body rotation.



3.1.3 Stress-Strain Relations and Elastic Constants

The relation between stress and strain is the extension of the Hooke's law for a spring. (i.e., $F = k\Delta l$ where F is the force, Δl is the length change and k is the spring constant.)

We assume that the material is isotropic and perfectly elastic. If the medium is

perfectly elastic, the stress should be expressed as a homogeneous linear function of strain. Since there are six independent stress components and strain components, in general there can be $6 \times 6 = 36$ constants. However, if the material is isotropic, we can show that there are only two independent constants.

Consider an elastic parallelepiped shown in Figure 13. Apply a normal stress σ_{11} in x_1 direction. The extension in x_1 direction is e_{11} (Figure 13). In the linear theory, e_{11} is proportional to σ_{11}

$$e_{11} = \frac{1}{E} \sigma_{11}$$

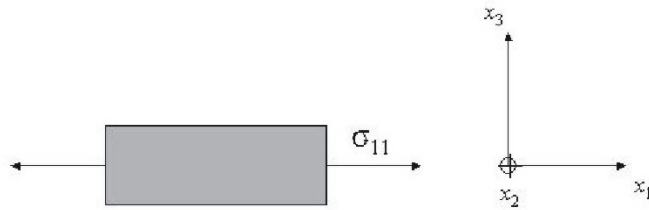


Fig. 13

The constant of proportionality is written as $\frac{1}{E}$, and is called the Young's modulus. Note that e_{11} is non-dimensional, so that E has the dimension of stress. Under this stress, there will be contraction in x_2 and x_3 directions that is proportional to e_{11} . Since the material is isotropic,

$$e_{22} = -\nu e_{11} = -\frac{\nu}{E} \sigma_{11} \quad \text{and} \quad e_{33} = -\nu e_{11} = -\frac{\nu}{E} \sigma_{11}$$

ν is called the Poisson's ratio.

If we apply σ_{11} , σ_{22} , and σ_{33} in x_1 , x_2 and x_3 directions simultaneously, then by superposition,

$$\begin{aligned}e_{11} &= \frac{\sigma_{11}}{E} - \frac{\nu}{E}(\sigma_{22} + \sigma_{33}) \\e_{22} &= \frac{\sigma_{22}}{E} - \frac{\nu}{E}(\sigma_{11} + \sigma_{33}) \\e_{33} &= \frac{\sigma_{33}}{E} - \frac{\nu}{E}(\sigma_{11} + \sigma_{22})\end{aligned}\tag{10}$$

Adding the three equations in (10) we obtain

$$\Delta = \frac{(1-2\nu)}{E}\Sigma\tag{11}$$

where

$$\Delta = e_{11} + e_{22} + e_{33}\tag{12}$$

and

$$\Sigma = \sigma_{11} + \sigma_{22} + \sigma_{33}$$

Consider deformation of a small parallelepiped. The initial volume is $V_0 = dx_1 dx_2 dx_3$ and the volume after deformation is

$$V = (1 + e_{11})dx_1(1 + e_{22})dx_2(1 + e_{33})dx_3$$

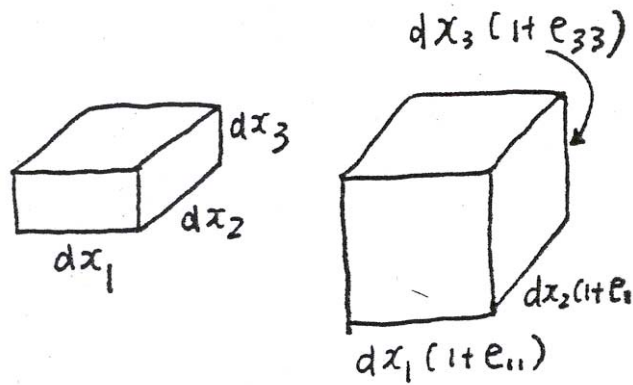


Fig. 14

Then, to the first order, the volume change is

$$dV = V - V_0 = V_0(e_{11} + e_{22} + e_{33})$$

Hence,

$$\Delta = dV / V_0$$

Thus, Δ represents relative change in the volume, and is called the volumetric strain or dilatation.

If $\sigma_{11} = \sigma_{22} = \sigma_{33} = \sigma$, then from (11), we obtain

$$\sigma = \frac{E}{3(1-2\nu)} \Delta = k\Delta$$

where

$$k = \frac{E}{3(1-2\nu)} \quad (13)$$

is called the bulk modulus or incompressibility.

Substituting (11) into (10), and solving for σ_{11} , σ_{22} , and σ_{33} , we obtain

$$\begin{aligned}\sigma_{11} &= \frac{\nu E}{(1-2\nu)(1+\nu)}\Delta + \frac{E}{(1+\nu)}e_{11} \\ \sigma_{22} &= \frac{\nu E}{(1-2\nu)(1+\nu)}\Delta + \frac{E}{(1+\nu)}e_{22} \\ \sigma_{33} &= \frac{\nu E}{(1-2\nu)(1+\nu)}\Delta + \frac{E}{(1+\nu)}e_{33}\end{aligned}$$

We introduce the Lamé's elastic constants λ and μ by

$$\lambda = \frac{\nu E}{(1-2\nu)(1+\nu)} \quad (14)$$

$$\mu = \frac{E}{2(1+\nu)} \quad (15)$$

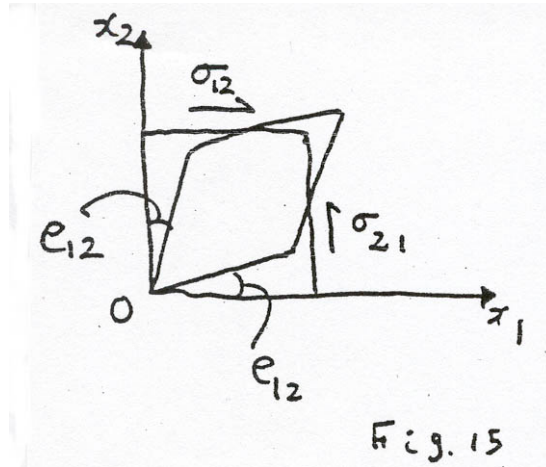
Then,

$$\begin{aligned}\sigma_{11} &= \lambda\Delta + 2\mu e_{11} \\ \sigma_{22} &= \lambda\Delta + 2\mu e_{22} \\ \sigma_{33} &= \lambda\Delta + 2\mu e_{33}\end{aligned} \quad (16)$$

Next, we consider shear stress and shear strain. From Figure 15, we see that the shear strain e_{12} is caused by the shear stress σ_{12} :

$$\sigma_{12} = 2Ge_{12}$$

where G is called the shear modulus.



Similarly,

$$\sigma_{13} = 2Ge_{13}$$

$$\sigma_{23} = 2Ge_{23}$$

It can be shown (homework problem) that G is equal to the Lamé constant μ . Hence,

$$\sigma_{12} = 2\mu e_{12}$$

$$\sigma_{13} = 2\mu e_{13}$$

$$\sigma_{23} = 2\mu e_{23}$$

(17)

Equations (16) and (17) give the stress-strain relations in isotropic media. (16) and (17) can be written collectively as

$$\sigma_{ij} = \lambda\Delta\delta_{ij} + 2\mu e_{ij}$$

(18)

Note that, although we have introduced five elastic constants E , ν , k , λ , and μ above, there are only two independent constants. If we choose E and ν as the basic constants then

$$k = \frac{E}{3(1-2\nu)}, \quad \lambda = \frac{\nu E}{(1+\nu)(1-2\nu)}, \quad \mu = \frac{E}{2(1+\nu)} \quad (19)$$

If we choose λ and μ as the basic constants, then

$$\nu = \frac{\lambda}{2(\lambda + \mu)}, \quad E = \frac{3\lambda + 2\mu}{\lambda + \mu} \mu, \quad k = \lambda + \frac{2}{3} \mu \quad (20)$$

Some Relations in Vector Analysis

In the theory of elasticity, the following definitions and relations are often used. Here, $\phi(x_1, x_2, x_3)$ is a scalar function and $\bar{u}(u_1, u_2, u_3)$ and $\bar{v}(v_1, v_2, v_3)$ are vectors. We assume that these functions are continuous and differentiable.

1) $\text{grad } \phi$ is a vector with the components

$$\left(\frac{\partial \phi}{\partial x_1}, \frac{\partial \phi}{\partial x_2}, \frac{\partial \phi}{\partial x_3} \right) \quad (21)$$

We often use an operator

$$\nabla \equiv \left(\frac{\partial}{\partial x_1}, \frac{\partial}{\partial x_2}, \frac{\partial}{\partial x_3} \right)$$

and write it as $\nabla\phi$.

2) $\operatorname{div} \bar{u}$ is a scalar defined by

$$\frac{\partial u_1}{\partial x_1} + \frac{\partial u_2}{\partial x_2} + \frac{\partial u_3}{\partial x_3} = u_{i,i} = \nabla \cdot \bar{u} \quad (22)$$

3) $\operatorname{curl} \bar{u}$ (rot \bar{u}) is a vector defined by

$$\left(\frac{\partial u_3}{\partial x_2} - \frac{\partial u_2}{\partial x_3}, \frac{\partial u_1}{\partial x_3} - \frac{\partial u_3}{\partial x_1}, \frac{\partial u_2}{\partial x_1} - \frac{\partial u_1}{\partial x_2} \right) = \nabla \times \bar{u} \quad (23)$$

4) Laplacian $\nabla^2\phi$ is a scalar defined by

$$\nabla^2\phi = \frac{\partial^2\phi}{\partial x_1^2} + \frac{\partial^2\phi}{\partial x_2^2} + \frac{\partial^2\phi}{\partial x_3^2} = \phi_{,ii} \quad (24)$$

5) Vector Laplacian $\nabla^2\bar{u}$ is a vector defined by

$$(\nabla^2 u_1, \nabla^2 u_2, \nabla^2 u_3) = (u_{1,ii}, u_{2,ii}, u_{3,ii}) \quad (25)$$

We use this only in the Cartesian coordinate.

6) $\nabla^2\bar{u} = \operatorname{grad} \operatorname{div} \bar{u} - \operatorname{curl} \operatorname{curl} \bar{u} = \nabla \nabla \cdot \bar{u} - \nabla \times \nabla \times \bar{u}$ (26)

For a non-Cartesian coordinate system, this should be considered as the definition of $\nabla^2\bar{u}$.

7) $\operatorname{curl} \operatorname{grad} \phi \equiv 0$

8) $\operatorname{div} \operatorname{curl} \bar{u} \equiv 0$

- 9) If $\text{curl}\bar{u} = 0$, \bar{u} is called an irrotational vector, and can be written as $\bar{u} = \text{grad}\phi$. ϕ is the scalar potential.
- 10) If $\text{div}\bar{u} = 0$, then \bar{u} is called a solenoidal vector, and can be written as $\bar{u} = \text{curl}\bar{v}$. \bar{v} is the vector potential.
- 11) Any vector field \bar{u} can be decomposed into an irrotational field \bar{u}^I and a solenoidal field \bar{u}^II , i.e.

$$\bar{u} = \bar{u}^I + \bar{u}^II$$

where $\text{curl}\bar{u}^I = 0$ and $\text{div}\bar{u}^II = 0$. Using 9) and 10) \bar{u} can be written as

$$\bar{u} = \text{grad}\phi + \text{curl}\bar{v} \quad (27)$$

Relations 6), 7), and 8) can be easily verified. Proof of 9), 10) and 11) requires some knowledge of Potential Theory.

3.1.4 Equation of Motion Expressed in Terms of Displacement

From (18) and the expression for e_{ij} , we obtain

$$\begin{aligned} \sigma_{ij,j} &= \lambda\Delta_{,j}\delta_{ij} + \mu(u_{i,jj} + u_{j,ij}) \\ &= \lambda\Delta_{,i} + \mu(\nabla^2 u_i + \Delta_{,i}) = (\lambda + \mu)\Delta_{,i} + \mu\nabla^2 u_i \end{aligned}$$

where we assume that the medium is homogeneous, i.e., λ and μ are constants.

Substituting this into (7), we obtain

$$\rho\ddot{u}_i = \rho f_i + (\lambda + \mu)\Delta_{,i} + \mu\nabla^2 u_i$$

or in a vector form,

$$\rho \ddot{\bar{u}} = \rho \bar{f} + (\lambda + \mu) \text{grad div } \bar{u} + \mu \nabla^2 \bar{u} \quad (28)$$

Using (26), this can be rewritten as,

$$\rho \ddot{\bar{u}} = \rho \bar{f} + (\lambda + 2\mu) \text{grad div } \bar{u} - \mu \text{curl curl } \bar{u} \quad (29)$$

or

$$\rho \ddot{\bar{u}} = \rho \bar{f} + (\lambda + 2\mu) \nabla^2 \bar{u} + (\lambda + \mu) \text{curl curl } \bar{u} \quad (30)$$

Equations (28), (29) and (30) are among the most fundamental equations in seismology.

If we decompose \bar{u} into irrotational field \bar{u}^I ($\text{curl } \bar{u}^I = 0$) and solenoidal field \bar{u}^H ($\text{div } \bar{u}^H = 0$), we obtain for \bar{u}^I , using (30)

$$\rho \ddot{\bar{u}}^I = \rho \bar{f} + (\lambda + 2\mu) \nabla^2 \bar{u}^I \quad (31)$$

For \bar{u}^H , we obtain, using (28)

$$\rho \ddot{\bar{u}}^H = \rho \bar{f} + \mu \nabla^2 \bar{u}^H \quad (32)$$

(31) and (32) are the wave equations for the irrotational field and the solenoidal field, respectively.

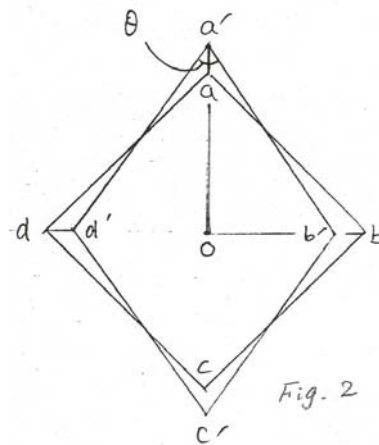
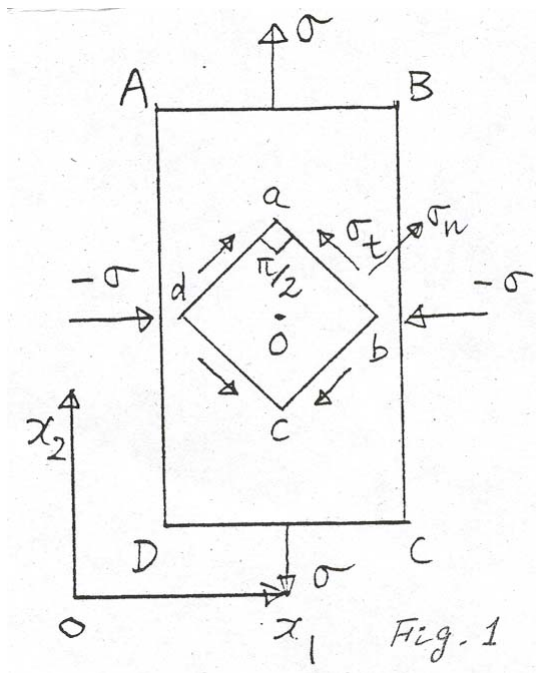
Ge 162 Problem #3

1. Show that the Lamé's elastic constant $\mu = E/2(1+\nu)$ (E : Young's modulus, ν : Poisson's ratio) is actually equal to the shear modulus G defined by

$$\sigma_{ij} = 2Ge_{ij} \quad (i \neq j)$$

Follow the steps described below for a 2-dimensional problem.

1) Consider a rectangular parallelepiped ABCD shown in Figure 1, and apply a normal stress $-\sigma$ uniformly on BC and AD, and $+\sigma$ on AB and DC.



Consider equilibrium of a beam with the square cross section abcd in the parallelepiped. The square abcd is now deformed into a parallelogram a'b'c'd' as shown in Figure 2.

Show that

$$\frac{ob'}{ob} = 1 - \frac{(1 + \nu)}{E} \sigma \quad (1)$$

$$\frac{oa'}{oa} = 1 + \frac{(1 + \nu)}{E} \sigma \quad (2)$$

2) Now consider equilibrium of a triangular beam with the cross section aob. The normal stress is $-\sigma$ on oa and σ on ob.

Show that

$$\sigma_t = \sigma, \text{ and } \sigma_n = 0,$$

where σ_t and σ_n are the shear and normal stresses on ab, respectively (see Figure 1).

3) Referring to the square abcd, this deformation can be viewed as shear deformation due to the shear stress σ_t .

Show that the corresponding shear strain e_t is given by

$$e_t = (\pi/4) - (1/2)\angle d' d b' \quad (\angle d' d b' \text{ is } \theta \text{ in Figure 2}) \quad (3)$$

4) From (1), (2) and (3),

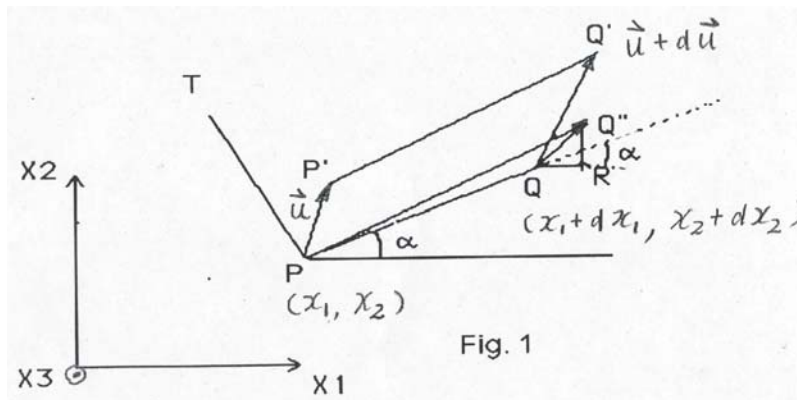
$$\tan((\pi/4) - e_t) = \frac{ob'}{oa'} = \frac{E - (1 + \nu)\sigma}{E + (1 + \nu)\sigma} \quad (4)$$

Assuming that e_t is small (i.e. you can put $\sin e_t = e_t$, $\cos e_t = 1$), obtain the expression for G by relating e_t to σ_t .

Ge 162, Problem #2

Strain at a Point, Principal Strain

Consider a 2-D problem shown in Fig. 1.



A line element PQ becomes $P'Q'$ after deformation. The strain components for this deformation are given by e_{11} , e_{22} , and e_{12} .

Determine the unit elongation in the direction of PQ and the shear strain for the directions of PQ and PT (PT is perpendicular to PQ). Follow the steps given below.

Let the displacement of P and Q be $\vec{u}(\vec{x})$ and $\vec{u} + d\vec{u}$, respectively. Observe that vector QQ' represents $d\vec{u}(du_1, du_2)$, where du_1 and du_2 are the x_1 and x_2 components of $d\vec{u}$, and are given by QR and RQ' in the figure, respectively.

1. Referring to the geometry shown in Fig. 1, show that the difference in the length between PQ" and PQ (elongation in PQ direction) is given by:

$$dl = du_1 \cos \alpha + du_2 \sin \alpha$$

Then dividing this by PQ, show that the unit elongation in the direction of PQ is given by:

$$e_\alpha = e_{11} \cos^2 \alpha + e_{22} \sin^2 \alpha + 2e_{12} \sin \alpha \cos \alpha$$

(Use the relations like $du_1 = \frac{\partial u_1}{\partial x_1} dx_1 + \frac{\partial u_1}{\partial x_2} dx_2$ and $\frac{dx_1}{PQ} = \cos \alpha$ etc.)

2. Referring to the geometry shown in Fig. 1, show that the angle through which PQ is rotated is given by:

$$\frac{du_2 \cos \alpha - du_1 \sin \alpha}{PQ} = \frac{\partial u_2}{\partial x_1} \cos^2 \alpha + (e_{22} - e_{11}) \cos \alpha \sin \alpha - \frac{\partial u_1}{\partial x_2} \sin^2 \alpha$$

3. The line segment PT makes an angle $\alpha + \pi/2$ with the x_1 axis. Using the result obtained above, show that the rotation of PT is given by:

$$\frac{\partial u_2}{\partial x_1} \sin^2 \alpha - (e_{22} - e_{11}) \cos \alpha \sin \alpha - \frac{\partial u_1}{\partial x_2} \cos^2 \alpha$$

4. Using the results of 2 and 3, show that the shear strain for the directions of PQ and PT (i.e. 1/2 of the change in angle between PQ and PT) is given by:

$$e_s = e_{12}(\cos^2 \alpha - \sin^2 \alpha) + (e_{22} - e_{11}) \sin \alpha \cos \alpha$$

From this result we see that there are two values of α , differing by $\pi/2$, for which shear strain vanishes. They are given by:

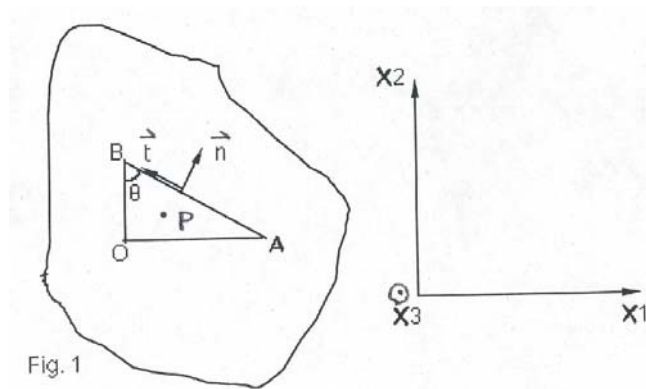
$$\tan 2\alpha = \frac{2e_{12}}{e_{11} - e_{22}}$$

The corresponding strains e_α are called the principal strains.

Ge 162 Problem #1

Stress at a point, principal axes and stresses

Consider a 2-D problem shown in Fig. 1.



Consider a (infinitesimally) small prism BOA at P with the three sides parallel to the x_3 axis. Let \bar{n} and \bar{t} be the unit vectors normal and parallel to BA respectively (the directions are shown in the figure.). In class, we showed that the x_1 and x_2 components of stress acting on plane BA are given by,

$$\begin{pmatrix} \sigma_{1n} \\ \sigma_{2n} \end{pmatrix} = \begin{pmatrix} \sigma_{11} & \sigma_{12} \\ \sigma_{21} & \sigma_{22} \end{pmatrix} \begin{pmatrix} n_1 \\ n_2 \end{pmatrix}$$

1. Show that the normal stress and shear stress on the plane BA are given by,

$$\sigma_{nn} = \sigma_{11} \cos^2 \theta + \sigma_{22} \sin^2 \theta + 2\sigma_{12} \cos \theta \sin \theta \tag{1}$$

$$\sigma_m = \sigma_{12}(\cos^2 \theta - \sin^2 \theta) + (\sigma_{22} - \sigma_{11}) \cos \theta \sin \theta$$

Show that if the angle θ is chosen such that

$$\tan 2\theta = \frac{2\sigma_{12}}{\sigma_{11} - \sigma_{22}}$$

the shear stress vanishes.

The directions of \bar{n} and \bar{t} for this θ are called the principal directions. If we take x'_1 and x'_2 axes in \bar{n} and \bar{t} directions, they are the principal axes. The normal stresses on the plane normal to x'_1 and x'_2 axes are the principal stresses.

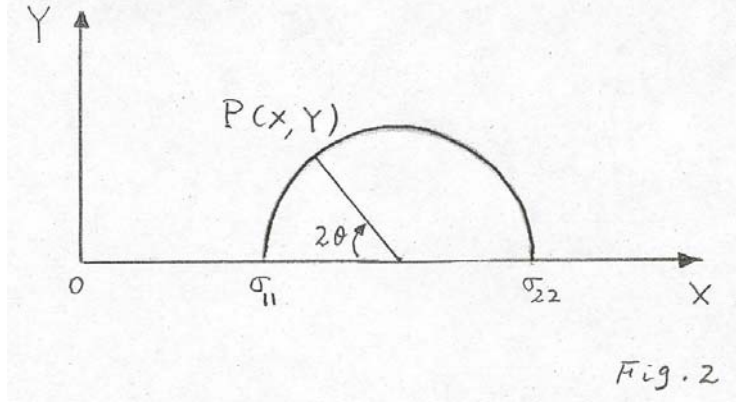
If x_1 and x_2 axes were the principal axes, (1) becomes

$$\sigma_m = \sigma_{11} \cos^2 \theta + \sigma_{22} \sin^2 \theta$$

$$\sigma_m = (\sigma_{22} - \sigma_{11}) \cos \theta \sin \theta$$

2. Refer to Fig. 2.

Show that the X and Y coordinates of point P is given by σ_m and σ_m , respectively. The circle shown in Fig. 2 is called Mohr's circle which is used for graphical representation of the normal stress and shear stress on plane AB. Note that x_1 and x_2 axes are the principal axes.



3.2 Wave Equation and Seismic Waves

Wave Equations

Following (31) and (32) of 3.1.4, and ignoring the body force, we obtain for the irrotational field \bar{u}^I ($\text{curl}\bar{u}^I = 0$),

$$\ddot{\bar{u}}^I = \alpha^2 \nabla^2 \bar{u}^I \quad (1)$$

where

$$\alpha = \sqrt{\frac{\lambda + 2\mu}{\rho}} \quad (2)$$

For the solenoidal field \bar{u}^{II} ($\text{div}\bar{u}^{II} = 0$),

$$\ddot{\bar{u}}^{II} = \beta^2 \nabla^2 \bar{u}^{II} \quad (3)$$

where

$$\beta = \sqrt{\frac{\mu}{\rho}} \quad (4)$$

Equations (1) and (3) are three-dimensional wave equations which are of fundamental importance in seismology.

3.3 Seismic *P* Wave (Compressional Wave) and *S* Wave (Shear Wave)

We first examine the property of \bar{u}^I . Here we use a coordinate system (x, y, z) instead of (x_1, x_2, x_3) , and denote the x , y , and z components of displacement by u , v , and w , respectively.

Let us consider a plane elastic wave propagating in the x direction, that is, a wave in which \bar{u}^I is a function of x and t . Since all derivatives with respect to y and z are zero, we have from $\text{curl} \bar{u}^I = 0$,

$$\frac{\partial w}{\partial x} = 0, \quad \text{and} \quad \frac{\partial v}{\partial x} = 0$$

which give $v = w = 0$. (Actually v and w are constant, but constant displacement is not important in wave propagation problems and they are set equal to 0.) Therefore, only non-zero displacement component is u . This means, \bar{u}^I represents a wave in which the particle motion is in the direction of propagation. The propagation velocity is, from (2),

$$\alpha = \sqrt{\frac{\lambda + 2\mu}{\rho}}$$

Because of this particle motion, this wave is also called longitudinal wave (Fig.1).

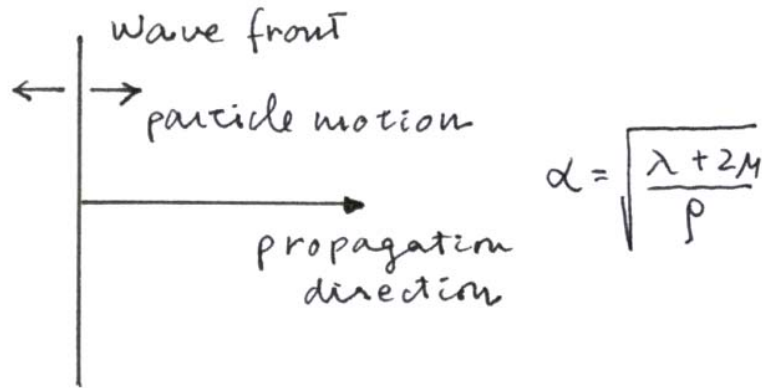


Fig. 1

Similarly, for \bar{u}'' , we have from $\text{div}\bar{u}'' = 0$,

$$\frac{\partial u}{\partial x} = 0$$

which gives $u = 0$. Then the non-zero components are v and w . This means, \bar{u}'' represents a wave in which the particle motion is confined on the plane perpendicular to the propagation direction; the propagation velocity is, from (4),

$$\beta = \sqrt{\frac{\mu}{\rho}}$$

Because of this particle motion, this wave is called a shear wave (Fig. 2). Since $\text{div} \bar{u}'' = 0$, it does not involve volume change.

In seismology, the longitudinal wave is often called P wave, and the shear wave is called S wave.

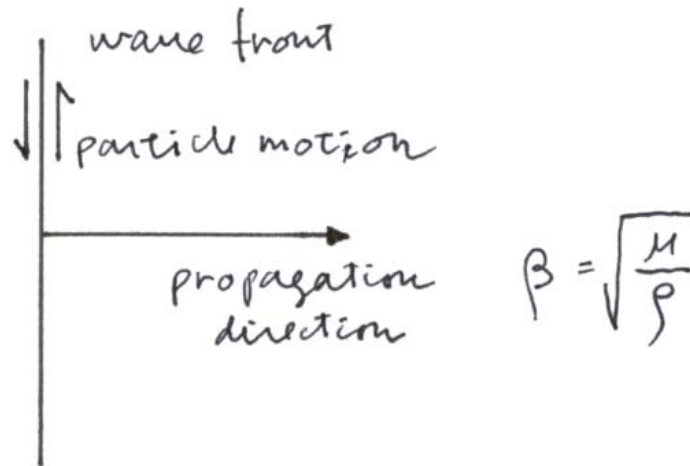


Fig. 2

3.4 Ray Theory

In the above, we assumed that the medium is homogeneous (in addition to being isotropic). That is the elastic constants λ and μ do not vary spatially. The equations (28), (29), and (30) in 3.1.4 were all derived with this assumption.

Once we obtain a 1-D wave equation in the form,

$$\ddot{u}(x,t) = c^2 u''(x,t) \quad (5)$$

we can obtain the solution,

$$u(x,t) = f(x-ct) + g(x+ct) \quad (6)$$

where $f(\xi)$ and $g(\xi)$ are twice differentiable arbitrary functions of ξ . f and g represent a plane wave propagating in positive and negative x directions, respectively, with velocity c . For a wave propagating in the positive x direction, we can consider a wave front $x=ct+\text{constant}$. The line perpendicular to the wave front determines the path along which the wave front propagates. This line (or curve, in general) is called a ray. Thus, in case of a homogeneous medium, we can use rays to describe wave propagation completely (ray theory). Ray theory is more intuitive than wave theory, and has been used very extensively in seismology.

However, in the real medium, λ and μ are usually a function of x , y , and z . The equation of motion is consequently far more complex than (28), (29), or (30) in 3.1.4, and we cannot obtain simple wave equations; consequently we cannot use the ray theory (rays cannot be defined rigorously). Fortunately, however, if the medium is only weakly heterogeneous, we can define a “ray” approximately, and use the ray theory. This is a common practice in seismology. The question is “what is considered weakly heterogeneous?” This problem can be discussed in detail in the Appendix to this section. Here we only discuss this condition qualitatively.

Suppose that the wave velocity $c(x)$ is a function of position x . Then the change in velocity c over a wave length λ is given by

$$\Delta c = \lambda c'$$

If this is much smaller than c itself, we can consider that the medium is “weakly heterogeneous”. The condition then can be stated as

$$\Delta c / c = \lambda c' / c = 2\pi c' / \omega \ll 1$$

Ignoring 2π , we can say that if

$$\omega \gg c' \quad (7)$$

then we can use the ray theory to discuss wave propagation problem in a heterogeneous medium. In this sense, the ray theory represents a high-frequency approximation.

As shown in the Appendix, a harmonic wave in a 1-D homogeneous medium is given by,

$$u(x, t) = \exp[i\omega(t - x/c)] \quad (8)$$

while in a 1-D weakly heterogeneous medium, it is given by

$$u(x, t) \propto \sqrt{\frac{1}{\rho c}} \exp\left[i\omega\left(t - \int \frac{dx}{c(x)}\right)\right] \quad (9)$$

Equation (9) shows that the wavefront propagates at the local velocity $c(x)$, and the amplitude varies as $\sqrt{1/\rho c}$.

A similar relation can be obtained for a 3-D medium. The most important result here is that a “wavefront” can be defined and it propagates at the local velocity, which leads to the well-known “Snell’s Law” (see the Appendix, for more details).

If a ray is incident from a medium with velocity c_1 into a medium with velocity c_2 , then the incidence angle i_1 and the angle of emergence i_2 are related by (Figure 3),

$$\frac{\sin i_1}{c_1} = \frac{\sin i_2}{c_2} \quad (10)$$

In general, if the velocity varies vertically as $c(z)$, then, for a given ray on a vertical plane, we have (Figure 3)

$$\frac{\sin i(z)}{c(z)} = p = \text{const.}$$

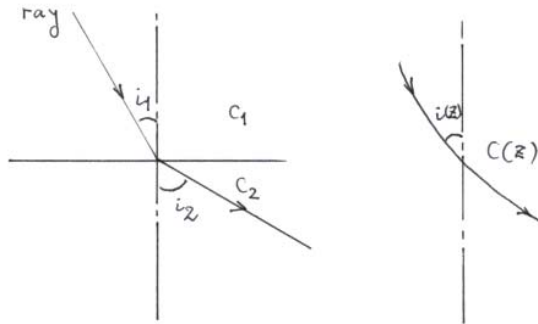


Fig. 3

Ge 162 Appendix to 3.4

Wave Propagation in a Slightly Heterogeneous Medium - Solution with the WKBJ Method-

1. One-Dimensional Case

The equation of motion

$$\rho \frac{\partial^2 u}{\partial t^2} = \frac{\partial}{\partial x} \left(E \frac{\partial u}{\partial x} \right)$$

does not reduce to the simple wave equation because $\frac{\partial E}{\partial x} \neq 0$ in general. We obtain

$$\rho \frac{\partial^2 u}{\partial t^2} = E \frac{\partial^2 u}{\partial x^2} + \frac{\partial E}{\partial x} \frac{\partial u}{\partial x}$$

Introducing a new variable v by

$$u = E^{-1/2} v$$

and ignoring the term containing E'' , we obtain

$$\rho \frac{\partial^2 v}{\partial t^2} = E \frac{\partial^2 v}{\partial x^2} + \frac{1}{4} \frac{E'^2}{E} v$$

We consider a harmonic wave

$$v(x, t) = V(x) e^{i\omega t}$$

Then, we have

$$\frac{d^2 V}{dx^2} + \left[k^2 + \frac{1}{4} \left(\frac{E'}{E} \right)^2 \right] V = 0$$

where

$$k = \frac{\omega}{c} \quad \text{and} \quad c = \sqrt{\frac{E}{\rho}}$$

If

$$\left(\frac{E'}{E}\right)^2 \ll k^2, \text{ or } \omega \gg c'$$

Then

$$\frac{d^2V}{dx^2} + k^2V = 0 \quad (\text{A-1})$$

Note that if $k = k_0 = \text{const}$, then the solution is

$$V = e^{\pm ik_0x} = e^{\pm i \int k_0 dx}$$

If k is a slowly varying function of x , we can solve this equation with the WKBJ method.

We seek a solution in the form

$$V = \exp\left(\pm i \int \kappa dx\right)$$

Substituting this into (1), we find that κ must satisfy the equation

$$-\kappa^2 \pm i\kappa' + k^2 = 0 \quad (\text{A-2})$$

1-st Approximation

Since

$$|\kappa'^2| \ll \kappa^2$$

we obtain for the first approximation of κ by

$$\kappa^{(1)2} = k^2 \quad \text{or} \quad \kappa^{(1)} = k$$

2nd Approximation

The 2nd approximation can be obtained by using $\kappa^{(1)}$ for the second term of (A-2). Then, the 2nd approximation

$$\kappa^{(2)} = \left(k^2 \pm i\kappa^{(1)'} \right)^{1/2} = \left(k^2 \pm ik' \right)^{1/2} = k \left(1 \pm i \frac{k'}{k^2} \right)^{1/2} \quad (\text{A-3})$$

If, $\omega \gg c'$, then $\frac{k'}{k^2} \ll 1$, and

$$\kappa^{(2)} = k \pm \frac{i k'}{2 k}$$

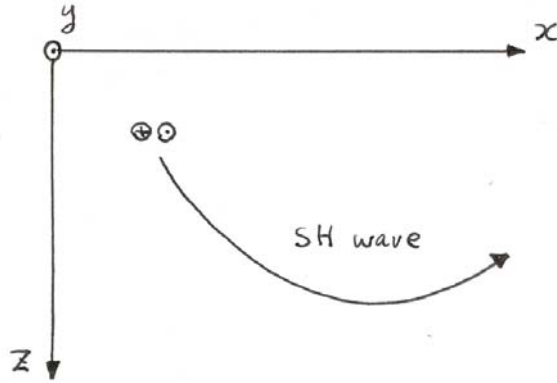
$$\therefore V(x) = \exp \left[\pm i \int \left(k \pm \frac{i k'}{2 k} \right) dx \right] = \frac{1}{\sqrt{k}} \exp \left(\pm i \int k dx \right)$$

$$\therefore u(x,t) = \frac{1}{\sqrt{E}} V \exp(i\omega t) = \sqrt{\frac{1}{\rho\omega c}} \exp \left[\pm i\omega \left(t \pm \int \frac{dx}{c} \right) \right] \quad (\text{A-4})$$

This is the WKBJ solution. This solution is valid under the condition $\omega \gg c'$.

2. Vertically Heterogeneous Medium

We consider a SH wave, i.e., the displacement vector is given by $(0, v(x, z), 0)$.



Then the equation of motion is given by

$$\rho \frac{\partial^2 v}{\partial t^2} = \mu \left(\frac{\partial^2 v}{\partial x^2} + \frac{\partial^2 v}{\partial z^2} \right) + \mu' \frac{\partial v}{\partial z}$$

As is in the 1-D case, we put

$$v(x,t) = \mu^{-1/2} e^{ikx} V(z) e^{i\omega t}$$

Then, we obtain

$$\frac{d^2 V}{dz^2} + \left[k_\beta^2(z) - k^2 + \frac{1}{4} \left(\frac{\mu'}{\mu} \right)^2 \right] V = 0$$

where

$$k_\beta = \frac{\omega}{\beta} \quad \text{and} \quad \beta = \sqrt{\frac{\mu}{\rho}}$$

We introduce $\chi(z)$ by

$$\chi^2(z) = k_\beta^2(z) - k^2$$

If,

$$\chi^2(z) \gg \frac{1}{4} \left(\frac{\mu'}{\mu} \right)^2 \quad (\text{A-5})$$

then,

$$\frac{d^2V}{dz^2} + \chi^2(z)V = 0 \quad (\text{A-6})$$

For (A-5) to be satisfied, at least $\omega \gg \beta'$ must be satisfied. If $k_\beta^2(z) - k^2 = 0$, then this condition is never satisfied.

Then the solution of (A-6) is

$$V(z) = \frac{1}{\sqrt{\chi}} \exp\left(\pm i \int \chi(z) dz\right)$$

Then,

$$v(x, z, t) = \frac{1}{\sqrt{\mu}} \frac{1}{(k_\beta^2 - k^2)^{1/4}} \exp\left[i\left(\omega t + kx \pm \int \sqrt{k_\beta^2 - k^2} dz\right)\right]$$

The wave front (i.e., plane of constant phase) is defined by

$$kx \pm \int \sqrt{k_\beta^2 - k^2} dz = \text{const}$$

\therefore

$$\frac{dz}{dx} = \pm \frac{k}{\sqrt{k_\beta^2 - k^2}}$$

at $z = z_0$

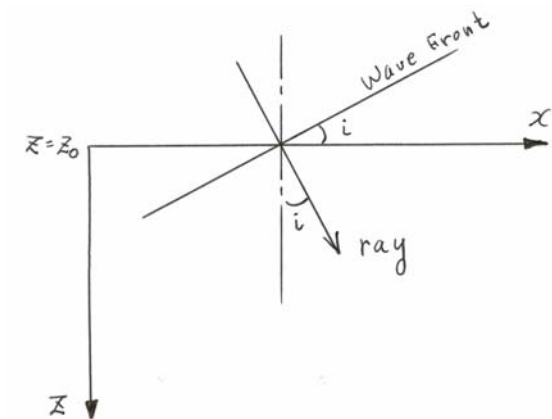
$$\frac{k}{\sqrt{k_\beta^2 - k^2}} = \text{const}$$

$$\sin i = \frac{dz}{\sqrt{d^2x + d^2z}} = \frac{1}{\sqrt{1 + \frac{k_\beta^2 - k^2}{k^2}}} = \frac{k}{k_\beta} = \frac{\beta}{\omega} k$$

\therefore

$$\frac{\sin i(z)}{\beta(z)} = \text{const for a given ray.}$$

However, if $k_\beta = k$ or $i = \pi/2$, which occurs at the turning point of a ray, the condition (A-5) cannot be satisfied and the WKBJ method breaks down.



Ge 162 Problem #4

Reflection and Transmission of SH wave at a Plane Boundary

An incident SH wave S1, reflected SH wave Sr and refracted (transmitted) SH wave S2 can be written as follows. (The displacement has only z component, w.)

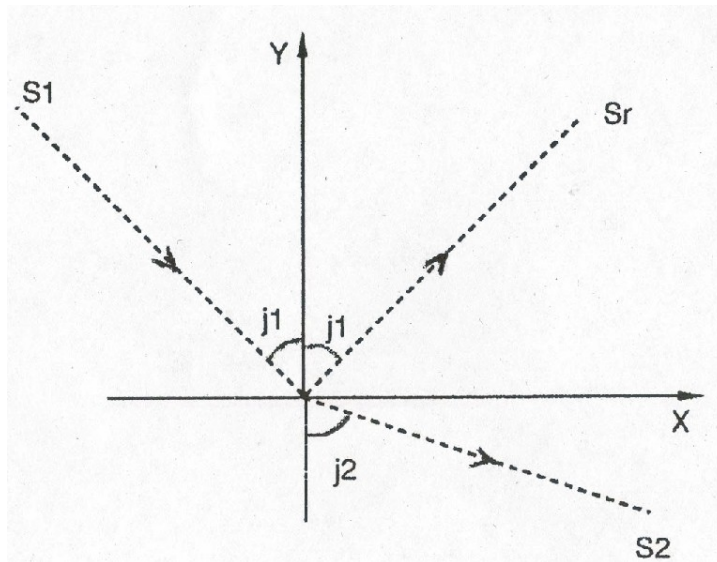
$$w_1 = \exp \left[i\omega \left(\frac{\sin j_1}{\beta_1} x - \frac{\cos j_1}{\beta_1} y - t \right) \right] \quad (1)$$

$$w_r = R \exp \left[i\omega \left(\frac{\sin j_1}{\beta_1} x + \frac{\cos j_1}{\beta_1} y - t \right) \right] \quad (2)$$

$$w_2 = T \exp \left[i\omega \left(\frac{\sin j_2}{\beta_2} x - \frac{\cos j_2}{\beta_2} y - t \right) \right] \quad (3)$$

where

$$\frac{\sin j_1}{\beta_1} = \frac{\sin j_2}{\beta_2} = \frac{1}{c}$$



Here, the amplitude of the incident wave is assumed to be 1. R and T are reflection and transmission coefficients respectively. c is the phase velocity along the boundary. (The above relations are solutions of the wave equation in each layer.)

Using c , the above equations can be written as,

$$w_1 = \exp \left[i\omega \left(\frac{x}{c} - \frac{\cos j_1}{\beta_1} y - t \right) \right] \quad (4)$$

$$w_r = R \exp \left[i\omega \left(\frac{x}{c} + \frac{\cos j_1}{\beta_1} y - t \right) \right] \quad (5)$$

$$w_2 = T \exp \left[i\omega \left(\frac{x}{c} - \frac{\cos j_2}{\beta_2} y - t \right) \right] \quad (6)$$

Two boundary conditions must be satisfied at the boundary: one for displacement and the other for stress (traction).

Show that these conditions are given by

$$1 + R = T$$

$$-\frac{\mu_1}{\beta_1} \cos j_1 + \frac{\mu_1}{\beta_1} \cos j_1 R = -\frac{\mu_2}{\beta_2} \cos j_2 T$$

where μ_1 and μ_2 are the rigidity.

Solving these equations, show that

$$R = \frac{-\mu_2\beta_1 \cos j_2 + \mu_1\beta_2 \cos j_1}{\mu_1\beta_2 \cos j_1 + \mu_2\beta_1 \cos j_2} \quad (7)$$

$$T = \frac{2\mu_1\beta_2 \cos j_1}{\mu_1\beta_2 \cos j_1 + \mu_2\beta_1 \cos j_2} \quad (8)$$

Determine the reflection and transmission coefficients for normal incidence (e.g., $j_1=0$).

$$R = \frac{-\mu_2\beta_1 + \mu_1\beta_2}{\mu_1\beta_2 + \mu_2\beta_1} \quad (9)$$

$$T = \frac{2\mu_1\beta_2}{\mu_1\beta_2 + \mu_2\beta_1} \quad (10)$$

If $\beta_2 > \beta_1$, $\sin j_2$ exceeds 1 for j_1 larger than the critical angle. In this case,

$$\cos j_2 = (1 - \sin^2 j_2)^{1/2}$$

becomes purely imaginary, i.e., $\cos j_2 = ib$ (b is real).

Referring to (6), briefly describe the behavior of the "transmitted" wave S2 for this case.

Also, the reflection coefficient R becomes complex. Determine the amplitude and phase (with respect to the incident wave) of the reflected wave.

3.5 Reflection and Refraction (LW, pp. 96-104)

When the elastic constant, say velocity, changes discontinuously in the medium, the condition (7) cannot be satisfied for any wavelength, because $|c'|$ becomes infinity there. Thus, in this case the ray theory cannot be used, and the wave equation must be solved with the appropriate boundary conditions (continuity of

displacements and traction) on the discontinuity surfaces. The problem, in general, becomes very complicated, and complex reflection, refraction and energy coupling between P and S waves take place. The simplest case in which a homogeneous medium is bounded at a plane boundary by another homogeneous medium having different elastic property (Fig. 4) has been studied by many investigators.

First let us consider a plane S wave incident at the boundary from medium 1 to 2. Let β_1 and β_2 be S wave velocities in media 1 and 2, respectively. We assume $\beta_1 < \beta_2$. It is usually convenient to decompose an S wave into SH and SV components. SH wave is an S wave whose particle motion is parallel to the boundary, and the particle motion of SV wave is on the plane including the ray and perpendicular to the boundary (this plane is called the plane of incidence) (Fig. 4).

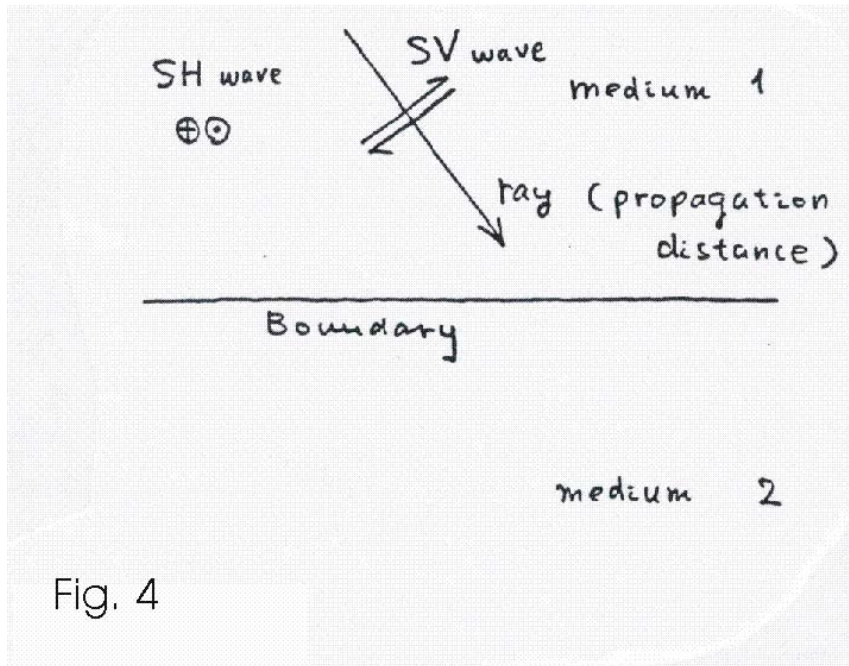


Fig. 4

Since SH wave does not have a component of particle motion perpendicular to the boundary, the situation is relatively simple. As shown in Fig. 5a, when SH wave is incident at the boundary with incident angle, j_1 , reflected SH wave, S_r , and refracted SH wave, S_2 , result. The angle of emergence, j_2 , is related to j_1 by

$$\frac{\sin j_1}{\beta_1} = \frac{\sin j_2}{\beta_2}$$

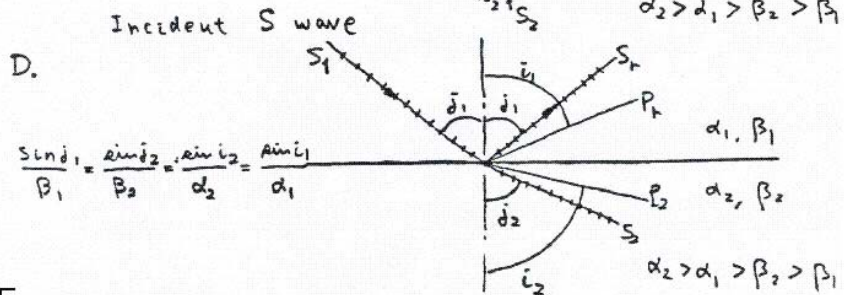
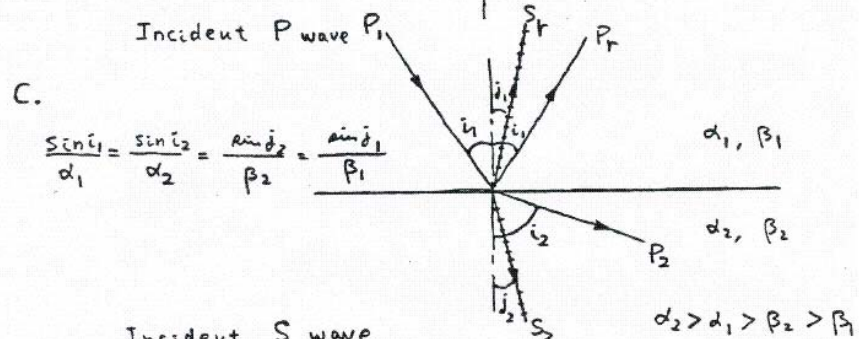
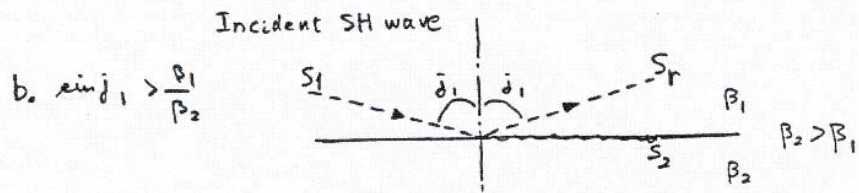
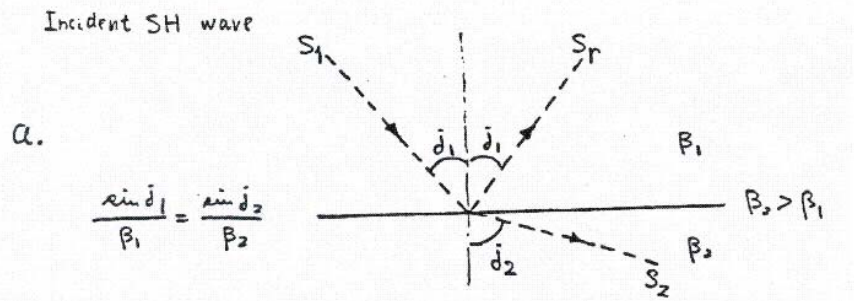


Fig. 5

This relation is similar to Snell's law (10) of 3.4. Thus, we see that, even in this case,

Snell's law can be used to determine the emergence angle. The amplitude ratios S_r / S_1 and S_2 / S_1 are functions of j_1 and, of course, β_2 / β_1 . When j_1 exceeds

$$j_{1,c} = \sin^{-1} \left(\frac{\beta_1}{\beta_2} \right)$$

(2)

no refracted wave results (Fig. 5b). In this case, part of the wave energy is trapped along the boundary, and total reflection occurs. At the same time phase shift occurs on reflection. The angle $j_{1,c}$ is called the critical angle.

When P wave is incident on the boundary, the situation is more complicated. We let α_1 and α_2 be the P wave velocities in media 1 and 2, respectively. We assume $\alpha_2 > \alpha_1 > \beta_2 > \beta_1$. In this case, in addition to refracted and reflected P waves, refracted and reflected SV waves result (Fig. 5c). The following relation holds,

$$\frac{\sin i_1}{\alpha_1} = \frac{\sin i_2}{\alpha_2} = \frac{\sin j_1}{\beta_1} = \frac{\sin j_2}{\beta_2} \quad (3)$$

where i_1 and i_2 are angles of incidence and emergence of the P wave, and j_1 and j_2 are angles of reflection and emergence of the SV wave. When i_1 exceeds

$$i_{1,c} = \sin^{-1} \left(\frac{\alpha_1}{\alpha_2} \right)$$

no refracted P wave results, and part of the wave energy is trapped along the boundary. The angle $i_{1,c}$ is the critical angle.

When SV wave is incident at the boundary, the situation is even more complicated. In this case, refracted and reflected P and SV waves result (Fig. 5d). As before, the following relations hold

$$\frac{\sin j_1}{\beta_1} = \frac{\sin j_2}{\beta_2} = \frac{\sin i_2}{\alpha_2} = \frac{\sin i_1}{\alpha_1} \quad (5)$$

where j_1 and j_2 are angles of incidence and emergence of SV waves, and i_1 and i_2 are angles of reflection and refraction of P waves. When j_1 exceeds

$$j_{1,c_1} = \sin^{-1} \left(\frac{\beta_1}{\alpha_2} \right) \quad (6)$$

P wave no longer propagates into medium 2. When j_1 exceeds

$$j_{1,c_2} = \sin^{-1} \left(\frac{\beta_1}{\alpha_1} \right) \quad (7)$$

no P wave is reflected into medium 1.

When j_1 exceeds

$$j_{1,c_3} = \sin^{-1} \left(\frac{\beta_1}{\beta_2} \right) \quad (8)$$

then no SV wave refraction takes place. In these cases, part of the energy is trapped along the boundary, and complicated phase shift occurs. The angles j_{1,c_1} , j_{1,c_2} and j_{1,c_3} are the critical angles.

When one medium is vacuum, the boundary becomes a free surface, and only reflections are to be considered. It is not difficult to see from Fig. 5 that there is no critical angle for incident SH and P waves, but for incident SV wave

$$j_{1,c_2} = \sin^{-1} \left(\frac{\beta_1}{\alpha_1} \right) \quad (9)$$

becomes critical angle at which no P wave reflection occurs.

Ge 162 Problem #5

Dispersion of Love Waves

We discussed the simplest case of plane Love wave in a single homogeneous layer overlying a homogeneous half-space. The phase velocity c of Love waves can be determined by the characteristic equation

$$\tan\left(\frac{\omega}{c} S_1 H\right) = \frac{\mu_2 S_2}{\mu_1 S_1} \quad (1)$$

where $S_1 = \sqrt{\frac{c^2}{\beta_1^2} - 1}$, and $S_2 = \sqrt{1 - \frac{c^2}{\beta_2^2}}$, and $\beta_1 < c < \beta_2$.

Equation (1) can be solved graphically to determine the phase velocity c for given μ_1 , μ_2 , β_1 , β_2 , and H . The roots of (1) are given by the intersection of the two curves corresponding to RHS (right-hand side) and LHS of (1) both of which are functions of phase velocity.

For the case

$$\begin{aligned} H &= 35 \text{ km} \\ \mu_1 &= 3 \times 10^{11} \text{ dyne/cm}^2, \quad \beta_1 = 3.5 \text{ km/sec} \\ \mu_2 &= 7 \times 10^{11} \text{ dyne/cm}^2, \quad \beta_2 = 4.6 \text{ km/sec} \end{aligned}$$

- Compute the values of RHS and LHS of (1) for phase velocities $c=3.52, 3.6, 3.8, 4.0, 4.2,$ and 4.5 km/sec, and for periods $T=20, 35, 50,$ and 80 sec.
- Plot the values computed above (vertical axis) as a function of phase velocity c (horizontal axis). Draw the two curves and find the phase velocity from the intersection of the two curves (this gives the phase velocity of the fundamental mode).
- Compare these phase velocities $c(T)$ with the dispersion curve for Love waves for the continental region (see Fig. 14 in class note 3.6).

Ge 162 Practice Session 3 Surface Wave Phase and Group Velocities

Figure 1 shows the Rayleigh wave trains from an earthquake (1/2/2002, $M=7.3$) in the Vanuatu Is., southwest Pacific, recorded at two TriNet stations, PAS (Pasadena) and NEE (Needles) (The SAC files, van2.pas.lhz.sac and van2.nee.lhz.sac are in /home/ftp/pub/hiroo/ge162.dir/practice3.dir, but they are not necessary to do this problem). These two stations and the epicenter are almost on a great circle, and the distance between the two stations, Δ , is 331 km. The unit of the time scale on the horizontal axis is sec (i.e., 2100 to 3100 sec).

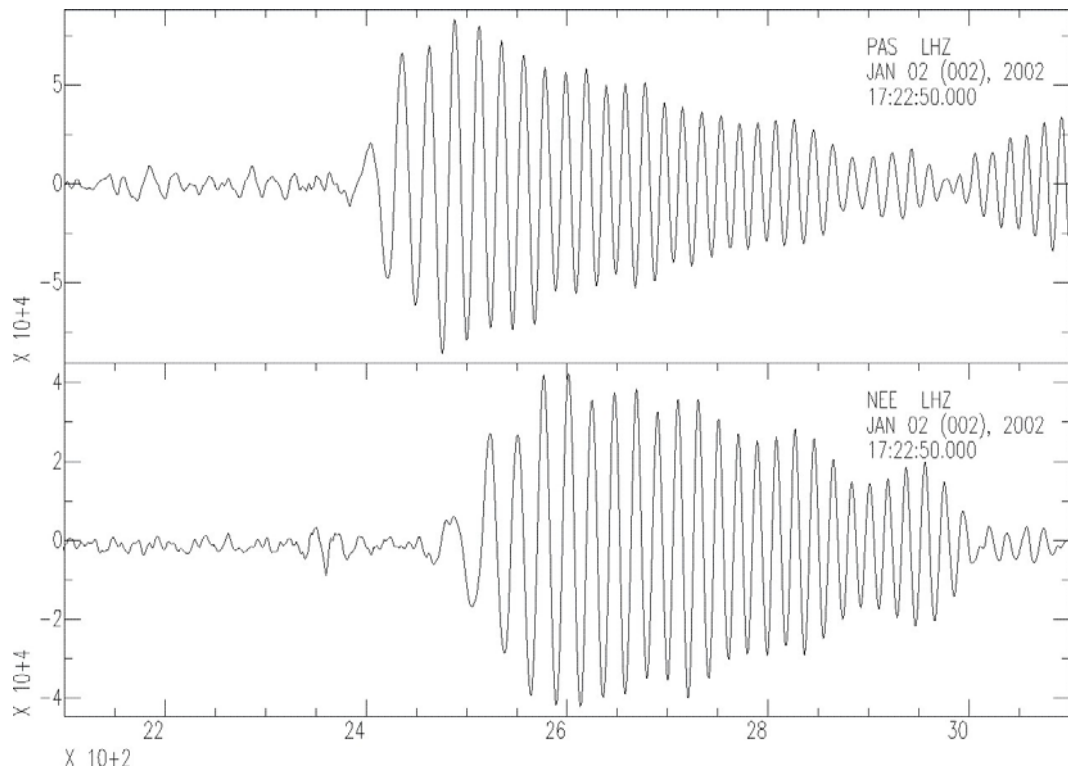


Fig. 1

Figures 2 and 3 show the original (top trace) and band-pass filtered records (at periods of about 20, 30, 40, 50, and 60 sec) of the seismograms shown in Figure 1.

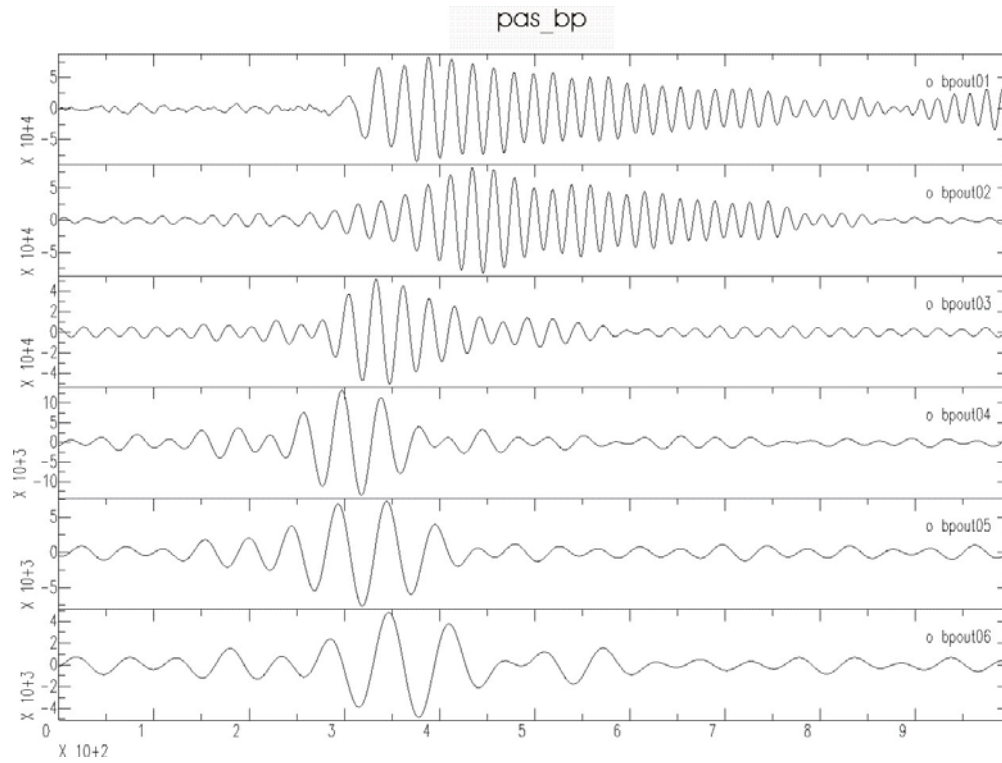


Fig. 2 (PAS)

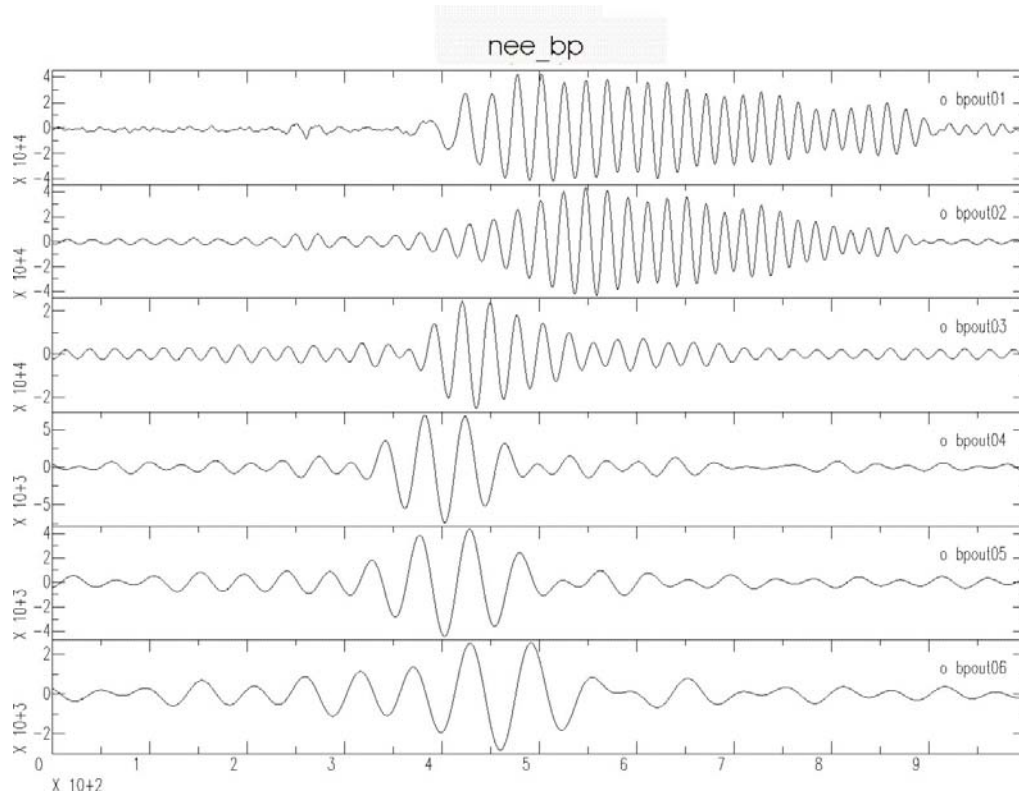


Fig. 3 (NEE)

The band-pass filtered records at $T=60$ sec are of marginal quality. Thus, we use the data from 20 to 50 sec.

1. Determine the group velocity, U , between PAS and NEE, at periods of 20, 30, 40, and 50 sec, by measuring the arrival times of the wave train. (Equation 57 in class handout), and plot the results on a $U-T$ diagram, and compare it with that for a simple crustal structure shown at the end.

The determination of the phase velocities, c , is a bit more difficult. Figures 4 and 5 show the plots of the harmonic components of the records at PAS and NEE. The top trace is the original and the six traces below it are the harmonic components at periods of 20.08, 30.12, 40.96, 51.20, 60.24, and 73.14 sec.

In principle, the phase velocities can be determined from the phase arrival times of the harmonic components using equation 51 in class handout. In this example, the records at PAS and NEE have the same starting time. The difficulty is that, if only harmonic components at discrete periods are given, it is not possible to determine the integer N . In other words, all the peaks look exactly the same. In this exercise, we assume that the phase velocities in southern California are approximately known within a certain range, and we determine N for each period so that the measured phase velocities fall in this range. (Note: If all the harmonics are given, as is the case in the real situation, we need to determine N only for one period.)

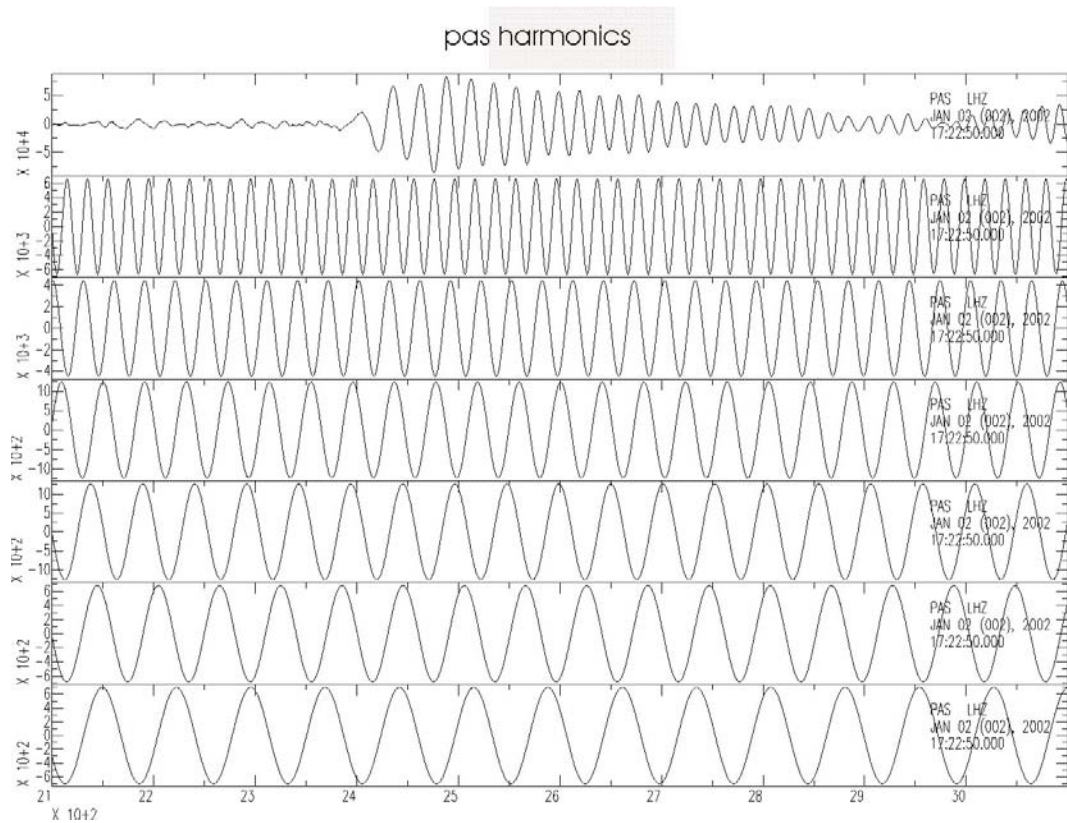


Fig. 4

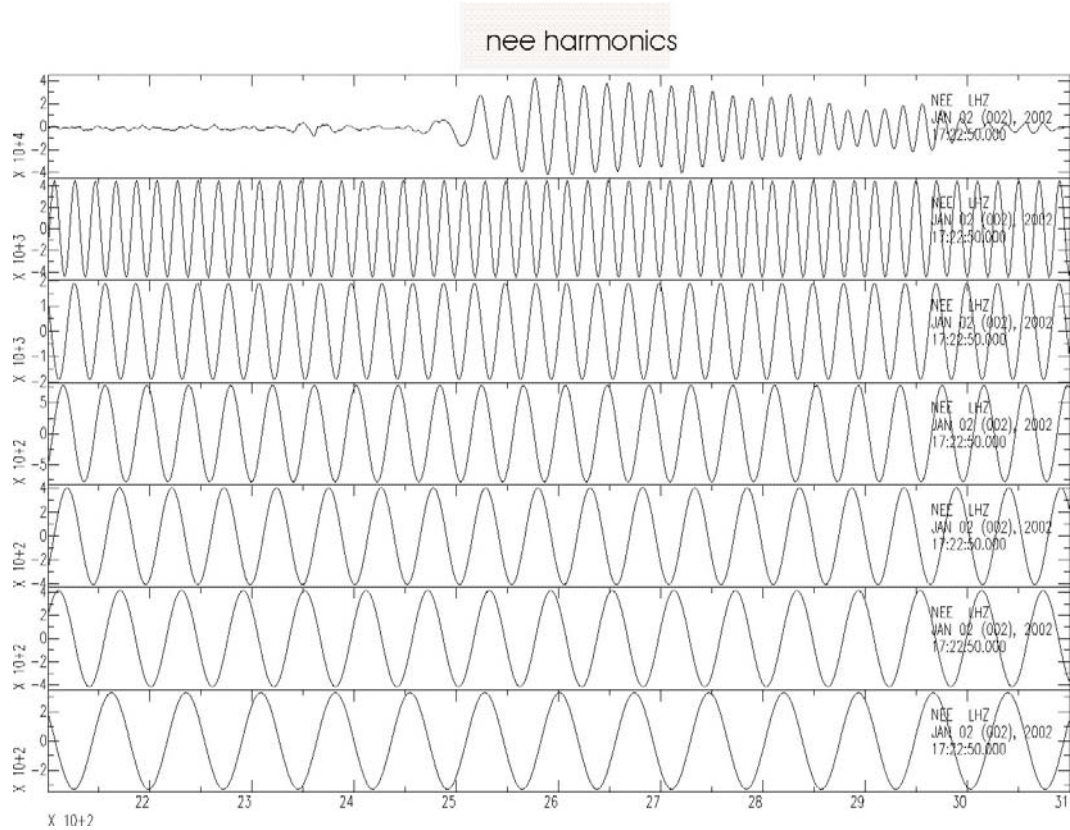
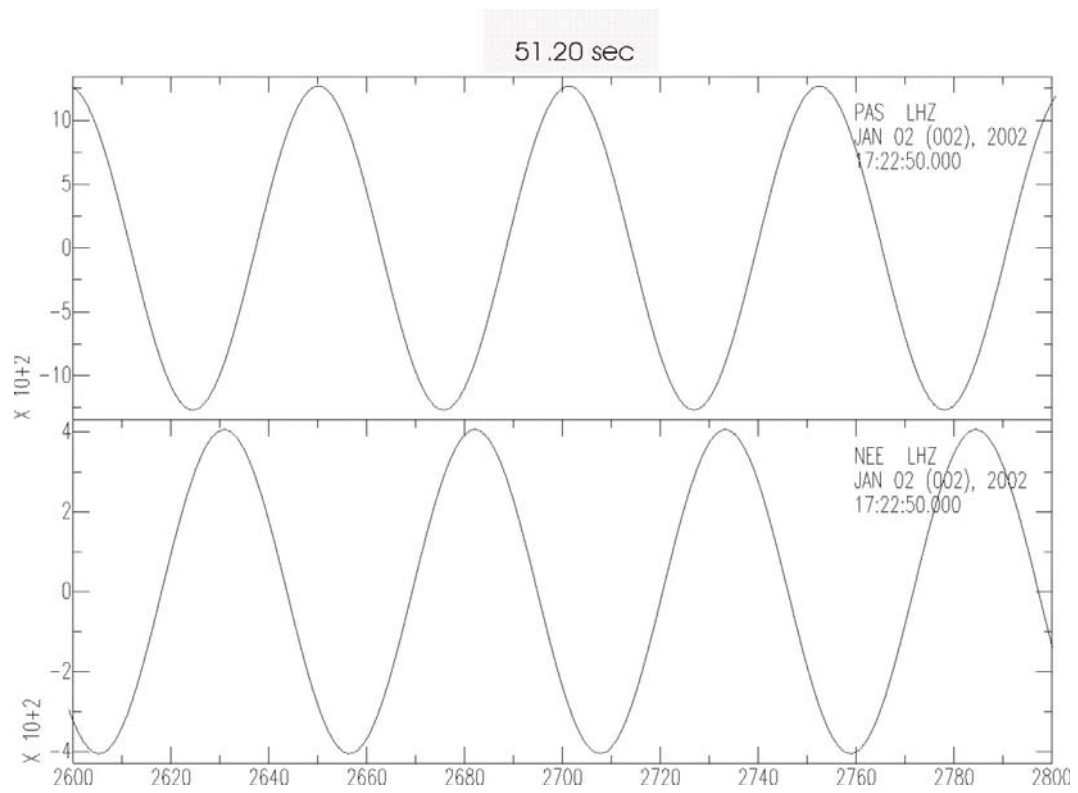


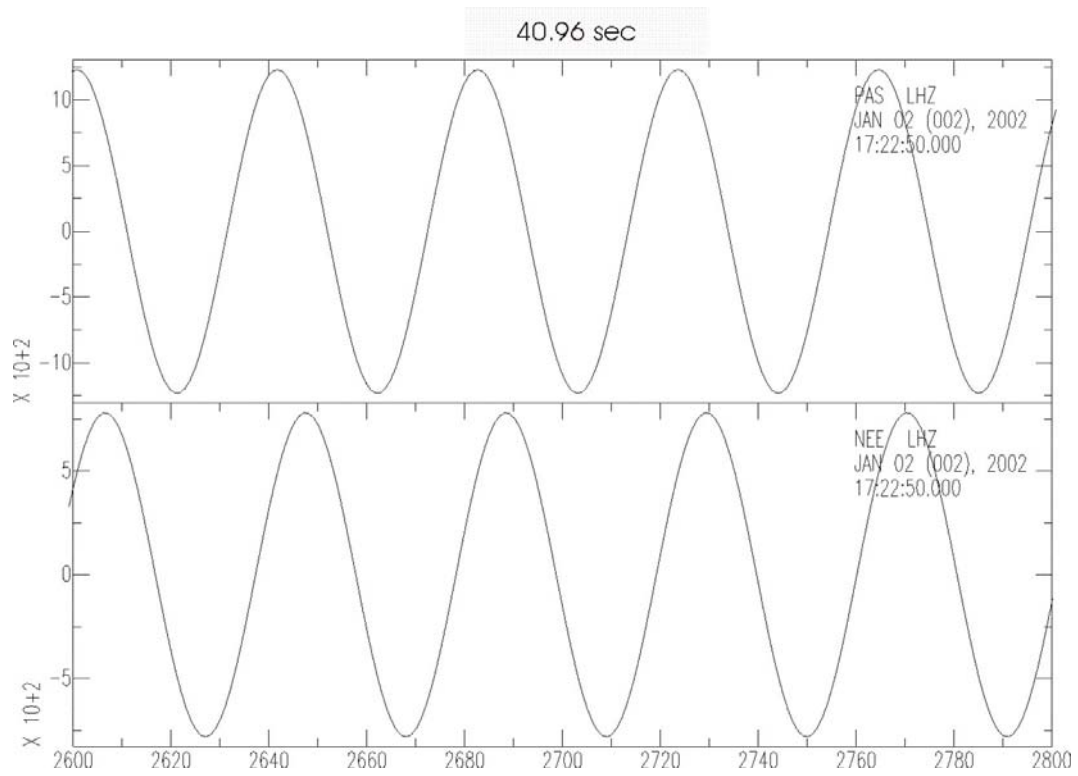
Fig. 5

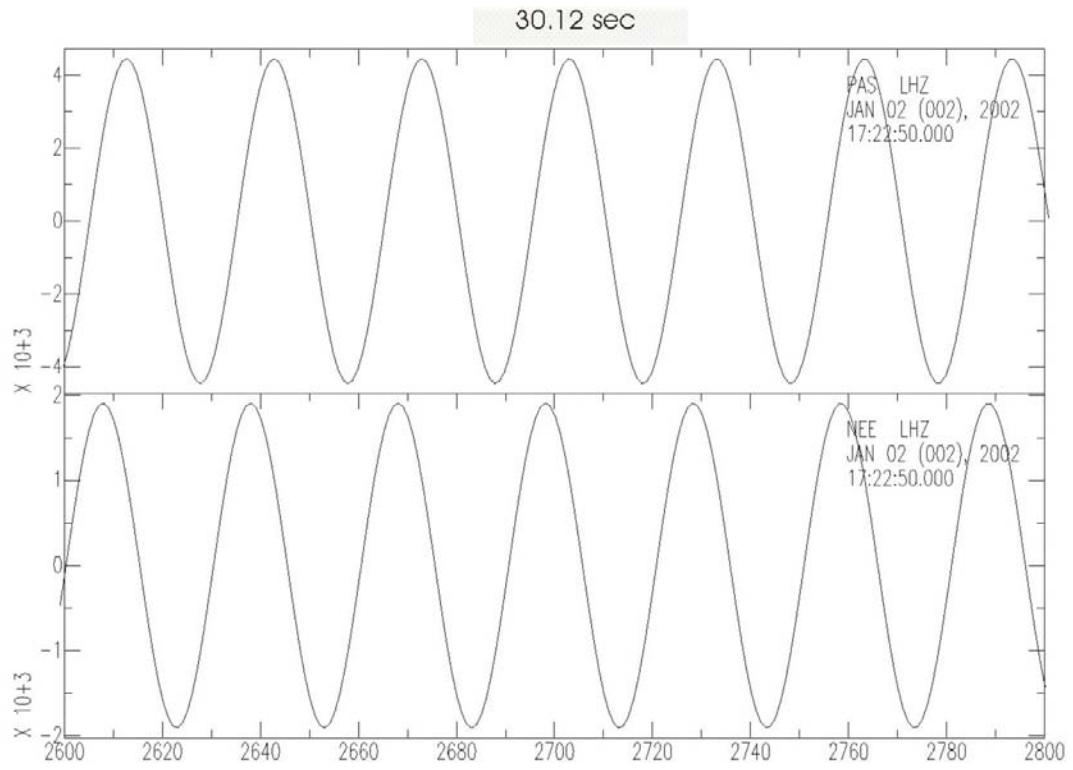
We assume that the phase velocities in southern California are within the following ranges.

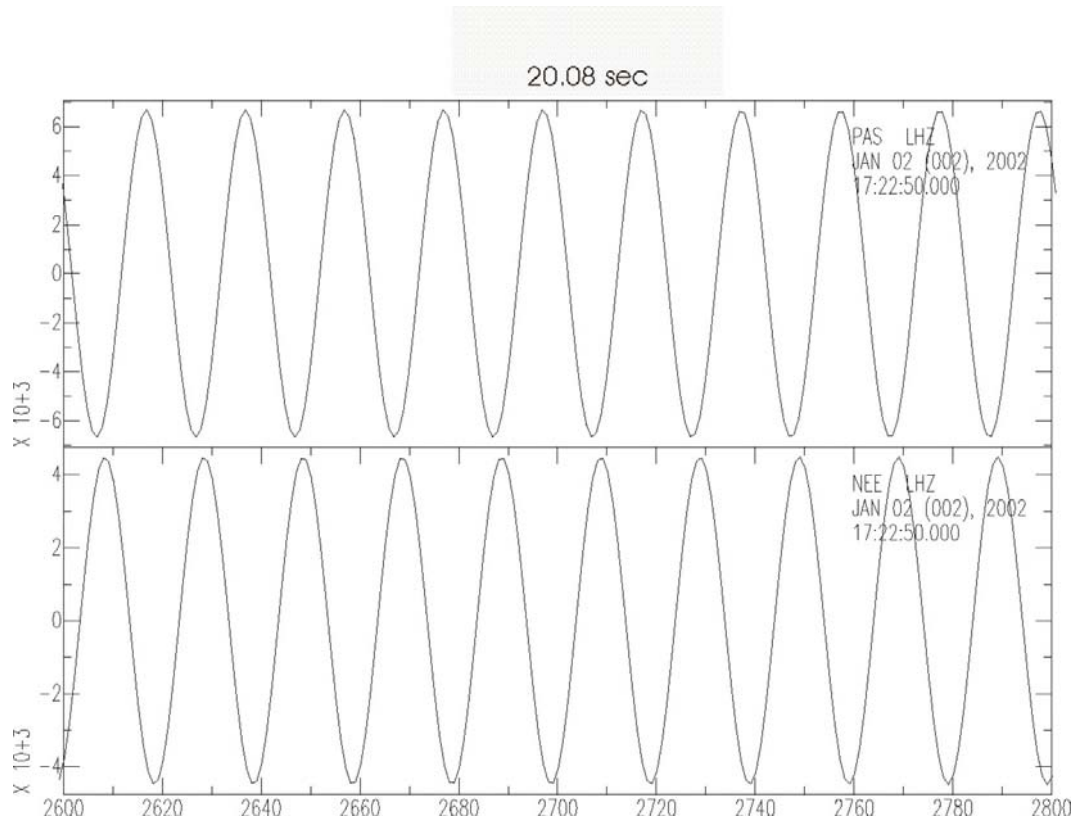
T (sec)	c (km/sec)
20	3.1-3.9
30	3.0-4.3
40	3.3-4.5
50	3.3-4.5

2. Determine the phase velocities between PAS and NEE using the pairs of harmonic waves shown below at periods of 20.08, 30.12, 40.97, and 51.20 sec, and plot them on a c - T diagram, and compare it with the phase velocity dispersion curve for a simple structure given at the end.

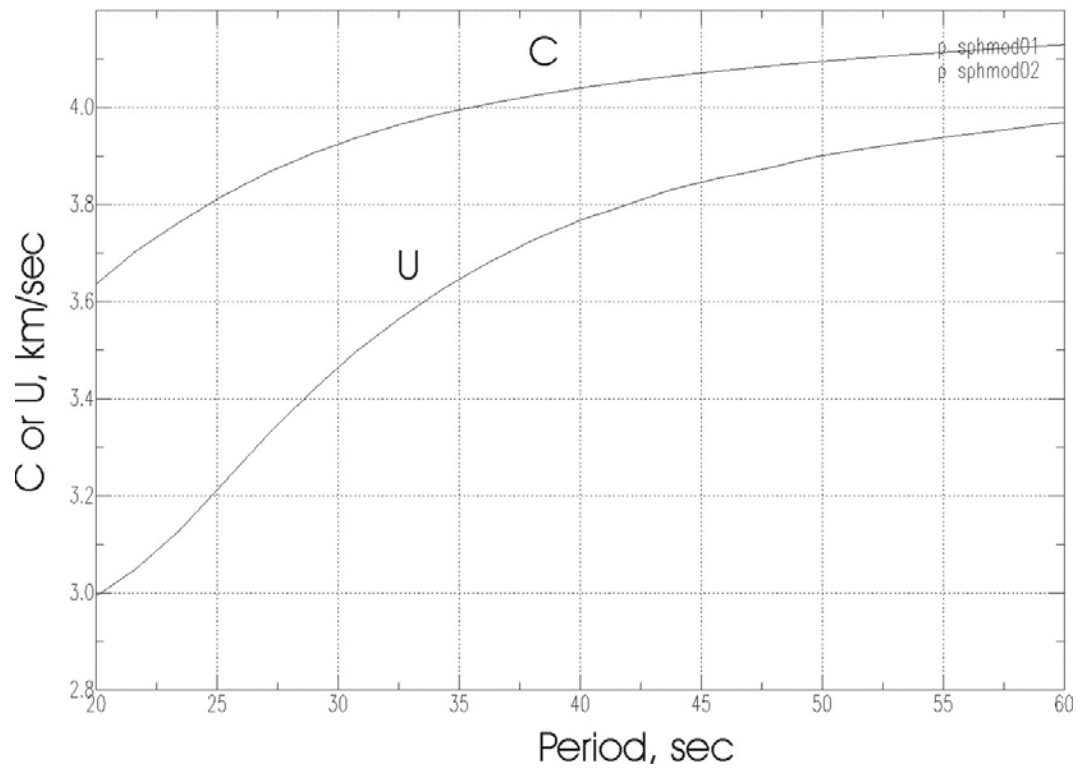




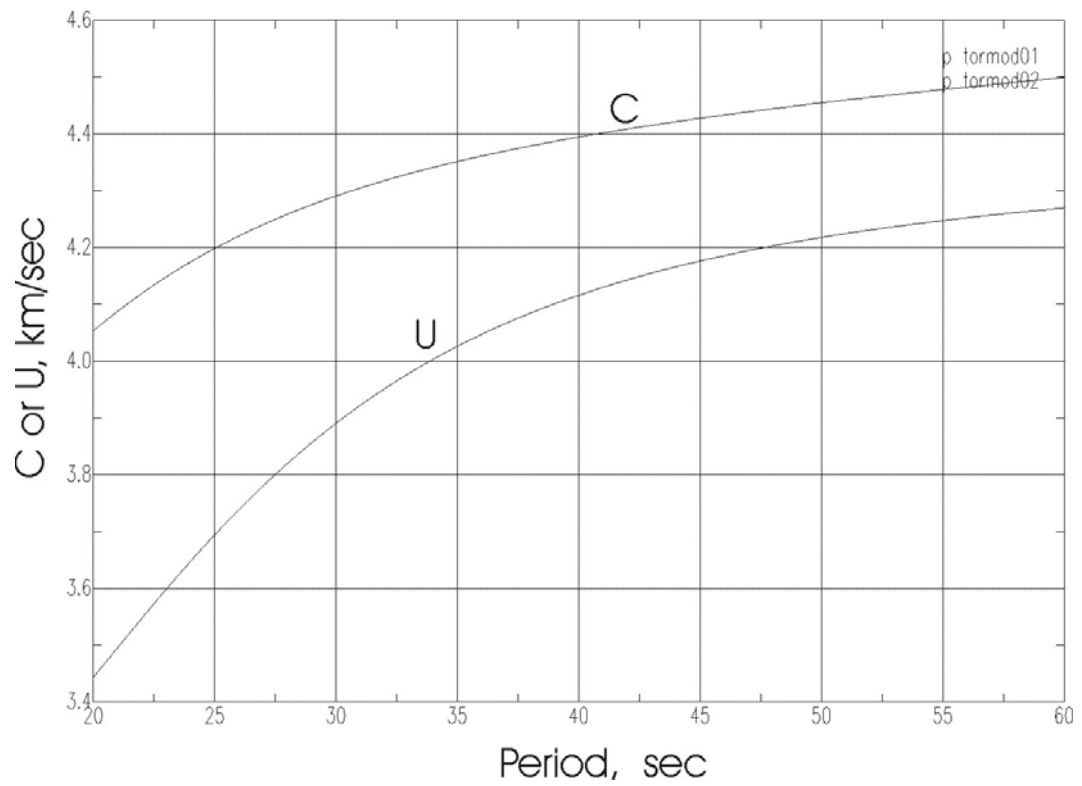




Rayleigh Wave Dispersion for a Simple Crustal Structure



Love Wave Dispersion for a Simple Crustal Structure



These dispersion curves are computed for a simple crustal structure:

Thickness (km)	P-velocity (km/sec)	S-velocity (km/sec)	Density (gm/cm ³)
4.0	5.5	3.18	2.6
23.4	6.3	3.64	2.67
5.0	6.8	3.93	2.8
100.	8.0	4.62	3.2

Note:

In this exercise, we use only 2 stations and the path is chosen to be a great circle. In practice, we use multiple stations and the wave is assumed to be a plane wave and the propagation azimuth and the phase velocities are simultaneously determined. Using a high-density network like TriNet, the accuracy can be improved significantly, and the method can be used for tomographic inversion.

3.6 Seismic Surface Waves (LW, pp. 116-153)

Rayleigh Wave

As we discussed in 3.5, when an SV wave is incident at a free surface, P and SV waves are, in general, reflected. However, when the incidence angle exceeds the critical angle, no P wave reflection occurs and part of the wave energy is trapped along the free surface. This situation suggests existence of surface waves whose energy is confined near the free surface. We consider here one of the simplest cases.

Consider a homogeneous elastic medium whose P wave velocity, S wave velocity, and density are α , β , and ρ , respectively. This medium is bounded by a plane surface, which we take as the x - y plane. We let the medium be in $z < 0$ (Fig. 6). Let us consider a harmonic surface wave propagating in x direction. Since we are considering a surface wave as a result of the coupling between P (irrotational) and SV (solenoidal) waves, we will look for a solution \bar{u} in a form,

$$\bar{u} = \bar{u}' + \bar{u}'' \quad (1)$$

where \bar{u}' is the irrotational field satisfying

$$\text{curl} \bar{u}' = 0 \quad \text{and} \quad \ddot{\bar{u}}' = \alpha^2 \nabla^2 \bar{u}' \quad (2)$$

and \bar{u}'' is the solenoidal field satisfying

$$\operatorname{div} \bar{u}'' = 0 \quad \text{and} \quad \ddot{\bar{u}}'' = \beta^2 \nabla^2 \bar{u}'' \quad (3)$$

Since we consider only *P* and *SV* type motions propagating in *x* direction, \bar{u}' and \bar{u}'' have only *x* and *z* components (u', w') and (u'', w'') which do not depend on *y*. We write $u', w', u'',$ and w'' in a form,

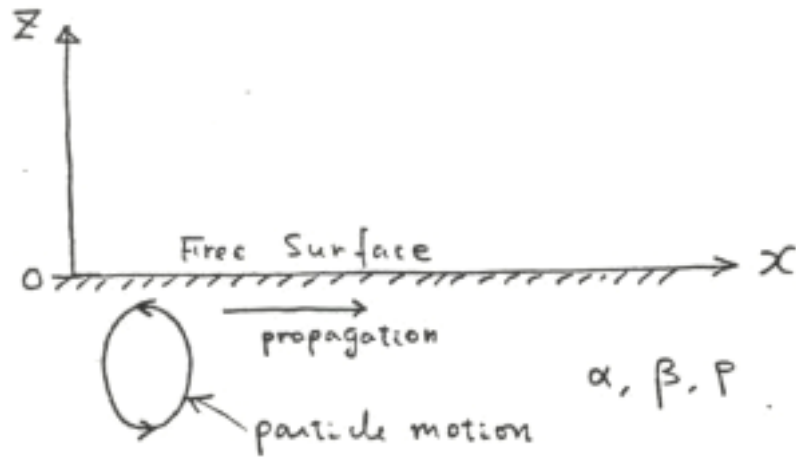


Fig. 6

$$\begin{aligned}
u^I &= f_1(z)e^{i\omega\left(t-\frac{x}{c}\right)} \\
w^I &= h_1(z)e^{i\omega\left(t-\frac{x}{c}\right)} \\
u^{II} &= f_2(z)e^{i\omega\left(t-\frac{x}{c}\right)} \\
w^{II} &= h_2(z)e^{i\omega\left(t-\frac{x}{c}\right)}
\end{aligned} \tag{4}$$

At this point, the phase velocity c is unknown, and we investigate whether we can find c which satisfies all the equations and the boundary conditions for surface waves.

From $\text{curl}\bar{u}^I = 0$, and $\text{div}\bar{u}^{II} = 0$, we have

$$\frac{\partial u^I}{\partial z} - \frac{\partial w^I}{\partial x} = 0, \quad \frac{\partial u^{II}}{\partial x} + \frac{\partial w^{II}}{\partial z} = 0$$

from which

$$h_1(z) = -\frac{1}{i} \frac{c}{\omega} f_1'(z) \quad \text{and} \quad f_2(z) = \frac{1}{i} \frac{c}{\omega} h_2'(z) \tag{5}$$

immediately follow.

Substituting u^I into (2), and w^{II} into (3), we have

$$f_1'' - \left(\frac{\omega}{c}\right)^2 \left(1 - \frac{c^2}{\alpha^2}\right) f_1 = 0 \tag{6}$$

and

$$h_2'' - \left(\frac{\omega}{c}\right)^2 \left(1 - \frac{c^2}{\beta^2}\right) h_2 = 0 \quad (7)$$

respectively. If $\left(1 - \frac{c^2}{\beta^2}\right) < 0$, then h_2 becomes a periodic function which does not decay in the medium. We therefore require

$$\left(1 - \frac{c^2}{\beta^2}\right) > 0 \quad (8)$$

Then, we have

$$f_1 = Ae^{\pm \frac{\omega}{c} S_\alpha z}, \quad h_2 = Be^{\pm \frac{\omega}{c} S_\beta z} \quad (9)$$

$$S_\alpha = \sqrt{1 - \frac{c^2}{\alpha^2}}, \quad S_\beta = \sqrt{1 - \frac{c^2}{\beta^2}}$$

where A and B are constants,

The solution with the minus sign gives an infinite amplitude in the medium at $z = -\infty$ which is physically implausible; the plus sign must be taken. Thus, we have

$$u(x, z, t) = \left(A e^{\frac{\omega}{c} S_{\alpha} z} + \frac{S_{\beta}}{i} B e^{\frac{\omega}{c} S_{\beta} z} \right) e^{i\omega \left(t - \frac{x}{c} \right)} \quad (10)$$

$$w(x, z, t) = \left(-\frac{S_{\alpha}}{i} A e^{\frac{\omega}{c} S_{\alpha} z} + B e^{\frac{\omega}{c} S_{\beta} z} \right) e^{i\omega \left(t - \frac{x}{c} \right)} \quad (11)$$

These solutions must satisfy the stress-free boundary conditions at the free surface $z = 0$, i.e.,

$$0 = \sigma_{zz} = \lambda \left(\frac{\partial u}{\partial x} + \frac{\partial w}{\partial z} \right) + 2\mu \frac{\partial w}{\partial z}, \quad \text{at } z=0 \quad (12)$$

$$0 = \sigma_{zx} = \mu \left(\frac{\partial u}{\partial z} + \frac{\partial w}{\partial x} \right), \quad \text{at } z=0 \quad (13)$$

Substituting (10) and (11) into (12) and (13), and setting $z = 0$, we have

$$-i \left(\frac{c^2}{\beta^2} - 2 \right) A + 2 \sqrt{1 - \frac{c^2}{\beta^2}} B = 0 \quad (14)$$

$$2 \sqrt{1 - \frac{c^2}{\alpha^2}} A - i \left(2 - \frac{c^2}{\beta^2} \right) B = 0 \quad (15)$$

For non-trivial A and B to exist, we must have

$$\left(2 - \frac{c^2}{\beta^2} \right)^2 = 4 \left(1 - \frac{c^2}{\alpha^2} \right)^{1/2} \left(1 - \frac{c^2}{\beta^2} \right)^{1/2} \quad (16)$$

or

$$\frac{c^6}{\beta^6} - 8\frac{c^4}{\beta^4} + c^2\left(\frac{24}{\beta^2} - \frac{16}{\alpha^2}\right) - 16\left(1 - \frac{\beta^2}{\alpha^2}\right) = 0 \quad (17)$$

Since LHS of this equation becomes $-16\left(1 - \frac{\beta^2}{\alpha^2}\right) < 0$ and 1 at $c = 0$ and $c = \beta$,

respectively, (17) has a real root at

$$0 < \frac{c}{\beta} < 1 \quad (18)$$

This satisfies the condition (8) assumed previously. Thus, we have proved that the surface wave given by (10) and (11) exists, and that it propagates with a velocity smaller than the shear wave velocity β . This kind of wave is called Rayleigh wave, and the propagation velocity c is called the phase velocity. Combining (14), (10), and (11), we have

$$u(x, z, t) = A \left(e^{\frac{\omega}{c} S_\alpha z} - \left(1 - \frac{1}{2} \frac{c^2}{\beta^2}\right) e^{\frac{\omega}{c} S_\beta z} \right) e^{i\omega\left(t - \frac{x}{c}\right)} \quad (19)$$

$$w(x, z, t) = -iA \left(-S_\alpha e^{\frac{\omega}{c} S_\alpha z} + \frac{1}{S_\beta} \left(1 - \frac{1}{2} \frac{c^2}{\beta^2}\right) e^{\frac{\omega}{c} S_\beta z} \right) e^{i\omega\left(t - \frac{x}{c}\right)} \quad (20)$$

The amplitude ratio at $z = 0$ becomes

$$\left(\frac{u}{w}\right)_{z=0} = \frac{\frac{1}{2} \frac{c^2}{\beta^2}}{-S_\alpha + \frac{1}{S_\beta} \left(1 - \frac{1}{2} \frac{c^2}{\beta^2}\right)} \quad (21)$$

and the phase of w is advanced by $\pi/2$ with respect to u ,

When $\alpha = \sqrt{3}\beta$ (this corresponds to the Poisson's solid for which Poisson's ratio $\nu = 0.25$), (17) has three real roots of $\frac{c^2}{\beta^2}$, namely, 4 , $2 + \frac{2}{\sqrt{3}}$, and $2 - \frac{2}{\sqrt{3}}$. The first two do not satisfy the condition (8), and therefore do not yield a surface wave. From the last value, we have

$$c = 0.92\beta \quad (22)$$

which satisfies (8). In this case, from (9), $S_\alpha = 0.85$, and $S_\beta = 0.39$. The particle motion at the surface for simple harmonic waves can be obtained by taking the real part of (19) and (20):

$$u(x, t) = 0.42A \cos \omega(t - x/c) \quad (23)$$

$$w(x, t) = 0.62A \sin \omega(t - x/c) \quad (24)$$

and the amplitude ratio becomes 0.68. Equations (23) and (24) show that the orbital motion is elliptic and counter-clockwise (for a wave propagating in positive x direction) (Fig.6).

The decay of the amplitude with depth is governed by factors like

$$e^{\frac{\omega}{c} S_\alpha z} = e^{2\pi S_\alpha \frac{z}{\lambda}} \quad \text{and} \quad e^{\frac{\omega}{c} S_\beta z} = e^{2\pi S_\beta \frac{z}{\lambda}}$$

where λ is the wave length. Thus short wave length components are more quickly attenuated than long wave length components.

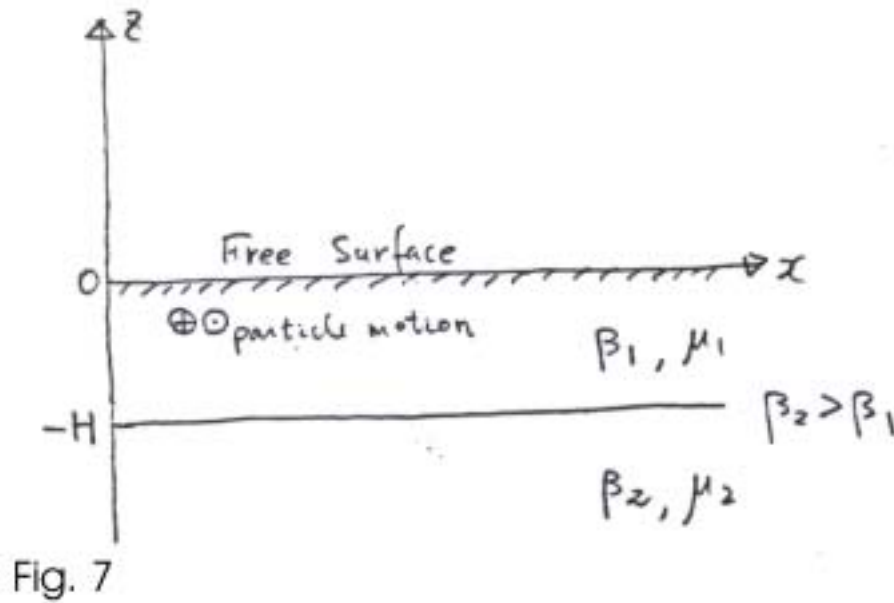
In the above, the medium is assumed homogeneous. Waves like Rayleigh waves also exist in heterogeneous (usually only in z direction) medium. In this case, the phase velocity c is in general a function of wave period (or wave length), and therefore the propagation becomes dispersive. Curves which relate the phase velocity to the period are called phase velocity

dispersion curves. Calculation of such dispersion curves for a vertically heterogeneous medium is usually made numerically,

Love Wave

As we saw in Fig. 5, SH wave is totally reflected when the incidence angle exceeds the

critical angle $j_{1,c} = \sin^{-1}\left(\frac{\beta_1}{\beta_2}\right)$ ($\beta_2 > \beta_1$). Also, it is totally reflected at a free surface, regardless of the incident angle. Therefore if we have a layer underlain by a half space (Fig. 7), and assume that $\beta_2 > \beta_1$, we can consider a SH wave bouncing between the free surface and the boundary without major loss of energy into the half space. This situation suggests propagation of wave energy which is trapped within the layer.



Let us consider propagation of this kind of wave. We take the free surface and the boundary to coincide with the plane $z=0$ and $z=-H$ respectively. The half space occupies $z < -H$. As before we consider a wave propagating in positive x direction. Since we consider an SH field, the displacement vector has only y component. We let v_1 and v_2 be the displacements in the layer and the half space, and look for the solutions in a form

$$v_1 = f_1(z)e^{i\omega\left(t-\frac{x}{c}\right)} \quad (25)$$

$$v_2 = f_2(z)e^{i\omega\left(t-\frac{x}{c}\right)} \quad (26)$$

v_1 and v_2 satisfy the SH wave equation (3) in the layer and the half space respectively. Thus, f_1 and f_2 must satisfy

$$f_1'' + \frac{\omega^2}{c^2} \left(\frac{c^2}{\beta_1^2} - 1 \right) f_1 = 0 \quad (27)$$

$$f_2'' - \frac{\omega^2}{c^2} \left(1 - \frac{c^2}{\beta_2^2} \right) f_2 = 0 \quad (28)$$

The solutions of these equations are

$$f_1 = A \cos \frac{\omega}{c} S_1 z + B \sin \frac{\omega}{c} S_1 z \quad (29)$$

$$f_2 = C e^{\frac{\omega}{c} S_2 z} \quad (30)$$

where

$$S_1 = \sqrt{\frac{c^2}{\beta_1^2} - 1} \quad \text{and} \quad S_2 = \sqrt{1 - \frac{c^2}{\beta_2^2}} \quad (31)$$

For f_2 to vanish at $z \rightarrow -\infty$, $1 - \frac{c^2}{\beta_2^2} > 0$, and we take only the term with positive sign in the exponent of f_2 . At this point S_1 can be either real or imaginary. f_1 and f_2 must satisfy the boundary conditions at the free surface and at the boundary. At the free surface

$$0 = \sigma_{zy} = \mu_1 \frac{\partial v_1}{\partial z} \quad \text{at } z=0 \quad (32)$$

At the boundary

$$v_1 = v_2 \quad \text{and} \quad \mu_1 \frac{\partial v_1}{\partial z} = \mu_2 \frac{\partial v_2}{\partial z} \quad \text{at } z=-H \quad (33)$$

where μ_1 and μ_2 are the rigidity of the layer and the half space, respectively. Substituting (29) and (30) into (32) and (33) leads to

$$B = 0 \quad (34)$$

$$A \cos \frac{\omega}{c} S_1 H - C e^{-\frac{\omega}{c} S_2 H} = 0 \quad (35)$$

$$A \mu_1 S_1 \sin \frac{\omega}{c} S_1 H - C \mu_2 S_2 e^{-\frac{\omega}{c} S_2 H} = 0 \quad (36)$$

For non-trivial A and C to exist, we must have

$$\tan \frac{\omega}{c} S_1 H = \frac{\mu_2}{\mu_1} \frac{S_2}{S_1} \quad (37)$$

This is the characteristic equation. If this equation is satisfied, the surface wave exists, and the phase velocity c is determined from (37). Since S_2 is required to be real, this equation implies that S_1 is also real. Therefore, from (31),

$$\beta_1 < c < \beta_2$$

If $\omega \rightarrow \infty$, or $\lambda (= 2\pi c / \omega) \rightarrow 0$ then (37) gives $c = \beta_1$, and $\omega \rightarrow 0$, or $\lambda \rightarrow \infty$, then (37) gives $c = \beta_2$. Since RHS of (37) varies continuously from ∞ to 0, as c changes from β_1 to β_2 , and LHS changes from 0 to $\tan \frac{\omega}{\beta_2} \sqrt{(\beta_2 / \beta_1)^2 - 1} H$ as c changes from β_1 to β_2 , there is at least one solution of (37) between β_1 and β_2 for any value of ω . For large values of ω ($\omega > \beta_2 \pi / \sqrt{(\beta_2 / \beta_1)^2 - 1} H$), more than one solution exists (Fig. 8).

Thus, the existence of the surface wave is proved. This kind of wave is called Love wave. As is evident from the previous discussion, Love wave is of purely SH type, and is dispersive (i.e., c depends on ω).

As we can see from (35), (29) and (30), the amplitudes in the layer and the half space become

$$f_1 = A \cos \frac{\omega}{c} S_1 z \quad (38)$$

$$f_2 = A \cos \frac{\omega}{c} S_1 H e^{\frac{\omega}{c} S_2 (z+H)} \quad (39)$$

It can be shown that for a fixed ω , the solution (mode) with the lowest value of c ($c = c_1$ in Fig. 8), gives an amplitude function which does not have a zero crossing (node). This mode is called fundamental mode. When more than one solution exists, the modes with higher phase velocities than c_1 have an amplitude function with zero crossings (nodes) (Fig. 8). These modes are called overtones or higher modes.

We can consider this type of wave for more complex medium, for example, a medium which has more than one layer or continuous velocity variation with depth. The computation of the dispersion curves for such complex media must be made numerically,

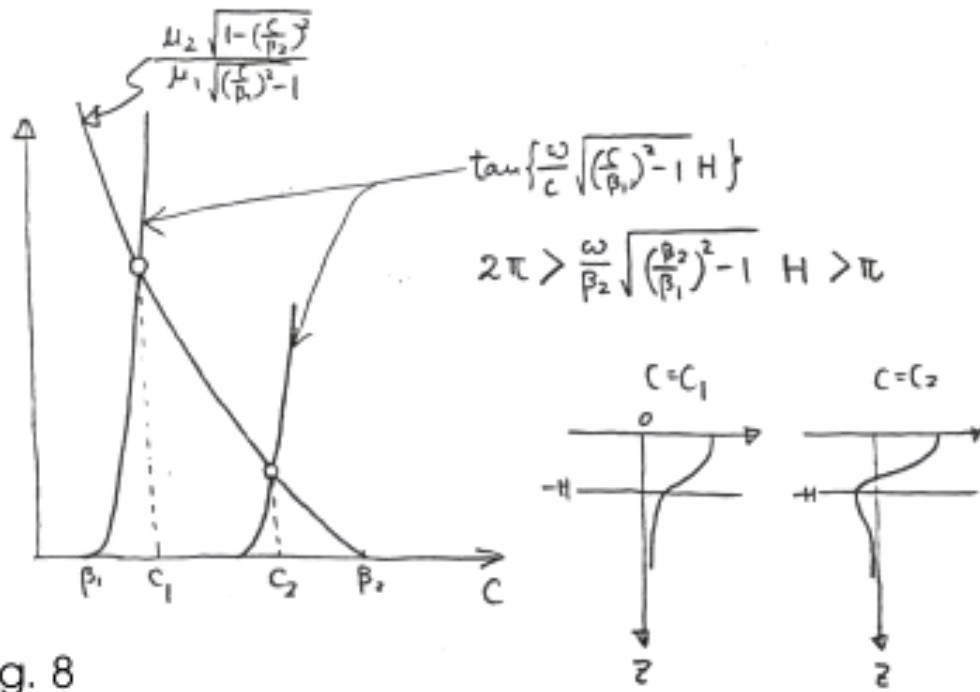
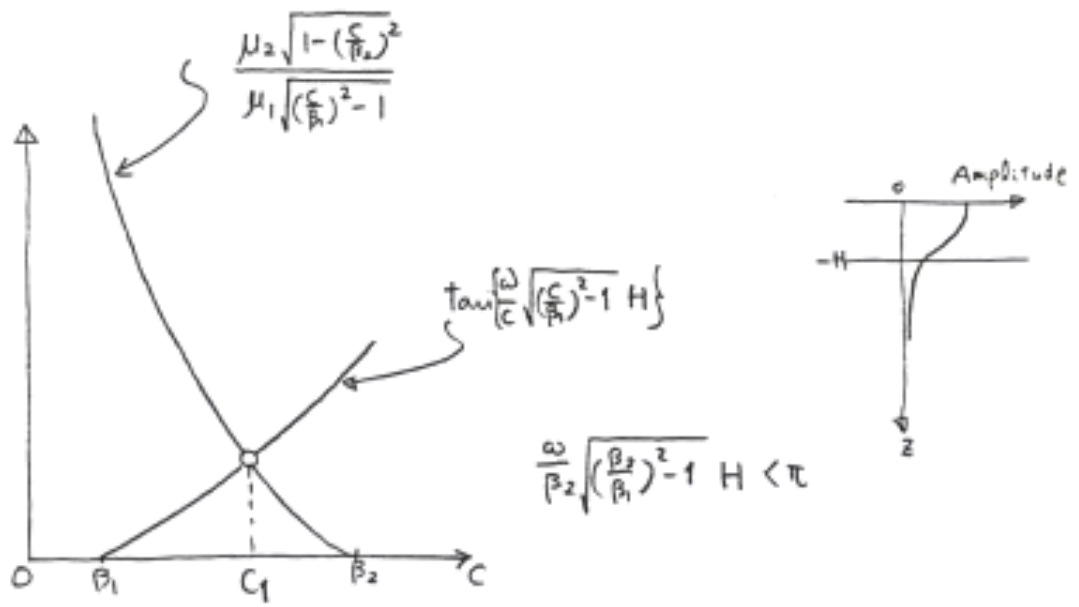


Fig. 8

Dispersion Curve and Structure

Dispersion curves $c(\omega)$ or $c(T)$ are important when we use surface waves to determine the structure of the medium. As we discussed earlier, both Love and Rayleigh waves are dispersive in layered media, and the dispersion curves are determined by the structure. Figures 9, 10, and 11 show several examples of dispersed Love and Rayleigh waves.

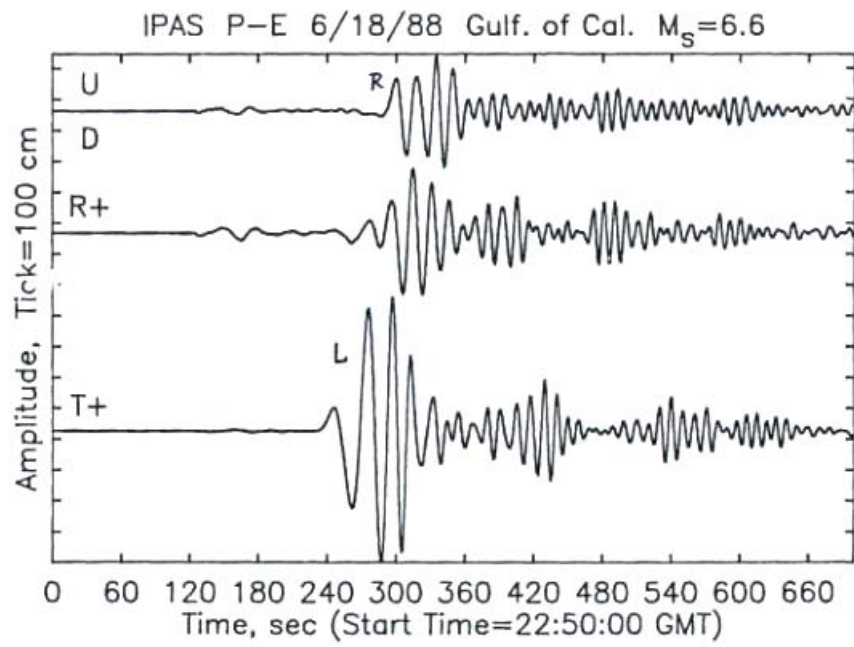


Fig. 9

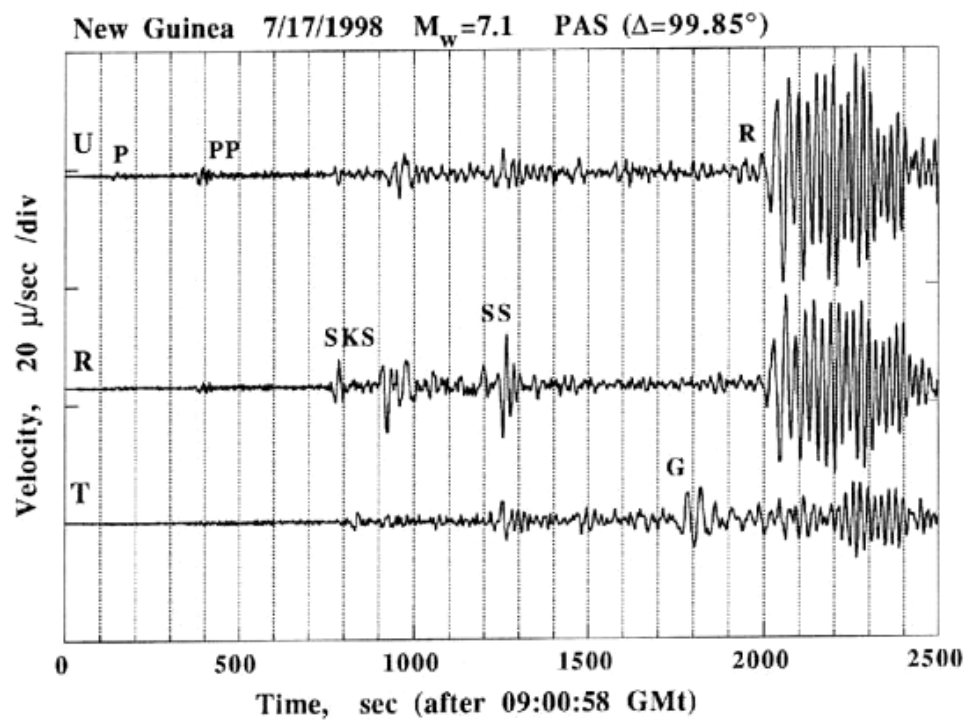


Fig. 10a

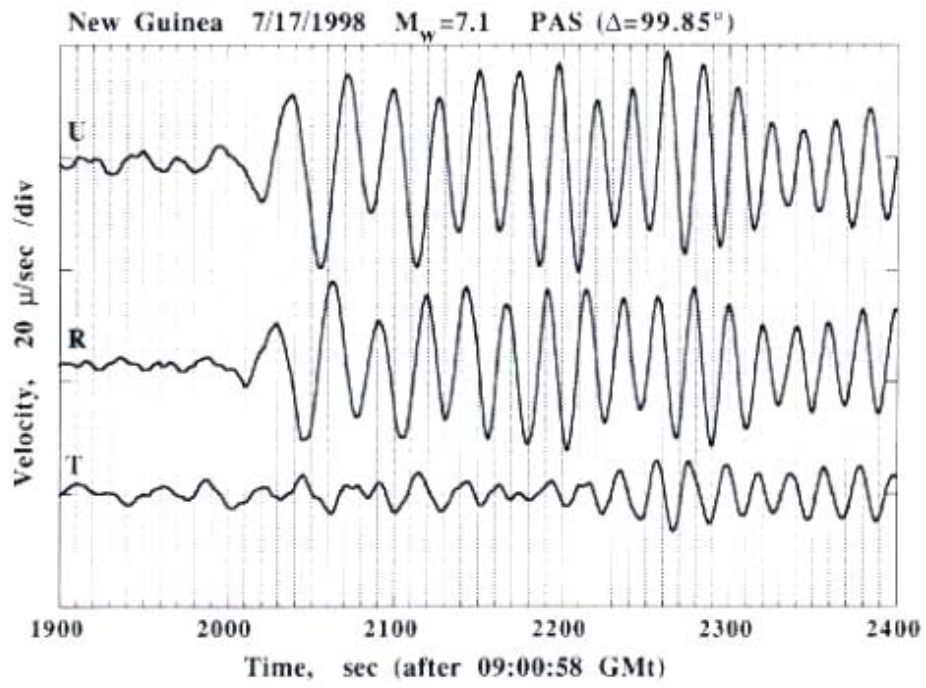


Fig. 10b

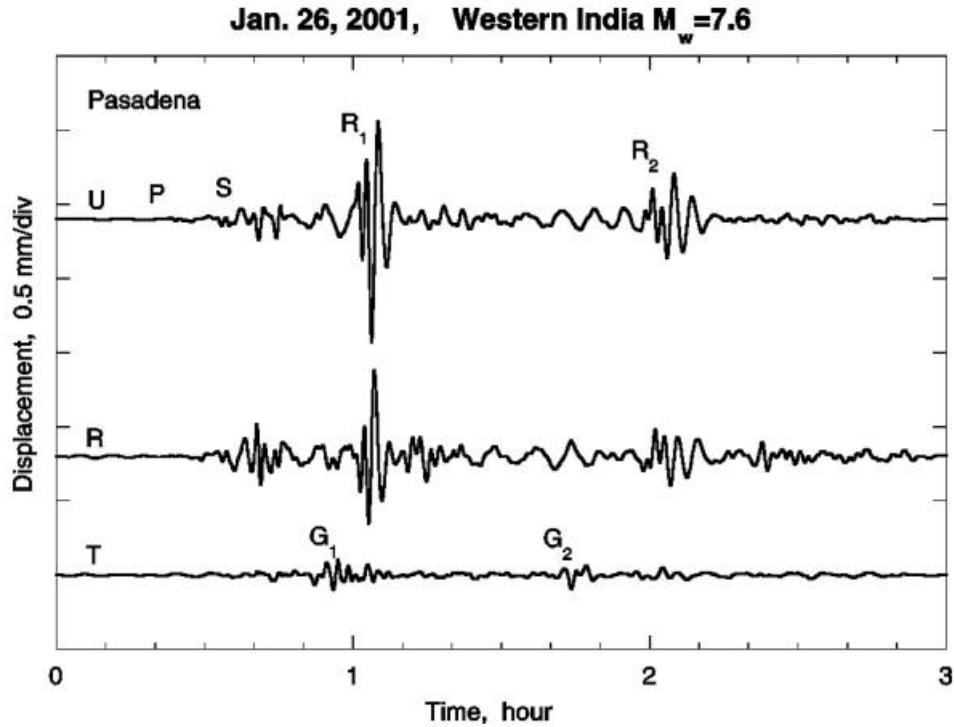


Fig. 11

Consider a layer-over-half space (Figure 12). Let the thickness of the layer be H , and the shear velocity in the layer and the half space be β_1 and β_2 , respectively ($\beta_2 > \beta_1$). At short period, the Love wave energy will be in the layer and the phase velocity approaches β_1 . At long period, Love wave energy penetrates into the half space. At very long period, the velocity approaches β_2 . Thus, the phase velocity dispersion curve would look like the one shown in Figure 12.

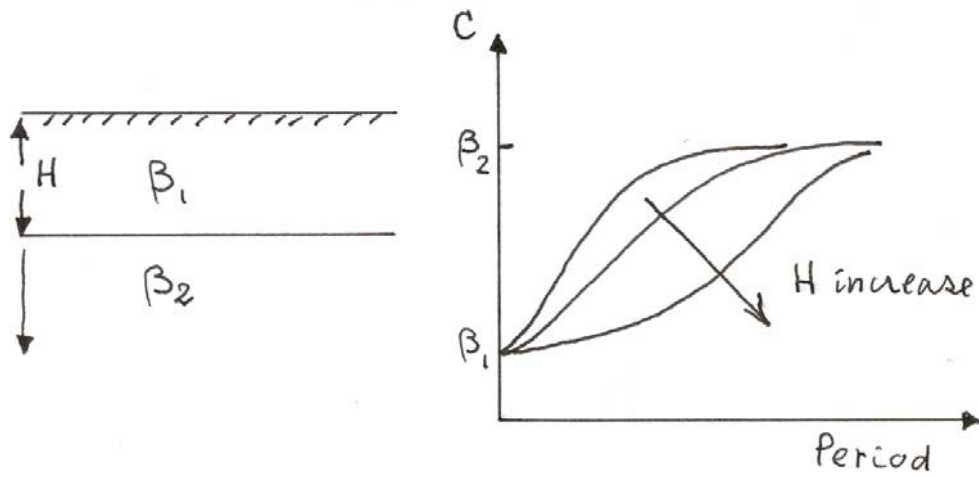


Fig. 12

Then, how would the shape of the dispersion curve change as H varies? If H decreases, the Love wave would "feel" the higher speed half space at a shorter period. Thus, the shape of the dispersion curves would change as shown. For a more complex multi-layered structure, a similar pattern is expected. Thus, we can determine the structure from the shape of the dispersion curve.

We can make the same argument for Rayleigh waves except that the phase velocities at the long-period and the short-period ends are $0.92\beta_2$ and $0.92\beta_1$ (for Poisson solid), respectively.

Figures 13 and 14 show the examples of phase velocity dispersion curves for oceanic, continental and shield structures.

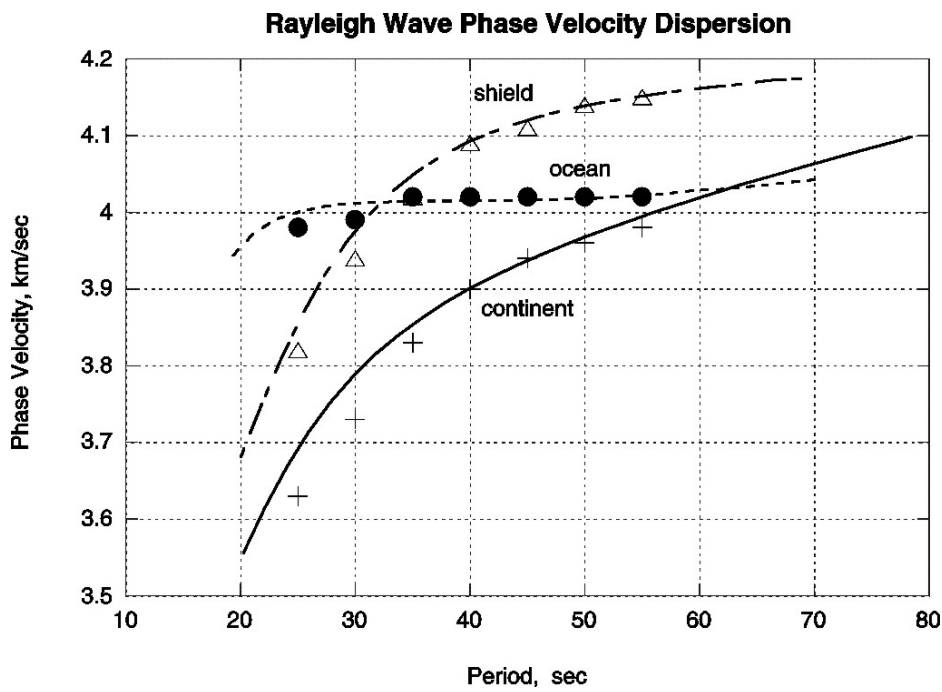


Fig. 13

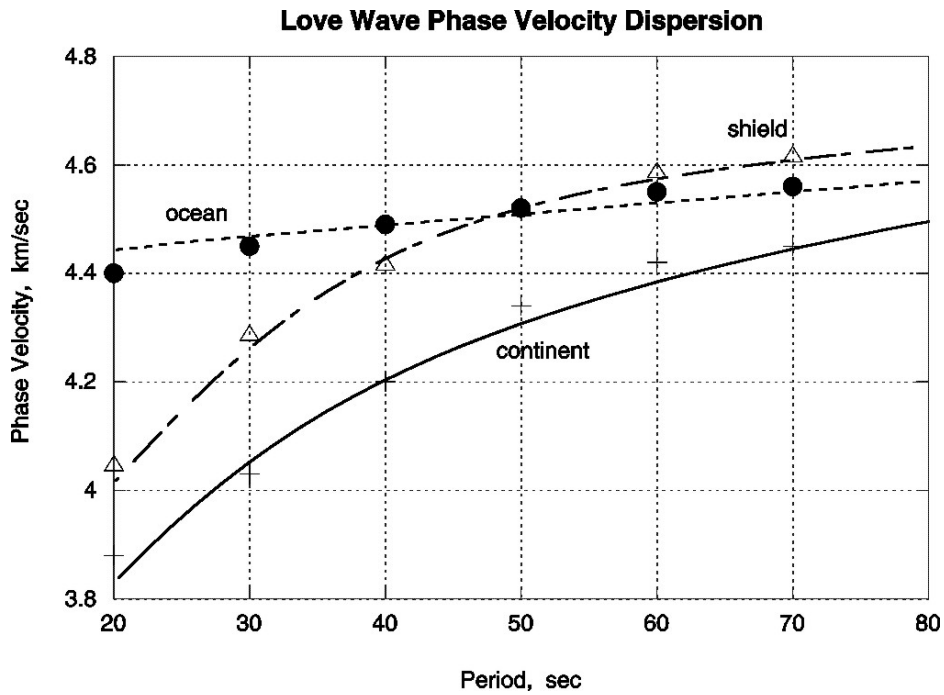


Fig. 14

The structures and the data are given in the following tables.

Models

Ocean

Thickness (km)	P velocity (km/sec)	S-velocity (km/sec)	Density (g/cm ³)
5.0	1.52	0.0	1.03
1.0	2.10	1.00	2.10
5.0	6.41	3.70	2.84
49.	7.82	4.61	3.34

160.	8.17	4.30	3.44
100.	8.49	4.60	3.53

Continent

Thickness (km)	P velocity (km/sec)	S-velocity (km/sec)	Density (g/cm ³)
15.0	5.57	3.36	2.65
18.0	6.50	3.74	2.87
17.0	7.775	4.36	3.33
25.0	7.83	4.39	3.35
35.0	7.92	4.44	3.37
40.0	8.04	4.49	3.41
50.0	8.19	4.56	3.45
50.0	8.35	4.64	3.49
50.0	8.50	4.72	3.53

Shield

Thickness (km)	P velocity (km/sec)	S-velocity (km/sec)	Density (g/cm ³)
6.0	5.64	3.47	2.70
10.5	6.15	3.64	2.80
18.7	6.60	3.85	2.85
80.0	8.10	4.72	3.30
100.0	8.20	4.54	3.44
100.0	8.30	4.51	3.53

Data

Rayleigh Wave

Period O C S

(sec)	(km/sec)	(km/sec)	(km/sec)
55	4.02	3.98	4.15
50	4.02	3.96	4.14
45	4.02	3.94	4.11
40	4.02	3.90	4.09
35	4.02	3.83	4.02
30	3.99	3.73	3.94
25	3.98	3.63	3.82

Love Wave

Period (sec)	O (km/sec)	C (km/sec)	S (km/sec)
70	4.56	4.45	4.62
60	4.55	4.42	4.59
50	4.52	4.34	4.52
40	4.49	4.20	4.42
30	4.45	4.03	4.29
20	4.40	3.88	4.05

Phase and Group Velocity of Dispersive Waves

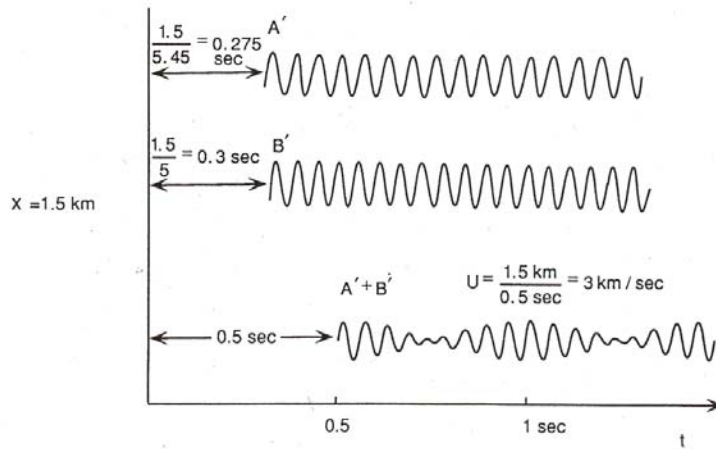
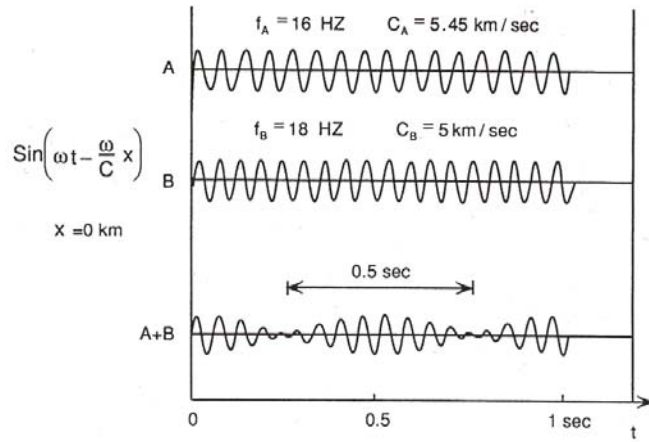
Surface waves are usually dispersive. That is, the phase velocity c is a function of angular frequency ω . In the treatment of dispersive waves we need to distinguish phase velocity $c(\omega)$ and group velocity $U(\omega)$.

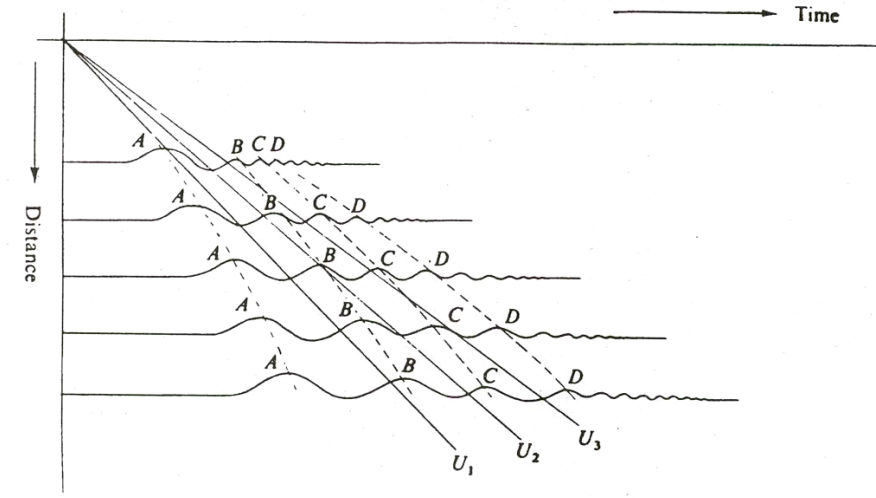
In order to understand the propagation of a dispersive wave train, we consider a wave packet made up of many harmonic wave trains like

$$g(x, t) = A_0 \exp[i(kx - \omega t + \text{const})] \quad (40)$$

The phase velocity is given by

$$c = \omega / k \quad (41)$$





Consider a case in which all components are in phase at $x=0, t=0$. Then, we have constructive interference at $t=0$, and destructive interference elsewhere leading to negligible disturbance. Thus, we have an impulse at $x=0$. At some later time t and at a distance x , a disturbance will be observable if any of the wave trains are in phase over a frequency band. The condition for reinforcement is

$$kx - \omega t = \text{const.}$$

within the frequency band. Differentiating with respect to k , we obtain

$$x - \left(\frac{d\omega}{dk} \right) t = 0 \quad (42)$$

The ratio x/t gives the velocity with which the disturbance (wave group) at the frequency band propagates, and is called the group velocity U . From (42),

$$U = \frac{d\omega}{dk} = c + k \frac{dc}{dk} \quad (43)$$

In general U is also a function of ω .

Determination of Phase Velocity $c(\omega)$

Let a surface wave train at $x = x_1$ be

$$g(x_1, t) = \int_{-\infty}^{+\infty} \hat{g}(x_1, f) \exp(2\pi ift) df = \int_{-\infty}^{+\infty} |\hat{g}(x_1, f)| \exp[i(2\pi ft + \phi_1)] df \quad (44)$$

where

$$\hat{g}(x, f) = |\hat{g}(x, f)| \exp[i\phi(f)] = \int_{-\infty}^{+\infty} g(x, t) \exp(-2\pi ift) dt \quad (45)$$

$|\hat{g}(x, f)|$ and $\phi(f)$ are the amplitude and phase spectrum of $g(x, t)$.

If the wave train propagates in x direction without changing the amplitude, then at $x = x_2$,

$$\begin{aligned} g(x_2, t) &= \int_{-\infty}^{+\infty} |\hat{g}(x_1, f)| \exp\{i[2\pi f(t - (x_2 - x_1)/c(f)) + \phi_1]\} df \\ &= \int_{-\infty}^{+\infty} |\hat{g}(x_1, f)| \exp[i(2\pi ft + \phi_2)] df \end{aligned}$$

and (46)

$$\phi_2 = \phi_1 - 2\pi f(x_2 - x_1) / c(f) \quad (47)$$

If the wave is non-dispersive (i.e., $c = c_0 = \text{constant}$), then

$$g(x_2, t) = g(x_1, t - x/c_0) \quad (48)$$

That is, the wave propagates without changing its waveform. In a dispersive medium, c is a function of frequency, and the waveform changes with propagation.

Since, adding $2\pi N$ (N is an integer) to ϕ_2 does not change (46), (47) is actually

$$\phi_2 = \phi_1 - 2\pi f(x_2 - x_1) / c(f) + 2\pi N \quad (49)$$

Using (49), we can determine the phase velocity from the two wave trains measured at distances x_1 and x_2 by measuring the phases ϕ_1 and ϕ_2 at these distances. Solving (49) for $c(f)$, we obtain,

$$c(f) = \frac{f(x_2 - x_1)}{N - (\phi_2 - \phi_1) / 2\pi} \quad (50)$$

or,

$$c(T) = \frac{(x_2 - x_1)}{NT + (-\phi_2 T / 2\pi + \phi_1 T / 2\pi)} \quad (51)$$

where $(-\phi_2 T / 2\pi) - (-\phi_1 T / 2\pi)$ is the phase travel time.

In the above, the records at the two stations are assumed to have a common origin time. In actual computations, we may use the records (seismograms) starting at different times; at $t = t_1$ at $x = x_1$ and at $t = t_2$ at $x = x_2$. Then, if we let ψ_1 , and ψ_2 be the Fourier phases measured from these records, then we have

$$\phi_2 - \phi_1 = \psi_2 - \psi_1 - 2\pi f(t_2 - t_1) \quad (52)$$

Substituting this in (50), we obtain

$$c(f) = \frac{f(x_2 - x_1)}{N - (\psi_2 - \psi_1)/2\pi + f(t_2 - t_1)} \quad (53)$$

If the propagation path is very long, and involves antipolar or polar passages, a small correction is necessary to correct for the polar phase shift. In this case,

$$c(f) = \frac{f(x_2 - x_1)}{N + m/4 - (\psi_2 - \psi_1)/2\pi + f(t_2 - t_1)} \quad (54)$$

where m is the number of polar or antipolar passages.

Determination of Group Velocity $U(\omega)$

Once the phase velocity is determined as a function of ω (or, frequency, f), then the group velocity $U(\omega)$ can be computed from phase velocity using (43), i.e.,

$$\frac{1}{U(\omega)} = \frac{dk}{d\omega} = \frac{1}{c(\omega)} - \frac{\omega}{c^2(\omega)} \frac{dc(\omega)}{d\omega} \quad (55)$$

Another way of determining the group velocity is to use narrow band-pass filtering of the seismograms.

Let a propagating wave be given by,

$$g(x, t) = \frac{1}{2\pi} \int_{-\infty}^{+\infty} \hat{g}(x, \omega) \exp[i(\omega t - kx)] d\omega = \frac{1}{2\pi} \int_{-\infty}^{+\infty} |\hat{g}(x, \omega)| \exp[i(\omega t - kx + \phi)] d\omega \quad (56)$$

If we consider a contribution over a narrow frequency band $\Delta\omega$ around ω_0 , we obtain from (56)

$$\begin{aligned} \tilde{g}(x, t) &\approx \frac{1}{\pi} |\hat{g}(x, \omega_0)| \int_{\omega_0 - \Delta\omega}^{\omega_0 + \Delta\omega} \cos(\omega t - kx + \phi) d\omega \\ &= \frac{\Delta\omega}{\pi} |\hat{g}(x, \omega_0)| \left(\frac{\sin\left(\frac{\Delta\omega}{2}(t - k'_0 x + \phi'_0)\right)}{\frac{\Delta\omega}{2}(t - k'_0 x + \phi'_0)} \right) \cos(\omega_0 t - k_0 x + \phi_0) \end{aligned} \quad (57)$$

where k_0 and ϕ_0 are the values of k and ϕ at $\omega = \omega_0$, respectively, and k'_0 and ϕ'_0 are the values of $\frac{dk}{d\omega}$ and $\frac{d\phi}{d\omega}$ at $\omega = \omega_0$, respectively. Equation (57) gives a wave train which propagates at a speed

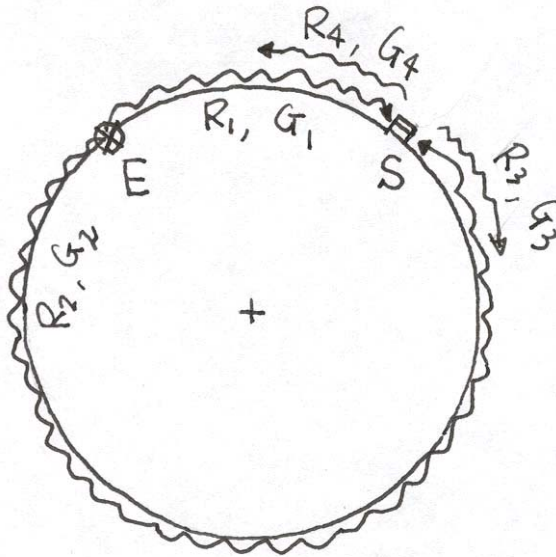
$$U(\omega_0) = \frac{1}{k'_0} = \left. \frac{d\omega}{dk} \right|_{\omega=\omega_0} \quad (58)$$

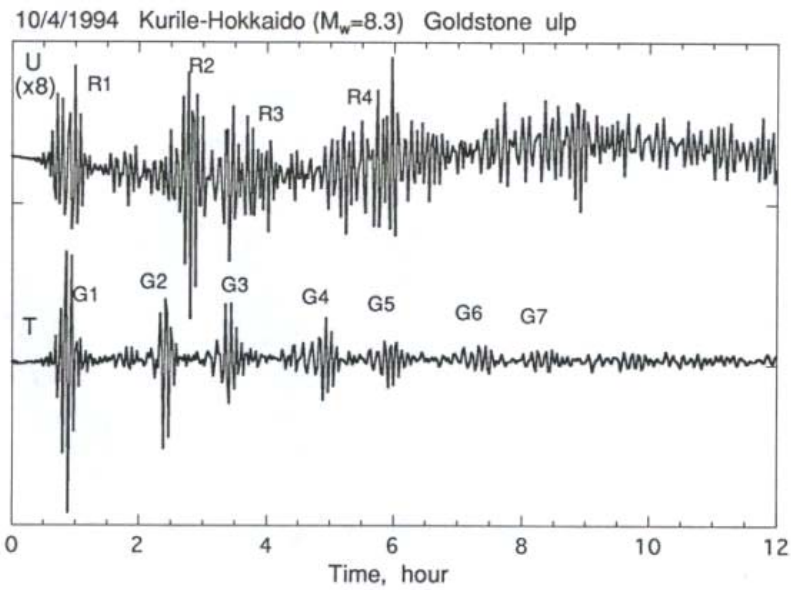
Thus, if we measure the propagation velocity of a band-pass filtered record, we can determine the group velocity.

Ge 162

3.7 Normal Mode Theory (LW, pp. 154-172)

Since the Earth is a bounded medium, the wave propagation problem can be treated as a normal-mode problem.

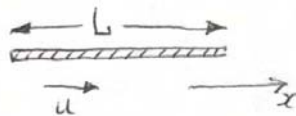




The basic physics can be understood with a simple 1-D problem.

1. 1-D Problem

Consider free oscillations of a homogeneous elastic rod shown below.



The equation of motion is

$$\rho \frac{\partial^2 u}{\partial t^2} = E \frac{\partial^2 u}{\partial x^2}$$

where ρ is the density and E is the Young's modulus.
For harmonic motion,

$$u(x, t) = y(x)e^{i\omega t} \quad (1)$$

then,

$$y'' + k^2 y = 0, \quad k^2 = \rho \omega^2 / E \quad (2)$$

The solution is

$$y = A \cos kx + B \sin kx$$

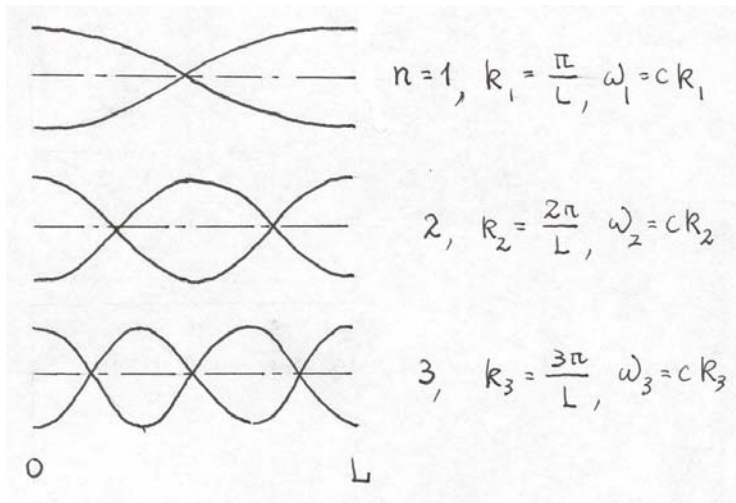
If both ends of the rod are free (i.e., $y' = 0$ at $x = 0$ and L), then $B = 0$ and $k_n = n\pi/L$ ($n = \text{integer}$). Then, the eigen functions are

$$y_n = A \cos(n\pi x/L)$$

and the eigen frequencies are

$$\omega_n = \sqrt{E / \rho} k_n$$

Here, n determines the number of nodes.



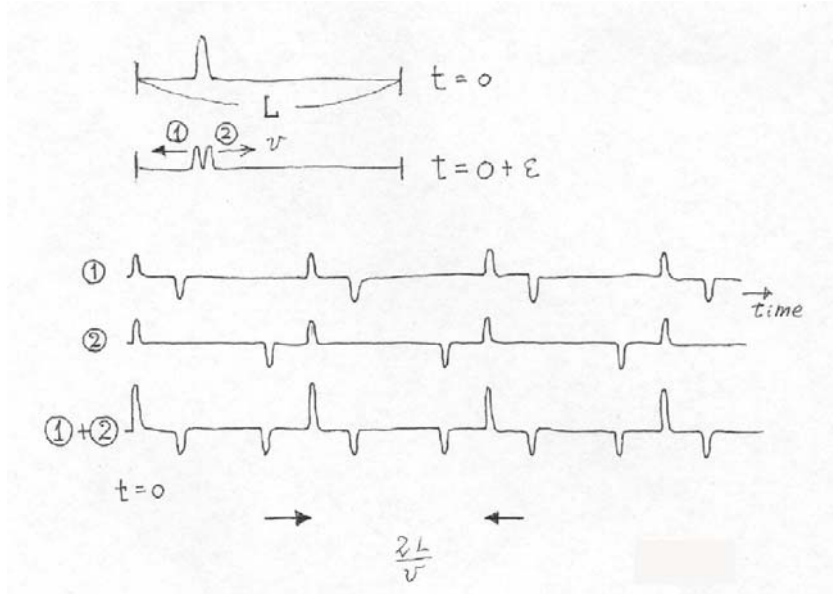
The eigen functions y_n are orthogonal, i. e.,

$$\int_0^L \rho y_n y_m dx \propto \delta_{nm} \quad (3)$$

(this relation can be derived directly from (2), if y_n and y_m satisfy the homogeneous boundary conditions $ay_n + y'_n = 0$ and $cy_m + y'_m = 0$ at $x=0$ and L .)

Example

If a stretched string is plucked at a point, a localized disturbance is produced. The disturbance propagates in the string and the time history of the disturbance is given as shown in the following figure.



This is a seismogram. This displacement can be viewed as superposition of normal modes as follows.

Normal modes for a string with length L , clamped at both ends are given by

$$y_n(x) = \sin(n\pi x / L)$$

The displacement of the string $u(x, t)$ is given by the superposition of $y_n(x)$ with weights A_n , and can be written as

$$u(x, t) = \sum_{n=1}^{\infty} A_n \sin(n\pi x / L) \cos \omega_n t$$

where $\omega_n = n\pi c / L$ are the eigen frequencies, and c is the velocity of wave traveling in the string.

The initial (at $t=0$) shape of the displacement $u(x, 0)$ is then given by

$$u(x, 0) = \sum_{n=1}^{\infty} A_n \sin(n\pi x / L)$$

which can be considered as a Fourier series of $u(x, 0)$.

If we assume that the initial disturbance is given by a delta function at $x = x_s$, $u(x, 0) = \delta(x - x_s)$, then A_n above can be determined by multiplying $u(x, 0)$ by $\sin(n\pi x / L)$ and integrating it from 0 to L . Since

$$\int_0^L \sin(n\pi x / L) \sin(m\pi x / L) dx = \frac{L}{2} \delta_{nm} \quad \text{and} \quad \int_0^L \delta(x - x_s) \sin(n\pi x / L) dx = \sin(n\pi x_s / L),$$

we obtain

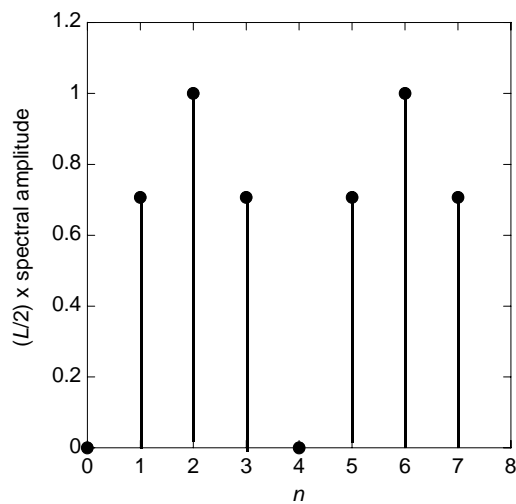
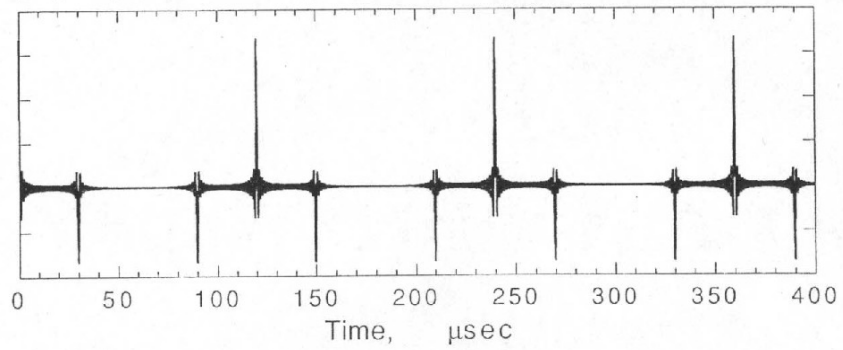
$$A_n = (2/L) \sin(n\pi x_s / L)$$

Then the displacement is given by

$$u(x, t) = \frac{2}{L} \sum_{n=1}^{\infty} \sin(n\pi x / L) \sin(n\pi x_s / L) \cos \omega_n t$$

The following figure shows $u(x, t)$ for $x = x_s = L/4$, and is essentially the same as the seismogram shown above. This equation can be viewed as superposition of normal modes, $\sin(n\pi x / L) \cos \omega_n t$, with the amplitudes $(2/L) \sin(n\pi x_s / L)$ shown as "spectrum".

Propagating pulse in string $L=30$ cm, $c=50$ m/sec, $x_s = x_o = L/4$

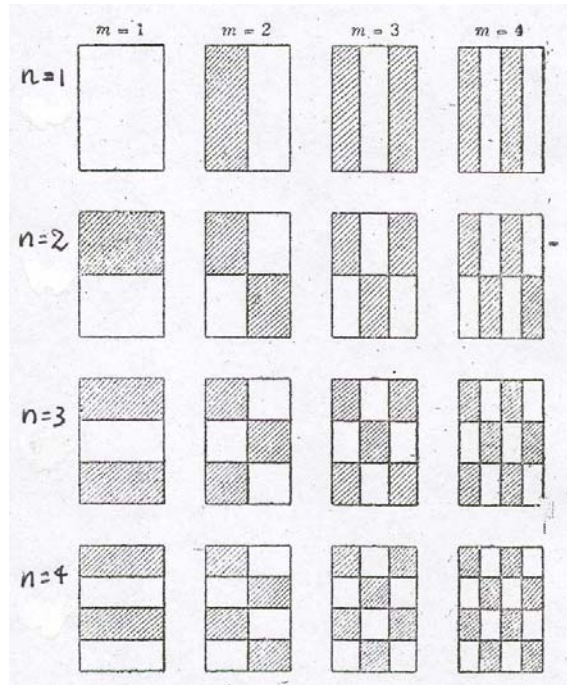
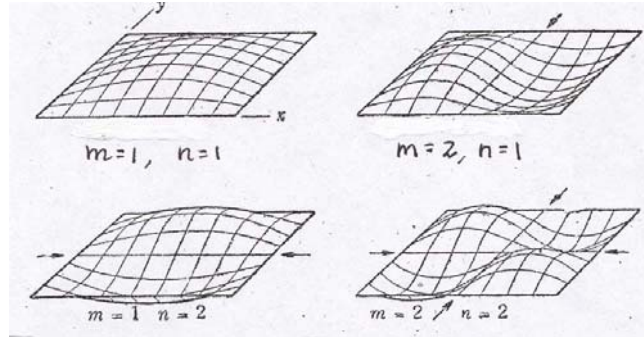


2. 2-D and 3-D Problems

The above result can be easily extended to 2-D and 3-D problems. For example, free oscillations of a homogeneous rectangular membrane can be expressed by eigen functions of the form,

$$y_n^m = A \sin(m\pi x / L_x) \sin(n\pi y / L_y)$$

Here, m and n determine the number of nodes in x and y directions, respectively (see the attached figure.).



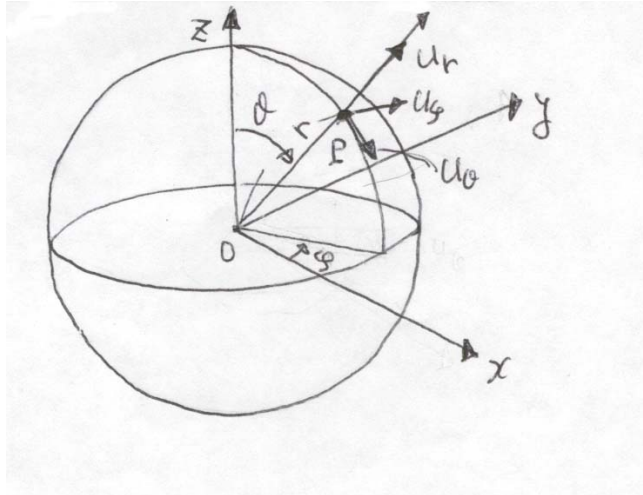
For free oscillations of a homogeneous elastic rectangular block, the eigen functions can have a form

$$y_l^m = A \cos(l\pi x / L_x) \cos(m\pi y / L_y) \cos(n\pi z / L_z)$$

the order numbers l , m and n determine the number of nodes in x , y and z directions, respectively.

3. Free Oscillations of the Earth --- General ---

The free oscillations of the Earth can be formulated similarly as free oscillations of an elastic sphere. The only difference is that it is more convenient to use a spherical coordinate system (r, θ, ϕ) instead of the Cartesian coordinate system (x, y, z) .

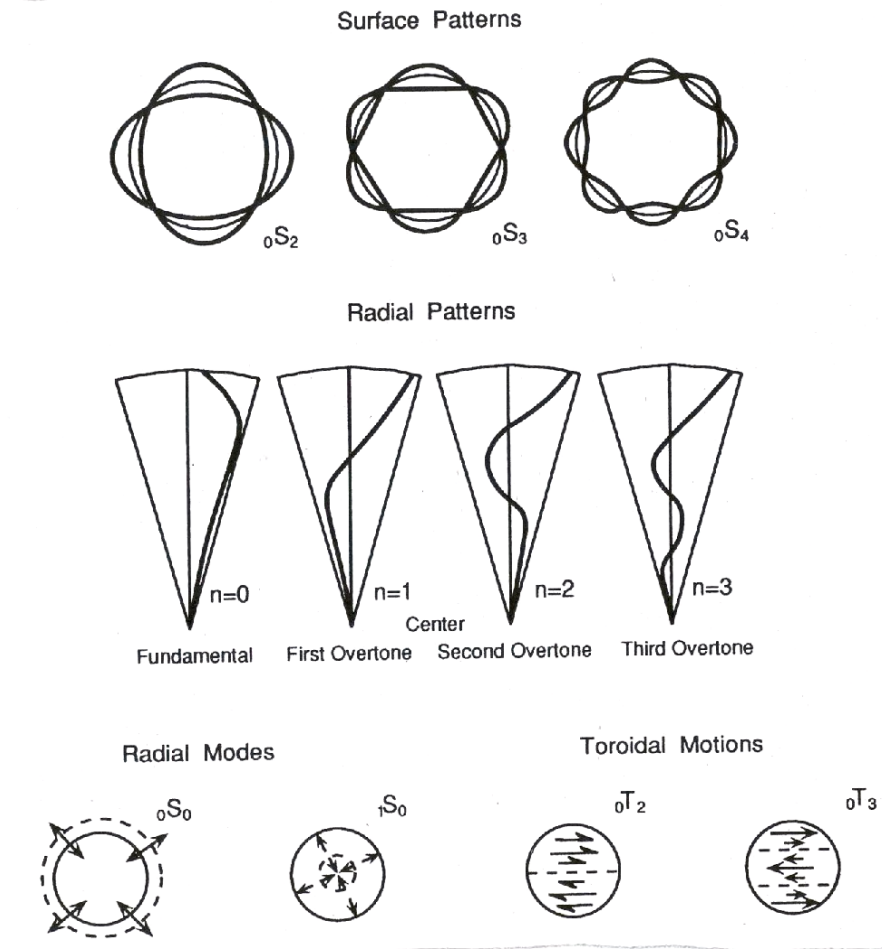


For a sphere with a laterally homogeneous structure, the eigen functions can be written as,

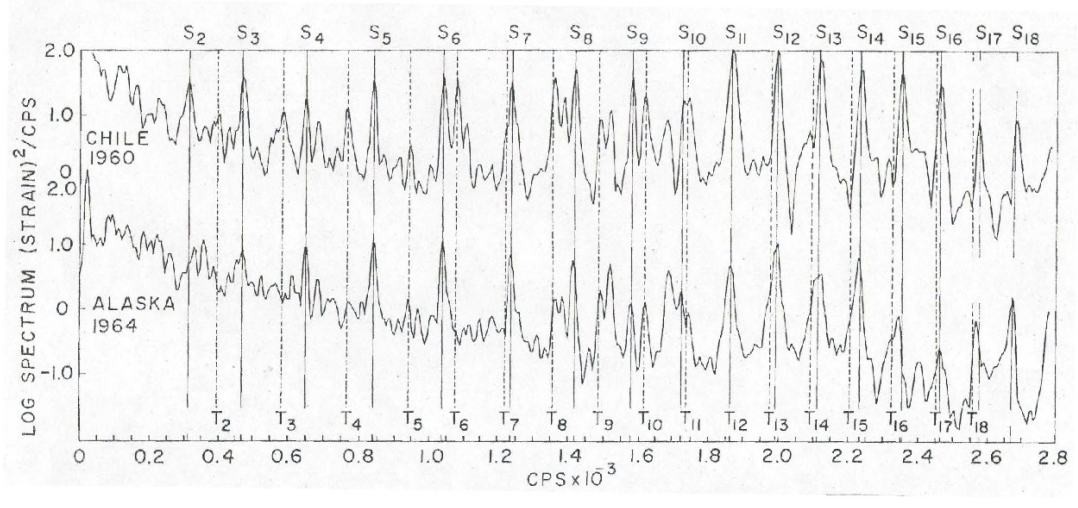
$${}_n y_l^m = A R_n(r) \Theta_l(\theta) \Phi_m(\phi) \quad (4)$$

For a homogeneous elastic sphere, $R_n(r)$ are Bessel functions, $\Theta_l(\theta)$ are (associated) Legendre functions and $\Phi_m(\phi)$ are trigonometric functions. The three indices l , m , and n determine the number of nodes in θ direction (meridional direction), ϕ direction (longitudinal direction) and r direction (radial direction).

In general eigen frequencies depend on l , m , and n and can be written as ${}_n \omega_l^m$. However, for a spherically symmetric, non-rotating Earth model, eigen frequencies do not depend on m .



Free oscillations of the Earth can be thought of as extensions of Love and Rayleigh waves propagating many times around the Earth. When Love waves propagate many times around the Earth, torsional free oscillations are set up. Similarly, when Rayleigh waves propagate around the Earth many times, spheroidal oscillations are set up. Torsional and spheroidal oscillations (modes) with order numbers l , m , and n are written as ${}_nT_l^m$ and ${}_nS_l^m$ and are shown in the attached figures and tables.

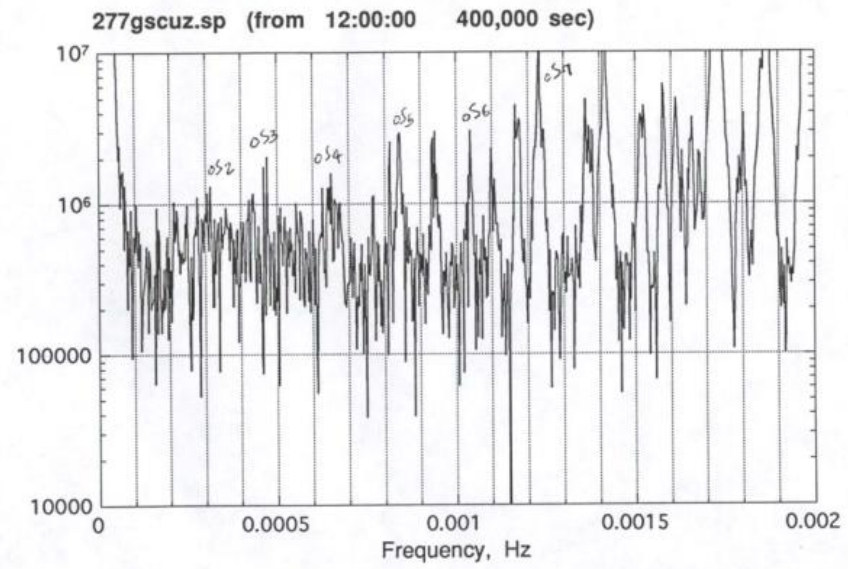


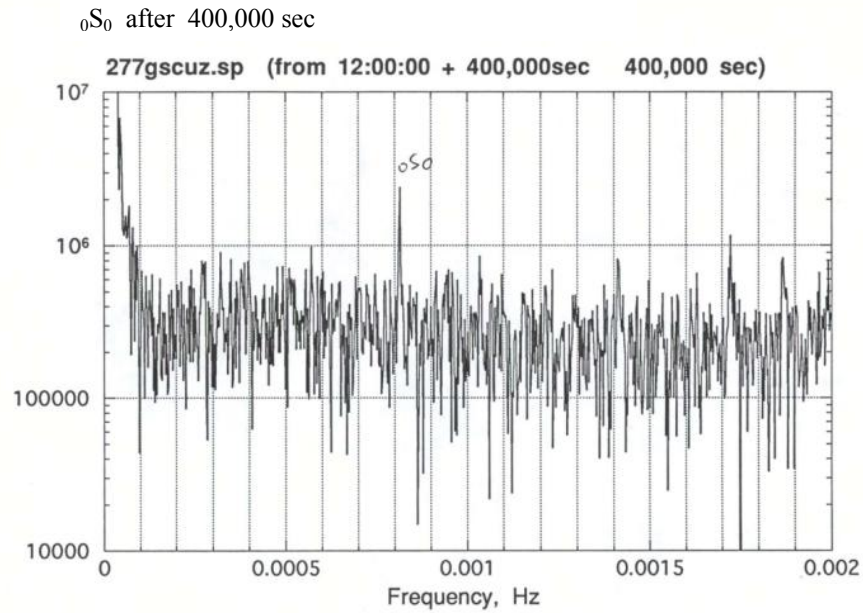
Some Observed Normal-Mode

Periods

Spheroidal modes	$T(s)$	Toroidal modes	$T(s)$
${}_0S_0$	1227.52	${}_0T_2$	2636.38
${}_0S_2$	3233.25	${}_0T_{10}$	618.97
${}_0S_{15}$	426.15	${}_0T_{20}$	360.03
${}_0S_{30}$	262.09	${}_0T_{30}$	257.76
${}_0S_{45}$	193.91	${}_0T_{40}$	200.95
${}_0S_{60}$	153.24	${}_0T_{50}$	164.70
${}_0S_{150}$	66.90	${}_0T_{60}$	139.46
${}_1S_2$	1470.85	${}_1T_2$	756.57
${}_1S_{10}$	465.46	${}_1T_{10}$	381.65
${}_2S_{10}$	415.92	${}_2T_{40}$	123.56

Spheroidal Modes, Bolivian Earthquake





4. Free Oscillations of the Earth --- Some Details ---

The equations of motion can be written using displacements and stresses expressed in spherical coordinates (r, θ, φ) . (Appendix 1)

Torsional Oscillations

We seek the solution in a form

$$\begin{pmatrix} u_r \\ u_\theta \\ u_\phi \end{pmatrix} = y_1(r) \begin{pmatrix} 0 \\ \frac{1}{\sin \theta} \frac{\partial Y_l^m}{\partial \phi} \\ -\frac{\partial Y_l^m}{\partial \theta} \end{pmatrix} e^{i\omega t} \quad (5)$$

$$Y_l^m(\theta, \phi) = P_l^m(\cos \theta)(A \cos m\phi + B \sin m\phi) \quad m=0, 1, 2, \dots, l \quad (6)$$

$$\bar{T}_l^m = \left(0, \frac{1}{\sin \theta} \frac{\partial Y_l^m}{\partial \phi}, -\frac{\partial Y_l^m}{\partial \theta}\right) \quad (7)$$

are called the vector spherical harmonics. It is easy to show that \bar{T}_l^m make up an orthogonal system:

$$\int_0^{2\pi} \int_0^\pi (\bar{T}_l^m \cdot \bar{T}_l^{m'}) \sin \theta d\theta d\phi = \frac{4\pi l(l+1)(l+m)!}{\varepsilon_m (2l+1)(l-m)!} \delta_{ll'} \delta_{mm'} \quad (8)$$

$$\varepsilon_m = 1 \quad \text{if } m = 0$$

$$\varepsilon_m = 2 \quad \text{if } m \neq 0$$

Substituting this into the equation of motion, we have

$$\mu \left(\frac{d^2 y_1}{dr^2} + \frac{2}{r} \frac{dy_1}{dr} \right) + \frac{d\mu}{dr} \left(\frac{dy_1}{dr} - \frac{y_1}{r} \right) + \left(\omega^2 \rho - \frac{l(l+1)}{r^2} \mu \right) y_1 = 0 \quad (9)$$

if we put

$$y_2(r) = \mu(r) \left(\frac{dy_1(r)}{dr} - \frac{y_1(r)}{r} \right)$$

(9) can be written as

$$\begin{aligned}\frac{dy_1(r)}{dr} &= \frac{1}{r} y_1(r) + \frac{1}{\mu} y_2(r) \\ \frac{dy_2(r)}{dr} &= \left(\frac{(l^2 + l - 2)}{r^2} \mu - \omega^2 \rho \right) y_1(r) - \frac{3}{r} y_2(r)\end{aligned}\quad (10)$$

The boundary conditions are

$$\sigma_{rr} = 0, \quad \sigma_{r\theta} = 0, \quad \sigma_{r\phi} = 0$$

at $r=r_1$ (the Earth's surface) and $r=r_2$ (core-mantle boundary).

Note that, using $y_2(r)$, we can write

$$\sigma_{r\theta} = y_2(r) \frac{1}{\sin \theta} \frac{\partial Y_l^m}{\partial \phi} e^{i\omega t} \quad \text{and} \quad \sigma_{r\phi} = -y_2(r) \frac{\partial Y_l^m}{\partial \theta} e^{i\omega t}$$

Thus, $y_2(r)$ gives the radial factor of stresses.

When $\mu=\text{const}$, the above equation can be reduced to

$$\frac{d^2 y_1}{dr^2} + \frac{2}{r} \frac{dy_1}{dr} + \left(\frac{\omega^2 \rho}{\mu} - \frac{l(l+1)}{r^2} \right) y_1 = 0 \quad (11)$$

Equation (11) is one of the variations of the Bessel's differential equation. The general solution is

$$y_1(r) \approx \frac{1}{\sqrt{r}} Z_{l+\frac{1}{2}}(kr) \quad (12)$$

$$k = \frac{\omega}{\sqrt{\mu / \rho}} \quad (13)$$

where $Z_l(\xi)$ represents a Bessel function.

In order to satisfy the boundary conditions, an appropriate kind of Bessel function should be taken and k must take certain discrete values ${}_n k$. Since (12) depends on l , these values depend on l , and we write these values as ${}_n k_l$. Using (13), the eigen frequencies ${}_n \omega_l$ can be given by

$${}_n \omega_l = {}_n k_l \sqrt{\frac{\mu}{\rho}}$$

Note that, since (11) does not contain m , the eigen values do not depend on m . Thus, there are $2l+1$ eigen functions belonging to ${}_n \omega_l$, i.e. there is degeneracy of $2l+1$ degree.

For a radially heterogeneous sphere where $\mu = \mu(r)$, the solution of (9) cannot be given by Bessel functions, but numerical integration of (10) with appropriate boundary conditions yields eigen functions similar to (12), and eigen values ${}_n \omega_l$. Since (10) does not contain m , the eigen values do not depend on m .

For large l , the asymptotic expansion of P_l^n gives

$$P_l^n \approx e^{m\pi i} m^l \sqrt{\frac{2}{\pi l \sin \theta}} \cos \left[\left(l + \frac{1}{2} \right) \theta + \frac{m}{2} \pi - \frac{\pi}{4} \right] \quad (14)$$

Thus, u_ϕ represents a wave propagating in θ direction. For $l \gg 1$, and $l \gg m$,

$$\left| \frac{\partial Y_l^m}{\partial \theta} \right| \approx l |Y_l^m| \quad \text{and} \quad \left| \frac{\partial Y_l^m}{\partial \phi} \right| \approx m |Y_l^m|$$

Thus, $|u_\phi| \gg |u_\theta|$, which represents "torsional" or "Love wave" motion.

Spheroidal Oscillation

We seek the solution in a form

$$\begin{pmatrix} u_r \\ u_\theta \\ u_\phi \end{pmatrix} = y_1(r) \begin{pmatrix} Y_l^m \\ 0 \\ 0 \end{pmatrix} e^{i\omega t} + y_3(r) \begin{pmatrix} 0 \\ \frac{\partial Y_l^m}{\partial \theta} \\ \frac{1}{\sin \theta} \frac{\partial Y_l^m}{\partial \phi} \end{pmatrix} e^{i\omega t} \quad (15)$$

where

$$\begin{aligned} \bar{S}_{1,l}^m &= (Y_l^m, 0, 0) \\ \bar{S}_{2,l}^m &= \left(0, \frac{\partial Y_l^m}{\partial \theta}, \frac{1}{\sin \theta} \frac{\partial Y_l^m}{\partial \phi}\right) \end{aligned}$$

are vector spherical harmonics which satisfy the orthogonality condition

$$\int_0^{2\pi} \int_0^\pi (\bar{S}_{2,l}^m \cdot \bar{S}_{2,l'}^{m'}) \sin \theta d\theta d\phi = \int_0^{2\pi} \int_0^\pi (\bar{S}_{1,l}^m \cdot \bar{S}_{1,l'}^{m'}) \sin \theta d\theta d\phi = \frac{4\pi l(l+1)(l+m)!}{\varepsilon_m (2l+1)(l-m)!} \delta_{l'l'} \delta_{mm'}$$

Using the expression (15), the equation of motion for a radially heterogeneous sphere can be reduced to a set of ordinary differential equations for y_1 and y_3 . It can be shown that y_1 and y_3 satisfy the orthogonality condition,

$$\int_{r_1}^{r_2} \rho r^2 [y_{1,n} y_{1,n'} + l(l+1) y_{3,n} y_{3,n'}] dr = C \delta_{nn'}$$

and the eigen values ${}_n \omega_l$ do not depend on m .

For $l \gg 1$ and $l \gg m$, $|\mu_r|$ and $|\mu_\theta|$ become much larger than $|\mu_\phi|$, and the displacement field represents "spheroidal" or "Rayleigh wave" motion.

Appendix 1 Cartesian, Cylindrical, and Spherical Coordinates

Strain Tensor

\bar{u} : Displacement Vector

Cartesian Coordinates (x_1, x_2, x_3)

$$e_{ik} = \frac{1}{2} \left(\frac{\partial u_i}{\partial x_k} + \frac{\partial u_k}{\partial x_i} \right)$$

Cylindrical Coordinates (r, ϕ, z)

$$\begin{aligned} e_{rr} &= \frac{\partial u_r}{\partial r}, \quad e_{\phi\phi} = \frac{1}{r} \frac{\partial u_\phi}{\partial \phi} + \frac{u_r}{r}, \quad e_{zz} = \frac{\partial u_z}{\partial z} \\ 2e_{z\phi} &= \frac{1}{r} \frac{\partial u_z}{\partial \phi} + \frac{\partial u_\phi}{\partial z}, \quad 2e_{rz} = \frac{\partial u_r}{\partial z} + \frac{\partial u_z}{\partial r} \\ 2e_{r\phi} &= \frac{\partial u_\phi}{\partial r} - \frac{u_\phi}{r} + \frac{1}{r} \frac{\partial u_r}{\partial \phi} \end{aligned}$$

Spherical Coordinates (r, θ, ϕ)

$$\begin{aligned} e_{rr} &= \frac{\partial u_r}{\partial r}, \quad e_{\theta\theta} = \frac{1}{r} \frac{\partial u_\theta}{\partial \theta} + \frac{u_r}{r}, \quad e_{\phi\phi} = \frac{1}{r \sin \theta} \frac{\partial u_\phi}{\partial \phi} + \frac{u_\theta}{r} \cot \theta + \frac{u_r}{r} \\ 2e_{\theta\phi} &= \frac{1}{r} \left(\frac{\partial u_\phi}{\partial \theta} - u_\phi \cot \theta \right) + \frac{1}{r \sin \theta} \frac{\partial u_\theta}{\partial \phi}, \quad 2e_{r\theta} = \frac{\partial u_\theta}{\partial r} - \frac{u_\theta}{r} + \frac{1}{r} \frac{\partial u_r}{\partial \theta} \\ 2e_{r\phi} &= \frac{1}{r \sin \theta} \frac{\partial u_r}{\partial \phi} + \frac{\partial u_\phi}{\partial r} - \frac{u_\phi}{r} \end{aligned}$$

Stress-Strain Relation

For all coordinate systems,

$$\sigma_{ij} = \lambda \delta_{ij} e_{ll} + 2\mu e_{ij}$$

Cartesian Coordinate $(1, 2, 3) \rightarrow (x_1, x_2, x_3)$

Cylindrical Coordinates $(1, 2, 3) \rightarrow (r, \phi, z)$

Spherical Coordinates $(1, 2, 3) \rightarrow (r, \theta, \phi)$

Examples

$$\sigma_{xx} = \lambda(e_{xx} + e_{yy} + e_{zz}) + 2\mu e_{xx}$$

$$\sigma_{xy} = 2\mu e_{xy}$$

$$\sigma_{\theta\theta} = \lambda(e_{rr} + e_{\theta\theta} + e_{\phi\phi}) + 2\mu e_{\theta\theta}$$

$$\sigma_{r\phi} = 2\mu e_{r\phi}$$

Equations of Motion

Cartesian Coordinates (x_1, x_2, x_3)

$$\rho \frac{\partial^2 u_i}{\partial t^2} = \rho f_i + \frac{\partial \sigma_{ik}}{\partial x_k}$$

Cylindrical Coordinates (r, ϕ, z)

$$\rho \frac{\partial^2}{\partial t^2} \begin{pmatrix} u_r \\ u_\phi \\ u_z \end{pmatrix} = \rho \begin{pmatrix} f_r \\ f_\phi \\ f_z \end{pmatrix} + \frac{1}{r} \frac{\partial}{\partial r} \begin{pmatrix} r\sigma_{rr} \\ r\sigma_{\phi r} \\ r\sigma_{zr} \end{pmatrix} + \frac{1}{r} \frac{\partial}{\partial \phi} \begin{pmatrix} \sigma_{r\phi} \\ \sigma_{\phi\phi} \\ \sigma_{z\phi} \end{pmatrix} + \frac{\partial}{\partial z} \begin{pmatrix} \sigma_{rz} \\ \sigma_{\phi z} \\ \sigma_{zz} \end{pmatrix} + \frac{1}{r} \begin{pmatrix} -\sigma_{\phi\phi} \\ \sigma_{r\phi} \\ 0 \end{pmatrix}$$

Spherical Coordinates (r, θ, ϕ)

$$\rho \frac{\partial^2}{\partial t^2} \begin{pmatrix} u_r \\ u_\theta \\ u_\phi \end{pmatrix} = \rho \begin{pmatrix} f_r \\ f_\theta \\ f_\phi \end{pmatrix} + \frac{1}{r^2} \frac{\partial}{\partial r} \begin{pmatrix} r^2 \sigma_{rr} \\ r^2 \sigma_{\theta r} \\ r^2 \sigma_{\phi r} \end{pmatrix} + \frac{1}{r \sin \theta} \frac{\partial}{\partial \theta} \begin{pmatrix} \sin \theta \sigma_{r\theta} \\ \sin \theta \sigma_{\theta\theta} \\ \sin \theta \sigma_{\phi\theta} \end{pmatrix} + \frac{1}{r \sin \theta} \frac{\partial}{\partial \phi} \begin{pmatrix} \sigma_{r\phi} \\ \sigma_{\theta\phi} \\ \sigma_{\phi\phi} \end{pmatrix} + \frac{1}{r} \begin{pmatrix} -\sigma_{\theta\theta} - \sigma_{\phi\phi} \\ \sigma_{r\theta} - \sigma_{\phi\phi} \cot \theta \\ \sigma_{\phi r} + \sigma_{\theta\phi} \cot \theta \end{pmatrix}$$

Appendix 2

Bessel Functions

$J_\nu(z)$, 1st kind, Bessel Function

$N_\nu(z)$, 2nd kind, Neumann Function

$H_\nu^{(1)}(z) = J_\nu(z) + iN_\nu(z)$, Hankel Function 1st kind

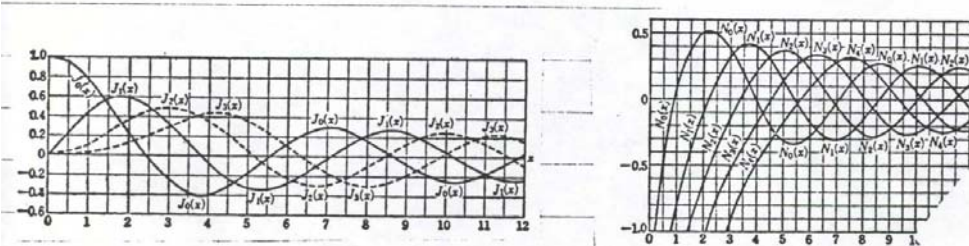
$H_\nu^{(2)}(z) = J_\nu(z) - iN_\nu(z)$, Hankel Function 2nd kind

$$J_{1/2}(z) = \sqrt{\frac{2}{\pi z}} \sin z, \quad J_{-1/2}(z) = \sqrt{\frac{2}{\pi z}} \cos z$$

$$J_{3/2}(z) = \sqrt{\frac{2}{\pi z}} \left(\frac{\sin z}{z} - \cos z \right), \quad J_{-3/2}(z) = -\sqrt{\frac{2}{\pi z}} \left(\sin z + \frac{\cos z}{z} \right)$$

$$J_{5/2}(z) = \sqrt{\frac{2}{\pi z}} \left(\left(\frac{3}{z^2} - 1 \right) \sin z - \frac{3}{z} \cos z \right)$$

$$J_{-5/2}(z) = \sqrt{\frac{2}{\pi z}} \left(\frac{3}{z} \sin z + \left(\frac{3}{z^2} - 1 \right) \cos z \right)$$



Appendix 3

Legendre Functions

$$P_n(x) = \frac{1}{2^n n!} \frac{d^n}{dx^n} (x^2 - 1)^n$$

$$x = \cos \theta$$

$$P_0(x) = 1, \quad P_1(x) = x = \cos \theta,$$

$$P_2(x) = (1/2)(3x^2 - 1) = (1/4)(3 \cos 2\theta + 1),$$

$$P_3(x) = (1/2)(5x^3 - 3x) = (1/8)(5 \cos 3\theta + 3 \cos \theta),$$

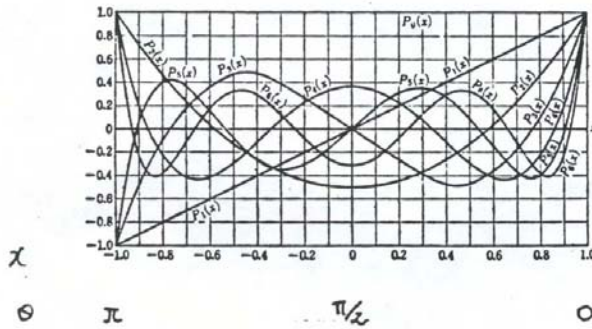
$$P_4(x) = (1/8)(35x^4 - 30x^2 + 3) = (1/64)(35 \cos 4\theta + 20 \cos 2\theta + 9),$$

$$P_5(x) = (1/8)(63x^5 - 70x^3 + 15x) \\ = (1/128)(63 \cos 5\theta + 35 \cos 3\theta + 30 \cos \theta),$$

$$P_6(x) = (1/16)(231x^6 - 315x^4 + 105x^2 - 5) \\ = (1/512)(231 \cos 6\theta + 126 \cos 4\theta + 105 \cos 2\theta + 50),$$

$$P_7(x) = (1/16)(429x^7 - 693x^5 + 315x^3 - 35x) \\ = (1/2^{10})(429 \cos 7\theta + 231 \cos 5\theta + 189 \cos 3\theta + 175 \cos \theta),$$

$$P_8(x) = (1/128)(6435x^8 - 12012x^6 + 6930x^4 - 1260x^2 + 35) \\ = (1/2^{14})(6435 \cos 8\theta + 3432 \cos 6\theta + 2772 \cos 4\theta \\ + 2520 \cos 2\theta + 1225).$$



Associated Legendre Functions

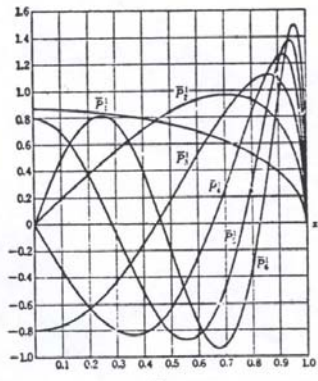
$$P_h^m(x) = \frac{(1-x^2)^{\frac{m}{2}}}{n! 2^n} \frac{d^{n+m}}{dx^{n+m}} (1-x^2)^n$$

$$= (1-x^2)^{\frac{m}{2}} \frac{d^m}{dx^m} P_n(x)$$

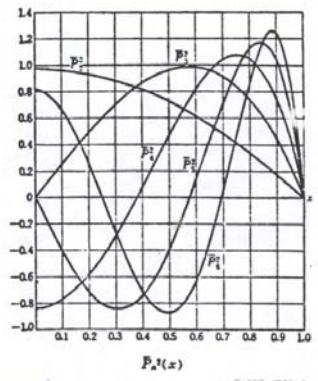
$P_1^1(x) = (1-x^2)^{1/2} = \sin \theta$
 $P_2^1(x) = 3(1-x^2)^{1/2}x = 3 \sin \theta \cos \theta = (3/2)(1-\cos 2\theta)$
 $P_2^2(x) = 3(1-x^2) = 3 \sin^2 \theta = (3/2)(1-\cos 2\theta)$
 $P_3^1(x) = (3/2)(1-x^2)^{1/2}(5x^2-1) = (3/8)(\sin \theta + 5 \sin 3\theta)$
 $P_3^2(x) = 15(1-x^2)x = (15/4)(\cos \theta - \cos 3\theta)$
 $P_3^3(x) = 15(1-x^2)^{3/2} = 15 \sin^3 \theta = (15/4)(3 \sin \theta - \sin 3\theta)$
 $P_4^1(x) = (5/2)(1-x^2)^{1/2}x(7x^2-3) = (5/16)(2 \sin 2\theta + 7 \sin 4\theta)$
 $P_4^2(x) = (15/2)(1-x^2)(7x^2-1) = (15/16)(3+4 \cos 2\theta - 7 \cos 4\theta)$
 $P_4^3(x) = 105(1-x^2)^{3/2}x = (105/8)(2 \sin 2\theta - \sin 4\theta)$
 $P_4^4(x) = 105(1-x^2)^2 = 105 \sin^4 \theta = (105/8)(3-4 \cos 2\theta + \cos 4\theta)$

$P_5^1(x) = (15/8)(1-x^2)^{1/2}(21x^4-14x^2+1)$
 $= (15/2^7)(2 \sin \theta + 7 \sin 3\theta + 21 \sin 5\theta)$
 $P_5^2(x) = (105/2)(1-x^2)x(3x^2-1)$
 $= (105/32)(2 \cos \theta + \cos 3\theta - 3 \cos 5\theta)$
 $P_5^3(x) = (105/2)(1-x^2)^{3/2}(9x^2-1)$
 $= (105/32)(6 \sin \theta + 13 \sin 3\theta - 9 \sin 5\theta)$
 $P_5^4(x) = 945(1-x^2)^2x = (945/16)(2 \cos \theta - 3 \cos 3\theta + \cos 5\theta)$
 $P_5^5(x) = 945(1-x^2)^{5/2} = 3 \cdot 5 \cdot 7 \cdot 9 \sin^5 \theta$
 $= (945/16)(10 \sin \theta - 5 \sin 3\theta + \sin 5\theta)$
 $P_6^1(x) = (21/8)(1-x^2)^{1/2}x(33x^4-30x^2+5)$
 $= (21/2^6)(5 \sin 2\theta + 12 \sin 4\theta + 33 \sin 6\theta)$
 $P_6^2(x) = (105/8)(1-x^2)(33x^4-18x^2+1)$
 $= (105/2^6)(10+17 \cos 2\theta + 6 \cos 4\theta - 33 \cos 6\theta)$
 $P_6^3(x) = (315/2)(1-x^2)^{3/2}x(11x^2-3)$
 $= (315/64)(9 \sin 2\theta + 12 \sin 4\theta - 11 \sin 6\theta)$
 $P_6^4(x) = (945/2)(1-x^2)^2(11x^2-1)$
 $= (945/64)(10+5 \cos 2\theta - 26 \cos 4\theta + 11 \cos 6\theta)$
 $P_6^5(x) = 10395(1-x^2)^{5/2}x = (10395/32)(5 \sin 2\theta - 4 \sin 4\theta + \sin 6\theta)$
 $P_6^6(x) = 10395(1-x^2)^3 = 3 \cdot 5 \cdot 7 \cdot 9 \cdot 11 \sin^6 \theta$
 $= (10395/32)(10-15 \cos 2\theta + 6 \cos 4\theta - \cos 6\theta)$
 $P_7^1(x) = (7/16)(1-x^2)^{1/2}(429x^6-495x^4+135x^2-5)$
 $= (7/2^{10})(25 \sin \theta + 81 \sin 3\theta + 165 \sin 5\theta + 429 \sin 7\theta)$
 $P_7^2(x) = (63/8)(1-x^2)x(143x^4-110x^2+15)$
 $= (63/2^8)(75 \cos \theta + 57 \cos 3\theta + 11 \cos 5\theta - 143 \cos 7\theta)$
 $P_7^3(x) = (315/8)(1-x^2)^{3/2}(143x^4-66x^2+3)$
 $= (315/2^8)(45 \sin \theta + 117 \sin 3\theta + 121 \sin 5\theta - 143 \sin 7\theta)$
 $P_7^4(x) = (3465/2)(1-x^2)^2x(13x^2-3)$
 $= (3465/2^7)(15 \cos \theta - 3 \cos 3\theta - 25 \cos 5\theta + 13 \cos 7\theta)$
 $P_7^5(x) = (10395/2)(1-x^2)^{5/2}(13x^2-1)$
 $= (10395/2^7)(25 \sin \theta + 33 \sin 3\theta - 43 \sin 5\theta + 13 \sin 7\theta)$

$P_7^6(x) = 135135x(1-x^2)^3$
 $= (135135/2^7)(5 \cos \theta - 9 \cos 3\theta + 5 \cos 5\theta + \cos 7\theta)$
 $P_7^7(x) = 135135(1-x^2)^{7/2} = 3 \cdot 5 \cdot 7 \cdot 9 \cdot 11 \cdot 13 \sin^7 \theta$
 $= (135135/2^8)(35 \sin \theta - 21 \sin 3\theta + 7 \sin 5\theta - \sin 7\theta)$
 $P_8^1(x) = (9/16)(1-x^2)^{1/2}x(715x^6-1001x^4+385x^2-35)$
 $= (9/2^{11})(70 \sin 2\theta + 154 \sin 4\theta + 286 \sin 6\theta + 715 \sin 8\theta)$
 $P_8^2(x) = (315/16)(1-x^2)(143x^6-143x^4+33x^2-1)$
 $= (315/2^{11})(35+274 \cos 2\theta + 44 \cos 4\theta - 143 \cos 6\theta)$
 $P_8^3(x) = (3465/8)(1-x^2)^{3/2}x(39x^4-26x^2+3)$
 $= (3465/2^{10})(18 \sin 2\theta + 30 \sin 4\theta + 26 \sin 6\theta - 39 \sin 8\theta)$
 $P_8^4(x) = (10395/8)(1-x^2)^2(65x^4-26x^2+1)$
 $= (10395/2^{10})(35+40 \cos 2\theta - 36 \cos 4\theta - 104 \cos 6\theta + 65 \cos 8\theta)$
 $P_8^5(x) = (135135/2)(1-x^2)^{5/2}x(5x^2-1)$
 $= (135135/2^{10})(10 \sin 2\theta + 6 \sin 4\theta - 14 \sin 6\theta + 5 \sin 8\theta)$
 $P_8^6(x) = (135135/2)(1-x^2)^3(15x^2-1)$
 $= (135135/2^9)(35-84 \cos 2\theta + 64 \cos 4\theta - 15 \cos 6\theta)$
 $P_8^7(x) = 2027025x(1-x^2)^4$
 $= (2027025/2^7)(14 \sin 2\theta - 14 \sin 4\theta + 6 \sin 6\theta - \sin 8\theta)$
 $P_8^8(x) = 2027025(1-x^2)^4 = 3 \cdot 5 \cdot 7 \cdot 9 \cdot 11 \cdot 13 \cdot 15 \sin^8 \theta$
 $= (2027025/2^7)(35-56 \cos 2\theta + 28 \cos 4\theta - 8 \cos 6\theta + \cos 8\theta)$



$$\bar{P}_n^m(x) = \sqrt{\frac{2n+1}{2} \frac{(n-m)!}{(n+m)!}} P_n^m(x)$$



Ge 162

4.1 Herglotz-Wiechert Method (LW, pp. 236-240)

Assume that $T(\Delta)$ and $p(\Delta)$ are continuous functions of Δ , as shown in Figures 1 and 2.

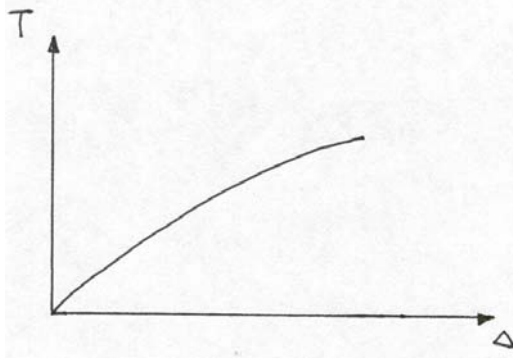


Fig.1

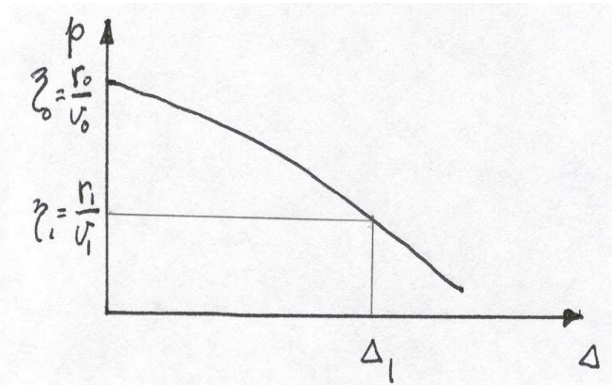


Fig. 2

Then, from Figure 3, $\tan i = r \frac{d\Delta}{dr}$. Since $p = \frac{r}{v} \sin i$,

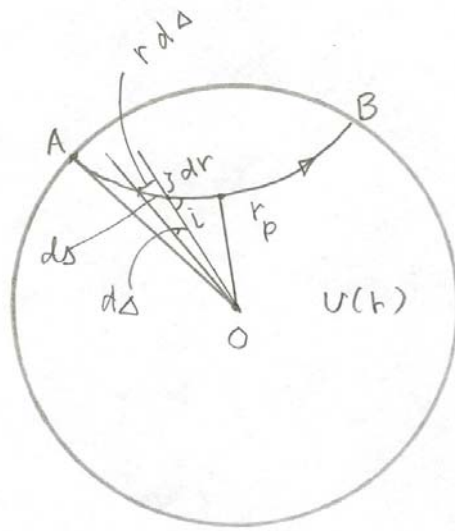


Fig. 3

$$d\Delta = \frac{p}{r \sqrt{\left(\frac{r}{v}\right)^2 - p^2}} dr \quad (1)$$

$$\Delta(p) = 2 \int_{r_p}^{r_0} \frac{p}{r \sqrt{\left(\frac{r}{v}\right)^2 - p^2}} dr \quad (2)$$

where the suffix 0 denotes the values at the surface (i.e., $r = r_0$) and r_p is the radial distance of the deepest point of a ray.

Introducing a new variable, $\eta = \frac{r}{v}$

$$\Delta(p) = 2 \int_p^{\eta_0} \frac{p}{r \sqrt{\eta^2 - p^2}} \frac{dr}{d\eta} d\eta \quad (3)$$

$\Delta(p)$ is known from observation, and $\eta(r) = \frac{r}{v(r)}$, or $v(r)$ is a unknown function of r which we wish to determine. (Note that since $p = \frac{r}{v} \sin i$, $p = \eta$ at the deepest point of the ray where $i = \pi/2$.)

Mathematically, this is a Volterra's integral equation of the second kind. The solution can be given by,

$$r_1 = r_0 \exp \left[-\frac{1}{\pi} \int_0^{\Delta_1} \ln \left[\left(\frac{p}{\eta_1} \right) + \sqrt{\left(\frac{p}{\eta_1} \right)^2 - 1} \right] d\Delta \right] \quad (11)$$

The suffix 1 is used to denote values of variables at the level r_1 , and let Δ_1 be the value of Δ for the ray whose deepest point is at r_1 .

To solve this, multiply (3) by $\frac{1}{\sqrt{p^2 - \eta_1^2}}$ and integrate with p from η_1 to η_0 (see Figure 4).

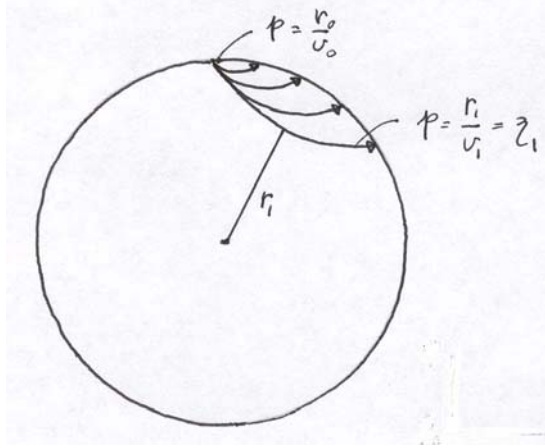


Fig. 4

The suffix 1 is used to denote values of variables at the level r_1 , and let Δ_1 be the value of Δ for the ray whose deepest point is at r_1 .

$$\int_{\eta_1}^{\eta_0} \Delta(p) \frac{1}{\sqrt{p^2 - \eta_1^2}} dp = 2 \int_{\eta_1}^{\eta_0} \frac{dp}{\sqrt{p^2 - \eta_1^2}} \int_p^{\eta_0} \frac{p}{r \sqrt{\eta^2 - p^2}} \frac{dr}{d\eta} d\eta \quad (4)$$

$$\text{LHS} = \Delta(p) \cosh^{-1} \left(\frac{p}{\eta_1} \right) \Big|_{\eta_1}^{\eta_0} - \int_{\eta_1}^{\eta_0} \frac{d\Delta}{dp} \cosh^{-1} \left(\frac{p}{\eta_1} \right) dp \quad (5)$$

Since $\Delta(\eta_0) = 0$ and $\cosh^{-1} \left(\frac{\eta_1}{\eta_1} \right) = \cosh^{-1}(1) = 0$,

$$\text{LHS} = - \int_{\Delta_1}^0 \cosh^{-1} \left(\frac{p}{\eta_1} \right) d\Delta \quad (6)$$

To evaluate the integral of RHS, we change the order of integration (see Figure 5),

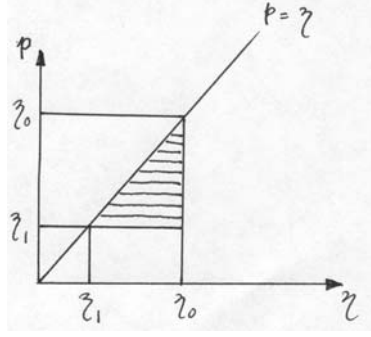


Fig. 5

$$\text{RHS} = 2 \int_{\eta_1}^{\eta_0} \frac{1}{r} \frac{dr}{d\eta} d\eta \int_{\eta_1}^{\eta} \frac{1}{\sqrt{p^2 - \eta_1^2}} \frac{p}{\sqrt{\eta^2 - p^2}} dp \quad (7)$$

Introducing θ , by

$$\sin^2 \theta = \frac{\sqrt{p^2 - \eta_1^2}}{\sqrt{\eta^2 - \eta_1^2}}$$

we obtain,

$$\int_{\eta_1}^{\eta} \frac{1}{\sqrt{p^2 - \eta_1^2}} \frac{p}{\sqrt{\eta^2 - p^2}} dp = \int_0^{\frac{\pi}{2}} d\theta = \frac{\pi}{2} \quad (8)$$

Then,

$$\text{RHS} = \pi \int_{r_1}^{r_0} \frac{1}{r} dr = \pi \ln \left(\frac{r_0}{r_1} \right) \quad (9)$$

Hence.

$$\pi \ln \left(\frac{r_0}{r_1} \right) = \int_0^{\Delta_1} \cosh^{-1} \left(\frac{p}{\eta_1} \right) d\Delta = \int_0^{\Delta_1} \ln \left[\left(\frac{p}{\eta_1} \right) + \sqrt{\left(\frac{p}{\eta_1} \right)^2 - 1} \right] d\Delta \quad (10)$$

or,

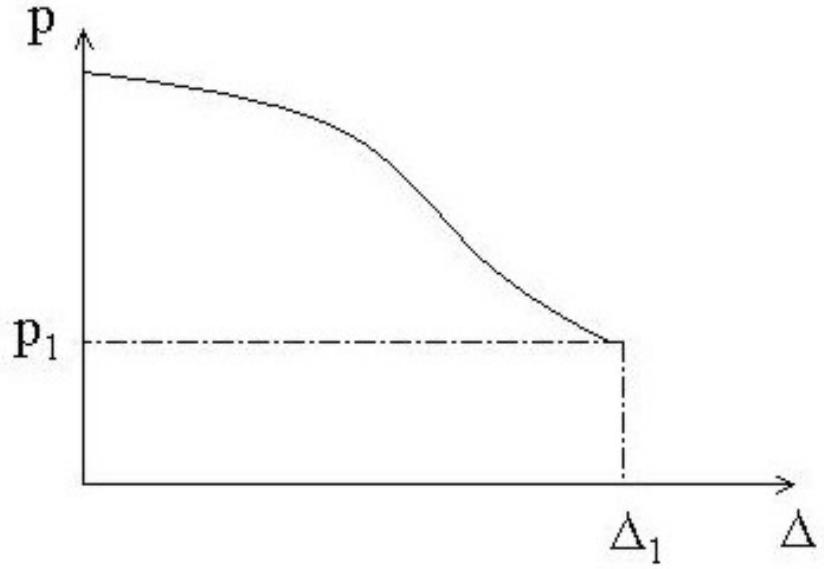
$$r_1 = r_0 \exp \left[-\frac{1}{\pi} \int_0^{\Delta_1} \ln \left[\left(\frac{p}{\eta_1} \right) + \sqrt{\left(\frac{p}{\eta_1} \right)^2 - 1} \right] d\Delta \right] \quad (11)$$

If $p(\Delta)$ is known, RHS of (11) can be evaluated for a given η_1 to determine r_1 (η_1 is the apparent velocity at $\Delta = \Delta_1$). Once r_1 is determined, v_1 is given by $v_1 = \frac{r_1}{\eta_1}$. More details are in the practice session.

Ge 162 Practice Session 4 Herglotz-Wiechert Method

The Herglotz-Wiechert (H-W) method is an elegant 'inversion' method which determines the velocity distribution in the Earth from a given p - Δ curve obtained from the observation. It is essential that a p - Δ curve is given continuously as a function of Δ . If a low-velocity zone exists and a shadow zone is produced, then the travel time curve is segmented. In this case the p - Δ curve is not continuous and the H-W method cannot be used. In general, the H-W method is applicable to a structure without low-velocity zones. This is the limitation of the method.

Figure 1 gives a p - Δ curve.



From equations (11) in class note, we obtain,

$$r_1 = r_0 \exp \left[-\frac{1}{\pi} \int_0^{\Delta_1} \ln \left[\left(\frac{p}{\eta_1} \right) + \sqrt{\left(\frac{p}{\eta_1} \right)^2 - 1} \right] d\Delta \right] \quad (1)$$

where

$$\eta(r) = \frac{r}{v(r)} \quad (2)$$

Here, r_1 is the radial distance to the bottoming point of the ray reaching the distance Δ_1 , and

$$\eta_1 = \frac{r_1}{v(r_1)} \quad (3)$$

Since $i = \pi/2$ at the bottoming point, the ray parameter for the ray reaching $\Delta = \Delta_1$ is given by

$$p_1 = \frac{r_1}{v(r_1)} \sin i_1 = \frac{r_1}{v(r_1)} \equiv \eta_1 \quad (4)$$

Thus, if a p - Δ curve is given, then for a given Δ_1 , we can determine η_1 . Then, we can integrate (1) to obtain r_1 . Once r_1 is determined, then $v(r_1)$ can be computed from

$$v(r_1) = \frac{r_1}{\eta_1} \quad (5)$$

Doing this for all Δ_1 , we can determine $v(r)$ as a function of r .

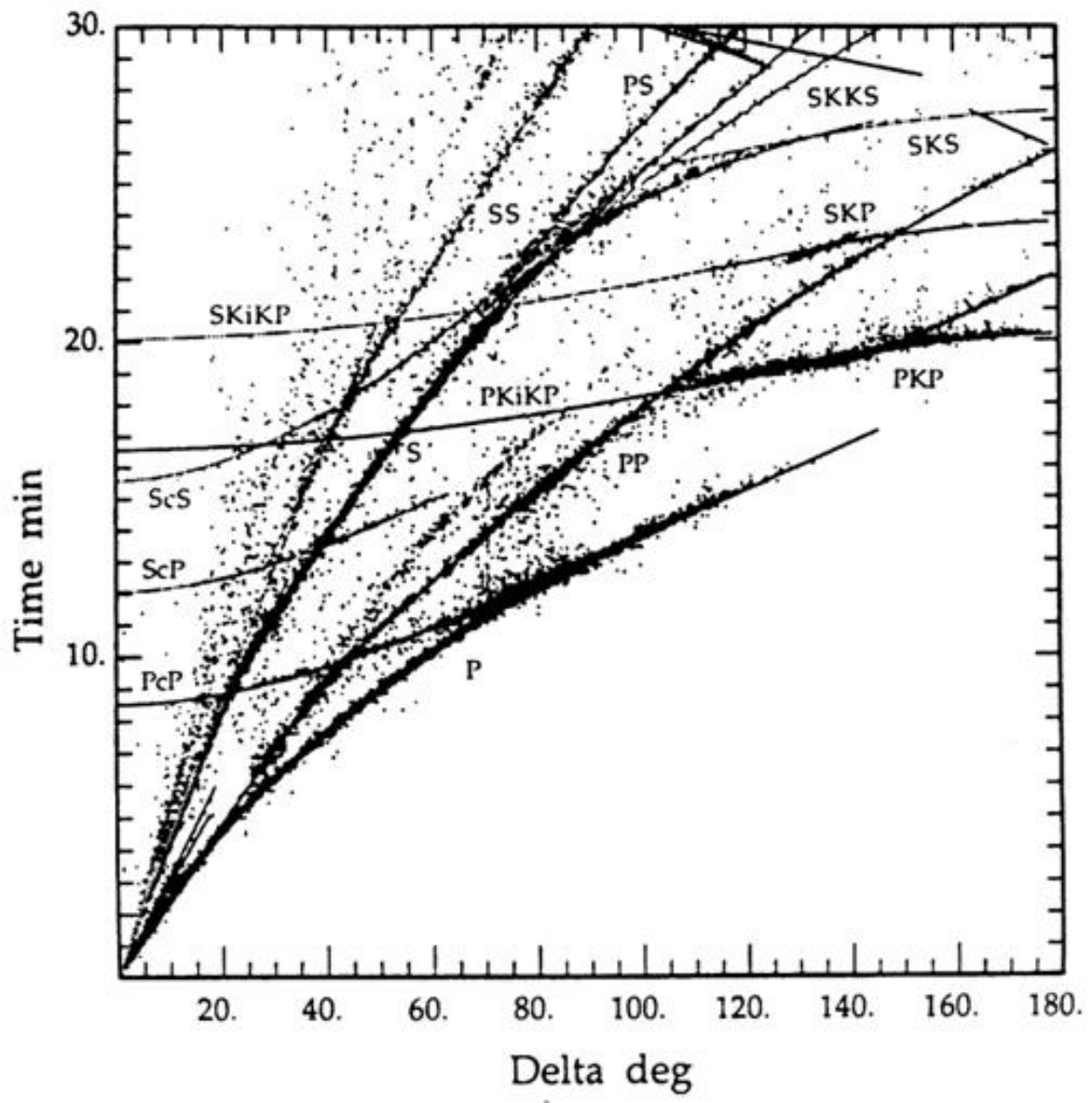
1. The following table shows the travel times (2nd column) which are consistent with the ISC travel-time curve given in class handout. Then the travel time data are numerically differentiated to compute the ray parameter p which is shown on the 3rd column. The unit of p is sec (i.e., the unit of the distance is converted to radian in this computation.). The following table lists the data up to $\Delta = 30^\circ$, and a more complete table up to $\Delta = 98^\circ$ is given in `i_p-delta_2` in `/home/ftp/pub/hiroo/ge162.dir/practice_4.dir`.

Plot the travel time and p in `i_p-delta_2` as a function of distance, and make sure that the travel times are consistent with the ISC data. Also, check the consistency between t and p . An enlarged travel-time curve is shown below. (Spot checks at $\Delta = 30^\circ, 60^\circ, 90^\circ$ are sufficient.)

Table

dist(deg)	t(sec)	p(sec)
0.00000	0.00000	1145.91516
2.00000	35.38889	828.24194
4.00000	63.90000	813.59973
6.00000	92.22500	807.87048

8.00000	120.30000	802.14056
10.00000	147.98334	788.77106
12.00000	175.25000	773.49268
14.00000	201.87500	753.43927
16.00000	227.92500	736.25037
18.00000	253.14999	710.46747
20.00000	276.72501	627.38831
22.00000	297.45001	572.95752
24.00000	317.10001	555.76868
26.00000	336.14999	532.85071
28.00000	354.47501	518.52673
30.00000	372.45001	509.93188
.....



2. Then, compute r_1 for $\Delta_1=0^\circ$ to 98° at 2° intervals by carrying out the integral given by (1)*.
3. Then, from r_1 thus computed and η_1 , determine $v(r_1)$.
4. Plot $v(r_1)$ as a function of r_1 , and compare the result with the P -wave structure shown in class handout (section 2.1, a numerical table, jeffreys_model, for the Jeffreys model is in practice_4.dir).

* Preferably, you should write a simple integration program (trapezoidal rule is adequate), but if you find it difficult, a simple program hw3.f is provided in practice_4.dir.

Note: The trapezoidal rule is given by,

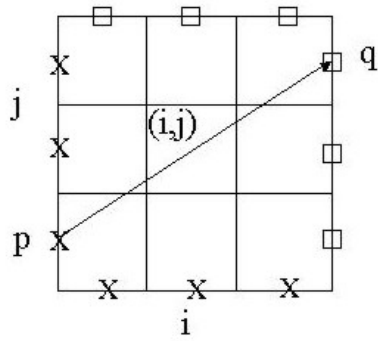
$$\int_0^L f(x)dx \approx \sum_{i=2}^N (f_{i-1} + f_i)\Delta x / 2, \text{ where } \Delta x = L/(N-1), \text{ and } f_i = f((i-1)*\Delta x)$$

Ge162

4.2 Tomography (LW, pp. 240-249)

The structure of the Earth is heterogeneous in 3 dimensions. To determine such a 3-dimensional structure, various tomographic methods are used. The basic principle can be illustrated as follows.

Consider a square area as shown in the figure.



Then, assume that seismic sources (X) and stations (square) are distributed on the sides. The velocity is a function of space. Divide the whole area into cells (i, j) . The wave speed in cell (i, j) is v_{ij} (or slowness $s_{ij} = 1/v_{ij}$) which we wish to determine from observations. If we assume that the ray paths are straight (this assumption is not valid in general for heterogeneous media). The travel time from source p to station q can be written as

$$t_{pq} = \sum_{i,j} l_{ijpq} / v_{ij} = \sum_{i,j} l_{ijpq} s_{ij} \quad (1)$$

where l_{ijpq} is the path length in the (i, j) cell for the p-q source-station ray. If the geometry and paths are fixed, as in this case, the problem is linear, but the problem is in general nonlinear, and the problem is usually linearized, as is done in the earthquake location problem.

If the problem is linear, or is linearized, (1) can be solved by the method of least squares or some other inversion methods.

We renumber the cells sequentially such that

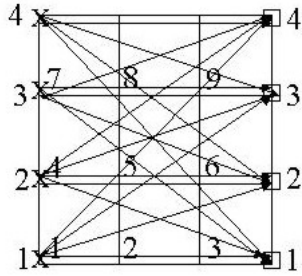
$$k = i + (j-1)n_x$$

where n_x is the number of cells in a row. Then (1) can be written as

$$t_{pq} = \sum_k l_{kpq} s_k \quad (2)$$

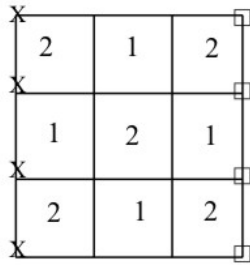
Simple examples are given in the following.

If we place the sources $p=1, 2, 3,$ and $4,$ and the receivers $q=1, 2, 3,$ and $4,$ as shown, we can have the ray geometry as shown in the following figure.



cross-hole

Then equation (2) can be written as



The solution is given as follows.

```

checker_b
cross_hole_simple
cell      s      Δs
1:      1.892    0.011
2:      1.218    0.015
3:      1.890    0.011
4:      0.892    0.010
5:      2.219    0.010
6:      0.890    0.010
7:      1.891    0.011
8:      1.219    0.015
9:      1.890    0.011

RMS  of residual 0.01160

```

Actually, for this geometry the inverse problem is fairly ill-posed, and even if no noise is applied, the solution is unstable (i.e., the standard error is large), as shown above.

If random noise of up to 10% is added to t_{pq} , the error becomes very large, as shown below.

```

checker_b
cross_hole_simple
cell      s      Δs
1:      2.149    3.187
2:      0.646    4.242
3:      2.091    3.190
4:      1.110    2.745
5:      2.083    2.750
6:      0.687    2.743
7:      1.478    3.176
8:      2.104    4.222
9:      1.538    3.179

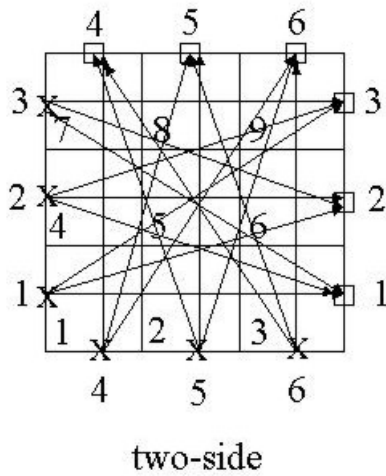
RMS  of residual  3.31218

```

This instability arises from the inadequate source-receiver geometry.

Example 2.

The source-receiver geometry is now changed to that shown in the following figure.



Then the solution becomes more stable as shown below.

No- noise case

```
checker_b
two_sides
cell      s      Δs
1:      1.999    0.001
2:      1.001    0.001
3:      1.999    0.001
4:      1.001    0.001
5:      2.000    0.001
6:      1.001    0.001
7:      1.999    0.001
8:      1.001    0.001
9:      1.999    0.001
```

RMS of residual 0.01479

With random noise of up to 10 %:

```
checker_b
two_sides
cell      s      Δs
1:      2.046    0.138
2:      0.922    0.154
3:      1.831    0.138
4:      0.856    0.154
5:      1.814    0.144
6:      1.222    0.154
7:      2.011    0.138
8:      1.062    0.154
9:      2.203    0.138
```

RMS of residual 2.90495

Caveats

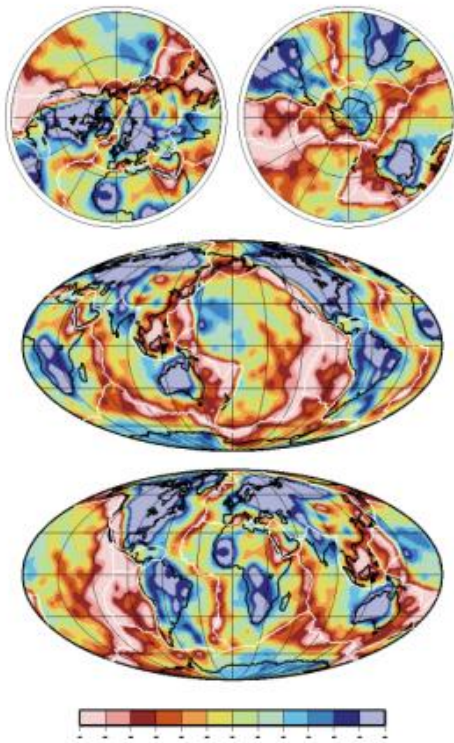
Although tomographic methods provide interesting 3-D structures of the Earth, the following caveats are in order.

1. The results depend on the initial parameterization of the cells and rays.
2. In a heterogeneous medium, the rays are not straight, and ray bending must be considered.
3. The effect of finite wave length must be considered in resolution.
4. The solutions are often regularized (damped) to avoid instability.

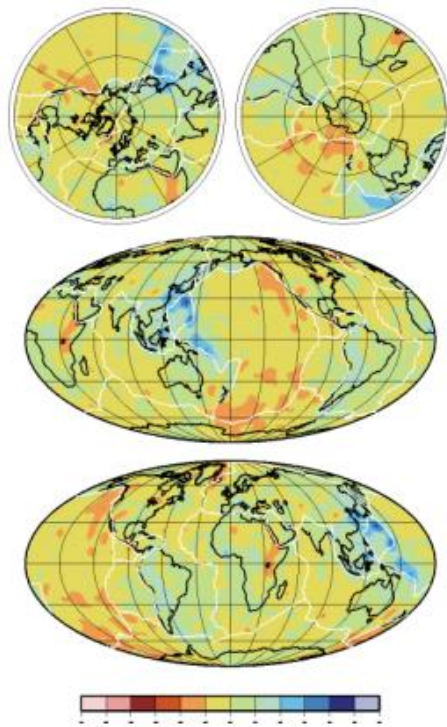
Several recent examples are shown in the following

Global Depth Slices

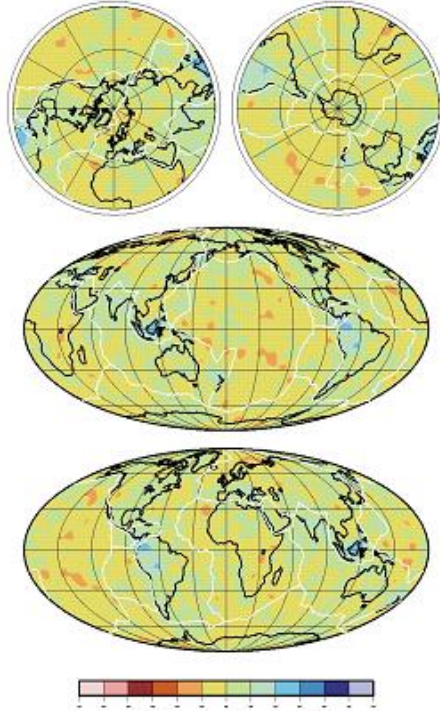
S30RTS
Ritsama & van Heijst [2001]
(100 km depth: -4% to +4% shear velocity variation)



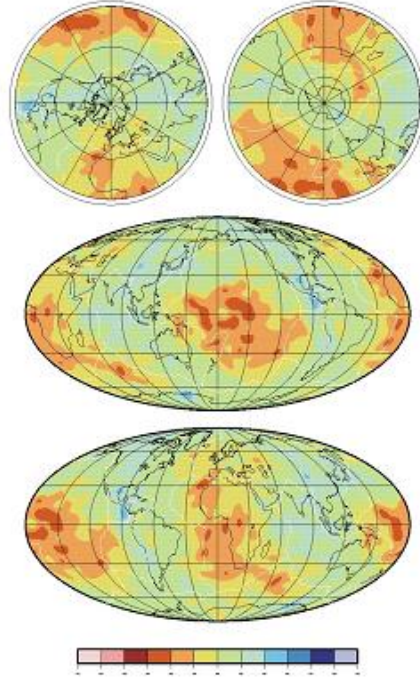
S30RTS
Ritsama & van Heijst [2001]
(300 km depth: -4% to +4% shear velocity variation)



S30RTS
Ritsema & van Hoolst [2001]
[1100 km depth: -4% to +4% shear velocity variation]



S30RTS
Ritsema & van Hoolst [2001]
[2050 km depth: -4% to +4% shear velocity variation]



J. Ritsema [written communication, 2002]

Spectral Structure of the Structural Heterogeneity in Earth

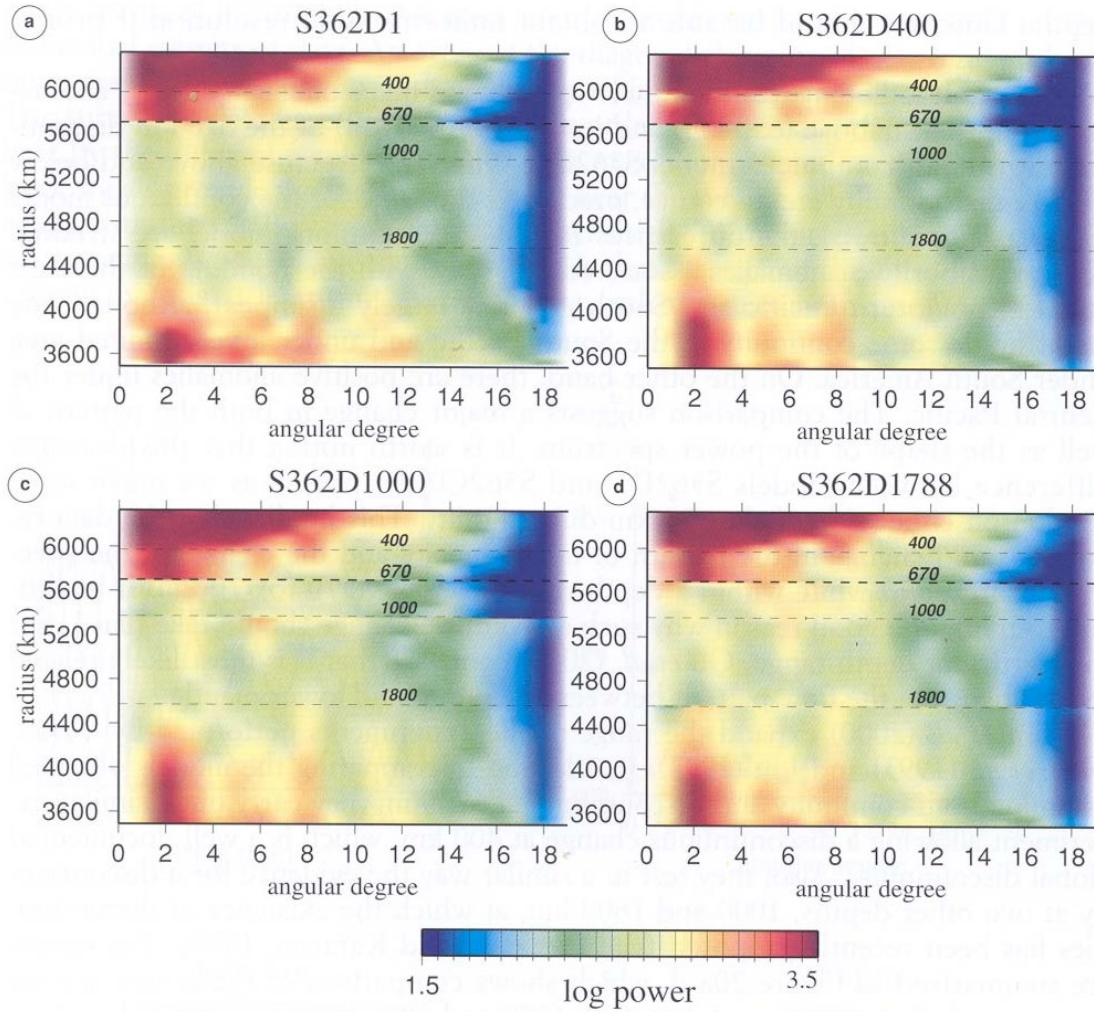
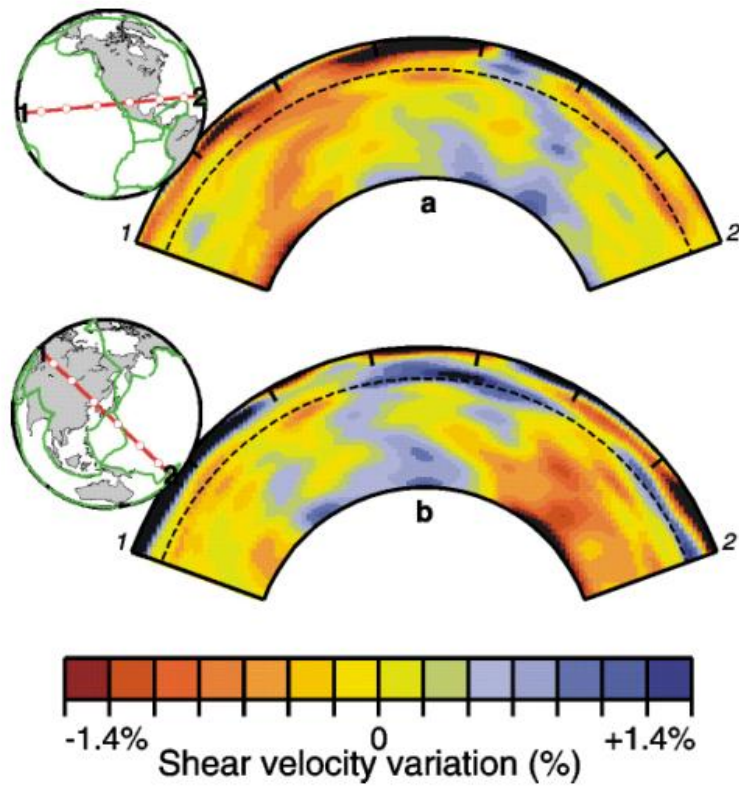


Figure 20a-d Power spectra as a function of depth in four Earth models in which a discontinuous change has been allowed at depths: 400 km (b); 670 km (a); 1000 km (c), and 1800 km (d). Only the model S362D1 shows a major change in the spectral pattern across the discontinuity, even though 400 km is also associated with a global discontinuity. The results imply a major change in the flow pattern across the 670 km discontinuity. From Gu *et al.* (2000).

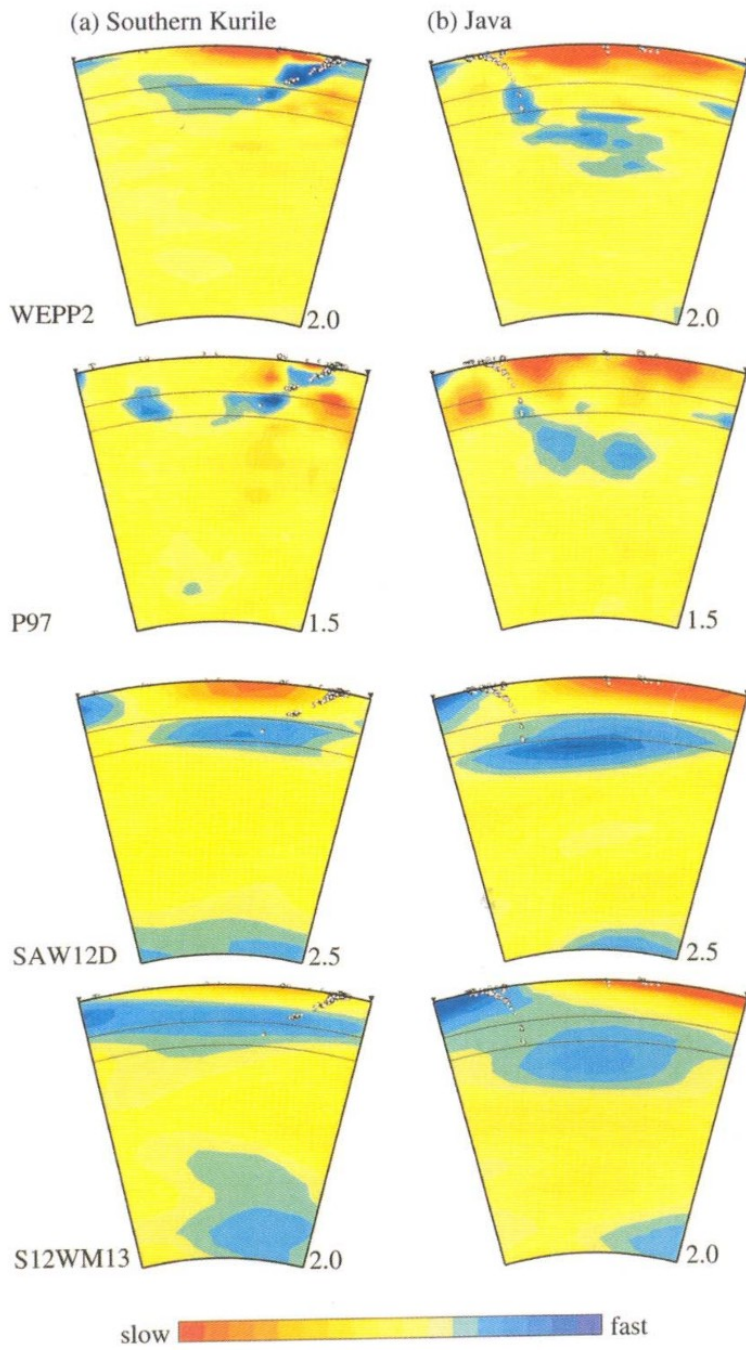
A. M. Dziewonski, Global seismic tomography: past, present and future, in Problems in Geophysics for the New Millennium, Editrice Compositori, 2000.

"Slab" Structure in Deep Interior



Ritsema, J., and van Heijst, H. J., Seismic imaging of structural heterogeneity in Earth's mantle: evidence for large-scale mantle flow, *Science Progress*, 83 (3), 243-259, 2000.

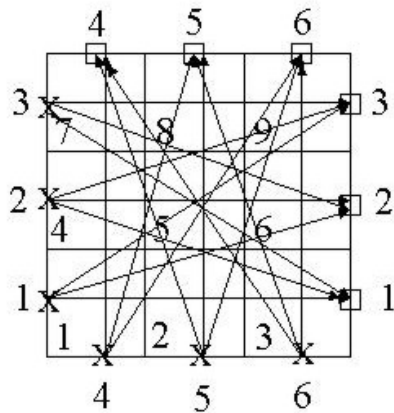
"Slab" Structures



Fukao, et al., Reviews of Geophysics, **39**, 291, 2001.

Ge162 Practice Session 5 (Optional) Simple Tomography

From class note, a tomography problem given below can be formulated by



two-side

If $A^T A$ is not singular, the formal least-squares solution is given by

$$\bar{m} = (A^T A)^{-1} A^T \bar{d} \quad (6)$$

and the error estimates are determined by the variance of the data and the diagonal elements of the inverse matrix of the normal equation (6). Usually, we write the uncertainty in m_i by Δm_i , and compute it by

$$\Delta m_i = \sqrt{c_{ii}} \sqrt{\sum_{(kl)=1}^N (t_{(kl)}^o - t_{(kl)}^c)^2 / (N - N_p)}, \quad i=1, 2, 3, \dots, 9 \quad (7)$$

where N_p is the number of parameters (here 9) and c_{ii} are the diagonal elements of $(A^T A)^{-1}$.

1. Determine the slowness s_i , $i=1, 2, 3, \dots, 9$, and the associated errors.

The matrix elements and the data are in `o_lsqr_mat_ts_0.1` and `o_lsqr_rhs_ts_0.1` in `/home/ftp/pub/hiroo/ge162.dir/practice5.dir`, respectively. In this computation, the

length of the side is 10 km, and errors up to 10% are added to the data. (This is the same geometry as Example 2 in class note. The numerical values of the standard errors may be slightly different, because of the difference in the definition.)

Actually, in the real problems, the computations of the ray paths and the path lengths in each cell are most difficult. In this problem, they are computed and the values are put in `o_lsq_mat_ts_0.1`. (there are small round-off errors of the order of 0.3 %.) Check the values for the first 3 rows of `o_lsq_mat_ts_0.1`.

Try to write your own program to do this problem, but if you find it difficult, you can use the program `tomo2.f` provided in `practice_5.dir`. It takes an input file `i_tomo2` which contains the names of the files for the matrix elements and the data. It also requires `c_tomo2`, but this should not be changed (it has a constant for regularization of the matrix inversion.).

2. Drop the data for source #6, and try the same.

3. Drop the data for sources #5 and #6, and try the same.

o_lsq_mat_ts_0.1

checker_b

two_sides

9	18	0.1000							
10.02	9.99	10.02	0.00	0.00	0.00	0.00	0.00	0.00	0.00
10.56	5.28	0.00	0.00	5.28	10.56	0.00	0.00	0.00	0.00
9.05	0.00	0.00	3.03	12.01	3.03	0.00	0.00	0.00	9.05
0.00	5.28	10.56	10.56	5.28	0.00	0.00	0.00	0.00	0.00
0.00	0.00	0.00	10.02	9.99	10.02	0.00	0.00	0.00	0.00
0.00	0.00	0.00	10.56	5.28	0.00	0.00	5.28	10.56	0.00
0.00	0.00	9.05	3.03	12.01	3.03	9.05	0.00	0.00	0.00
0.00	0.00	0.00	0.00	5.28	10.56	10.56	5.28	0.00	0.00
0.00	0.00	0.00	0.00	0.00	0.00	10.02	9.99	10.02	0.00
10.02	0.00	0.00	9.99	0.00	0.00	10.02	0.00	0.00	0.00
10.56	0.00	0.00	5.28	5.28	0.00	0.00	10.56	0.00	0.00
9.05	3.03	0.00	0.00	12.01	0.00	0.00	3.03	9.05	0.00
0.00	10.56	0.00	5.28	5.28	0.00	10.56	0.00	0.00	0.00
0.00	10.02	0.00	0.00	9.99	0.00	0.00	10.02	0.00	0.00
0.00	10.56	0.00	0.00	5.28	5.28	0.00	0.00	10.56	0.00
0.00	3.03	9.05	0.00	12.01	0.00	9.05	3.03	0.00	0.00
0.00	0.00	10.56	0.00	5.28	5.28	0.00	10.56	0.00	0.00
0.00	0.00	10.02	0.00	0.00	9.99	0.00	0.00	10.02	0.00

o_lsqrhs_ts_0.1

checker_b

two_sides

9 18 0.1000

(47.28
44.36
67.07
44.95
39.69
43.15
60.62
51.73
51.76
49.93
49.19
68.50
45.47
36.96
51.15
61.99
46.84
53.53)

Ge 162

5. Earthquake Source Theory

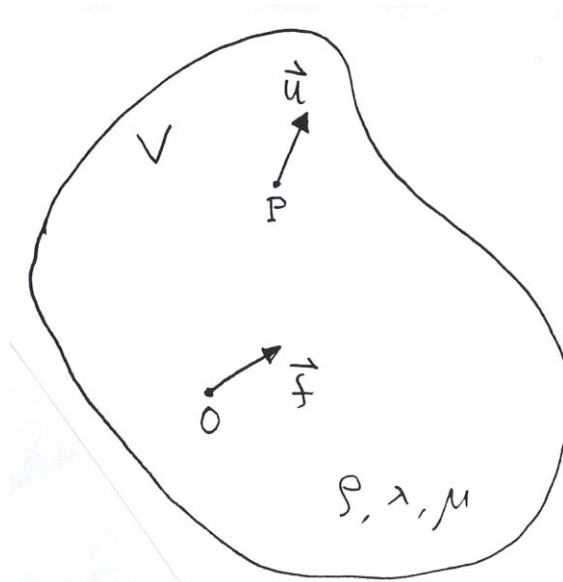
5.1 Static Source

5.1.1 Static Displacement Field Due to a Single Point Force in Infinite Homogeneous Medium (LW, pp. 323-331)

1. Description of the Problem

Consider an isotropic infinite homogeneous elastic medium with density ρ and elastic constants λ and μ .

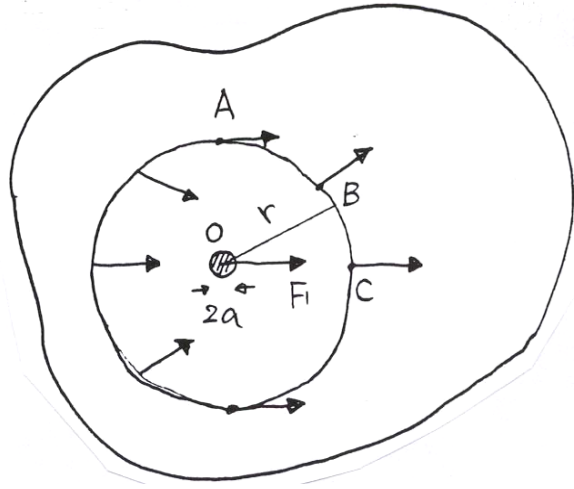
We apply a force at point O, and want to determine the displacement \vec{u} at point P. We assume that the outer boundary at infinity is constrained, *i.e.*, $|\vec{u}|=0$ at infinity.



2. Qualitative Solution

Suppose we apply a force F to a small sphere of radius a at the origin. We consider the displacement on the plane containing the force. It is not difficult to imagine that the resulting displacement field is given by the arrows shown in the following figure. The magnitude of u may be approximately determined as follows.

Consider a sphere with radius r . In equilibrium, the body force F acting at the center of this sphere must be balanced by stresses acting on the surface. The figure suggests that the stress on the surface of this sphere is compressional at C, shear at A, and half shear and half compression at B.



Let σ be the magnitude of this stress. Then, to the first approximation

$$F = 4\pi r^2 \sigma \quad (1)$$

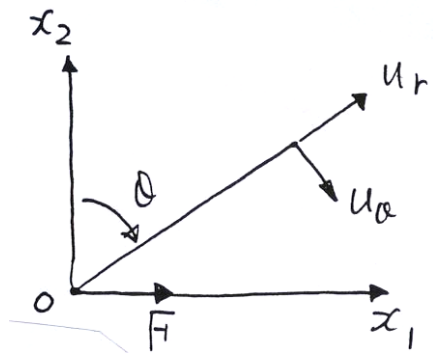
Let $u(r)$ be the magnitude of the displacement at r , then, from the geometry shown in the figure, du/dr gives the magnitude of the strain at r .

$$-\tilde{E} \frac{du}{dr} \approx \sigma \approx \frac{F}{4\pi r^2} \quad (2)$$

(The negative sign is taken because $u(r)$ decreases as r increases.) Here \tilde{E} represents an appropriate elastic constant, and is of the order of λ or μ . Integrating (4), and using $u(r \rightarrow \infty) = 0$, we obtain

$$u(r) \approx \frac{F}{4\pi\tilde{E}r} \quad (3)$$

Actually, a rigorous derivation shows (in the next section) that, if we define the polar coordinates as shown in the figure,



$$\begin{aligned} u_r &= \frac{F}{4\pi\mu r} \sin \theta \\ u_\theta &= \frac{F}{4\pi\mu r} \left(1 - \frac{\alpha}{2}\right) \cos \theta \end{aligned} \quad (4)$$

where

$$\alpha = \frac{\lambda + \mu}{\lambda + 2\mu}$$

Since for most solids, $\lambda = \mu$ and $\alpha=2/3$, we see that (3) is a good approximation of (4) and that the directions of the displacement shown in the figure are consistent with (4).

3. Elasto-static Solution of the Problem

Definition

a. Point Force of Strength F

When we consider a force in continuum, we introduce force per unit volume, or force per unit mass. Let \vec{f} be a force per unit mass, then $\rho \vec{f}$ gives force per unit volume.

Consider a small volume δV , and apply $\rho \vec{f}$ to this volume. Then

$$\vec{F} = \lim_{\delta V \rightarrow 0} (\rho \vec{f} \delta V)$$

defines a point force. $|\vec{F}| = F$ is the strength of this force.

b. Three-Dimensional Delta Function

Three-Dimensional Delta Function $\delta(r)$ can be defined by

$$\delta(r) = 0, \quad r \neq 0, \quad \int_V \delta(r) dV = 1$$

where V is a volume which includes the origin $r=0$. A convenient expression for this is

$$\delta(r) = -\frac{1}{4\pi} \nabla^2 (1/r) \quad (5)$$

Direct differentiation shows that

$$\nabla^2 (1/r) = 0, \quad \text{if } r \neq 0.$$

We can show that

$$\int_V \nabla^2(1/r)dV = -4\pi, \quad V \text{ contains the origin.} \quad (6)$$

Here, following the expression for the Gauss' theorem, $\int_V \nabla^2(1/r)dV$ is understood to mean $\int_S \nabla(1/r) \cdot \bar{n}dS$.

Although this looks like a very simple problem, it is not that easy. We have to start with elasto-static equation of equilibrium. From equation (29) of 3.1, we have

$$\rho \bar{f} + (\lambda + 2\mu)\text{graddiv}\bar{u} - \mu\text{curlcurl}\bar{u} = 0 \quad (7)$$

where \bar{f} is the force per unit mass. Consider a point force of magnitude F at the origin.

$$\rho \bar{f} = F\bar{a}\delta(r) \quad (8)$$

where \bar{a} is the unit vector in the direction of the force. By using (5) we have

$$\rho \bar{f} = -F\nabla^2\left(\frac{\bar{a}}{4\pi r}\right) = -F\left[\text{graddiv}\left(\frac{\bar{a}}{4\pi r}\right) - \text{curlcurl}\left(\frac{\bar{a}}{4\pi r}\right)\right] \quad (9)$$

We look for a solution in the form

$$\bar{u} = \text{graddiv}\bar{A}_p - \text{curlcurl}\bar{A}_s \quad (10)$$

This form may appear somewhat artificial, but it is suggested from the fact that any displacement field can be represented by a sum of solenoidal and irrotational fields and that the forcing term (9) is given in this form. Substituting (9) and (10) into (7), we have

$$\begin{aligned}
& -F \text{graddiv} \left(\frac{\bar{a}}{4\pi r} \right) + F \text{curlcurl} \left(\frac{\bar{a}}{4\pi r} \right) + (\lambda + 2\mu) \text{graddiv}(\text{graddiv}\bar{A}_p - \text{curlcurl}\bar{A}_p) \\
& -\mu \text{curlcurl}(\text{graddiv}\bar{A}_s - \text{curlcurl}\bar{A}_s) = 0
\end{aligned}$$

In the third term $\text{curlcurl}\bar{A}_s$ is replaced by $\text{curlcurl}\bar{A}_p$, because its divergence vanishes anyway. Similarly, $\text{graddiv}\bar{A}_p$ in the fourth term is replaced by $\text{graddiv}\bar{A}_s$. Using the relation

$$\text{graddiv}\bar{A}_p - \text{curlcurl}\bar{A}_p = \nabla^2 \bar{A}_p$$

and the similar relation for \bar{A}_s , we obtain

$$\text{graddiv} \left(-F \frac{\bar{a}}{4\pi r} + (\lambda + 2\mu) \nabla^2 \bar{A}_p \right) + \text{curlcurl} \left(F \frac{\bar{a}}{4\pi r} - \mu \nabla^2 \bar{A}_s \right) = 0 \quad (11)$$

This equation is satisfied if,

$$(\lambda + 2\mu) \nabla^2 \bar{A}_p = F \frac{\bar{a}}{4\pi r} \quad (12)$$

$$\mu \nabla^2 \bar{A}_s = F \frac{\bar{a}}{4\pi r} \quad (13)$$

If we put $\bar{A}_p = A_p \bar{a}$ and $\bar{A}_s = A_s \bar{a}$, (12) and (13) can be reduced to Poisson's equation,

$$\nabla^2 A_p = \frac{F}{4\pi(\lambda + 2\mu)r} \quad \text{and} \quad \nabla^2 A_s = \frac{F}{4\pi\mu r} \quad (14)$$

Since $\nabla^2 r = \frac{2}{r}$, we have

$$A_p = \frac{F}{8\pi(\lambda + 2\mu)} r \quad (15)$$

and

$$A_s = \frac{F}{8\pi\mu} r \quad (16)$$

Using (10)

$$\bar{u} = \text{graddiv}\bar{A}_p - \text{graddiv}\bar{A}_s + \nabla^2\bar{A}_s \quad (17)$$

Substituting (15) and (10) into (17), we have for the i -th component of displacement for a unit force ($F=1$) in j -th direction, u_i^j ,

$$\begin{aligned} u_i^j &= \frac{1}{8\pi(\lambda + 2\mu)} \frac{\partial}{\partial x_i} \frac{\partial r}{\partial x_j} - \frac{1}{8\pi\mu} \frac{\partial}{\partial x_i} \frac{\partial r}{\partial x_j} + \delta_{ij} \frac{1}{8\pi\mu} \nabla^2 r \\ &= \frac{1}{8\pi\mu} \left(\delta_{ij} \nabla^2 r - \frac{\lambda + \mu}{\lambda + 2\mu} \frac{\partial^2 r}{\partial x_i \partial x_j} \right) = \frac{1}{8\pi\mu} (\delta_{ij} \nabla^2 r - \alpha r_{,ij}) = u_j^i \end{aligned} \quad (18)$$

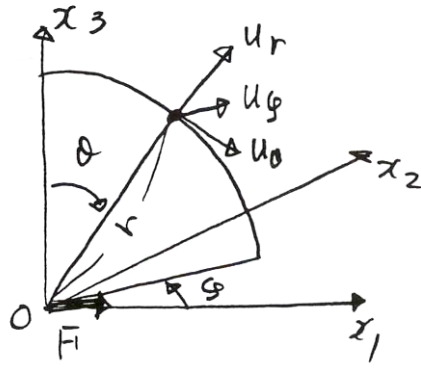
where

$$\alpha = \frac{\lambda + \mu}{\lambda + 2\mu} \quad (2/3 \text{ for most solids}) \quad (19)$$

Equation (18) gives the solution of our problem. Note that $u_j^i = u_i^j$ (symmetric). u_i^j is often called the Somigliana Tensor. We write all the components explicitly,

$$\begin{aligned}
u_1^1 &= \frac{1}{8\pi\mu} \left[\frac{2}{r} - \alpha \left(\frac{1}{r} - \frac{x_1^2}{r^3} \right) \right], & u_1^2 &= \frac{1}{8\pi\mu} \left(\alpha \frac{x_1 x_2}{r^3} \right) \\
u_1^3 &= \frac{1}{8\pi\mu} \left(\alpha \frac{x_1 x_3}{r^3} \right), & u_2^2 &= \frac{1}{8\pi\mu} \left[\frac{2}{r} - \alpha \left(\frac{1}{r} - \frac{x_2^2}{r^3} \right) \right] \\
u_2^3 &= \frac{1}{8\pi\mu} \left(\alpha \frac{x_2 x_3}{r^3} \right), & u_3^3 &= \frac{1}{8\pi\mu} \left[\frac{2}{r} - \alpha \left(\frac{1}{r} - \frac{x_3^2}{r^3} \right) \right]
\end{aligned} \tag{20}$$

Let us consider the simplest case. A force with a magnitude F is applied in x_1 direction. We take the polar coordinates (r, θ, ϕ) as shown in the figure.



Then

$$\begin{pmatrix} u_r \\ u_\theta \\ u_\phi \end{pmatrix} = \begin{pmatrix} \sin \theta \cos \phi & \sin \theta \sin \phi & \cos \theta \\ \cos \theta \cos \phi & \cos \theta \sin \phi & -\sin \theta \\ -\sin \phi & \cos \phi & 0 \end{pmatrix} \begin{pmatrix} u_1^1 \\ u_2^1 \\ u_3^1 \end{pmatrix} \tag{21}$$

On $x_1 - x_3$ plane, $\phi=0$,

$$u_r = \sin \theta u_1^1 + \cos \theta u_3^1 = \frac{F}{4\pi\mu r} \sin \theta \tag{22}$$

$$u_\theta = \cos \theta u_1^1 - \sin \theta u_3^1 = \frac{F}{4\pi\mu r} \left(1 - \frac{\alpha}{2}\right) \cos \theta \quad (23)$$

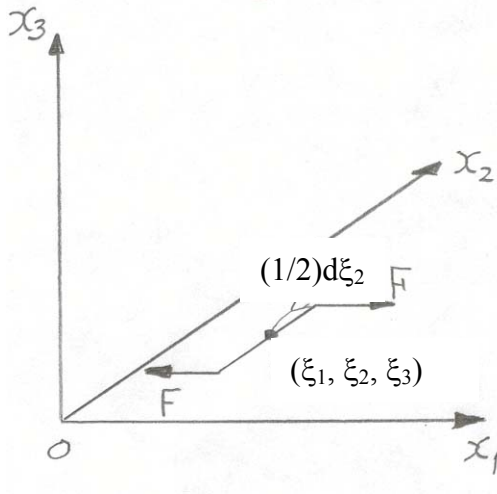
These are the results given by (4).

5.1.2 Static Displacement Field Due to Force Couples

Single Couple

If we apply a force at (ξ_1, ξ_2, ξ_3) instead of at the origin, the displacement at (x_1, x_2, x_3) can be still given by (18) with

$$r^2 = (x_1 - \xi_1)^2 + (x_2 - \xi_2)^2 + (x_3 - \xi_3)^2 \equiv (x_i - \xi_i)^2.$$



If we apply a force F in x_1 direction at $\xi_2 + \frac{1}{2}d\xi_2$, and F in $-x_1$ direction at $\xi_2 - \frac{1}{2}d\xi_2$,

the displacement at (x_1, x_2, x_3) is

$$\begin{aligned} & Fu_i^1(\xi_1, \xi_2 + \frac{1}{2}d\xi_2, \xi_3, x_1, x_2, x_3) - Fu_i^1(\xi_1, \xi_2 - \frac{1}{2}d\xi_2, \xi_3, x_1, x_2, x_3) \\ &= F \frac{\partial u_i^1}{\partial \xi_2} d\xi_2 + o(d^2\xi_2) \end{aligned}$$

(24)

Since $r^2 = (x_1 - \xi_1)^2 + (x_2 - \xi_2)^2 + (x_3 - \xi_3)^2 \equiv (x_i - \xi_i)^2$,

$$\frac{\partial r}{\partial \xi_i} = -\frac{\partial r}{\partial x_i} \quad (25)$$

(we often write this as $r^i = -r_i$.)

therefore, from (18)

$$\frac{\partial u_i^j}{\partial \xi_k} = -\frac{\partial u_i^j}{\partial x_k} \quad (26)$$

Thus, the displacement for this force couple is given by

$$-F \frac{\partial u_i^1}{\partial x_2} d\xi_2 + o(d^2 \xi_2) \quad (27)$$

If we make $d\xi_2 \rightarrow 0$, $F \rightarrow \infty$, so that $F d\xi_2 \rightarrow M$ (finite), the displacement due to this single couple (we will denote it by U_i) can be written as

$$U_i = M \frac{\partial u_i^1}{\partial \xi_2} = M u_i^{1,2} \quad (27')$$

or

$$U_i = -M \frac{\partial u_i^1}{\partial x_2} = -M u_{i,2}^1 \quad (27'')$$

Thus, the displacement due to this single couple placed at the origin can be obtained by replacing F by M in (20), taking the derivative of (20) with respect to x_2 , and changing the sign.

\therefore

$$U_1 = -\frac{M}{8\pi\mu} \left[-2 \frac{x_2}{r^3} - \alpha \left(-\frac{x_2}{r^3} + 3 \frac{x_1^2 x_2}{r^5} \right) \right] \quad (28)$$

$$U_2 = -\frac{M}{8\pi\mu} \alpha \left[\frac{x_1}{r^3} - 3 \frac{x_1 x_2^2}{r^5} \right] \quad (29)$$

$$U_3 = -\frac{M}{8\pi\mu} \alpha \left[-3 \frac{x_1 x_2 x_3}{r^5} \right] \quad (30)$$

Similarly if we apply a single couple as shown in the following figure, we obtain

$$U_i = M \frac{\partial u_i^2}{\partial \xi_1} = M u_{i,1}^{2,1}$$

or

$$U_i = -M \frac{\partial u_i^2}{\partial x_1} = -M u_{i,1}^2$$

and the x_1, x_2, x_3 components of the displacement can be given by

$$U_1 = -\frac{M}{8\pi\mu} \alpha \left[\frac{x_2}{r^3} - 3 \frac{x_2 x_1^2}{r^5} \right] \quad (31)$$

$$U_2 = -\frac{M}{8\pi\mu} \left[-2 \frac{x_1}{r^3} - \alpha \left(-\frac{x_1}{r^3} + 3 \frac{x_2^2 x_1}{r^5} \right) \right] \quad (32)$$

$$U_3 = -\frac{M}{8\pi\mu} \alpha \left[-3 \frac{x_1 x_2 x_3}{r^5} \right] \quad (33)$$

Double Couple

It is evident that for a double couple as shown in the figure, the displacements can be given by

$$U_i = M \frac{\partial u_i^2}{\partial \xi_1} = M(u_i^{1,2} + u_i^{2,1}) \quad (34)$$

or

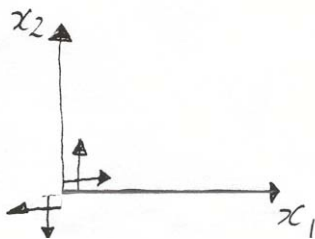
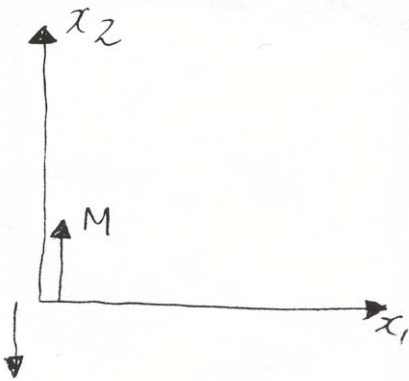
$$U_i = -M \frac{\partial u_i^2}{\partial x_1} = -M(u_{i,2}^1 + u_{i,1}^2) = -M(u_{1,2}^i + u_{2,1}^i) \quad (35)$$

From the sum of (28) and (31), (29) and (32), and (30 and (33), we obtain

$$U_1 = \frac{M}{8\pi\mu} \left(2 \frac{x_2}{r^3} \right) - \frac{2\alpha M}{8\pi\mu} \left(\frac{x_2}{r^3} - 3 \frac{x_1^2 x_2}{r^5} \right) = \frac{M}{4\pi\mu r^2} \frac{x_2}{r} \left[1 - \alpha \left(1 - 3 \frac{x_1^2}{r^2} \right) \right] \quad (36)$$

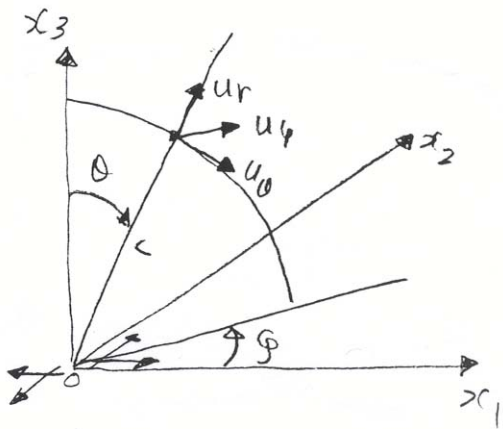
$$U_2 = \frac{M}{8\pi\mu} \left(2 \frac{x_1}{r^3} \right) - \frac{2\alpha M}{8\pi\mu} \left(\frac{x_1}{r^3} - 3 \frac{x_2^2 x_1}{r^5} \right) = \frac{M}{4\pi\mu r^2} \frac{x_1}{r} \left[1 - \alpha \left(1 - 3 \frac{x_2^2}{r^2} \right) \right] \quad (37)$$

$$U_3 = \frac{M}{8\pi\mu} \left(6\alpha \frac{x_1 x_2 x_3}{r^5} \right) = \frac{M}{4\pi\mu r^2} \left(3\alpha \frac{x_1 x_2 x_3}{r^3} \right) \quad (38)$$



For double couples with different orientations, similar expressions can be obtained.

Using the polar coordinates (r, θ, ϕ) ,



the displacement components, u_r, u_θ, u_ϕ are given by

$$u_r = \frac{M}{4\pi\mu r^2} \left(1 + \frac{\alpha}{2}\right) \sin^2 \theta \sin 2\phi \quad (39)$$

$$u_\theta = \frac{M}{4\pi\mu r^2} \left(\frac{1}{2} - \frac{\alpha}{2}\right) \sin 2\theta \sin 2\phi \quad (40)$$

$$u_\phi = \frac{M}{4\pi\mu r^2} (1 - \alpha) \sin \theta \cos 2\phi \quad (41)$$

Or,

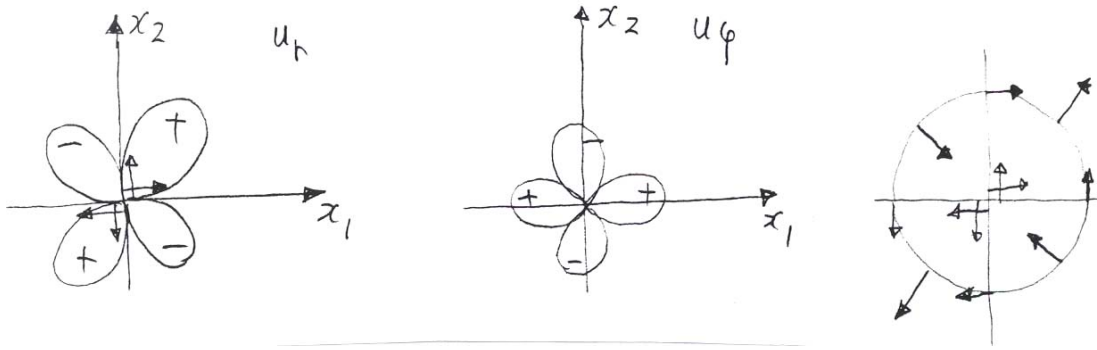
$$\begin{pmatrix} u_r \\ u_\theta \\ u_\phi \end{pmatrix} = \frac{M}{4\pi\mu r^2} \begin{pmatrix} \left(1 + \frac{\alpha}{2}\right) \sin^2 \theta \sin 2\phi \\ \left(\frac{1}{2} - \frac{\alpha}{2}\right) \sin 2\theta \sin 2\phi \\ (1 - \alpha) \sin \theta \cos 2\phi \end{pmatrix} \quad (42)$$

On the $x_1 - x_2$ plane, $\theta = \pi/2$, $u_\theta = 0$, and

$$u_r \approx \left(1 + \frac{\alpha}{2}\right) \sin 2\phi$$

$$u_\phi \approx (1 - \alpha) \cos 2\phi$$

The azimuthal variation of u_r and u_ϕ is shown in the following figure.



The displacement field on a circle $x_1^2 + x_2^2 = \text{const}$ is also shown.

Single Couple and Double Couple with Arbitrary Orientation

If the force is in $\bar{k} = (k_1, k_2, k_3)$ direction and the arm is in $\bar{l} = (l_1, l_2, l_3)$ direction, then

$$U_i^{SC} = \frac{\partial u_i^k}{\partial s_l}$$

Here, $\frac{\partial}{\partial s_l}$ is the derivative in \bar{l} direction, and \bar{l} is taken positive in the direction towards

the force oriented in positive \bar{k} direction. Then, since $\frac{\partial}{\partial s_l} = l_q \frac{\partial}{\partial \xi_q}$ and $u_i^k = u_i^p k_p$,

$$U_i^{SC} = u_i^{p,q} k_p l_q \quad (43)$$

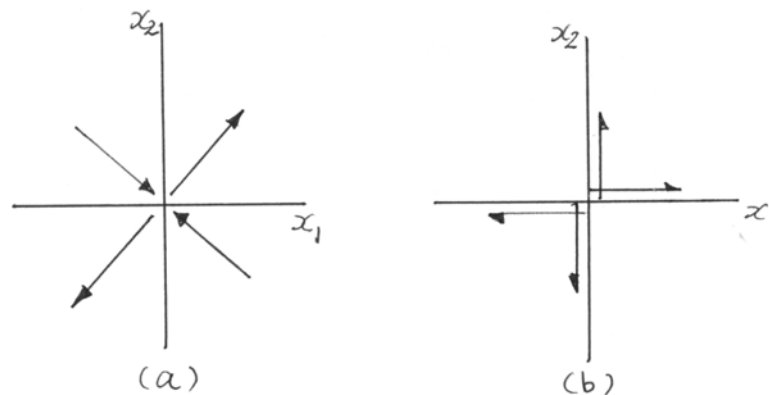
Then, the displacement due to a unit double couple is

$$U_i^{DC} = u_i^{p,q} (k_p l_q + k_q l_p) \quad (44)$$

Ge 162 Problem #6 Double Couple and Dipole

Using the expressions discussed in 5.1.2 (i.e., $u_i^{SC} = u_i^{p,q} k_p l_q$), we can write the displacement due to a force dipole as $u_i^{DP} = u_i^{p,q} k_p l_q$ where \vec{k} and \vec{l} are the unit vectors in the direction of force and the arm, respectively. \vec{k} and \vec{l} are parallel but they can be of either opposite or the same direction, depending on the orientation of the force (i.e., inward or outward).

Show that the force system with two dipoles (a) shown below is equivalent to the double couple (b) (all the dipoles and the couples are with unit moment.).

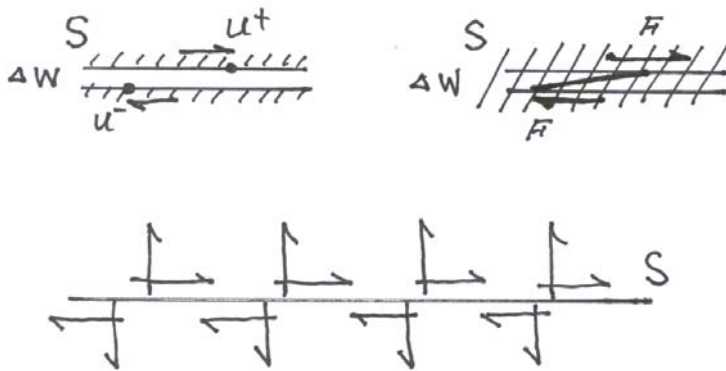


Ge 162

5.1.3 Elastic Dislocation

1. Qualitative Description of the Problem

Consider a fault shown in the figure. The displacement on one side is u^+ and the other side is u^- , so that the displacement discontinuity is $\Delta u = u^+ - u^-$. This is called fault offset and is often denoted by D . Since we already know the displacement field due to a point force and force couples, we will first try to produce, by applying forces or force couples to the medium without dislocation, a displacement field similar to that caused by faulting.



Since an earthquake represents transition from one equilibrium state to another, there should be no net force and no net moment. Thus, a single force or a single couple is not appropriate to represent an earthquake. A double couple is an appropriate force system to represent an earthquake.

Now, we try to find a double couple applied in a medium without dislocation which yields a displacement field similar to that produced by a fault (i.e. dislocation).

As shown in the figure, to produce D over a small distance of Δw , in the medium without dislocation, we need to apply a force couple with one force approximately equal to

$$F = \mu \frac{u^+ - u^-}{\Delta w} S \quad (1)$$

where S is the fault area.

We reduce Δw while maintaining $D = u^+ - u^-$,

$$\lim_{\Delta w \rightarrow \infty} F \Delta w = \mu(u^+ - u^-)S = \mu DS$$

which means a moment

$$M = \mu DS \quad (2)$$

is required to produce the offset D over S .

To produce D over an extended area S , we can distribute double couples on S as shown in the figure. In this case, the effects of the vertical forces are cancelled within S , and the overall force system can produce a dislocation-like displacement field.

2. Definition of Elastic Dislocation

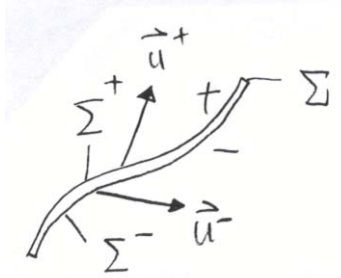
First we need to give a precise definition of "Elastic Dislocation". Create a thin cavity in an elastic medium. Let one side of this cavity be Σ^+ and the other be Σ^- . Apply force on these surfaces to move the Σ^+ side by \bar{u}^+ and Σ^- side by \bar{u}^- . Then,

make the gap very small so that Σ^+ and Σ^- form an open surface Σ . Then weld the two surfaces and remove the force. Now we have a displacement discontinuity

$$\Delta \bar{u} = \bar{u}^+ - \bar{u}^-$$

across Σ . This is called the elastic dislocation. Note that, for a dislocation created this way, the traction must be continuous across Σ .

If \bar{u}^+ and \bar{u}^- are tangential to Σ , $\Delta \bar{u}$ is called the shear dislocation.



3. Description of the Problem

Consider an infinite homogeneous (isotropic) elastic medium in equilibrium. Then create a dislocation $\Delta \bar{u}$ on Σ .

This dislocation causes deformation throughout the medium which is in new equilibrium state.

We want to determine the displacement field \bar{u} in the medium caused by this dislocation.

4. Elasto-Static Theory of Dislocation

We use Volterra's dislocation theory to show

$$u^k(Q) = \int_{\Sigma} \Delta u_i \tau_{ij}^k \nu_j dS \quad (3)$$

where $u^k(Q)$ is the k -th component of displacement at Q ; τ_{ij}^k is the ij component of stress on Σ due to a unit force in k -th direction at Q (the unit of τ_{ij}^k should be understood as stress/force=1/area); Δu_i is the displacement discontinuity (dislocation) across Σ . i.e. $\Delta u_i = u_i(\text{on } \Sigma^+) - u_i(\text{on } \Sigma^-)$. Also,

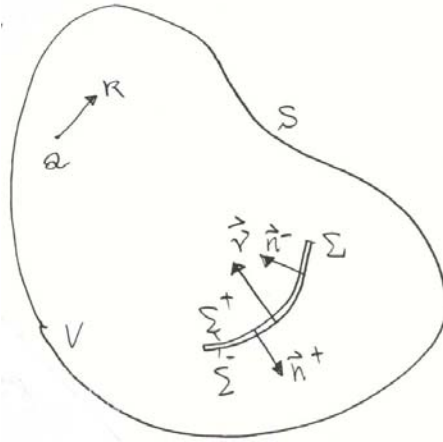
$\Sigma^+ + \Sigma^-$: Closed surface defining the dislocation surface.

Σ : Open surface formed by Σ^+ and Σ^- when they are made coincident with each other.

$\bar{\nu}$: unit vector normal to Σ pointing from the negative side to the positive side.

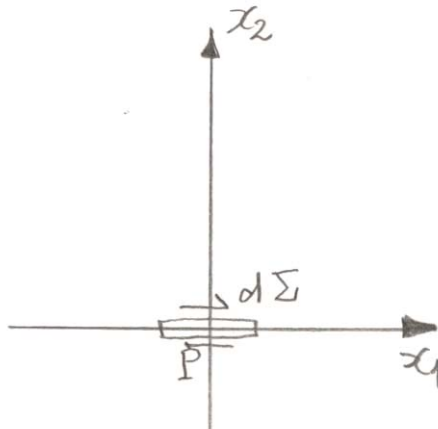
$$\bar{n}^+ = \bar{\nu} \text{ on } \Sigma^+, \quad \bar{n}^- = -\bar{\nu} \text{ on } \Sigma^-$$

Equation (3) will be proved in the next section.



Let us consider one of the simplest cases.

Suppose we have a very small planar shear dislocation surface $d\Sigma$ at P which is perpendicular to x_2 axis. We consider a displacement discontinuity in x_1 direction.



Then $\Delta u_1 \neq 0, \Delta u_2 = \Delta u_3 = 0$ and $\vec{v} = (0, 1, 0)$.

In this case (3) gives

$$\begin{aligned}
u^k(Q) &= d\Sigma[\Delta u_1(\tau_{11}^k v_1 + \tau_{12}^k v_2 + \tau_{13}^k v_3) \\
&\quad + \Delta u_2(\tau_{21}^k v_1 + \tau_{22}^k v_2 + \tau_{23}^k v_3) \\
&\quad + \Delta u_3(\tau_{31}^k v_1 + \tau_{32}^k v_2 + \tau_{33}^k v_3)] \\
&= d\Sigma \Delta u_1 \tau_{12}^k
\end{aligned} \tag{4}$$

Note that

$$\tau_{12}^k = \mu(u_{1,2}^k + u_{2,1}^k)$$

Referring to (34) of 5.1.2, this means that $(\tau_{12}^k / \mu) = (u_{1,2}^k + u_{2,1}^k)$ is the k -th component of displacement, U^k , at Q due to a unit double couple placed on the $x_1 - x_2$ plane at P.

Thus,

$$u^k(Q) = d\Sigma \Delta u_1 (\mu U^k) = (\mu \Delta u_1 d\Sigma) U^k \tag{5}$$

This means that $u^k(Q)$ is equal to the k -th component of displacement at Q due to a double couple of moment $M = \mu \Delta u_1 d\Sigma$ placed at P. Since this relation evidently holds for any $d\Sigma$, we can conclude that a shear dislocation Δu_s over a surface S is equivalent to a double couple whose total moment is

$$M = \int_S \mu \Delta u_s d\Sigma = \mu \Delta \bar{u}_s S \tag{6}$$

5. Volterra's Dislocation Theory

We first introduce the following notation for the stress strain relation:

$$\tau_{ij} = \lambda \delta_{ij} u_{k,k} + \mu (u_{i,j} + u_{j,i}) = c_{ijpq} u_{p,q} \quad (7)$$

where

$$c_{ijpq} = \lambda \delta_{ij} \delta_{pq} + \mu (\delta_{ip} \delta_{jq} + \delta_{jp} \delta_{iq}) \quad (8)$$

Then the following symmetry relations hold.

$$c_{ijpq} = c_{jipq} = c_{ijqp} = c_{pqij} \quad (9)$$

Note:

Among 81 components of c_{ijpq} , most of them are zero. Nonzero components are

$$\begin{aligned} c_{1111} &= c_{2222} = c_{3333} = \lambda + 2\mu \\ c_{1122} &= c_{2211} = c_{1133} = c_{3311} = c_{2233} = c_{3322} = \lambda \\ c_{1212} &= c_{1221} = c_{2112} = c_{2121} = c_{1313} = c_{1331} = \mu \\ c_{3113} &= c_{3131} = c_{2323} = c_{2332} = c_{3223} = c_{3232} = \mu \end{aligned}$$

Then, the equation of equilibrium can be written as:

$$\rho f_i + \tau_{ij,j} = 0, \text{ or } \rho f_i + c_{ijpq} u_{p,qj} = 0 \quad (10)$$

This notation is convenient for the derivation given in the following.

Consider an elastic medium (homogeneous, isotropic) bounded by a closed surface S_1 . Within this medium consider a closed surface consisting of Σ^+ and Σ^- . Σ^+ and Σ^- are made coincident with each other to make an open surface Σ .

We let V be the volume inside of S_1 , and outside of $\Sigma^+ + \Sigma^-$.

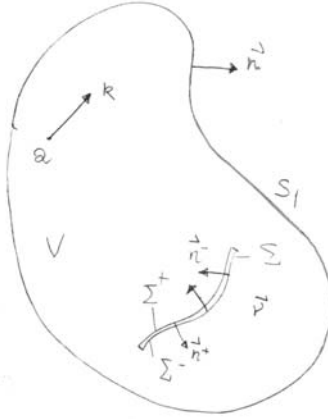
We let u_i be a solution of equation of equilibrium

$$c_{ijpq} u_{p,qj} = -\rho f_i \quad (11)$$

u_i is continuous throughout V . On Σ^+ , $u_i = u_i^+$ and on Σ^- , $u_i = u_i^-$; $u_i^+ - u_i^- = \Delta u_i$.

Also, u_i satisfies the boundary conditions, either $u_i = 0$ (rigid) or $c_{ijpq} u_{p,qj} n_j = 0$ (free) on S_1 , where \bar{n} is a unit vector normal to S_1 (positive outward).

Let v_i be another solution of (10) and represent the displacement field due to a body force $\rho \bar{g}$ (per unit volume). v_i is continuous everywhere and satisfies the boundary condition on S_1 (either $v_i = 0$ (rigid) or $c_{ijpq} v_{p,qj} n_j = 0$ (free)).



$$c_{ijpq} v_{p,qj} = -\rho g_i \quad (12)$$

Multiplying (11) by v_i and (12) by u_i , subtracting and integrating over the volume V , we obtain

$$\int_V (c_{ijpq} u_{p,qj} v_i - c_{ijpq} v_{p,qj} u_i) dV = -\int_V (\rho f_i v_i - \rho g_i u_i) dV \quad (13)$$

Note that

$$(c_{ijpq} u_{p,q} v_i - c_{ijpq} v_{p,q} u_i)_{,j} = (c_{ijpq} u_{p,qj} v_i - c_{ijpq} v_{p,qj} u_i) + (c_{ijpq} u_{p,q} v_{i,j} - c_{ijpq} v_{p,q} u_{i,j})$$

Owing to the symmetry of c_{ijpq} , the second term of RHS vanishes. Hence,

$$\int_V (c_{ijpq} u_{p,q} v_i - c_{ijpq} v_{p,q} u_i)_{,j} dV = -\int_V (\rho f_i v_i - \rho g_i u_i) dV \quad (14)$$

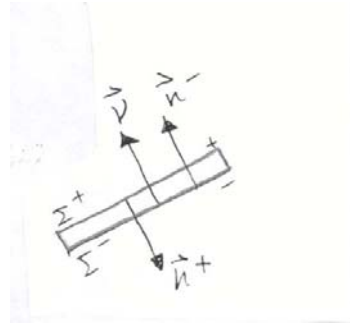
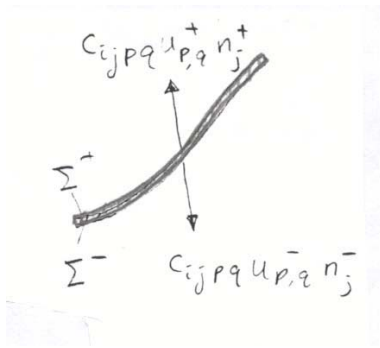
Applying the Gauss' theorem to LHS,

$$\int_{S_1+\Sigma^++\Sigma^-} (c_{ijpq}u_{p,q}v_i n_j - c_{ijpq}v_{p,q}u_i n_j) dS = -\int_V (\rho f_i v_i - \rho g_i u_i) dV \quad (15)$$

Due to the boundary conditions on S_1 , the integral on S_1 vanishes. Since v_i is continuous on Σ

$$\begin{aligned} \int_{\Sigma^++\Sigma^-} c_{ijpq}u_{p,q}v_i n_j dS &= \int_{\Sigma^+} c_{ijpq}u_{p,q}^+ v_i n_j^+ dS + \int_{\Sigma^-} c_{ijpq}u_{p,q}^- v_i n_j^- dS \\ &= \int_{\Sigma} v_i (c_{ijpq}u_{p,q}^+ n_j^+ + c_{ijpq}u_{p,q}^- n_j^-) dS \end{aligned}$$

In equilibrium, the traction on the Σ^+ side $c_{ijpq}u_{p,q}^+ n_j^+$ should be balanced by that on the Σ^- side, $c_{ijpq}u_{p,q}^- n_j^-$. Hence this integral vanishes.



On the other hand

$$\begin{aligned} \int_{\Sigma^+ + \Sigma^-} c_{ijpq} \nu_{p,q} u_i n_j dS &= \int_{\Sigma^+} c_{ijpq} \nu_{p,q} u_i^+ (-\nu_j) dS + \int_{\Sigma^-} c_{ijpq} \nu_{p,q} u_i^- (+\nu_j) dS \\ &= - \int_{\Sigma} c_{ijpq} \nu_{p,q} \Delta u_i \nu_j dS \end{aligned}$$

Hence,

$$- \int_{\Sigma} c_{ijpq} \nu_{p,q} \Delta u_i \nu_j dS = \int_V (\rho f_i \nu_i - \rho g_i u_i) dV \quad (16)$$

We put $\rho f_i = 0$, and, for g_i , consider a unit force in k -th direction at point Q:

$$\rho g_i = \delta_{ik} \delta(Q)$$

Then (16) becomes

$$u^k(Q) = \int_{\Sigma} \Delta u_i \tau_{ij}^k \nu_j dS \quad (17)$$

This is the Volterra's relation. τ_{ij}^k is the stress due to a unit force in k -th direction at Q, and its unit should be stress/force = 1/area.

6. Moment Tensor

Applying the Veltterra's relation

$$u^k(\bar{y}) = \int_{\Sigma} \Delta u_i \tau_{ij}^k \nu_j dS = \int_{\Sigma} \Delta u_i c_{ijpq} u_{p,q}^k \nu_j dS$$

to a small surface element ΔS over which $\bar{\nu}$, $\Delta \bar{u}$ and $u_{p,q}^k$ are constant, we obtain

$$u^k(\bar{y}) = c_{ijpq} u_{p,q}^k \Delta u_i \nu_j \Delta S \quad (18)$$

$$= M_{pq} u_{p,q}^k \quad (19)$$

where

$$M_{pq} = c_{ijpq} \Delta u_i \nu_j \Delta S \quad (20)$$

M_{pq} is a symmetric tensor called the moment tensor. Then (19) can be written as

$$\begin{pmatrix} u^1 \\ u^2 \\ u^3 \end{pmatrix} = \begin{pmatrix} u_{1,1}^1 & u_{2,2}^1 & u_{3,3}^1 & u_{1,2}^1 + u_{2,1}^1 & u_{1,3}^1 + u_{3,1}^1 & u_{2,3}^1 + u_{3,2}^1 \\ u_{1,1}^2 & u_{2,2}^2 & u_{3,3}^2 & u_{1,2}^2 + u_{2,1}^2 & u_{1,3}^2 + u_{3,1}^2 & u_{2,3}^2 + u_{3,2}^2 \\ u_{1,1}^3 & u_{2,2}^3 & u_{3,3}^3 & u_{1,2}^3 + u_{2,1}^3 & u_{1,3}^3 + u_{3,1}^3 & u_{2,3}^3 + u_{3,2}^3 \end{pmatrix} \begin{pmatrix} M_{11} \\ M_{22} \\ M_{33} \\ M_{12} \\ M_{13} \\ M_{23} \end{pmatrix} \quad (21)$$

Using the explicit expressions for c_{ijpq} , (20) can be written as,

$$\begin{aligned}
 M_{11} &= \Delta S [(\lambda + 2\mu) \Delta u_1 v_1 + \lambda \Delta u_2 v_2 + \lambda \Delta u_3 v_3] \\
 M_{22} &= \Delta S [\lambda \Delta u_1 v_1 + (\lambda + 2\mu) \Delta u_2 v_2 + \lambda \Delta u_3 v_3] \\
 M_{33} &= \Delta S [\lambda \Delta u_1 v_1 + \lambda \Delta u_2 v_2 + (\lambda + 2\mu) \Delta u_3 v_3] \\
 M_{12} &= \Delta S \mu (\Delta u_2 v_1 + \Delta u_1 v_2) \\
 M_{13} &= \Delta S \mu (\Delta u_3 v_1 + \Delta u_1 v_3) \\
 M_{23} &= \Delta S \mu (\Delta u_2 v_3 + \Delta u_3 v_2)
 \end{aligned} \tag{22}$$

For shear dislocation, i.e., $\vec{v} \perp \Delta \vec{u}$,

$$\begin{aligned}
 M_{11} &= 2\Delta S \mu \Delta u_1 v_1 \\
 M_{22} &= 2\Delta S \mu \Delta u_2 v_2 \\
 M_{33} &= 2\Delta S \mu \Delta u_3 v_3 \\
 M_{12} &= \Delta S \mu (\Delta u_2 v_1 + \Delta u_1 v_2) \\
 M_{13} &= \Delta S \mu (\Delta u_3 v_1 + \Delta u_1 v_3) \\
 M_{23} &= \Delta S \mu (\Delta u_2 v_3 + \Delta u_3 v_2)
 \end{aligned} \tag{23}$$

which is often written as

$$\mathbf{M} = \mu \Delta S (\Delta \vec{u} \vec{v}^T + \vec{v}^T \Delta \vec{u}) \tag{23'}$$

By taking the limit, $\Delta S \Rightarrow 0$ ($\Delta u_i \Delta S$ is kept finite), we obtain a point dislocation source that is represented by a moment tensor M_{pq} .

As a special case, consider a case where

$$\bar{\nu} = (0,1,0), \text{ and } \Delta\bar{u} = (\Delta u_1, 0, 0).$$

Then, from (22)

$$M_{12} = \Delta S \mu \Delta u_1 \quad \text{and} \quad M_{pq} = 0 \quad (p \neq 1, q \neq 2)$$

and, from (21)

$$\begin{aligned} u^1 &= (u_{1,2}^1 + u_{2,1}^1) M_{12} \\ u^2 &= (u_{1,2}^2 + u_{2,1}^2) M_{12} \\ u^3 &= (u_{1,2}^3 + u_{2,1}^3) M_{12} \end{aligned}$$

This is the case considered earlier.

Equation (21) can be used to determine the moment tensor from the observed displacement u^k , if the Somigliana tensor u_i^k for the medium is known.

Suppose we observe the displacement ${}_l u^k$ ($l=1,2,3,\dots,L$) at L locations. Then, we can compute ${}_l u_{p,q}^k$ by using the known Somigliana tensor. Then (21) can be written as

$$({}_l u^k) = ({}_l U) (M_{pq}) \quad (24)$$

where $({}_l U)$ is the matrix on the RHS of (21) which can be computed by the known Somigliana tensor. Combining (24) for $l=1,2,3,\dots,L$, we obtain a set of linear equations

with 6 unknowns M_{pq} and $L \times 3$ data, and, for $L > 2$, the equations can be solved (unless the problem is ill-posed) to obtain M_{pq} .

Ge 162 Problem #7 Moment Tensor and Fault Parameters

Consider a fault model as sketched in Figure 1. Only the foot-wall block is shown. (ξ_1, ξ_2, ξ_3) is the fault coordinate system ($+\xi_1$ is in the direction of fault strike), and (x_1, x_2, x_3) is the geographical coordinate system (x_1 : North; x_2 : West; x_3 : Up).

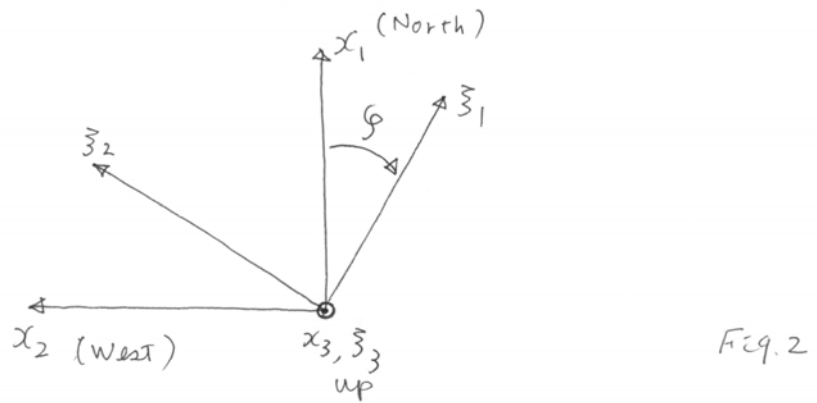
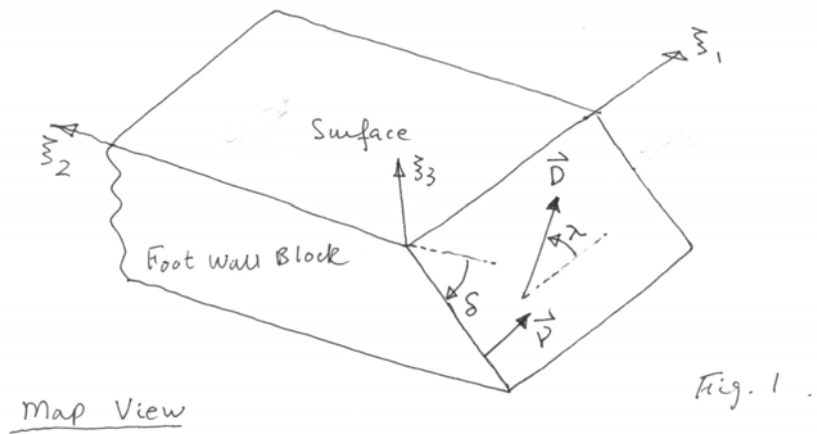
The top surface of the block coincides with the surface of the Earth. \bar{D} is the slip vector of the hanging-wall block (not shown). δ is the dip angle of the fault plane measured downward from the horizontal (i.e. from $-\xi_2$ direction.). λ is the slip angle (rake) measured counter-clockwise on the fault plane from the horizontal line as shown in the figure (i.e. from $+\xi_1$ direction.). \bar{v} is the unit vector normal to the fault plane. Let ΔS be the fault area.

Place this fault model in a homogeneous elastic medium with the rigidity μ at the origin of the Cartesian coordinates as shown in Figure 2. The strike of the fault, ϕ , is measured clockwise on the free surface from x_1 axis in Figure 2. We assume that ΔS is small so that the fault can be considered a point source.

- 1) Determine the ξ_1, ξ_2, ξ_3 components of the displacement vector \bar{D} (magnitude D) and the unit vector \bar{v} .
- 2) Determine the x_1, x_2, x_3 components of the displacement vector \bar{D} (magnitude D) and the unit vector \bar{v} .
- 3) Determine the moment tensor elements M_{ij} ($i, j = 1, 2, 3$) for this fault model. Write the result in terms of scalar moment $M_0 = \mu D \Delta S$, δ , λ , and ϕ . (The results are given in 5.1.4.) (Note that this is a shear dislocation.)

4) Determine the moment tensors for the Hector Mine earthquake, the Chi-Chi Taiwan earthquake, and the Bhuj India earthquake. The fault parameters for these events are given below (δ (dip in degree), λ (rake in degree), ϕ_f (strike in degree), M_0 (Seismic Moment in N-m)).

1999, Hector Mine	85,	179,	336,	5.9×10^{19}
1999, Chi-Chi, Taiwan	27,	82,	26,	4.1×10^{20}
2001, Bhuj, India	50,	50,	65,	3.6×10^{20}



Ge 162

5.1.4 Summary of Static Source Representation

1. Green's Function

Apply unit point force in k direction at $\bar{\xi} = (\xi_1, \xi_2, \xi_3)$. Then, the i -th component of the displacement at $\bar{x} = (x_1, x_2, x_3)$ is the Green' function $G_i^k(\bar{x}, \bar{\xi})$.

In a homogeneous whole space, this is given by the Somigliana tensor, u_i^k .

2. Single force at a point

The displacement for a single force $\bar{F}(F^1, F^2, F^3)$ is then

$$u_i = F^k G_i^k \quad (1)$$

3. Distributed force

The displacement due to a distributed force in V_0 can be written as.

$$u_i(\bar{x}) = \int_{V_0} \rho f^k(\bar{\xi}) G_i^k(\bar{x}, \bar{\xi}) dV \quad (3)$$

4. Force Couples

For a unit single couple on the $x_1 - x_2$ plane, the displacement is

$$u_i^{SC} = G_i^{1,2} \quad (3)$$

For a double couple,

$$u_i^{DC} = G_i^{1,2} + G_i^{2,1} \quad (4)$$

In a homogeneous whole space, (3) and (4) can be also written as $u_i^{SC} = -G_{i,2}^1$ and $u_i^{DC} = -(G_{i,2}^1 + G_{i,1}^2)$.

If the force is in $\bar{k} = (k_1, k_2, k_3)$ direction and the arm is in $\bar{l} = (l_1, l_2, l_3)$ direction, then

$$u_i^{SC} = G_i^{p,q} k_p l_q \quad (5)$$

This can be shown as follows. Let $G_i^{(f)}$ be the i -th component of displacement due to a unit force in \bar{k} direction, and $\frac{\partial}{\partial s_l}$ be the derivative in \bar{l} direction, then

$$u_i^{SC} = \frac{\partial G_i^{(f)}}{\partial s_l} = l_q \frac{\partial}{\partial x_q} (G_i^p k_p) = G_i^{p,q} k_p l_q \quad (5)$$

Then, the displacement due to a unit double couple is

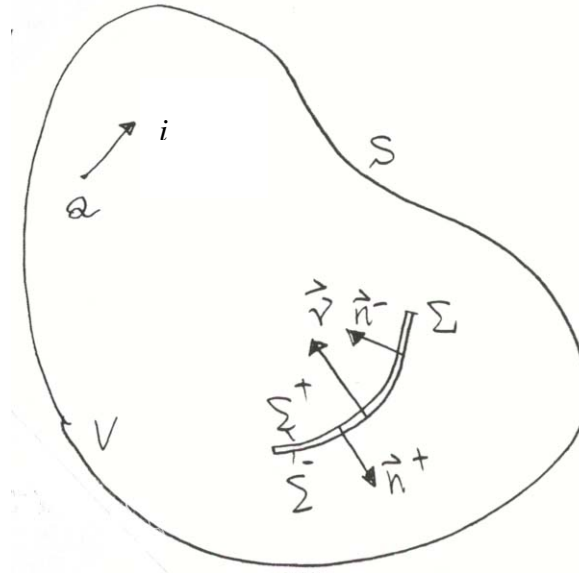
$$u_i^{DC} = G_i^{p,q} (k_p l_q + k_q l_p) \quad (6)$$

For a source represented by force couples and dipoles with the strength (moment) given by M_{kj} ,

$$u_i = M_{kj} G_i^{k,j} \quad (7)$$

5. Dislocation source

Referring to the figure below. the displacement due to an elastic dislocation $\Delta \bar{u}$ on the surface Σ can be written as



$$u^i = \int_{\Sigma} \tau_{pq}^i \Delta u_p v_q dS \quad (8)$$

$$\tau_{pq}^i = c_{pqkl} G_{k,l}^i \quad (9)$$

$$u^i = \int_{\Sigma} c_{pqkl} G_{k,l}^i \Delta u_p v_q dS = \int_{\Sigma} m_{kl} G_{k,l}^i dS \quad (10)$$

where

$$m_{kl} = c_{pqkl} \Delta u_p v_q \quad (11)$$

In the limit of point dislocation (i.e., $|\Delta \bar{u}| \rightarrow \infty$, $\Sigma \equiv \Delta S \rightarrow 0$ and $|\Delta \bar{u}| \Delta S \rightarrow \text{finite}$)

$$u^i = M_{kl} G_{k,l}^i \quad (12)$$

or, exchanging the source and the observation points,

$$u_i = M_{kl} G_i^{k,l} \quad (12')$$

where

$$M_{kl} = c_{pqkl} \Delta u_p v_q \Delta S = M_{lk} \quad (13)$$

This is the same as the expression for the displacement field due to force couples (7). Thus, a dislocation source is equivalent to force couples.

The explicit form of M_{lk} is:

$$\begin{aligned} M_{11} &= \Delta S \left[(\lambda + 2\mu) \Delta u_1 v_1 + \lambda \Delta u_2 v_2 + \lambda \Delta u_3 v_3 \right] \\ M_{22} &= \Delta S \left[\lambda \Delta u_1 v_1 + (\lambda + 2\mu) \Delta u_2 v_2 + \lambda \Delta u_3 v_3 \right] \\ M_{33} &= \Delta S \left[\lambda \Delta u_1 v_1 + \lambda \Delta u_2 v_2 + (\lambda + 2\mu) \Delta u_3 v_3 \right] \\ M_{12} &= \mu \Delta S (\Delta u_1 v_2 + \Delta u_2 v_1) \\ M_{13} &= \mu \Delta S (\Delta u_1 v_3 + \Delta u_3 v_1) \\ M_{23} &= \mu \Delta S (\Delta u_2 v_3 + \Delta u_3 v_2) \end{aligned} \quad (14)$$

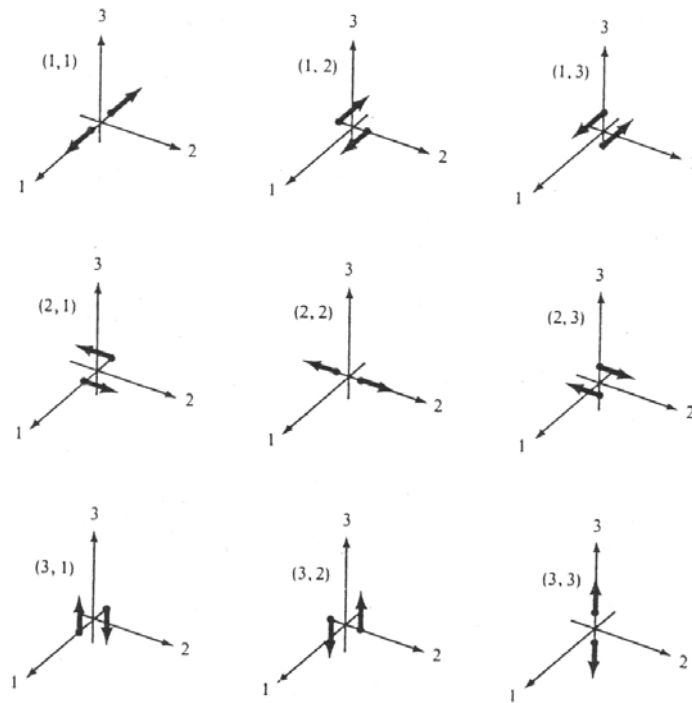
In case of shear dislocation (i.e., $\Delta \bar{u} \perp \bar{v}$), then

$$\begin{aligned} M_{11} &= 2\mu \Delta S \Delta u_1 v_1 \\ M_{22} &= 2\mu \Delta S \Delta u_2 v_2 \\ M_{33} &= 2\mu \Delta S \Delta u_3 v_3 \\ M_{12} &= \mu \Delta S (\Delta u_1 v_2 + \Delta u_2 v_1) \\ M_{13} &= \mu \Delta S (\Delta u_1 v_3 + \Delta u_3 v_1) \\ M_{23} &= \mu \Delta S (\Delta u_2 v_3 + \Delta u_3 v_2) \end{aligned} \quad (15)$$

or,

$$\mathbf{M} = \mu \Delta S (\Delta \bar{u} : \bar{v}) \quad (15')$$

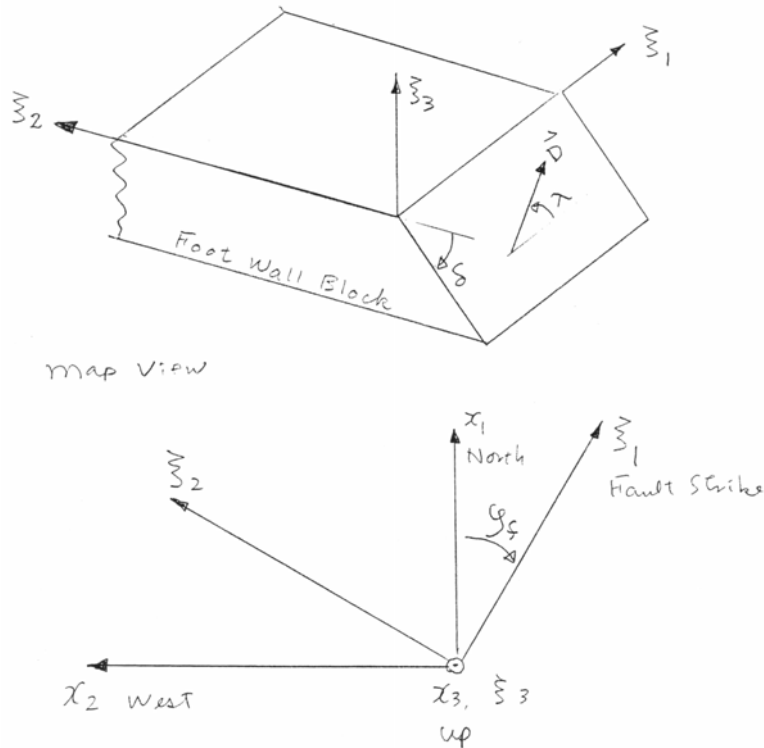
The following figure illustrates the force couples represented by each element of a moment tensor.



6. Fault parameters and Moment tensor elements.

The fault parameters (δ , λ , and ϕ_f) defined in the figure below can be transformed to moment tensor elements by (μDS is assumed to be 1),

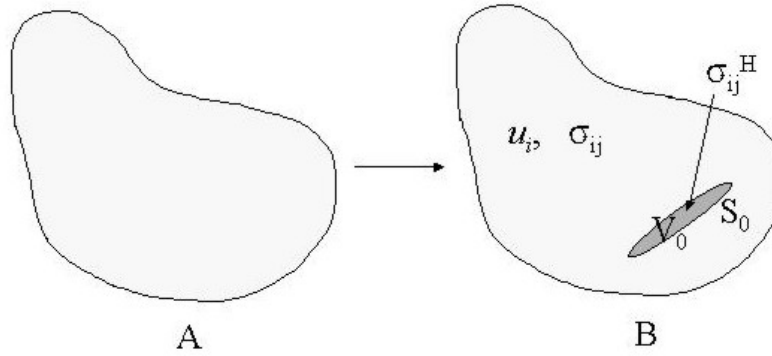
$$\begin{aligned}
 M_{11} &= -\sin^2 \phi_f \sin 2\delta \sin \lambda - \sin 2\phi_f \cos \lambda \sin \delta \\
 M_{22} &= -\cos^2 \phi_f \sin 2\delta \sin \lambda + \sin 2\phi_f \cos \lambda \sin \delta \\
 M_{33} &= \sin 2\delta \sin \lambda \\
 M_{12} &= -\frac{1}{2} \sin 2\phi_f \sin 2\delta \sin \lambda - \cos 2\phi_f \cos \lambda \sin \delta \\
 M_{13} &= \cos \phi_f \cos \delta \cos \lambda + \sin \phi_f \sin \lambda \cos 2\delta \\
 M_{23} &= -\sin \phi_f \cos \delta \cos \lambda + \cos \phi_f \sin \lambda \cos 2\delta
 \end{aligned} \tag{7}$$



(The following part is not complete yet)

6. General Representation

Suppose that the medium is in equilibrium in the beginning (A). Then a failure occurs in V_0 (B), and displacement u_i and stress σ_{ij} are produced in the medium.



The equation for static equilibrium,

$$\sigma_{ij,j} = 0 \quad (16)$$

holds everywhere including V_0 . In the region outside of V_0 , u_i and σ_{ij} are related by elastic constitutive relations; i.e., stress can be computed from u_i . However, the elastic constitutive relation does not hold in the failure zone V_0 . Thus, σ_{ij} cannot be computed from u_i . If we assume hypothetical elastic constants in V_0 , then, we can compute the stress in V_0 from u_i . We denote this stress by σ_{ij}^H (i.e., Hooke's stress). σ_{ij}^H is different from σ_{ij} . Then we can write (16) as

$$\sigma_{ij}^H - (\sigma_{ij}^H - \sigma_{ij}) = \sigma_{ij}^H - m_{ij} = 0 \quad (17)$$

where

$$m_{ij} = (\sigma_{ij}^H - \sigma_{ij}) \quad (18)$$

m_{ij} vanishes outside of V_0 .

The form of equation (17) suggests that $-m_{ij,j}$ can be considered as equivalent body force. Thus, the displacement can be written as

$$u_i = \int_{V_0} (-m_{kl,l} G_i^k) dV \quad (19)$$

Using the Gauss theorem,

$$\int_{V_0} (m_{kl} G_i^k)_{,l} dV = \int_{V_0} m_{kl,l} G_i^k dV + \int_{V_0} m_{kl} G_{i,l}^k dV = \int_{S_0} m_{kl} G_i^k n_l dS = 0$$

(S_0 can be taken slightly outside of V_0). Then, (19) can be written as

$$u_i = \int_{V_0} m_{kl} G_i^{k,l} dV \quad (20)$$

For a point source,

$$\int_{V_0} m_{kl} dV \rightarrow M_{kl} \quad (21)$$

and

$$u_i = M_{kl} G_i^{k,l} \quad (22)$$

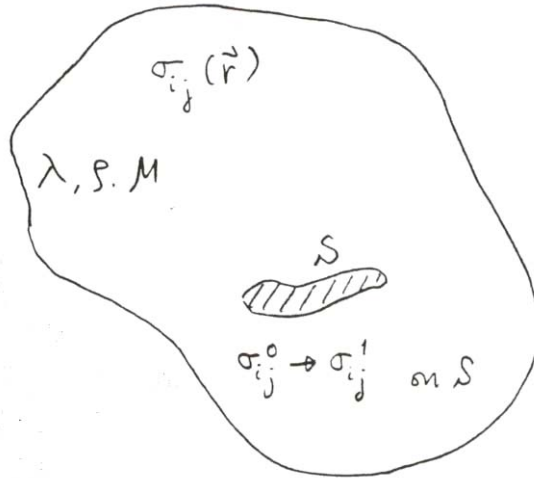
which is the same as (12').

m_{ij} defined by (18) can be considered as a general source representation, and is called the seismic moment tensor.

5.1.5 Stress Relaxation

1. Description of the Problem

Consider an elastic medium which is in equilibrium under stress $\sigma_{ij}(\vec{r})$. Let S be an open surface defined in this medium of which the stress is $\sigma_{ij}^{(0)}(\vec{r})$. Relax the stress from $\sigma_{ij}^{(0)}$ to $\sigma_{ij}^{(1)}$ by creating a cut on S and letting the material on either side of S to move. Let $\Delta\vec{u}$ be the resulting dislocation (displacement discontinuity). $\Delta\vec{u}$ is not necessarily parallel to S . We want to determine $\Delta\vec{u}$, and the difference in strain energy ΔW between the two states, before and after the crack formation.



2. Qualitative Solution of the Problem

Let us consider a planar crack S under uniform shear stress σ_0 . If the stress is relaxed on the crack surface to $\sigma_1 (= \text{const})$, there will be a displacement offset Δu across the crack. In general, this is not uniform on S . Let \bar{D} be the average of Δu on S . If the representative dimension of the crack is L , then the change in ε would be

$$\Delta\varepsilon \approx \bar{D}/(L/2)$$

This strain change is caused by the change in the stress $\Delta\sigma = \sigma_0 - \sigma_1$, which we call stress drop. Thus,

$$\Delta\sigma = \mu\Delta\varepsilon = c\mu\bar{D}/(L/2) \quad (1)$$

where c is a non-dimensional constant which depends upon the shape of the crack; it is apparent from the above argument that $c \sim 1$.

The simplest case is a circular crack. If a is the radius of the crack, we can show that $L = 2a$ and $c = 7\pi/16$ ($\lambda = \mu$ is assumed).

$$\Delta\sigma = (7\pi/16)\mu\bar{D}/a \quad (2)$$

The change in the strain energy ΔW is given by $S\bar{\sigma}\bar{D}$. This is analogous to the change in the strain energy of a spring (spring constant k) which is stretched from x_0 to x_1 . The change in the strain energy is

$$\Delta W = (1/2)k(x_0^2 - x_1^2) = (1/2)k(x_0 + x_1)(x_0 - x_1)$$

where $(1/2)k(x_0 + x_1)$ is the average force and $(x_0 - x_1)$ is the displacement.

Thus, for the circular crack

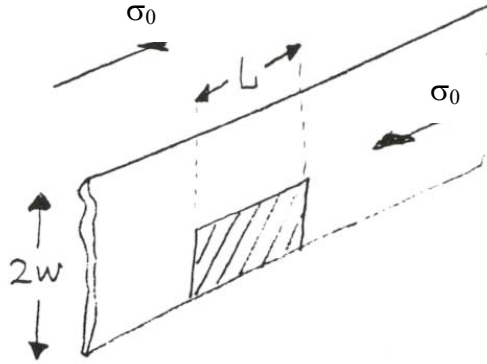
$$\Delta W = S\bar{\sigma}\bar{D} = (16/7\mu)a^3\Delta\sigma\bar{\sigma} \quad (3)$$

where $\bar{\sigma} = (\sigma_0 + \sigma_1)/2$ is the average stress.

If we use the dislocation theory, this crack can be represented by a distribution of double couples whose total moment M_0 is

$$M_0 = \mu S\bar{D} = (16/7)a^3\Delta\sigma \quad (4)$$

Next, we consider a crack as shown by the figure.



The crack is a strip with a width of $2w$ and of infinite length. We consider a uniform shear stress parallel to this strip. Because of the geometrical similarity between this crack and a strike slip fault, we call this crack a strike-slip crack. In mechanics, this is called Mode III crack. The argument similar to that made for the circular crack leads to

$$\Delta\varepsilon \approx \bar{D}/w \quad \text{and} \quad \Delta\sigma = \mu\Delta\varepsilon = c\mu(\bar{D}/w), \quad c \approx o(1)$$

we can prove that $c = 2/\pi$. If the crack is not infinitely long but of finite length L , the above relation is not exact. However, when L is very long, it is a good approximation.

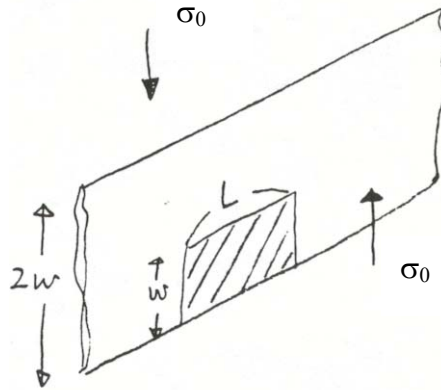
For practical applications, we often take one half of the crack as shown by the hatched portion in the figure. For this crack,

$$\Delta\sigma = (2/\pi)\mu(\bar{D}/w)$$

$$\Delta W = Lw\bar{\sigma}\bar{D} = (\pi/2\mu)w^2L\Delta\sigma\bar{\sigma} \quad (5)$$

$$M_0 = \mu wL\bar{D} = (\pi/2)w^2L\Delta\sigma \quad (6)$$

Another useful geometry is shown below.



The crack extends in the direction perpendicular to the uniform shear stress. In this case we can derive

$$\Delta\sigma = \frac{4(\lambda + \mu)\mu}{\pi(\lambda + 2\mu)} (\bar{D}/w)$$

We call this crack a dip-slip crack. In mechanics, this is called Mode II crack. For the hatched portion,

$$\Delta W = Lw\bar{\sigma}\bar{D} = \frac{\pi(\lambda + 2\mu)}{4(\lambda + \mu)\mu} w^2 L\Delta\sigma\bar{\sigma}$$

and

$$M_0 = \mu Lw\bar{D} = \frac{\pi(\lambda + 2\mu)}{4(\lambda + \mu)} w^2 L\Delta\sigma$$

These relations are summarized in the following table.

	Circular ($\lambda = \mu$)	Strike Slip (Mode III)	Dip Slip (Mode II)
Stress drop, $\Delta\sigma$	$(7\pi/16)\mu\bar{D}/a$	$(2/\pi)\mu(\bar{D}/w)$	$\frac{4(\lambda + \mu)\mu}{\pi(\lambda + 2\mu)} (\bar{D}/w)$

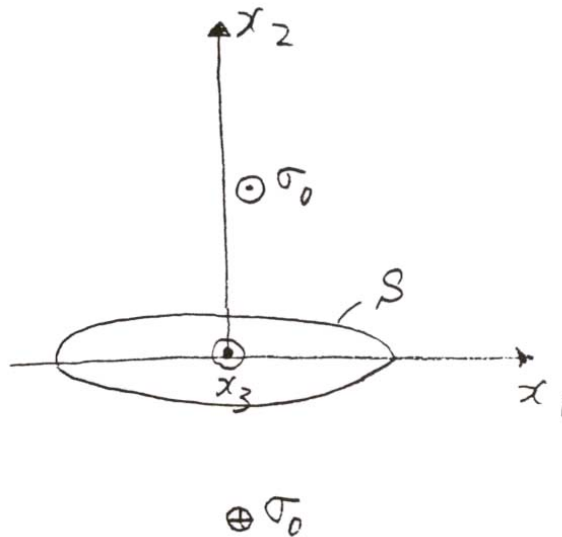
Strain Energy, $\Delta W = S\bar{\sigma}\bar{D}$	$(16/7\mu)a^3\Delta\sigma\bar{\sigma}$	$(\pi/2\mu)w^2L\Delta\sigma\bar{\sigma}$	$\frac{\pi(\lambda+2\mu)}{4(\lambda+\mu)\mu}w^2L\Delta\sigma\bar{\sigma}$
Moment, $M_0 = \mu S\bar{D}$	$(16/7)a^3\Delta\sigma$	$(\pi/2)w^2L\Delta\sigma$	$\frac{\pi(\lambda+2\mu)}{4(\lambda+\mu)}w^2L\Delta\sigma$

Relations between stress drop, strain energy change, offset, dimension, and moment for static cracks. Dimensions of the fault are a radius, L length, w width; initial stress is σ_0 ; final stress is σ_1 ; stress drop is $\Delta\sigma = (\sigma_0 - \sigma_1)$; average stress is $\bar{\sigma} = 1/2(\sigma_0 + \sigma_1)$; average dislocation is \bar{D} .

3. Elasto-Static Theory of Crack

Here, we consider only a strike-slip crack (Mode III). In this case, the displacement field has a component only in the direction parallel to the crack. Therefore, the problem becomes 2-dimensional.

Consider a crack extending in x_3 of which the cross-section is elliptic. We will later reduce this ellipse to a infinitesimally thin strip.



Initially the crack is not formed. We introduce initial displacement field

$$\bar{U}^{(0)} = (0, 0, U_3^{(0)})$$

where $U_3^{(0)} = A_0 x_2$. Since the stress corresponding to this displacement is

$$\sigma_0 = \mu \frac{\partial U_3^{(0)}}{\partial x_2} = \mu A_0 = \text{const},$$

we have a uniform initial shear stress $\sigma_0 = \mu A_0$. Let \bar{U} be

the displacement after the crack is formed. Because of the symmetry of the problem, \bar{U} has only x_3 component. i.e.,

$$\bar{U} = (0, 0, U_3) \quad (7)$$

where U_3 does not depend on x_3 , and

$$\text{div} \bar{U} = 0 \quad (8)$$

Thus, the equation of equilibrium

$$(\lambda + 2\mu) \text{grad} \text{div} \bar{U} - \mu \text{curl} \text{curl} \bar{U} = 0 \quad (9)$$

gives

$$\text{curl} \text{curl} \bar{U} = 0 \quad (10)$$

If we put

$$\bar{A} = \text{curl} \bar{U} \quad (11)$$

then, from (10),

$$\text{curl} \bar{A} = 0 \quad (12)$$

Also from (11),

$$\text{div} \bar{A} = 0 \quad (13)$$

From (12) we can put

$$\bar{A} = -grad\phi \quad (14)$$

where ϕ is a scalar potential. Substituting (14) into (13)

$$\nabla^2\phi = 0 \quad (15)$$

From (11) and (14),

$$\left(\frac{\partial U_3}{\partial x_2}, -\frac{\partial U_3}{\partial x_1}, 0 \right) = \left(-\frac{\partial \phi}{\partial x_1}, -\frac{\partial \phi}{\partial x_2}, -\frac{\partial \phi}{\partial x_3} \right) \quad (16)$$

Let us consider a case where the stress on the crack is completely released, i.e., $\tau_{32} = 0$ on S .

$$\mu \frac{\partial U_3}{\partial x_2} = 0 \quad \text{on } S$$

By (16), this condition can be restated as

$$\frac{\partial \phi}{\partial x_1} = 0 \quad \text{on } S$$

Since $\frac{\partial \phi}{\partial x_3} = 0$ (see (16)), $\phi = \phi(x_2)$. In the limit of a very thin crack $x_2 = 0$ on S ; thus,

$\phi = \text{const}$ on S . Since ϕ is a potential, we can put, for the boundary condition

$$\phi = 0, \quad \text{on } S \quad (17)$$

Thus, our problem is now reduced to a problem of finding a solution of (15), with a boundary condition (17). Note that this problem is equivalent to the well-known electro-static problem of finding an electro-static field due to a perfect conductor placed in vacuum.

To solve this, we introduce elliptic coordinates (ξ_1, ξ_2) by

$$x_1 = a \cosh \xi_1 \cos \xi_2 \quad \text{and} \quad x_2 = a \sinh \xi_1 \sin \xi_2 \quad (18)$$

Then

$$w = x_1 + ix_2 = a \cosh(\xi_1 + i\xi_2) = a \cosh(\zeta) \quad (19)$$

where $\zeta = \xi_1 + i\xi_2$. $\xi_1 = \text{const}$ gives an ellipse with a major axis $a \cosh \xi_1$, and a minor axis $a \sinh \xi_1$. Thus, the elliptic crack is given by $\xi_1 = \text{const}$, and the limiting case $\xi_1 = 0$ represents an infinitesimally thin crack of width $2a$.

We write

$$\phi = \phi_0 + \phi' \quad (20)$$

where ϕ_0 represents the initial field, and ϕ' , the perturbation due to the crack. Since the initial field is $U_3^{(0)} = A_0 x_2$,

$$\phi_0 = -A_0 x_1 = -A_0 a \cosh \xi_1 \cos \xi_2 \quad (21)$$

$$\phi = -A_0 a \cosh \xi_1 \cos \xi_2 + \phi' \quad (22)$$

Since $\nabla^2 \phi = 0$, and $\nabla^2 \phi_0 = 0$ (from (21)),

$$\nabla^2 \phi' = 0 \quad (23)$$

Since $\phi = 0$ on S ($\xi_1 = \text{const}$), ϕ' must have the form

$$\phi' = F(\xi_1) \cos \xi_2 \quad (24)$$

From $\nabla^2 \phi' = 0$, we have (use Laplacian for the elliptic coordinates),

$$\frac{d^2 F}{d\xi_1^2} = F$$

$$\therefore F(\xi_1) = A \exp(-\xi_1) + B \exp(+\xi_1) \quad (25)$$

Because $F(\xi_1)$ must be finite for $\xi_1 \rightarrow \infty$, we take only the first term

$$\phi = (A \exp(-\xi_1) - A_0 a \cosh \xi_1) \cos \xi_2 \quad (26)$$

From the condition that $\phi = 0$ at $\xi_1 = 0$,

$$\begin{aligned} A &= A_0 a \\ \phi &= -A_0 a \sinh \xi_1 \cos \xi_2 = -\frac{1}{2} A_0 a (\sinh \zeta + (\sinh \zeta)^*) \\ &= -A_0 a \operatorname{Re}(\sinh \zeta) = -A_0 a \operatorname{Re}(\cosh^2 \zeta - 1)^{1/2} = -A_0 \operatorname{Re}(w^2 - a^2)^{1/2} \end{aligned} \quad (27)$$

Since, from (16)

$$\frac{\partial \phi}{\partial x_1} = \frac{\partial(-U_3)}{\partial x_2} \quad \text{and} \quad \frac{\partial \phi}{\partial x_2} = -\frac{\partial(-U_3)}{\partial x_1}$$

From the Cauchy-Riemann relation, if ϕ is the real part of analytic function

$-A_0(w^2 - a^2)^{1/2}$ of $w = x_1 + ix_2$, as shown above, then $-U_3$ is the imaginary part of $-A_0(w^2 - a^2)^{1/2}$. Thus

$$U_3 = A_0 \operatorname{Im}(w^2 - a^2)^{1/2} = \frac{\sigma_0}{\mu} \operatorname{Im}(w^2 - a^2)^{1/2} \quad (28)$$

is the solution of the problem.

With the solution,

$$U_3 = A_0 \operatorname{Im}(w^2 - a^2)^{1/2} = \frac{\sigma_0}{\mu} \operatorname{Im}(w^2 - a^2)^{1/2} \quad (w = x_1 + ix_2) \quad (28)$$

first, consider the displacement field on $x_1 - x_3$ plane (plane of the crack).

In this case $x_2 = 0$, and $w = x_1$.

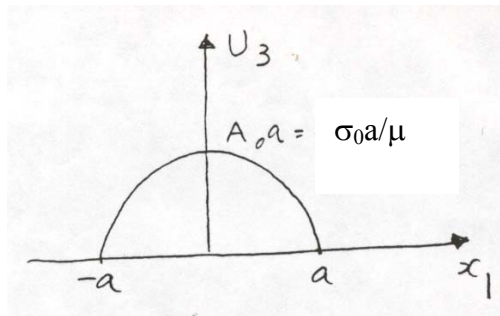
$$U_3 = \frac{\sigma_0}{\mu} \operatorname{Im}(x_1^2 - a^2)^{1/2}$$

$$U_3 = 0, \quad x_1 > a \quad (29)$$

\therefore

$$U_3 = \frac{\sigma_0}{\mu} (a^2 - x_1^2)^{1/2}, \quad x_1 \leq a$$

This is shown in the figure.



The maximum displacement $U_{3\max}$ is

$$U_{3\max} = \left(\frac{\sigma_0}{\mu} \right) a$$

and the average displacement is

$$\bar{U}_3 = \frac{1}{2a} \int_{-a}^a \frac{\sigma_0}{\mu} (a^2 - x_1^2)^{1/2} dx_1 = (\pi\sigma_0 / 4\mu)a \quad (30)$$

The average dislocation is

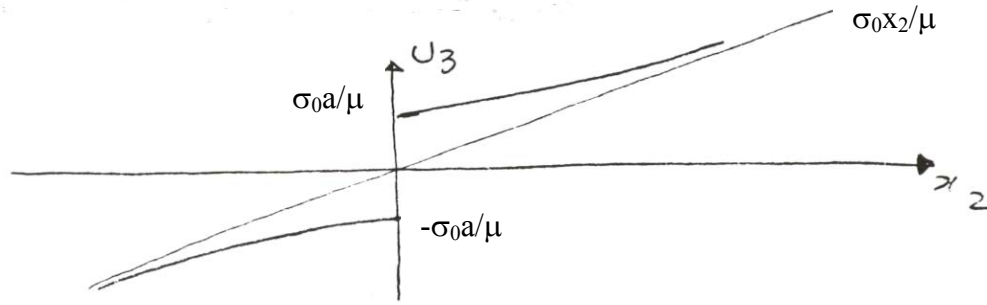
$$\bar{D} = 2\bar{U}_3 = (\pi\sigma_0 / 2\mu)a \quad (31)$$

For a partial stress drop in which stress drops from σ_0 to σ_1 , σ_0 in (31) should simply be replaced by $\Delta\sigma = \sigma_0 - \sigma_1$. If we replace a in (31) by width w , (31) leads to the relation given in the table.

Next, let us consider the displacement on $x_2 - x_3$ plane. Putting $x_1 = 0$, we have, from (28)

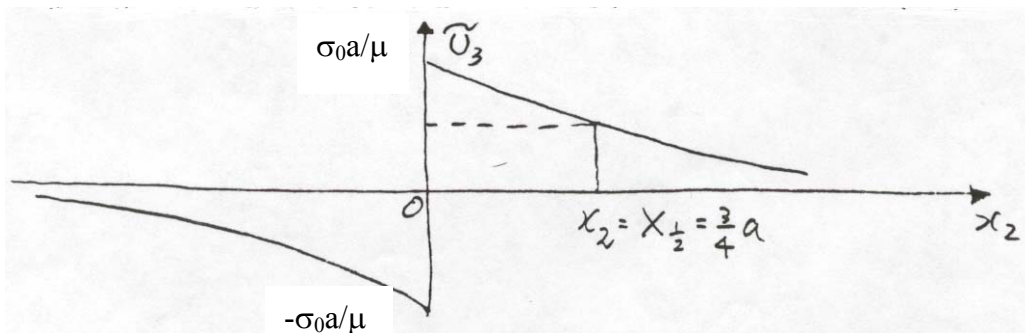
$$U_3 = \frac{\sigma_0}{\mu} \text{Im}(-x_2^2 - a^2)^{1/2} = \pm \left(\frac{\sigma_0}{\mu} \right) (x_2^2 + a^2)^{1/2} \quad (32)$$

+ sign is taken for $x_2 > 0$, and - sign for $x_2 < 0$.



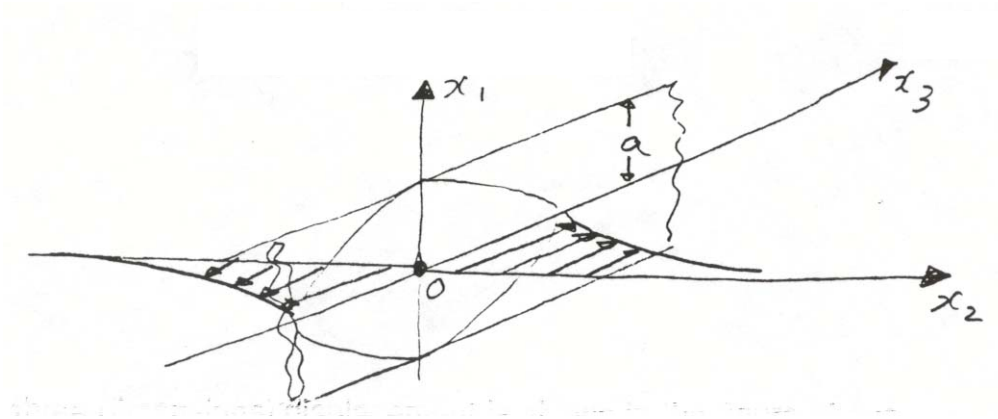
Since the initial field is $\left(\frac{\sigma_0}{\mu}\right)x_2$, the actual displacement caused by the crack is obtained by subtracting $\left(\frac{\sigma_0}{\mu}\right)x_2$ from (32):

$$\tilde{U}_3 = U_3 - \left(\frac{\sigma_0}{\mu}\right)x_2 = \left(\frac{\sigma_0}{\mu}\right)\left[\pm(x_2^2 + a^2)^{1/2} - x_2\right] \quad (33)$$



The x_2 coordinate where the displacement decays to half is given by

$$X_{1/2} = (3/4)a \quad \text{or} \quad a = (4/3)X_{1/2} \quad (34)$$

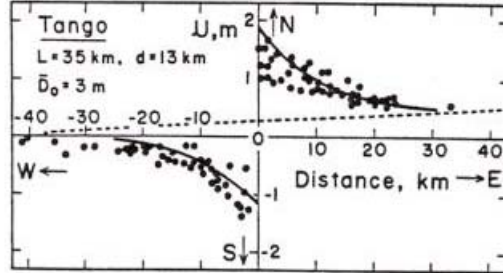
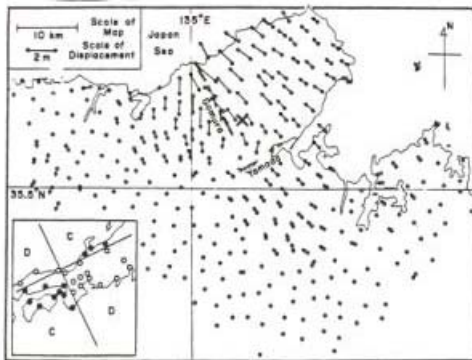


The three-dimensional displacement is shown in the figure above.

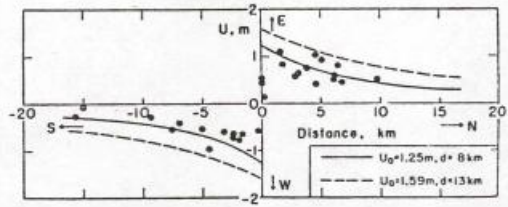
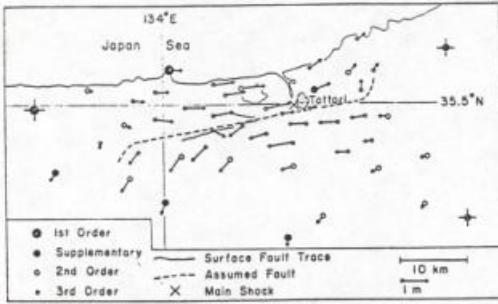
If we use this model, we can estimate the depth of the fault from the observed decay rate of the displacement field by using (34).

In the following examples, $U_3(x_1 = 0)$ is plotted as a function of x_2 . It is readily seen that $X_{1/2} = 10$ km for Tango, 7 km for Tottori and 5 km for the San Francisco earthquakes. From these values, $w \sim 13$ km, 9 km and 7 km are obtained for these earthquakes. However, because of the incompleteness of the data set for the San Francisco earthquake, the estimate of w for this event is very uncertain.

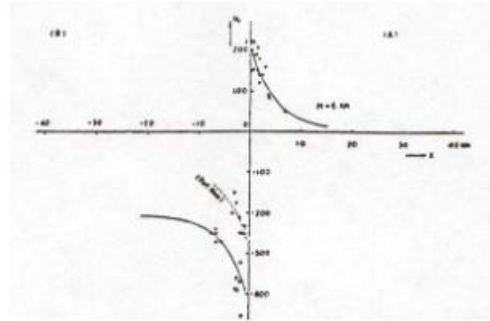
1927 Tango Earthquake (M=7.5)



1943 Tottori Earthquake (M=7.3)



1906 San Francisco Earthquake M=8



4. Stress

Next, let us consider the change in the stress. Since $U_1 = 0$, $U_2 = 0$, $U_3(x_1, x_2)$, only nonzero components of stress are $\tau_{32} = \mu \frac{\partial U_3}{\partial x_2}$ and $\tau_{31} = \mu \frac{\partial U_3}{\partial x_1}$.

Using (28), we have on $x_2 - x_3$ plane (i.e., $x_1 = 0$)

$$\tau_{31} = 0, \text{ and } \tau_{32} = \sigma_0 x_2 \frac{1}{(x_2^2 + a^2)^{1/2}} = \sigma_0 \frac{1}{(1 + (a/x_2)^2)^{1/2}} \quad (35)$$

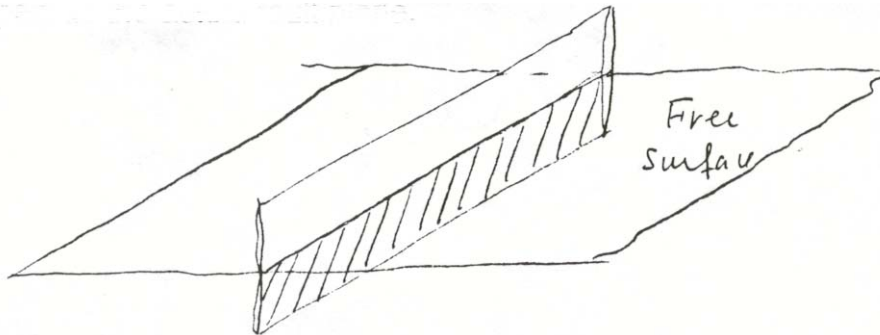
Note: (28) gives the solution as an imaginary part of an analytic function. The derivatives of U_3 with respect to x_1 and x_2 can be obtained using the following relation.

Consider an analytic function $\Psi(w) = P(x_1, x_2) + iQ(x_1, x_2)$ of $w = x_1 + ix_2$. Then

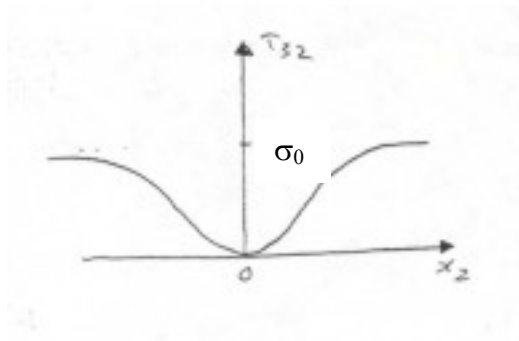
$$\frac{\partial \Psi}{\partial w} = \frac{\partial P}{\partial x_1} + i \frac{\partial Q}{\partial x_1}, \quad \text{and} \quad \frac{\partial \Psi}{\partial w} = \frac{\partial P}{\partial(ix_2)} + i \frac{\partial Q}{\partial(ix_2)} = -i \frac{\partial P}{\partial x_2} + \frac{\partial Q}{\partial x_2}$$

Hence, $\frac{\partial Q}{\partial x_1}$ is the imaginary part of $\frac{\partial \Psi}{\partial w}$, and $\frac{\partial Q}{\partial x_2}$ is the real part of $\frac{\partial \Psi}{\partial w}$.

Since $\tau_{11} \equiv 0$ and $\tau_{12} \equiv 0$, $\tau_{31} = 0$ obtained above means that the $x_2 - x_3$ plane can be considered as a stress free surface. Thus, it is convenient to take this plane as a free surface in modeling a shallow fault. In this case, we consider one half of the crack as shown by the hatched part as the actual fault plane.



The stress τ_{32} changes as a function of x_2 on $x_2 - x_3$ plane as shown in the following figure.

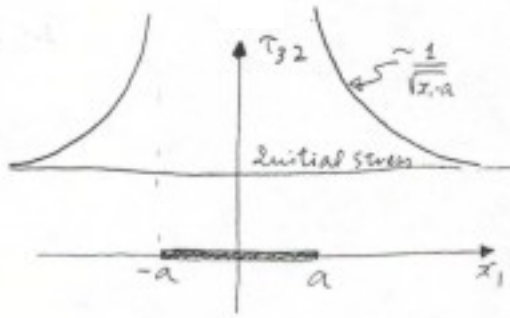


On $x_1 - x_3$ plane ($x_2 = 0$), we have

$$\begin{aligned} \tau_{32} &= 0, & |x_1| < a \\ \tau_{32} &= \sigma_0 x_1 \frac{1}{(x_1^2 - a^2)^{1/2}}, & |x_1| > a \end{aligned} \quad (36)$$

As shown in the figure τ_{32} has a singularity at $x_1 = a$ of the order of $(x_1 - a)^{-1/2}$ (i.e., square-root singularity). This singularity is typical of this type of thin cracks. Near, $x_1 = a$, i.e., at $x_1 = a + \varepsilon$ ($\varepsilon \ll a$), and

$$\tau_{32} = \sigma_0 x_1 \frac{1}{(x_1 - a)^{1/2} (x_1 + a)^{1/2}} \approx \sigma_0 \sqrt{\frac{a}{2}} \varepsilon^{-1/2} \quad (36')$$



5.2 Elasto-Dynamic Source ---Summary of 5.2.1. and 5.2.2. ---

5.2.1 Displacement Field due to a Point Force and Force Couples (Time-dependent case)

The derivation is more complex than that for the static case, but is similar. The displacement field consists of near-field and far-field. The field consists of "compressional" and "shear", propagating at P and S wave velocities, respectively. The near-field term yields displacement between P and S waves, as shown in the figure on page 5.

The following relation holds.

$$u_i^j(t; \tau) = u_i^j(-\tau; -t)$$

5.2.2 Force Couples

The derivation is essentially similar to that for the static case. In general, the displacement field consists of near-field and far-field.

Far field:

$$u \approx \frac{M'(\tau)}{4\pi\rho v^3 r}$$

Near field

$$u \approx \frac{M(\tau)}{4\pi\rho v^2 r^2}$$

The displacement is schematically shown on page 7

The most important relation is given by equation 17', which gives the radiation pattern and the amplitude of far-field P and S waves. The radiation pattern is exactly the same as that for the static field.

For a shear faulting, S wave is much larger than P wave.

$$\frac{|\max u_r|}{|\max u_\phi|} = \left(\frac{v_s}{v_p}\right)^3 \approx \frac{1}{5}$$

5.2 Elasto-Dynamic Source

5.2.1 Displacement Field due to a Point Force and Force Couples (Time-dependent case)

Single Force

The method is essentially the same as that used for static problem.

The equation of motion is:

$$\rho \frac{\partial^2 \bar{u}}{\partial t^2} = \rho \bar{f} + (\lambda + 2\mu) \text{graddiv} \bar{u} - \mu \text{curlcurl} \bar{u} \quad (1)$$

A point force is given by:

$$\begin{aligned} \rho \bar{f} &= F \bar{a} \delta(r) h(t) = -F h(t) \nabla^2 \left(\frac{\bar{a}}{4\pi r} \right) \\ &= -F h(t) \left[\text{graddiv} \left(\frac{\bar{a}}{4\pi r} \right) - \mu \text{curlcurl} \left(\frac{\bar{a}}{4\pi r} \right) \right] \end{aligned} \quad (2)$$

We seek a solution in the form

$$\bar{u} = \text{graddiv} \bar{A}_p - \mu \text{curlcurl} \bar{A}_s \quad (3)$$

Then, we obtain,

$$(\lambda + 2\mu) \nabla^2 \bar{A}_p = \frac{F h(t)}{4\pi r} \bar{a} + \rho \frac{\partial^2 \bar{A}_p}{\partial t^2} \quad (4)$$

$$\mu \nabla^2 \bar{A}_s = \frac{F h(t)}{4\pi r} \bar{a} + \rho \frac{\partial^2 \bar{A}_s}{\partial t^2} \quad (5)$$

Putting

$$\bar{A}_p = A_p \bar{a} \quad \text{and} \quad \bar{A}_s = A_s \bar{a} \quad (6)$$

$$\nabla^2 A_p = \frac{F h(t)}{4\pi(\lambda + 2\mu)r} \bar{a} + \frac{1}{v_p^2} \frac{\partial^2 A_p}{\partial t^2} \quad (7)$$

$$\nabla^2 A_s = \frac{F h(t)}{4\pi\mu r} \bar{a} + \frac{1}{v_s^2} \frac{\partial^2 A_s}{\partial t^2} \quad (8)$$

where

$$v_p = \sqrt{(\lambda + 2\mu) / \rho} \quad \text{and} \quad v_s = \sqrt{\mu / \rho} \quad (9)$$

are *P*- and *S*-wave velocities, respectively.

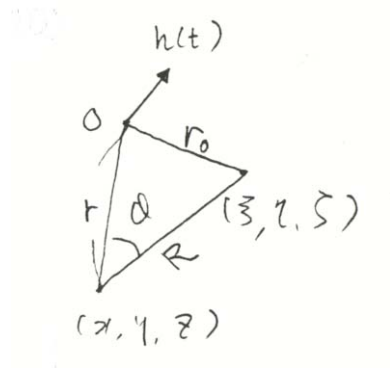
Note that, the solution of an inhomogeneous scalar wave equation,

$$\nabla^2 \phi(x, y, z, t) - \frac{1}{c^2} \frac{\partial^2 \phi(x, y, z, t)}{\partial t^2} = -g(x, y, z, t) \quad (10)$$

is given by,

$$\phi(x, y, z, t) = \frac{1}{4\pi} \int_V \frac{g(\xi, \eta, \zeta, t \pm R/c)}{R} d\xi d\eta d\zeta \quad (11)$$

where $R^2 = (x - \xi)^2 + (y - \eta)^2 + (z - \zeta)^2$



Using this relation, and carrying out the integration, we obtain

$$A_p(r, t) = \frac{F}{4\pi\rho} \left[\frac{1}{r} \int_0^\infty h(t \pm r/v_p \pm v) v dv - \frac{1}{r} \int_0^\infty h(t \pm v) v dv \right] \quad (12)$$

$$A_s(r,t) = \frac{F}{4\pi\rho} \left[\frac{1}{r} \int_0^\infty h(t \pm r/v_s \pm v) v dv - \frac{1}{r} \int_0^\infty h(t \pm v) v dv \right] \quad (13)$$

Then, for a unit force ($F=1$),

$$u_i^j = \frac{1}{4\pi\rho} \left\{ \frac{\partial^2}{\partial x_i \partial x_j} \left[\frac{1}{r} \int_0^\infty (h(t \pm r/v_p \pm v) - h(t \pm r/v_s + v)) v dv \right] + \frac{1}{v_s^2} \frac{h(t \pm r/v_s)}{r} \delta_{ij} \right\} \quad (14)$$

This solution gives both outgoing and converging waves. For outgoing waves, we take the minus sign, and rewriting it

$$u_i^j = \frac{1}{4\pi\rho} \frac{\partial^2 r^{-1}}{\partial x_i \partial x_j} \int_{r/v_p}^{r/v_s} v h(t-v) dv + \frac{1}{4\pi\rho v_p^2 r} \frac{x_i x_j}{r^2} h(t-r/v_p) + \frac{1}{4\pi\rho v_s^2 r} \left(\delta_{ij} - \frac{x_i x_j}{r^2} \right) h(t-r/v_s) \quad (15)$$

u_i^j is called Love tensor.

It is easy to show that if a δ function force is applied at $Q(y_1, y_2, y_3)$ at time τ , then the displacement at $P(x_1, x_2, x_3)$ at time t is given by,

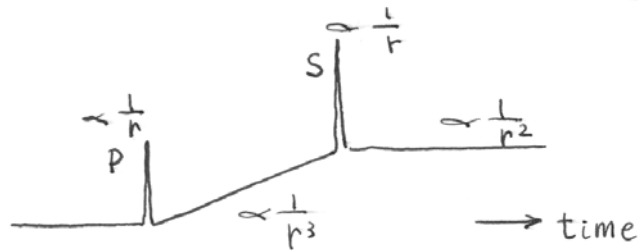
$$u_i^j = \frac{1}{4\pi\rho} \frac{\partial^2 r^{-1}}{\partial x_i \partial x_j} \int_{r/v_p}^{r/v_s} v \delta(t-\tau-v) dv + \frac{1}{4\pi\rho v_p^2 r} \frac{x_i x_j}{r^2} \delta(t-\tau-r/v_p) + \frac{1}{4\pi\rho v_s^2 r} \left(\delta_{ij} - \frac{x_i x_j}{r^2} \right) \delta(t-\tau-r/v_s) \quad (15')$$

where

$$r^2 = (x_i - y_i)^2$$

The 2nd and the 3rd terms decay as $1/r$ and represent propagating P and S waves, respectively. These terms are called far-field. The first term decays as $1/r^2$, and represents displacement between P and S wave arrivals. This term is called near-field.

The time history is schematically shown in the figure below.



Reciprocity

It is evident that

$$u_i^j(t; \tau) = u_j^i(t; \tau).$$

However, since t and τ appear as $t - \tau$,

$$u_i^j(t; \tau) \neq u_i^j(\tau; t)$$

but

$$u_i^j(t; \tau) = u_i^j(-\tau; -t)$$

5.2.2 Force Couples

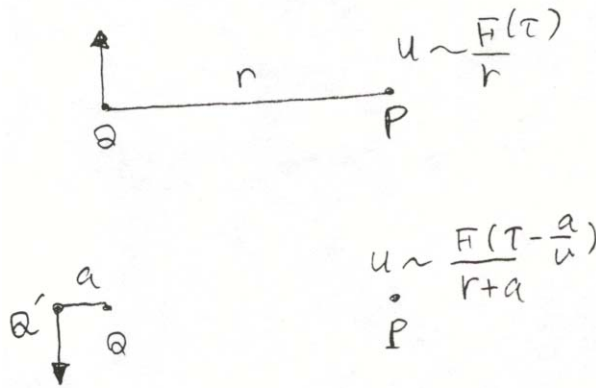
The displacement field for single couples and double couples can be obtained by differentiating (15) with respect to appropriate coordinates.

Qualitative Derivation

For a point force $F(t)$ placed at Q, the displacement at P due to the 2nd or 3rd term is

$$u \propto F(\tau)/r$$

where $\tau = t - r/v$ (v : wave velocity).



For a force at Q' (short distance a away from Q),

$$F(\tau - a/v)/(r + a)$$

Then for a couple

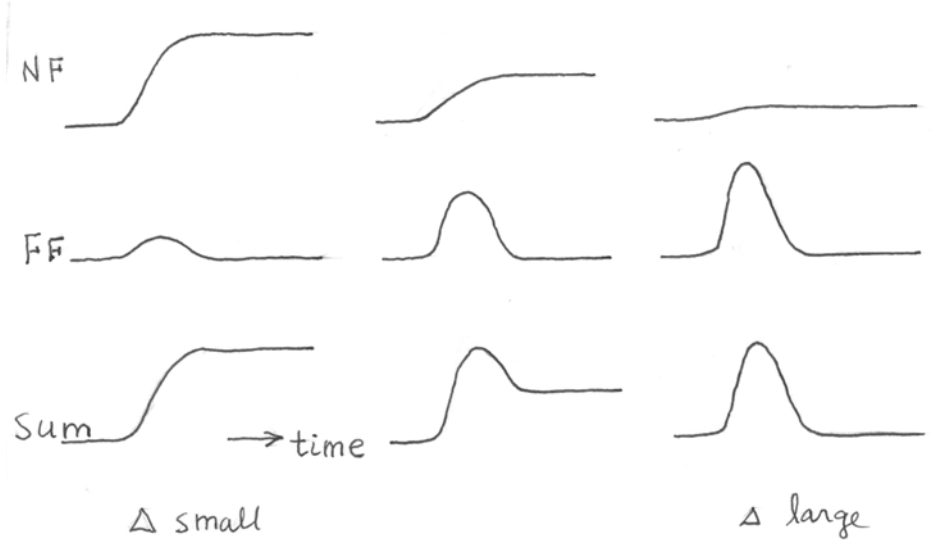
$$\begin{aligned} u &\propto F(\tau)/r - F(\tau - a/v)/(r + a) = F(\tau)/r - (1/r)(1 - a/r)(F(\tau) - (a/v)F'(\tau)) \\ &= aF(\tau)/r^2 + aF'(\tau)/rv = M(\tau)/r^2 + M'(\tau)/rv \end{aligned}$$

The first term decays as $1/r^2$; hence, at large r , we have $M'(\tau)/rv$ which is called far field. At short distance, the first term, $M(\tau)/r^2$, dominates, which is called near field.

Recovering the term $\frac{1}{4\pi\rho v^2}$, we obtain

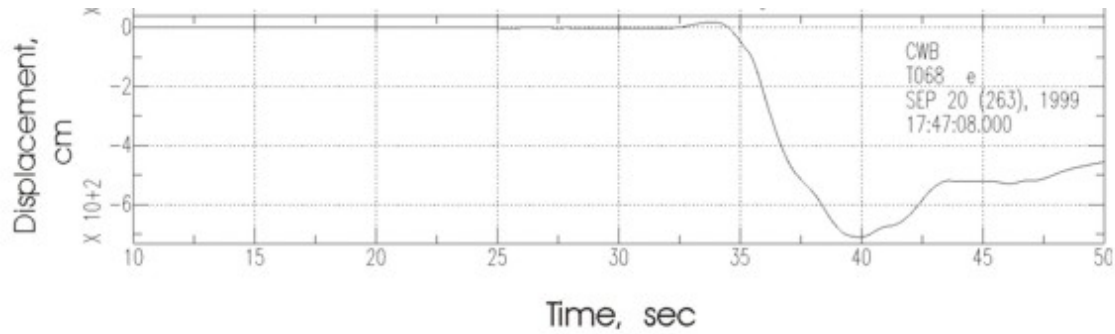
$$u \approx \frac{M(\tau)}{4\pi\rho v^2 r^2} + \frac{M'(\tau)}{4\pi\rho v^3 r} \quad (16)$$

The following figure illustrates the contributions of near-field and far-field displacements.



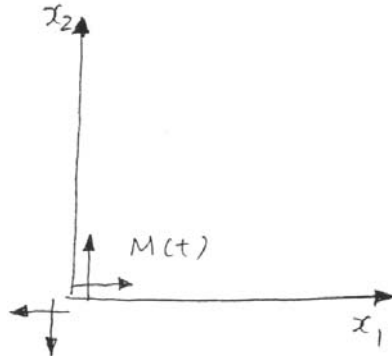
The actual displacement field is more complicated because we need to include the contribution of the 1st term in (15') too. However, at far field, the second term in (16) essentially gives the displacement field which propagates at either P or S wave.

The figure below shows the near-field (+far-field) displacement observed for the 1999 Chi-Chi, Taiwan earthquake.



Elasto-dynamic theory

Here, we consider only the far-field term. If we place a double couple with a moment $M(t)$ on $x_1 - x_2$ plane as shown in the figure,

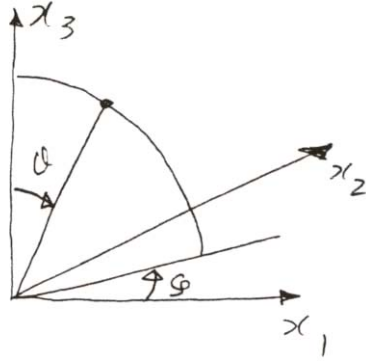


we have at large r (far-field),

$$\begin{aligned}
 u_i = & \frac{1}{4\pi\mu v_p r} 2 \left(\frac{v_s}{v_p} \right)^2 \gamma_i \gamma_1 \gamma_2 M'(t - r/v_p) \\
 & + \frac{1}{4\pi\mu v_s r} (-2\gamma_i \gamma_1 \gamma_2 + \gamma_2 \delta_{i1} + \gamma_1 \delta_{i2}) M'(t - r/v_s)
 \end{aligned} \tag{17}$$

where $\gamma_i = x_i / r$.

If we take the polar coordinates (r, θ, ϕ) ,



$$\gamma_1 = \sin \theta \cos \phi, \quad \gamma_2 = \sin \theta \sin \phi, \quad \gamma_3 = \cos \theta,$$

Then

$$\begin{pmatrix} u_r \\ u_\theta \\ u_\phi \end{pmatrix} = \frac{1}{4\pi\rho r v_p^3} M'(t-r/v_p) \begin{pmatrix} \sin^2 \theta \sin 2\phi \\ 0 \\ 0 \end{pmatrix} + \frac{1}{4\pi\rho r v_s^3} M'(t-r/v_s) \begin{pmatrix} 0 \\ 1/2 \sin 2\theta \sin 2\phi \\ \sin \theta \cos 2\phi \end{pmatrix} \quad (17')$$

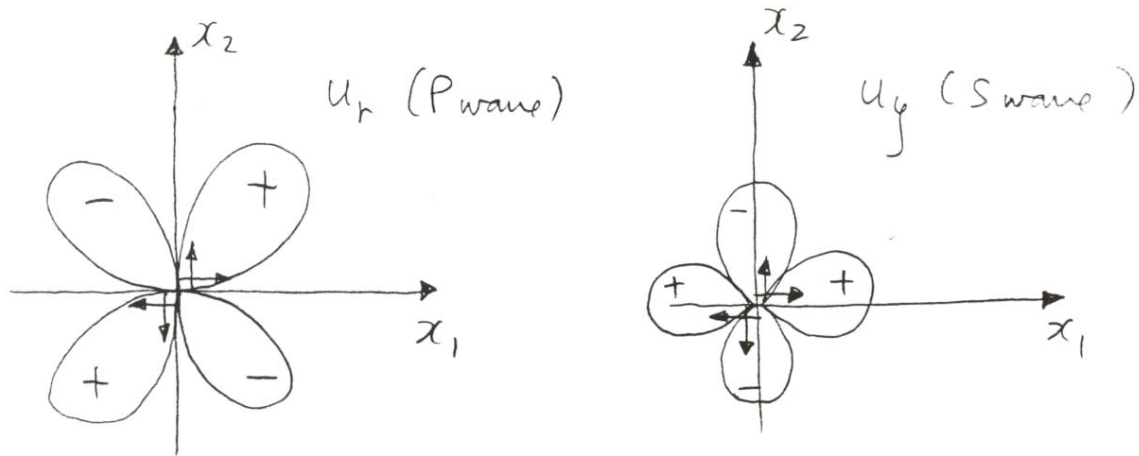
The first term on RHS represents *P* wave and the second term, *S* wave.
On $x_1 - x_2$ plane, $\theta = \pi/2$ and

$$u_r = \frac{1}{4\pi\rho r v_p^3} M'(t-r/v_p) \sin 2\phi$$

$$u_\theta = 0 \quad (18)$$

$$u_\phi = \frac{1}{4\pi\rho r v_s^3} M'(t - r/v_s) \cos 2\phi$$

The amplitude distribution is sketched in the following figures.



Note that the pattern (radiation pattern) is identical to that for the static case. The amplitude ratio

$$\frac{|\max u_r|}{|\max u_\phi|} = \left(\frac{v_s}{v_p}\right)^3 \approx \frac{1}{5}$$

Also the time history of the displacement is given by the time derivative of the moment time function. It is also important that the amplitude decays as $1/r$ in contrast to $1/r^2$ for the static field.

5.2.3 Radiation from a Double-Couple Source

The attached four figures show the waveforms computed for the following:

Fig. 1 and Fig. 2 show the responses in a whole space ($\alpha=6$ km/sec, $\beta=3.5$ km/sec, $\rho=2.6$ g/cm³). The "depth" is 10 km. This means that the displacements are computed at a level 10 km above the source. The mechanism is a N-S striking vertical strike slip with and the seismic moment is 10^{27} dyne-cm. The source time function is a triangle with a rise-time of 0.2 sec and fall-off time of 0.2 sec.

Fig. 1.

Station azimuth=90°. The transverse components are shown at 20 km distance intervals. *P*-wave arrivals are aligned.

Whole Space
Vertical Strike Slip $\phi=90^\circ$
 $M_0=10^{27}$ dyne-cm, $H=10$ km

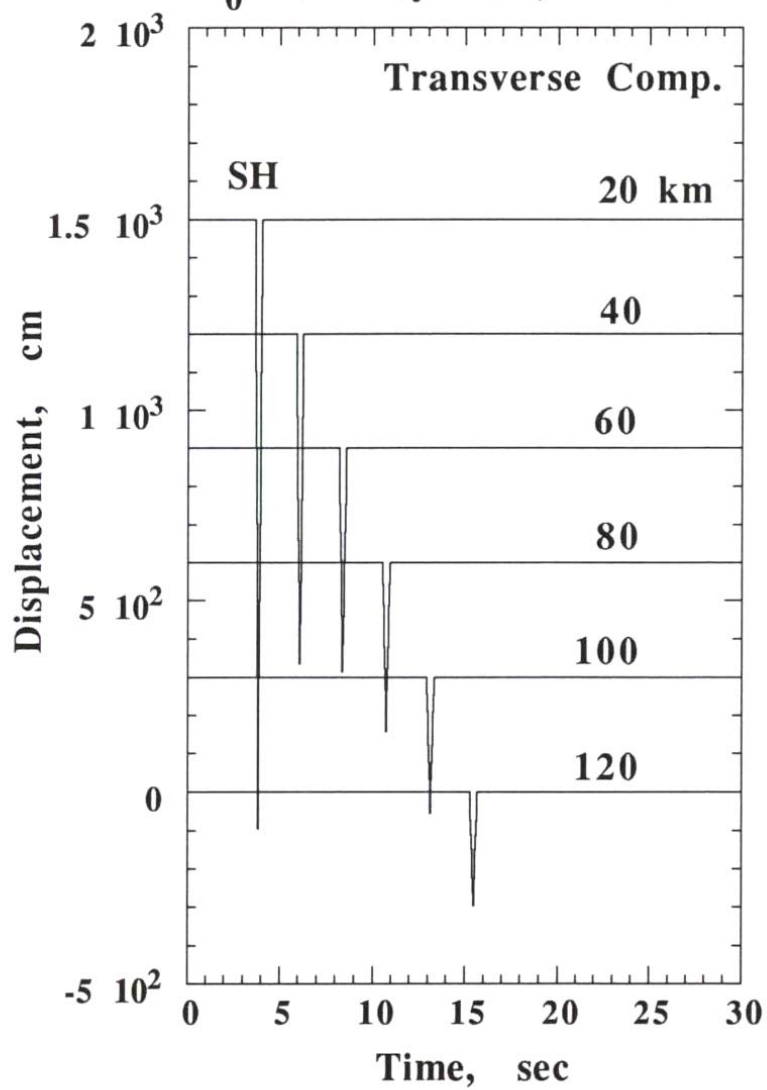


Fig. 2.

Station azimuth=45°. The vertical components are shown at 20 km distance intervals. *P*-wave arrivals are aligned.

Whole Space
Vertical Strike Slip $\phi=45^\circ$
 $M_0=10^{27}$ dyne-cm

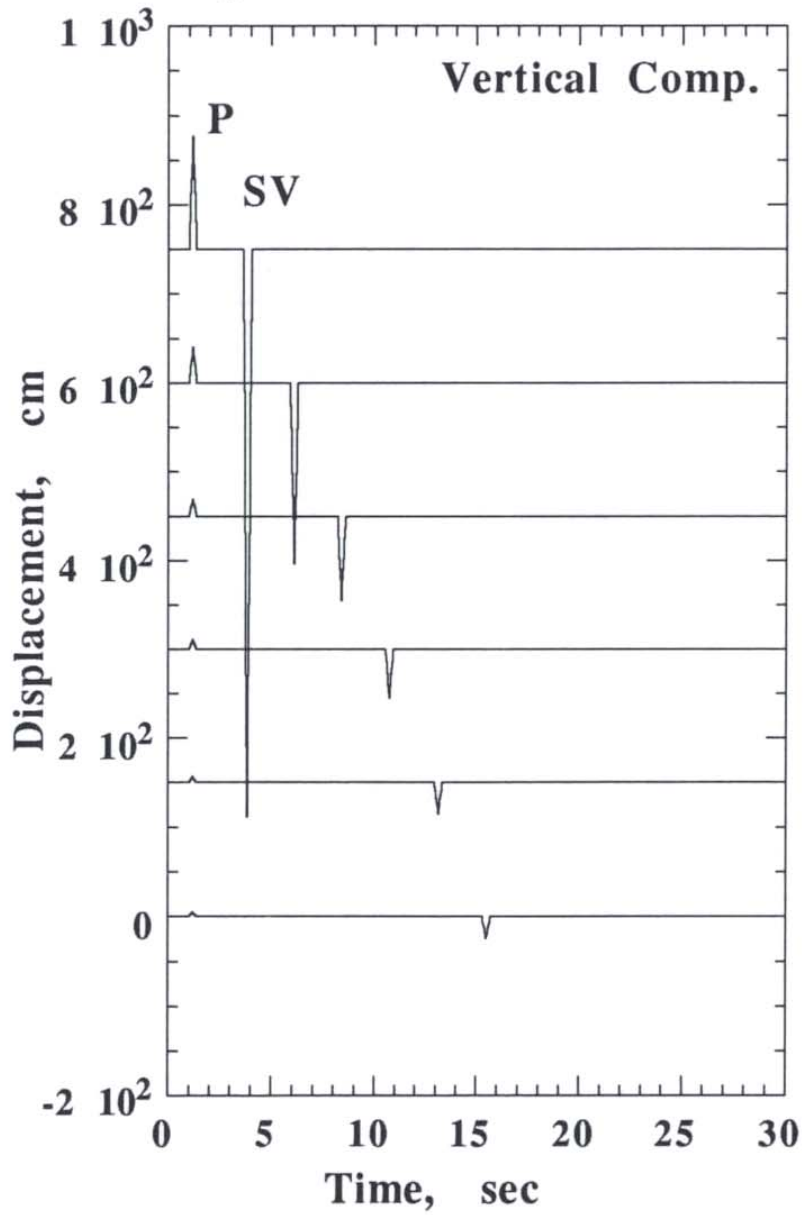


Fig. 3. and Fig. 4 show the responses in a southern California crustal model given below.

Thickness (km)	α (km/sec)	β (km/sec)	ρ (g/cm ³)
5.5	5.5	3.18	2.4
10.5	6.3	3.64	2.67
19.0	6.7	3.87	2.8
	7.8	4.5	3.0

The depth is 11 km. The mechanism is a vertical strike slip and the seismic moment is 10^{27} dyne-cm. The source time function is a 1/2 cycle cosine with half-width of 0.2 sec.

Fig. 3. Station azimuth = 90° . The transverse components are shown at 20 km distance intervals.

S. Calif. Crust
Vertical Strike Slip $\phi=90^\circ$
 $M_0=10^{27}$ dyne-cm, $H=11$ km

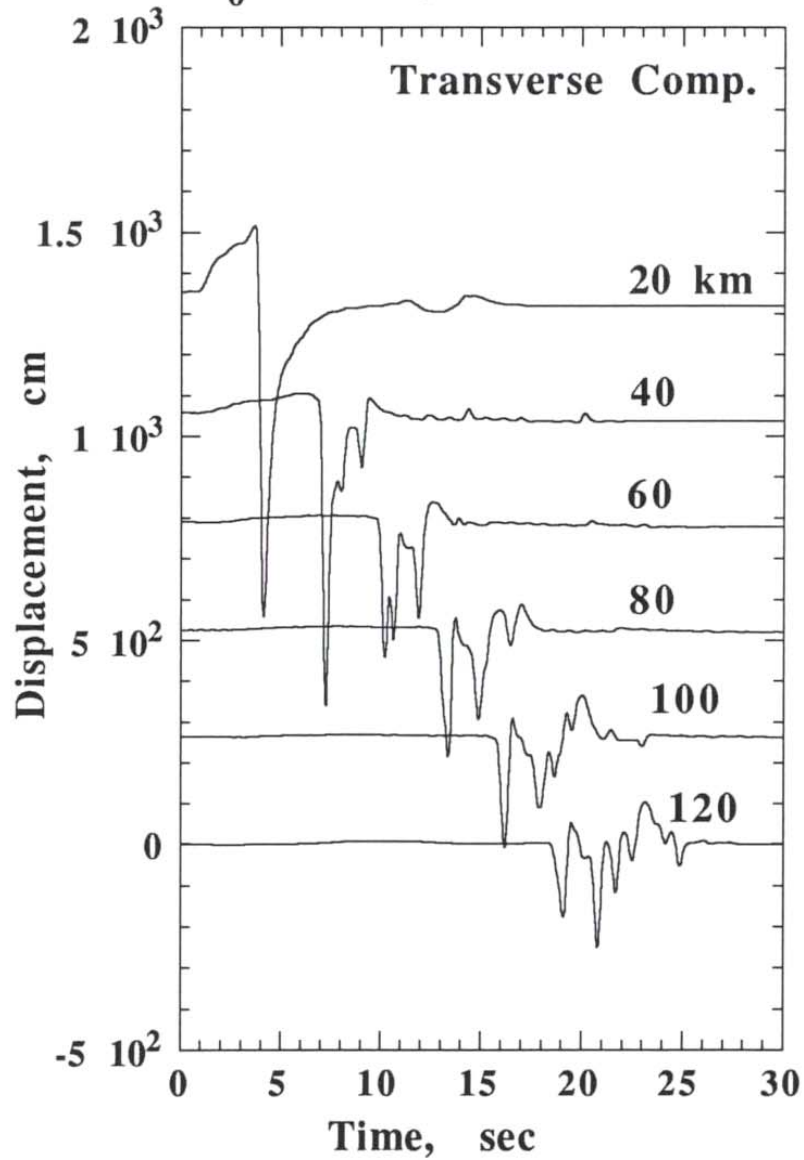
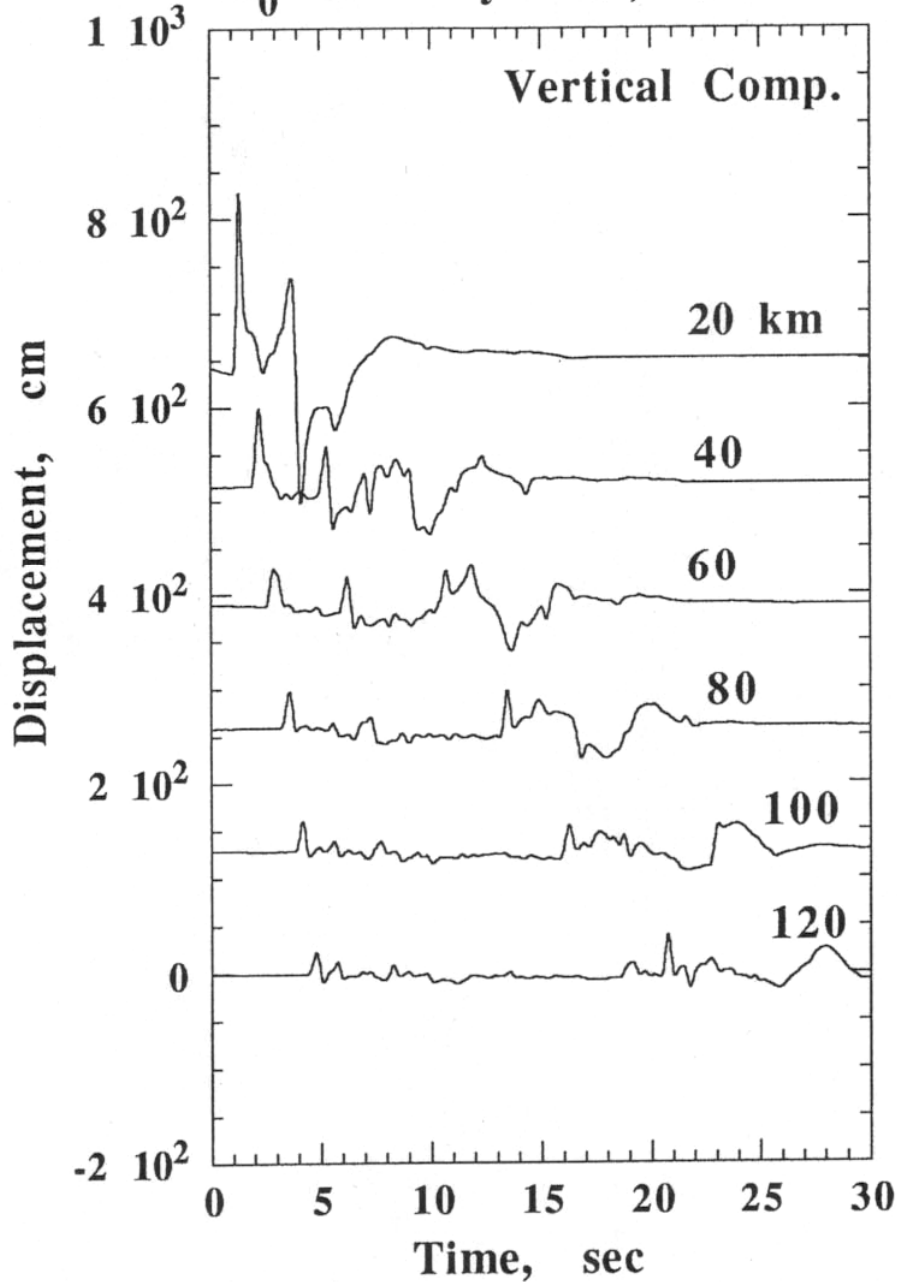


Fig. 4.
Station azimuth =45°. The vertical components are shown at 20 km distance intervals.

S. Calif. Crust
Vertical Strike Slip $\phi=45^\circ$
 $M_0=10^{27}$ dyne-cm, $H=11$ km



5.2.3 Elastic Dislocation ---- Summary ----

The equivalence between an elastic dislocation and a double couple shown for the static problem holds for the dynamic case, too. A point dislocation given by $D(t)$ over an infinitesimally small area is equivalent to a double couple with moment

$$M(t) = \mu D(t)S$$

Moment tensor, $M_{kl}(\bar{\xi}, t)$, can be defined in a similar manner.

The displacement due to a point double couple is given by

$$u_i(\bar{x}, t) = M_{kl}(\bar{\xi}, t) * G_i^{k,l}(\bar{x}, \bar{\xi}, t)$$

where * denotes convolution (i.e., $h(t) = f(t) * g(t)$ means $h(t) = \int_{-\infty}^{+\infty} f(t-\tau)g(\tau)d\tau$).

In the frequency domain,

$$\hat{u}_i(\bar{x}, \omega) = \hat{M}_{kl}(\bar{\xi}, \omega) \hat{G}_i^{k,l}(\bar{x}, \bar{\xi}, \omega)$$

This is formally equivalent to the expression we obtained for the static case. In practice, both the time-domain and the frequency-domain formulations are used for inversion. The time-domain representation is most commonly used in body-wave inversion, and the frequency-domain representation is more commonly used in inversion studies of normal modes.

5.2.3 Elastic Dislocation

1. Equivalence Between Double Couple and Dislocations

The equivalence between elastic dislocation and a double couple we showed for the static case holds for the dynamic case. In particular, the displacement field due to a point elastic dislocation D on S , can be computed with a double couple with a moment of $M_0 = \mu DS$. For a finite source, we use a distribution of double couples.

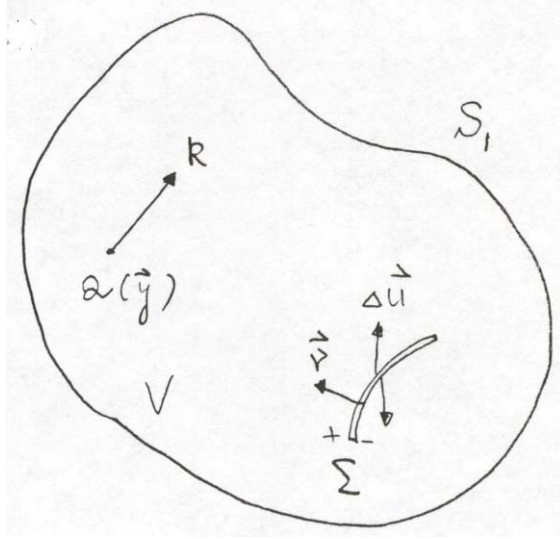
To prove this, we use the Volterra's theory (next section):

$$u^k(\bar{y}, t) = \int_{-\infty}^{+\infty} d\tau \int_{\Sigma} \Delta u_i(\bar{x}, \tau) \tau_{ij}^k v_j dS \quad (1)$$

where

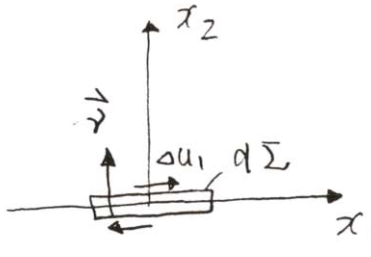
$$\begin{aligned} \tau_{ij}^k &= \lambda \delta_{ij} u_{i,i}^k(-\tau; -t) + \mu (u_{i,j}^k(-\tau; -t) + u_{j,i}^k(-\tau; -t)) \\ &= \lambda \delta_{ij} u_{i,i}^k(t; \tau) + \mu (u_{i,j}^k(t; \tau) + u_{j,i}^k(t; \tau)) \end{aligned}$$

(by reciprocity). τ_{ij}^k is the i - j component of stress at time $-\tau$ on Σ due to a δ function force applied in k direction at Q at time $-t$.



Thus, for a small planar dislocation $d\Sigma$ at P which is perpendicular to the x_2 axis, and on which u_1 , has discontinuity, $\Delta u_1(\tau)$

(19)



$$u^k(\bar{y}, t) = \int_{-\infty}^{+\infty} \Delta u_1(\tau) \tau_{12}^k d\Sigma d\tau \quad (2)$$

where

$$\tau_{12}^k = \mu(u_{1,2}^k(t; \tau) + u_{2,1}^k(t; \tau)) = -\mu(u_1^{k,2}(t; \tau) + u_2^{k,1}(t; \tau))$$

It is easy to see that τ_{12}^k / μ is the k th component of displacement at Q at time t due to a δ function double couple applied at τ on $x_1 - x_2$ plane.

Then it is clear from (2) that this dislocation is equivalent to a double couple of moment $\mu d\Sigma \Delta u_1(\tau)$.

2. Volterra's Dislocation Theory (Dynamic Case)

We use the same geometry and notation as those used for the static case.

The equations of motion for u_i and v_i are

$$c_{ijpq} u_{p,qj}(\bar{x}, t) - \rho \ddot{u}_i(\bar{x}, t) = -\rho f_i(\bar{x}, t) \quad (3)$$

$$c_{ijpq} v_{p,qj}(\bar{x}, t) - \rho \ddot{v}_i(\bar{x}, t) = -\rho g_i(\bar{x}, t) \quad (4)$$

$$f_i = g_i = 0 \quad \text{and} \quad u_i = v_i = 0 \quad \text{for} \quad t < -T \quad (5)$$

Define

$$\bar{v}_p(\bar{x}, t) = v_p(\bar{x}, -t) \quad (6)$$

$$\bar{g}_i(\bar{x}, t) = g_i(\bar{x}, -t) \quad (7)$$

then

$$\bar{g}_i(\bar{x}, t) = \bar{v}_p(\bar{x}, t) = 0 \quad \text{for} \quad t > T \quad (8)$$

For \bar{v}_p and \bar{g}_i , we have,

$$c_{ijpq} \bar{v}_{p,qj}(\bar{x}, t) - \rho \ddot{\bar{v}}_i(\bar{x}, t) = -\rho \bar{g}_i(\bar{x}, t) \quad (9)$$

Forming (3) x \bar{v}_i - (9) x u_i and integrating it with t and V

$$\int_{-\infty}^{+\infty} dt \int_V ((3)x\bar{v}_i - (9)xu_i)dV \quad (10)$$

Using the symmetry relations for c_{ijpq} and the relation

$$\frac{\partial}{\partial t}(\bar{v}_i\dot{u}_i - u_i\dot{\bar{v}}_i) = \bar{v}_i\ddot{u}_i - u_i\ddot{\bar{v}}_i$$

We have from (10)

$$\begin{aligned} & \int_{-\infty}^{+\infty} dt \int_{S_1+\Sigma^++\Sigma^-} dS [c_{ijpq}(\bar{v}_i u_{p,q} - u_i \bar{v}_{p,q})n_j] - \int_{-\infty}^{+\infty} dt \frac{\partial}{\partial t}(\bar{v}_i\dot{u}_i - u_i\dot{\bar{v}}_i) \\ & = \int_{-\infty}^{+\infty} dt \int_V dV \rho(u_i \bar{g}_i - \bar{v}_i f_i) \end{aligned} \quad (11)$$

The second term of LHS vanishes because

$$\begin{aligned} & \int_{-\infty}^{+\infty} dt \frac{\partial}{\partial t}(\bar{v}_i\dot{u}_i - u_i\dot{\bar{v}}_i) = (\bar{v}_i\dot{u}_i - u_i\dot{\bar{v}}_i)\Big|_{-\infty}^{+\infty} \\ & = \bar{v}_i(+\infty)\dot{u}_i(+\infty) - u_i(+\infty)\dot{\bar{v}}_i(+\infty) - \bar{v}_i(-\infty)\dot{u}_i(-\infty) + u_i(-\infty)\dot{\bar{v}}_i(-\infty) = 0 \end{aligned}$$

(owing to (5) and (8)).

As in the static case, we introduce

$$f_i = 0, \text{ and } \rho g_i(\bar{x}, t) = \delta_{ki} \delta(x_1 - y_1) \delta(x_2 - y_2) \delta(x_3 - y_3) \delta(t + s)$$

then,

$$\rho \bar{g}_i(\bar{x}, t) = \delta_{ki} \delta(x_1 - y_1) \delta(x_2 - y_2) \delta(x_3 - y_3) \delta(-t + s) \quad (12)$$

Substituting these into (11),

$$u^k(\bar{y}, s) = \int_{-\infty}^{+\infty} dt \int_{\Sigma} \Delta u_i(\bar{x}, t) \tau_{ij}^k \nu_j dS \quad (13)$$

where $\tau_{ij}^k = c_{ijpq} \bar{v}_{p,q}(\bar{x}, t)$ is for $\rho \bar{g}_i(\bar{x}, t)$ given by (12). From the definition, τ_{ij}^k is the ij component of stress at time $-t$ due to a δ function force applied in k direction at Q and at time $-s$.

Changing s to t and t to τ , we have

$$u^k(\bar{y}, t) = \int_{-\infty}^{+\infty} dt \int_{\Sigma} \Delta u_i(\bar{x}, \tau) \tau_{ij}^k \nu_j dS \quad (14)$$

This is the Volterra's relation used in (1).

3. Seismic Moment Tensor

In (14), the more explicit expression for τ_{ij}^k is

$$\tau_{ij}(-\tau; -t) = c_{ijpq} u_{p,q}^k(\bar{x}, -\tau; -t) = c_{ijpq} u_{p,q}^k(\bar{x}, t - \tau)$$

Substituting this in (14),

$$u^k(\bar{y}, t) = \int_{-\infty}^{+\infty} d\tau \int_{\Sigma} c_{ijpq} u_{p,q}^k(\bar{x}, t - \tau) \Delta u_i(\bar{x}, \tau) \nu_j dS \quad (15)$$

For a point source ($dS = d\Sigma \rightarrow 0$, $\Delta u_i \rightarrow \infty$, with $\Delta u_i d\Sigma = \text{constant}$),

$$u^k(\bar{y}, t) = \int_{-\infty}^{+\infty} d\tau c_{ijpq} u_{p,q}^k(\bar{x}, t - \tau) \Delta u_i(\bar{x}, \tau) \nu_j d\Sigma \quad (16)$$

Introducing M_{pq} by

$$M_{pq}(\bar{x}, \tau) = c_{ijpq} \Delta u_i(\bar{x}, \tau) \nu_j d\Sigma \quad (17)$$

we obtain,

$$u^k(\bar{y}, t) = \int_{-\infty}^{+\infty} M_{pq}(\bar{x}, \tau) u_{p,q}^k(\bar{x}, t - \tau) d\tau \quad (18)$$

M_{pq} is the seismic moment tensor.

The above integral is convolution of M_{pq} and $u_{p,q}^k$. Hence taking the Fourier transform of this, we obtain,

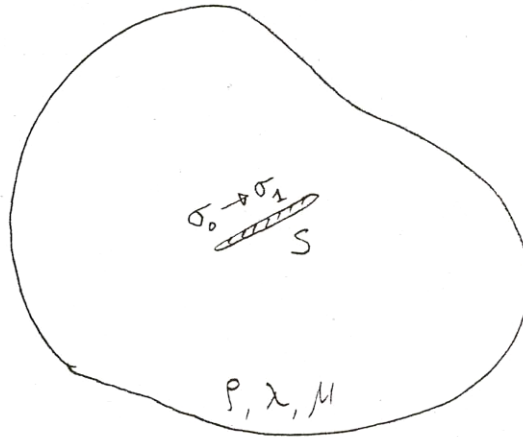
$$\hat{u}^k(\bar{y}, \omega) = \hat{M}_{pq}(\bar{x}, \omega) \hat{u}_{p,q}^k(\bar{x}, \omega) \quad (19)$$

where $\hat{u}^k(\bar{y}, \omega)$ etc are the Fourier transform of $u^k(\bar{y}, t)$ etc, respectively.

5.2.4 Stress Relaxation Model and Cracks (Dynamic Case)

1. Description of the Problem

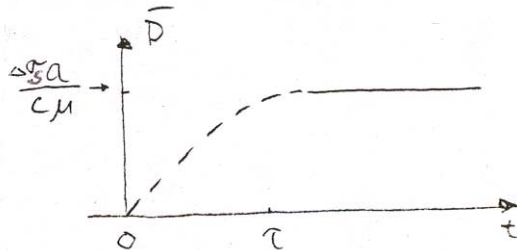
Consider an elastic medium which is in equilibrium under stress. Consider an open surface S . For simplicity, assume that the shear stress on this surface is uniform and σ_0 . At time $t = 0$ relax the stress on this surface from σ_0 to σ_1 . Then the static stress drop is $\Delta\sigma_s = \sigma_0 - \sigma_1$.



As discussed earlier, the resulting average dislocation \bar{D} and $\Delta\sigma$ are related by

$$\Delta\sigma_s = c\mu\bar{D}/a \quad (1)$$

where a is the representative dimension of the crack and c is a non-dimensional "shape factor" which is of the order of 1. Thus, if we plot \bar{D} as a function of time, it would look like the curve shown below.



For $t < 0$ $\bar{D} = 0$. At $t = 0$ when the stress is relaxed the side of the crack starts moving. After time τ , the medium is in another equilibrium state in which dislocation

$$\bar{D} = a\Delta\sigma_s / c\mu$$

is produced.

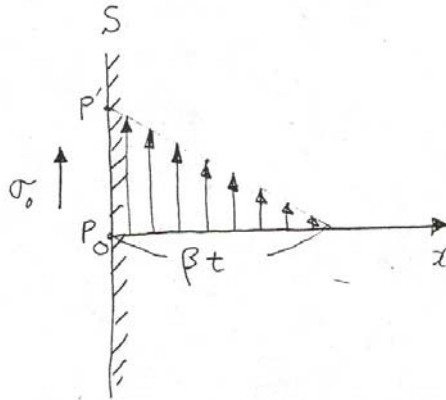
The behavior between $t = 0$ and $t = \tau$ depends on how stress is relaxed on S . If stress relaxation takes place smoothly, the change in \bar{D} may be also relatively smooth. The time constant τ depends on σ_0 and $\Delta\sigma$. To solve this problem rigorously using elasto-dynamics is difficult. In most cases no analytic solution is available, and we have to resort to numerical methods.

2. Qualitative Analysis of the Problem

Infinite Instantaneous Crack

First let us consider the simplest case. Consider an infinite homogeneous elastic medium under uniform shear stress σ_0 . At time $t = 0$, relax this stress over an infinite plane S (parallel to the applied shear stress) instantaneously. In order to see the displacement for $t \geq 0$ this problem can be replaced by the following problem.

Consider an homogeneous half space bounded by a plane S .



Apply a uniform shear stress σ_0 at $t = 0$ over the entire surface of S instantaneously. This is equivalent to relaxing the uniform shear stress σ_0 over S in an infinite medium. Then at time t , the point P on S will be moved to P' . Let this displacement be $u(t)$.

The disturbance applied to the surface propagates into the medium with shear velocity β . At time t , it propagates as far as βt . Thus, the instantaneous strain is

$$\varepsilon = u(t) / \beta t$$

Since this is caused by the applied shear stress σ_0 ,

$$\sigma_0 = \mu \varepsilon = \mu u(t) / \beta t$$

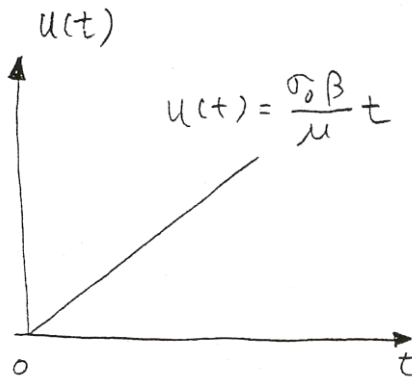
\therefore

$$u(t) = (\sigma_0 / \mu) \beta t \quad (2)$$

This gives the displacement for infinite instantaneous crack. From (2)

$$\dot{u}(t) = (\sigma_0 / \mu) \beta = \text{constant} \quad (3)$$

Note that the particle velocity is proportional to the initial stress, σ_0 .



This problem can be solved analytically.
The equation of motion for $x > 0$ is

$$\frac{\partial^2 u}{\partial x^2} = \frac{1}{\beta^2} \frac{\partial^2 u}{\partial t^2} \quad (4)$$

The solution is $u(z) = F(z)$ where $z = x - \beta t$.

The boundary condition at $x=0$ is

$$\mu \frac{\partial u}{\partial x} + \sigma_0 = 0, \quad t > 0$$

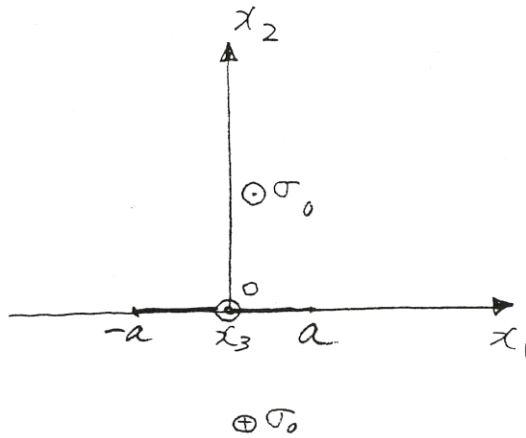
$$\therefore \mu F'(z) = -\sigma_0, \quad F(z) = -\sigma_0 z / \mu = -(\sigma_0 / \mu)(x - \beta t)$$

$$\therefore u = (\sigma_0 / \mu)(\beta t - x), \quad t > x / \beta$$

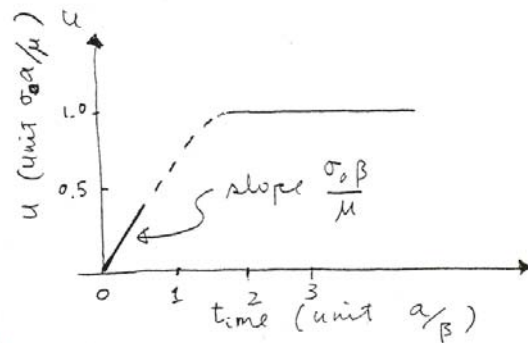
which gives (2).

3. Finite Instantaneous Crack

Next let us consider a strike-slip crack shown in the figure.



At $t = 0$, uniform shear stress σ_0 is applied in x_3 direction instantaneously over a surface ($x_2 = 0, |x_1| \leq a$). Let us consider the displacement at point O, the middle point of the crack. For small t (before the effect of the edge reaches this point), the displacement of this point should be the same as for infinite crack. Thus, the initial velocity should be given by $\sigma_0 \beta / \mu$. The effect of the edge arrives at this point at time $t = a / \beta$, and eventually the motion stops when a final equilibrium state is achieved. This is given by the solution of the static problem, i.e., $u = \sigma_0 a / \mu$. Hence, the displacement time function may be schematically given by the following figure.



One useful functional form which approximates this function is

$$u(t) = (\sigma_0 a / \mu)(1 - \exp(-\beta t / a)) \quad (5)$$

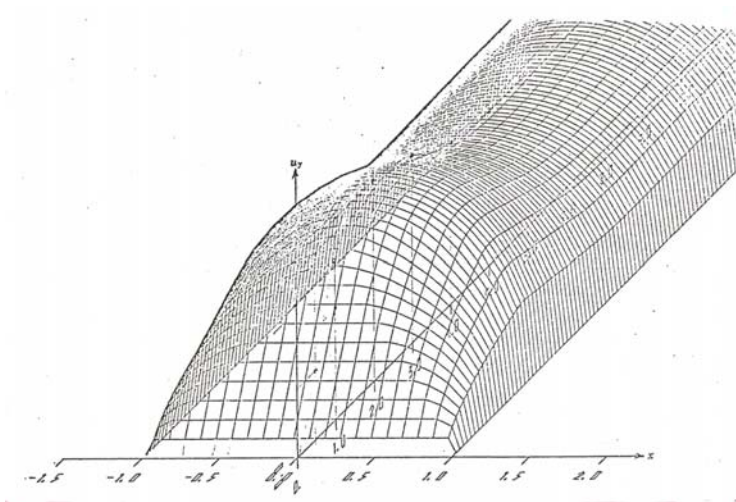
This problem can be solved numerically. The equation of motion in the medium is

$$\frac{1}{\beta^2} \frac{\partial^2 u}{\partial t^2} = \frac{\partial^2 u}{\partial x_1^2} \quad (6)$$

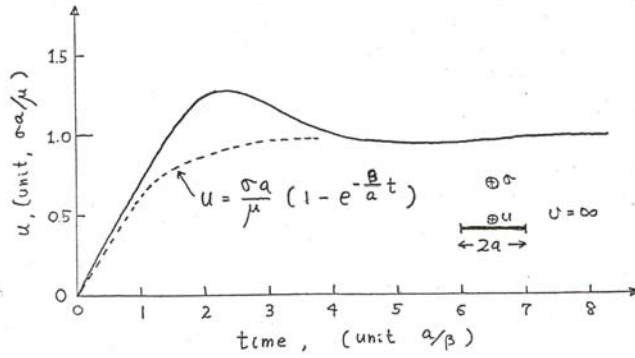
and the boundary condition is

$$\mu \frac{\partial u}{\partial x_2} + \sigma_0 = 0 \quad (x_2 = 0, |x_1| \leq a, t > 0) \quad (7)$$

The numerical solution is shown in the figure below and the displacement at the middle point is compared with the approximate solution given above. Note that the numerical solution shows a slight overshoot.



(Burridge, R., Phil. Trans. Roy. Soc. London, 265, 353-381, 1969)



4. Finite Propagating Crack

Let us consider the same geometry as before. Instead of applying the stress instantaneously, we apply a propagating stress,

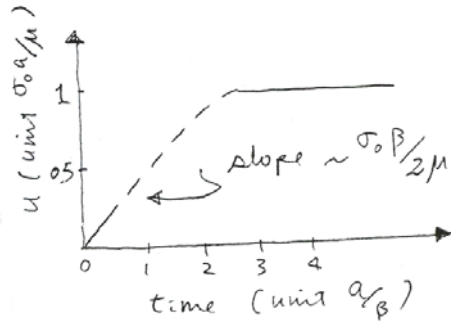
$$\sigma = \sigma_0 H(t \pm x_1/V), \quad |x_1| \leq a \quad (8)$$

where $H(t)$ is the Heaviside step function and V is the rupture velocity. V is usually slightly smaller than β . In this case, the final value of u is the same as before.

However, the point O starts feeling the edge effect even in the beginning, because at $t = 0$, the two edges are very close to this point. Thus, the motion is decelerated compared with the previous example. The effect of the edge $|x_1| = a$ will reach the point O at time $a(1/\beta + 1/V) \approx 2a/\beta$ after the stress application. Thus, the average velocity would be

$$\bar{u} \approx \frac{\sigma_0 a / \mu}{2a / \beta} \approx \sigma_0 \beta / 2\mu \quad (9)$$

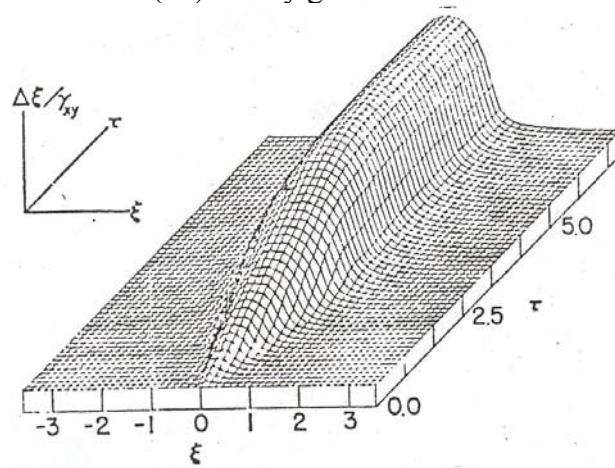
The schematic displacement time function may look like the one shown in the figure.



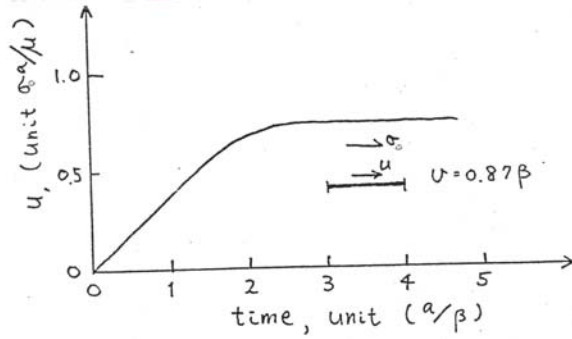
A useful functional form would be

$$u(t) = (\sigma_0 a / \mu)(1 - \exp(-\beta t / 2a)) \quad (10)$$

A result of numerical computation is shown in figure below (this is computed for a slightly different geometry). Note that, in this case there is no overshoot and that the agreement with (10) is very good.



(Hanson, M. E., A. R. Sanford, and R. J. Shaffer, J. Geophys. Res., 76, 3375-3383, 1971)



The above description, however, is very simplified. In a real propagating crack, the initial velocity could be faster than $\sigma_0\beta/2\mu$ due to the stress concentration near the crack tip. Equation (10) should be considered only approximate.

5. Comparison with the data

Regardless of all the details, the particle-motion velocity is governed by the relation,

$$\dot{u} \approx \sigma_0\beta / \mu$$

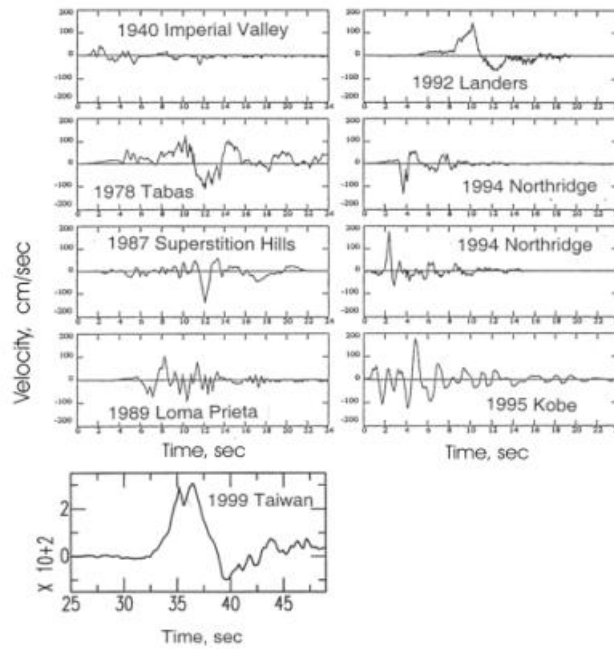
If $\sigma_0=100$ bar, $\beta=3$ km/sec, and $\mu=3\times 10^{11}$ dyne/cm², then

$$\dot{u} \approx 1 \text{ m/sec}$$

The observation of \dot{u} is difficult because of the complexity of faulting and the propagation effects, but the ground-motion velocity observed very close to a fault can be used as a good proxy of \dot{u} at least approximately. The following figure shows several examples of observed ground-motion velocity very close to the source. This comparison suggests that the above estimates are approximately correct, i.e., the magnitude of the driving stress is of the order of about 100 bar. However, the result from the 1999 Chi-Chi, Taiwan, earthquake stands out, suggesting that ground-motion velocity significantly larger than 1 m/sec can occur under certain conditions.

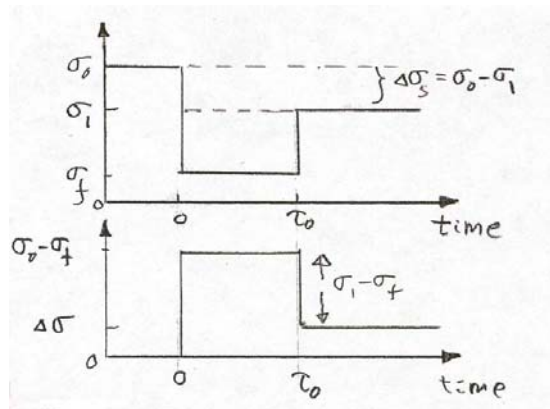
Large Earthquakes

Ground-Motion Velocity from Large Earthquakes



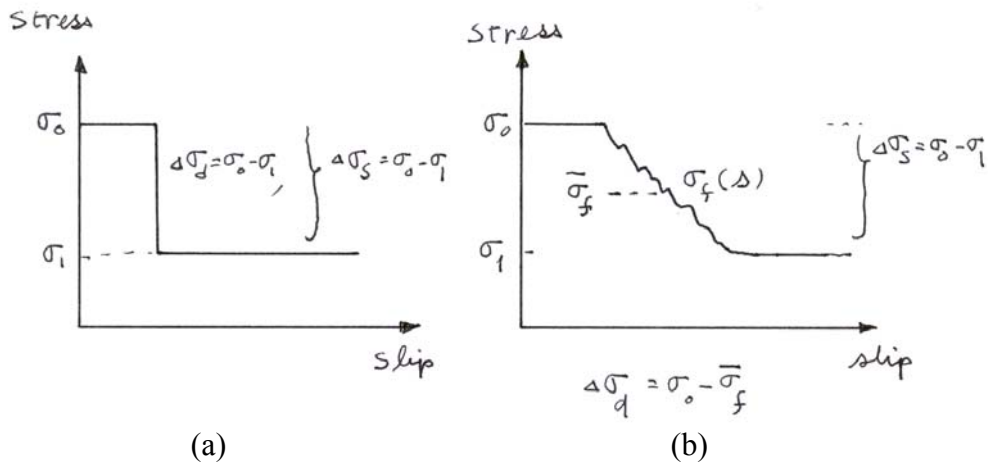
6. Frictional Stress Release

In actual earthquake faulting, the stress on the fault plane is released against frictional stress σ_f opposing the motion.



It is also possible that, at a certain time, say τ_0 , the fault motion slows down due to some locking mechanism. In this case, the time history of the stress drop on the fault surface may be schematically given by the curve shown in the figure above.

Actual stress release pattern can be very complex as shown by figure (b) below.



Since the details of the stress release are presently unknown, it is not meaningful to consider overly detailed models.

If the stress release is simple as shown on the left, then the fault motion

is driven by $\sigma_{0e} = \sigma_0 - \sigma_f$ ($\sigma_f = \sigma_1$) which is called the effective (tectonic) stress.

The particle velocity of the side of the crack (fault) will be given by $\sigma_{0e}\beta/\mu$ or $\sigma_{0e}\beta/2\mu$ depending upon whether the stress application is instantaneous or not (or in general $c\sigma_{0e}\beta/\mu$, c =constant).

Thus, if we can determine the approximate time function of the source dislocation function, we can determine the effective tectonic stress σ_{0e} from the initial slope and the stress drop $\Delta\sigma_s$ from the final dislocation (static field).

It is important to note that since only σ_{0e} and $\Delta\sigma_s$ appear in these expressions we cannot determine the actual tectonic stresses σ_0 and σ_1 , and the frictional stress, σ_f , by seismological methods alone.

7. Static Stress Drop and Dynamic Stress Drop

Referring to the figure shown above, the static stress drop of an earthquake, $\Delta\sigma_s$, is defined by

$$\Delta\sigma_s = \sigma_0 - \sigma_1 \quad (11)$$

where σ_0 and σ_1 are the initial and the final stresses, respectively. This definition is straightforward and unambiguous.

The dynamic stress drop, $\Delta\sigma_d$, is the stress that drives fault motion. Unfortunately, the definition of dynamic stress drop is not universal, and is ambiguous. For the simplest stress release pattern shown by figure (a) above, it is the same as the effective tectonic stress and is equal to the static stress drop, *i e.*,

$$\Delta\sigma_d = \sigma_{0e} (= \sigma_0 - \sigma_f) = \Delta\sigma_s (= \sigma_0 - \sigma_1) \quad (12)$$

In this case, the dynamic stress drop is unambiguous.

However, for more complex stress release patterns in which friction changes as a function of slip as shown by figure (b) above, we can define $\Delta\sigma_d$ by

$$\Delta\sigma_d = \sigma_0 - \bar{\sigma}_f \quad (13)$$

where

$$\bar{\sigma}_f = \frac{1}{D} \int_0^D \sigma_f ds \quad (14)$$

(s : slip).

This definition is similar to (12) and reasonable. In general, $\bar{\sigma}_f \neq \Delta\sigma_s$. Thus, it is important to distinguish $\Delta\sigma_d$ and $\Delta\sigma_s$.

Ge 162 Practice Session 6, Retrieval of Source Parameters

Figure 1 shows the ground-motion displacement, $U(t)$, of the Jan. 26, 2001, Bhuj, India, earthquake recorded at ESK (Eskdalemuir) in Scotland.

Estimate the seismic moment M_0 , and the approximate duration of the source (as viewed from ESK). It is also possible to constrain the depth, H , but, for simplicity, we fix H , except in the last step where the effect of H on the waveform will be examined.

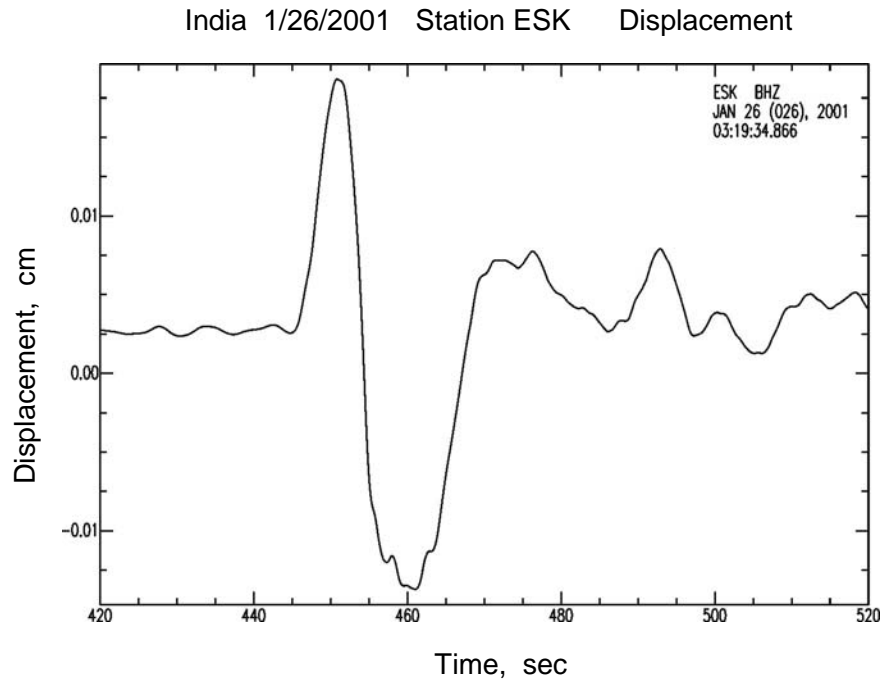


Fig. 1

The following is the general principle.

1) Waveform in the whole space.

As discussed in class, the far-field waveform in the Haskell model can be approximated by a trapezoidal function

$$T(t; \tau_0, t_c) \quad (1)$$

where τ_0 and t_c are the two time constants of the source. The area under $T(t; \tau_0, t_c)$ is unity. Then, the P-wave form in a whole space is given by

$$u_1(t) = \frac{M_0 R_{\theta\phi}}{4\pi\rho r\alpha^3} T(t - r/\alpha; \tau_0, t_c) \quad (2)$$

2) The source and receiver effects and the geometrical spreading.

In the real earth, the structure near the source and the receiver complicates the wave form. Here, we use a simple half space. Then, we need to include the near-source reflections pP and sP, and the effect of the free surface near the station. Here, the near-source effect is approximated by

$$C_S(t) = \delta(t) + a_1\delta(t - t_1) + a_2\delta(t - t_2) \quad (3)$$

The first, second, and third terms represent, the direct P, pP, and sP, respectively. a_1 , a_2 , t_1 , and t_2 depend on the radiation pattern, the depth, and the structure. In particular, changing the depth has a large effect on the waveform.

The receiver effect is simply given by a scalar factor, C_R . (For SH wave, $C_R=2$.)

The geometrical spreading factor is also simplified by a scalar factor g , and $1/r$ in (2) is replaced by g/R_E where R_E is the radius of Earth.

Including these, the wave form is now modified to,

$$u_2(t) = \frac{rg}{R_E} C_R u_1(t) * C_S(t) \quad (4)$$

Even for this simplified problem, computation of (4) is not that simple because of the complexity of $C_S(t) = 1 + a_1\delta(t - t_1) + a_2\delta(t - t_2)$. A simple program `pwsyn2g_asc.f` is provided in `/home/ftp/pub/hiroo/ge162.dir/practice_6.dir`. The output of this program is $u_2(t)$.

Run this program for various τ_0 , t_c , and the depth H . The constants, a_1 , a_2 , t_1 , and t_2 are computed in the program from the fault parameters and the depth. This program computes the displacement in cm for a unit moment ($M_0=10^{20}$ N-m).

(Another program pwsyn2g.f which does the same and outputs the results in SAC format is also provided.)

3) Observed Waveform

To simulate the observed waveform at the station, we need to add the effects of attenuation. The attenuation function, $F(t; t^*)$, for $t^* = 1$ sec is shown in Figures 2, and the file is in practice_6.dir (o_futtm.asc (ASCII file) and o_futtm (SAC file)).

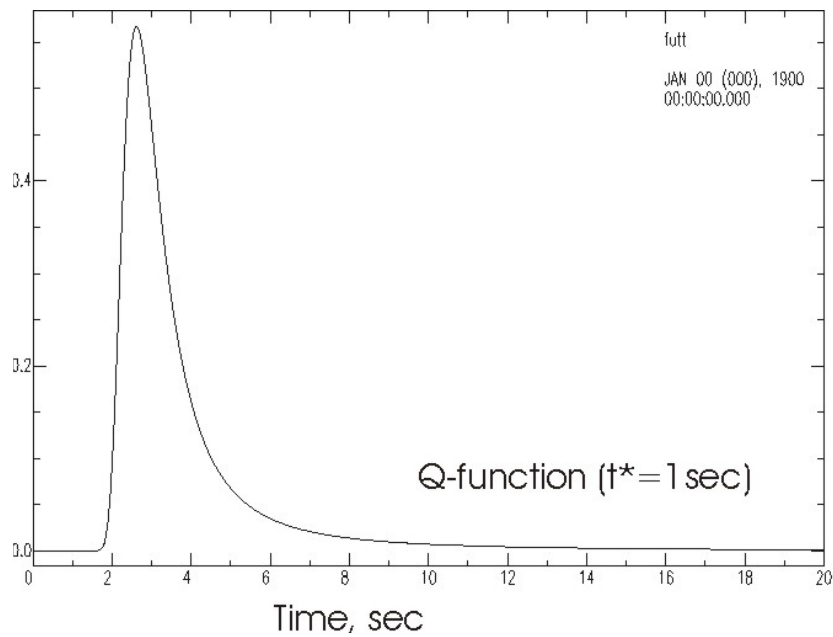


Fig. 2

The synthetic ground-motion displacement can be computed by

$$u_3(t) = u_2(t) * F(t) \quad (5)$$

This can be directly compared with the observed record, $U(t)$, shown in Figure 1.

4) Determination of M_0

Once the waveforms are matched satisfactorily, the amplitude ratio of the observed waveform

$$\frac{\text{amplitude}(U(t))}{\text{amplitude}(u_3(t))}$$

gives the seismic moment, M_0 , of the earthquake in the unit of 10^{20} N-m.

Since many approximations have been made, the waveforms cannot be matched completely, but try to match the overall waveform and the amplitude of the first 1 cycle.

Here, we use only one station, and the mechanism (i.e., radiation pattern) is assumed. However, if we have more than one station, we can determine the mechanism by matching the amplitudes at different stations with the same M_0 .

In general, matching the displacement record is much easier than matching the velocity record, $V(t)$, shown in Figure 3, because high-frequency components which are harder to model have been removed in the displacement record.

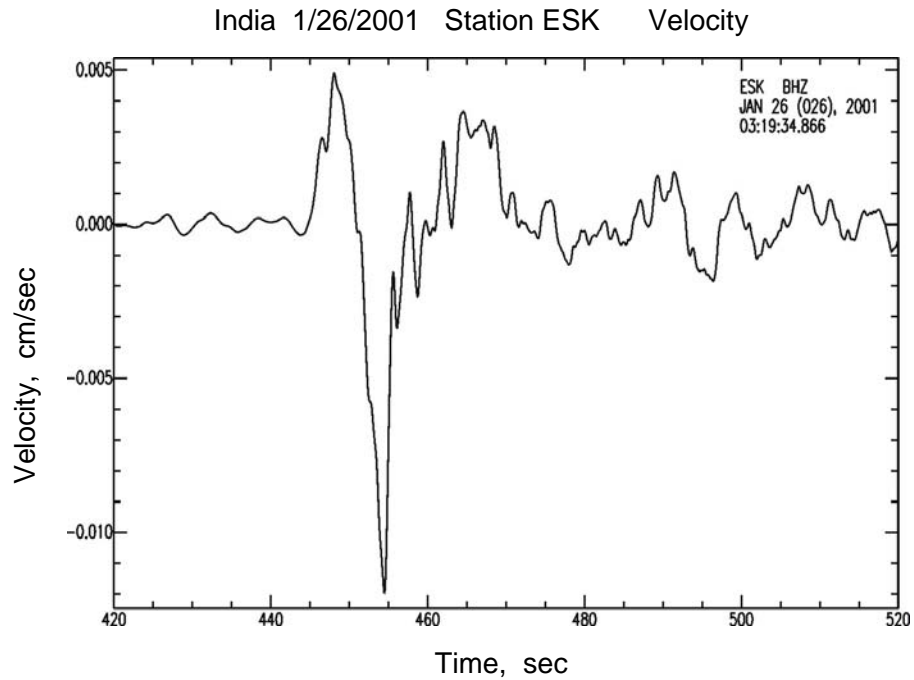


Fig. 3

The relevant parameters needed for the computation are in the following.

Bhuj, India, Earthquake

O.T. 03:16:41.0, 1/26/2001

Lat. 23.40° , Long. 70.32° , Depth (H), 10-40 km

Dip(δ)= 64° , rake(λ)= 60° , strike(ϕ_f)= 66°

Eskdalemuir

Lat.= 55.3167° , Long.= 3.2050° , Elevation=242m

Epicentral Distance (Δ)= 61° , Azimuth= 321° , Takeoff Angle (i_h)= 18°

Source Crustal Structure (Half Space)

$$\alpha = 6.0 \text{ km/sec}, \beta = 3.46 \text{ km/sec}, \rho = 2.67 \text{ g/cm}^3$$

For the mechanism and the takeoff angle given above, the radiation pattern factor for P-wave at the source

$$R_{\theta\phi} = 0.914 \quad (\text{this is computed in the program})$$

Geometrical spreading factor computed for a standard Earth model

$$g = 0.35$$

Steps for Practice

1. Compute $u_2(t)$ for

$$H = 10 \text{ km}, \tau_0 = 8 \text{ sec}, t_c = 12 \text{ sec}$$

using `pwsyn2g_asc.f`. Plot, `o_Pamp.asc` (direct P wave), `o_pPamp.asc` (pP wave), `o_sPamp.asc` (sP wave), and `o_Ptotalamp.asc` (sum of all). These are ASCII files with simple 2-column t vs. $u_2(t)$ data.

Observe, how P, pP and sP phases interact. Note that the far-field waveform in a whole space discussed in class should be a one-sided pulse, while the observed $U(t)$ is two sided. The interaction between these phases is the primary reason why the observed displacement is two-sided.

2. Convolve `o_Ptotalamp.asc` with $F(t; t^* = 1 \text{ sec})$ to compute $u_3(t)$. Program `convg3m.f` is provided, but you may want to write a simple program for convolution.*

3. Compare $u_3(t)$ with $U(t)$ to determine M_0 . The starting time is arbitrary so that you can shift the waveform arbitrarily in comparison.
4. Try 1, 2, and 3, for different combinations of τ_0 , and t_c (fix H) and find the best solution.
5. Compute $u_3(t)$ using a source time function shown below, and compare it with $U(t)$. Vary H from 5 to 35 km, and see the difference in the synthetic waveforms. (This source time function is not a trapezoid, which means that the source model is different from the Haskell model.)

Suggested source time function

0.0 sec	0.0
2.0	0.0
4.0	0.2
8.0	1.0
22.0	0.0
100.0	0.0

6. (Optional)

Compute the velocity $v_3(t_i) = [u_3(t_{i+1}) - u_3(t_i)] / \Delta t$ for the best model, and compare it with $V(t)$.

Explanation of the Programs

pwsyn2g.f

pwsyn2g.f takes input file i_pwsyn2g. Only the parameters in bald face need to be changed. (do not change c_pwsyn2g.)

i_pwsyn2g

```

line 1      station id

line 2  rho,  $\alpha$ , dt, *, *, * (density in g/cm3, P-velocity in km/s(S-
      velocity is assumed to be  $\alpha/1.732$ ), dt of data (0.05 sec for VBB)

line 3  fif, dip, rake (fault strike, dip and rake)

line 4  ih, fis, H(depth), g, * (take-off angle, station azimuth,
      depth, g factor)

line 5  flag for the choice of source time function (do not change)

line 6  nt (# of points where time function is defined_)

line 7  t1, y(t1) (time, amplitude (amplitude is arbitrary; the
      amplitude is eventually normalized in the program.)

line 8  t2, y(t2)

      etc

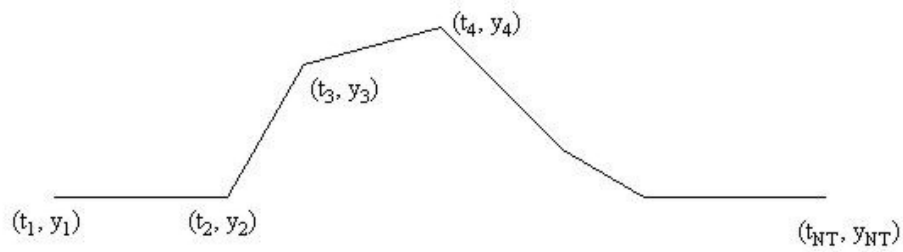
```

Example

```

ESK
2.67      6.0      0.05      0.01      0.01      0.01
66.      64.      60.
18.      321.     10.      0.35      1.0
      1
      6
0.0      0.0
2.0      0.0
10.0     1.0
14.0     1.0
22.0     0.0
100.0    0.0

```



The output file o_pwsyn2g contains the parameters used and other computed parameters.

Output files o_Pamp.asc, o_pPamp.asc, o_sPamp.asc, and o_Ptotalamp.asc contain the time series for P, pP, sP, and the sum in ASCII format.

convg3m.f

This program computes convolution of $x(t)$ and $y(t)$. The result is $z(t) = x(t) * y(t)$.

i_conv3m

line 1 file name of $x(t)$
line 2 file name of $y(t)$
line 3 file name of $z(t)$

Example

i_conv3m

o_Ptotalamp.asc

o_futtm.asc

o_Ptotalamp_q.asc

* convolution of x_i ($i=1,2, \dots, l$) and y_j ($j=1,2, \dots, m$) is

$$z_k = \left(\sum_{i=1}^l x_i y_{k-i} \right) \Delta t \quad k = 1, 2, \dots, l+m$$

(if $k-i \leq 0$, then $y_{k-i} = 0$)

Ge 162

6. Retrieval of Seismic Source Parameters

6.1 Far Field Body Waves

1. Introduction

Far-field body waves are widely used to determine the source mechanism (fault plane solution), seismic moment, and rupture patterns (complexity). The method is conceptually simple, but the actual procedure involves many steps. These steps include the calculation of the following:

1. Source time function (Dislocation time history)
2. Source finiteness function (rupture function), $T(t; \tau_0, t_c)$
3. Radiation pattern, R
4. Response of source and receiver structures, $C_S(t)$ and $C_R(t)$
5. Geometrical spreading function, $g(\Delta, h)$
6. Attenuation (Q operator), $q(t)$
7. Instrument response, $I(t)$

The displacement at far-field is then given by,

$$u(\Delta, t) = \frac{M_0 R g(\Delta, h)}{4\pi\rho v_c^3 R_E} T(t; \tau_0, t_c) * C_S(t) * C_R(t) * q(t) * I(t)$$

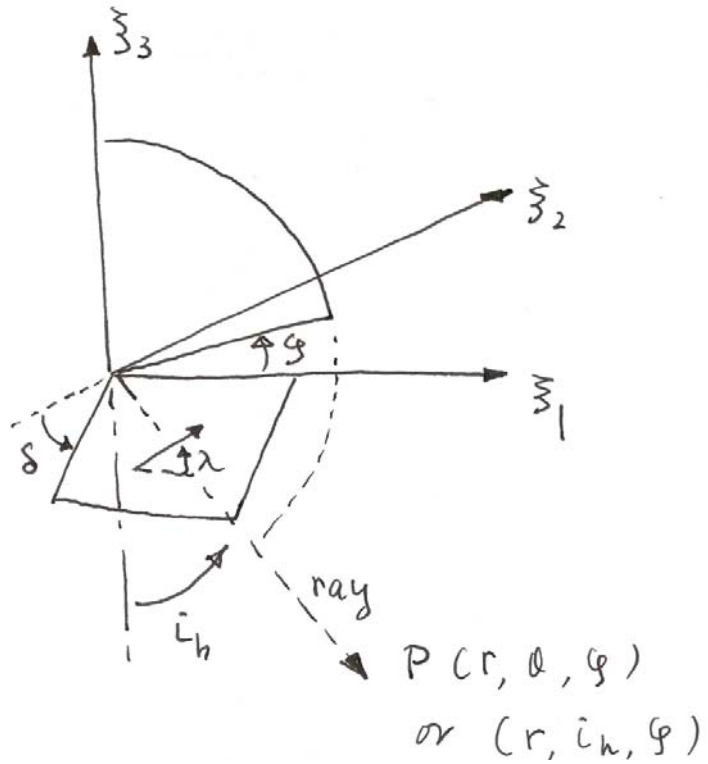
where M_0 is the seismic moment, ρ is the density, v_c is P- or S-wave velocity, and R_E is the radius of Earth.

These steps are described in detail in the following.

2. Radiation Pattern from a Point Double Couple

The radiation pattern from a point double couple has been already given with respect to the coordinates fixed to the double couple.

For actual applications it is convenient to express the radiation pattern by using a geographical coordinate system. For a fault model shown in the figure, the displacement at point P can be given by:



$$u_r(r, t) = \frac{1}{4\pi r \alpha^3} R^p \dot{M}(t - r/\alpha) \quad (1)$$

$$u_\theta(r, t) = \frac{1}{4\pi r \beta^3} R^\theta \dot{M}(t - r/\beta) \quad (2)$$

$$u_\phi(r, t) = \frac{1}{4\pi\rho r\beta^3} R^\phi \dot{M}(t - r/\beta) \quad (3)$$

where

$$R^P = s_R(3\cos^2 i_h - 1) - q_R \sin 2i_h - p_R \sin^2 i_h \quad (4)$$

$$R^\theta = \frac{3}{2}s_R \sin 2i_h + q_R \cos 2i_h + \frac{1}{2}p_R \sin 2i_h \quad (5)$$

$$R^\phi = -q_L \cos i_h - p_L \sin i_h \quad (6)$$

$$q_L = -(\cos \lambda \cos \delta) \sin \phi + (\sin \lambda \cos 2\delta) \cos \phi \quad (7)$$

$$p_L = (\sin \lambda \sin \delta \cos \delta) \sin 2\phi + (\cos \lambda \sin \delta) \cos 2\phi \quad (8)$$

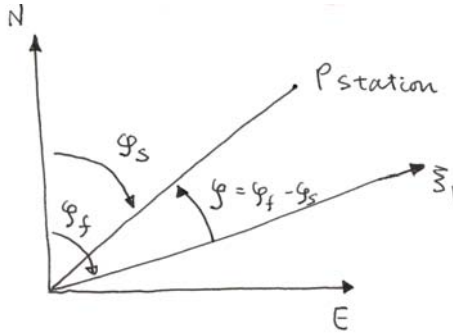
$$s_R = \sin \lambda \sin \delta \cos \delta \quad (9)$$

$$q_R = \sin \lambda \cos 2\delta \sin \phi + \cos \lambda \cos \delta \cos \phi \quad (10)$$

$$p_R = \cos \lambda \sin \delta \sin 2\phi - \sin \lambda \sin \delta \cos \delta \cos 2\phi \quad (11)$$

If the azimuth of the fault strike (x_1 axis) ϕ_f and the azimuth of the station (point P) ϕ_s are measured clockwise from N, then ϕ (measured counter-clockwise from ξ_1 axis) in the above formula should be given by

$$\phi = \phi_f - \phi_s \quad (12)$$

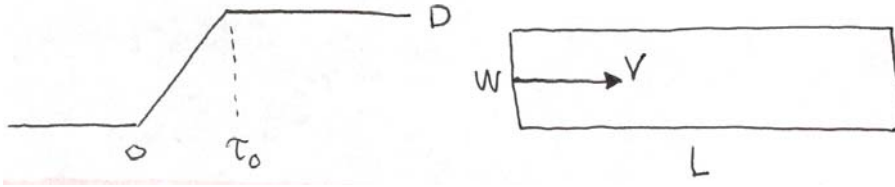


By using (1) to (12) we can compute the far-field displacements of body waves from a fault of arbitrary geometry. The station coordinates are given by (r, i_h, ϕ) rather than the conventional (r, θ, ϕ) .

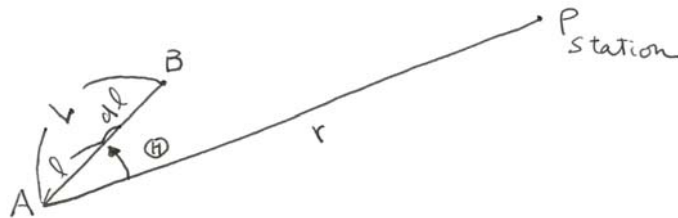
3. Source Finiteness-- Haskell Model

One of the useful kinematic source models is the Haskell(1964) model. In this model, a seismic source is represented by a rectangular fault with length L and width W . The dislocation (fault offset), D , on the fault plane is uniform in space, and its temporal variation is given by a linear ramp function with a rise time τ_0 .

The rupture propagation is assumed instantaneous in the width direction. Lengthwise, the rupture propagates from one end of the fault to the other with a uniform rupture speed V . In this sense, the rupture propagation is one-dimensional unilateral.



Assume that the rupture propagates from A to B over a length L . If the seismic moment per unit fault length is m , the moment per line element dl is mdl .



The far-field time function due to this line element is given by a box-car function of width τ_0 and height mdl / τ_0 .



If AP is very large compared with AB, the displacement at P (station) can be given by

$$\frac{R}{4\pi\rho r v_c^3} m d l s \left(t - \frac{r}{v_c} - \frac{l}{V} + \frac{l \cos \Theta}{v_c} \right)$$

where $r = AP$, v_c is either P or S wave velocity, R , the radiation pattern and V is the rupture velocity. $s(t)$ is defined above, and is called the local dislocation rate function. Therefore, for a source propagating from A to B, we have

$$u(r, t) = \frac{R}{4\pi\rho r v_c^3} m \int_0^L s \left(t - \frac{r}{v_c} - \frac{l}{V} + \frac{l \cos \Theta}{v_c} \right) dl \quad (13)$$

Introducing the following variables,

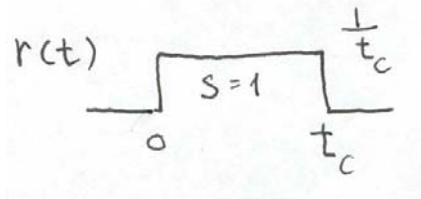
$$\tau = t - r/v_c, \quad t_c = L/V - L \cos \Theta / v_c, \quad t_1 = l t_c / L, \quad dl = L dt_1 / t_c \quad (14)$$

we obtain,

$$u(r, \tau) = \frac{R}{4\pi\rho r v_c^3} \frac{M_0}{t_c} \int_0^{t_c} s(\tau - t_1) dt_1 \quad (15)$$

where $M_0 = mL$ is the total seismic moment.

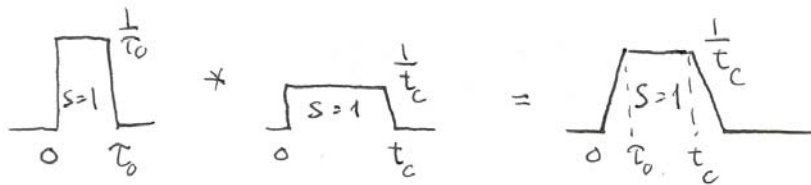
Introducing a function $r(t_1)$, as shown in the figure,



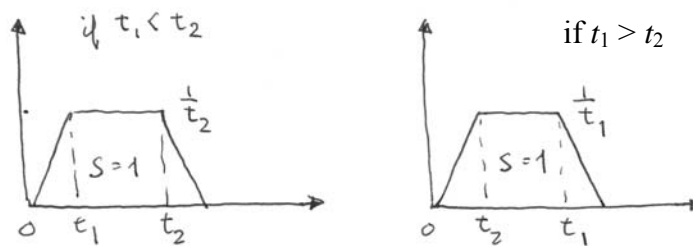
we obtain

$$\begin{aligned}
 u(r, \tau) &= \frac{RM_0}{4\pi\rho r v_c^3} \int_0^{\tau} r(t_1) s(\tau - t_1) dt_1 \\
 &= \frac{RM_0}{4\pi\rho r v_c^3} \int_{-\infty}^{+\infty} r(t_1) s(\tau - t_1) dt_1
 \end{aligned}
 \tag{16}$$

which is convolution of $r(t)$ and $s(t)$. $r(t)$ is called the rupture function.



The above convolution yields a trapezoidal function $T(t; t_1, t_2)$ given by the following figure.



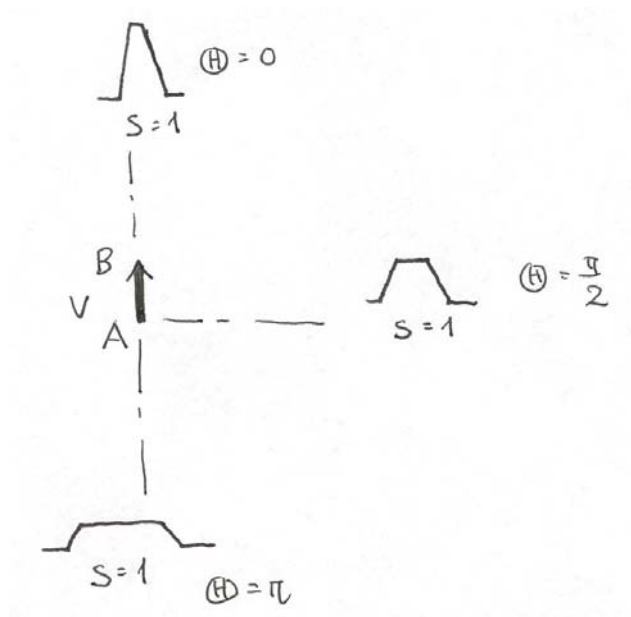
Note that

$$\int_{-\infty}^{+\infty} T(t; t_1, t_2) dt = \int_0^{t_1+t_2} T(t; t_1, t_2) dt = 1
 \tag{17}$$

Thus, the pulse width at the station in the azimuth Θ is

$$w(\Theta) = \tau_0 + \frac{L}{V} - \frac{L}{v_c} \cos \Theta \quad (18)$$

If τ_0 is small, the pulse shape at $\Theta = 0$, $\Theta = \pi/2$ and $\Theta = \pi$ may be schematically shown by the following figure.



Note that S is always equal to 1.

The amplitude spectrum of $T(t; \tau_0, t_c)$ is given by

$$|\hat{T}(\omega; \tau_0, t_c)| = \left| \frac{\sin(\omega\tau_0/2)}{(\omega\tau_0/2)} \right| \left| \frac{\sin(\omega t_c/2)}{(\omega t_c/2)} \right| \quad (19)$$

Note:

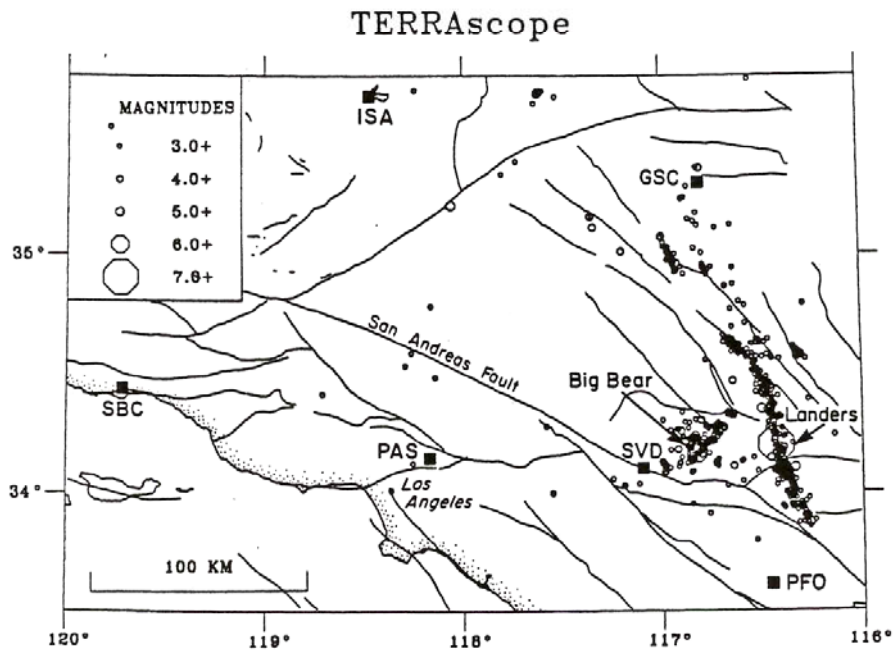
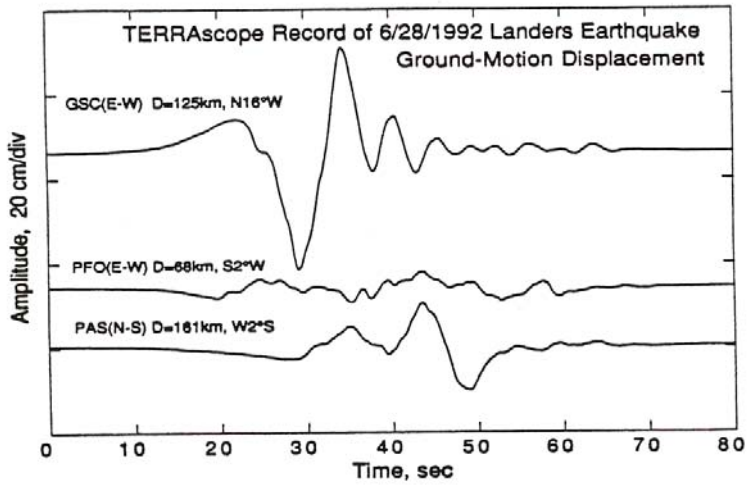
In applying the above results to body-wave radiation in the real earth, another factor needs to be considered. For example, if AB is horizontal, we let the take-off angle of the ray be i_h , and the azimuth of the station from AB measured on the earth's surface be Θ . Then the phase velocity along the Earth's surface is $v_c / \sin i_h$. Then we replace r / v_c and v_c in the argument of $s(t)$ by T and $v_c / \sin i_h$ respectively, where T is the travel time. Hence we have, instead of (14) and (15),

$$u(r, \tau) = \frac{RM_0}{4\pi\rho r v_c^3 t_c} \int_0^{t_c} s(\tau - t_1) dt_1 \quad (20)$$

where,

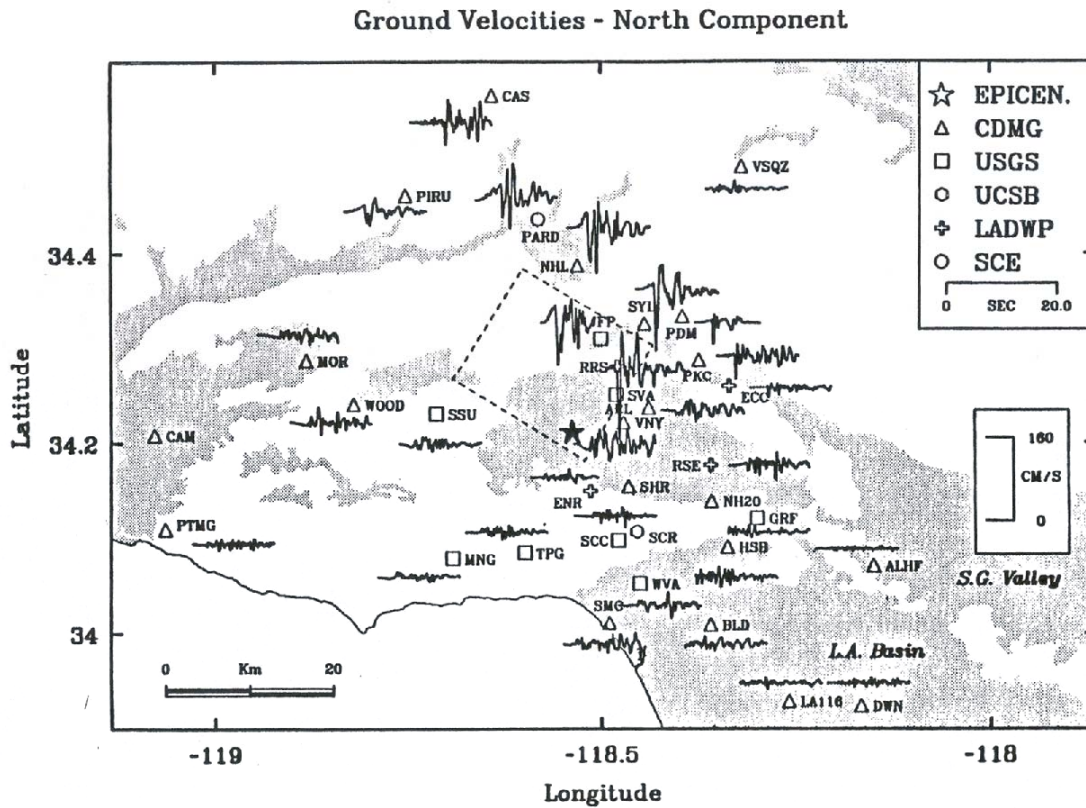
$$\tau = t - T, \text{ and } t_c = L/V - L \cos \Theta \sin i_h / v_c \quad (21)$$

For example, directivity observed for the 1999 Landers earthquake is illustrated in the following figure.

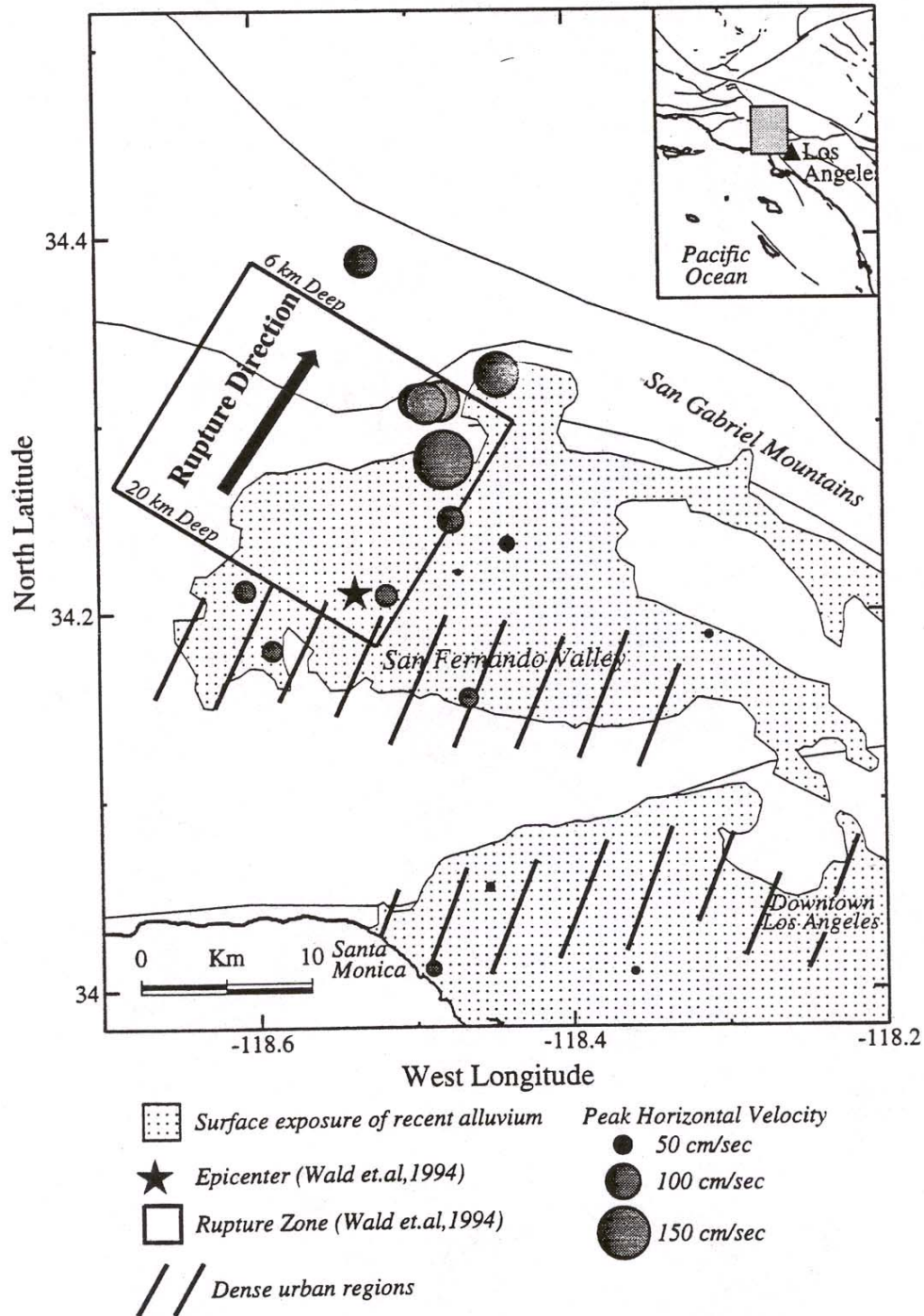


Directivity has strong influence on the distribution of strong ground motion as shown for the 1994 Northridge earthquake.

1994 Northridge Earthquake (M=6.7)

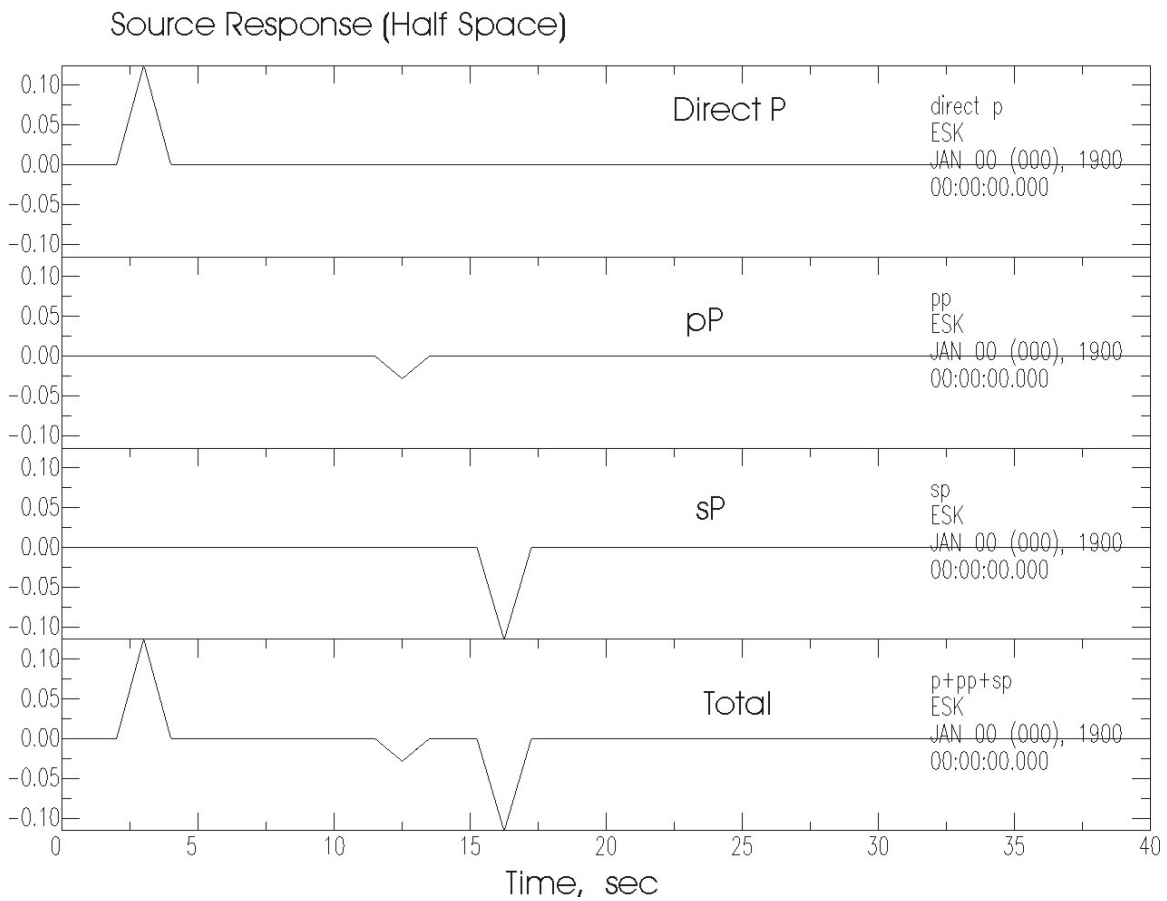


17 January 1994 Northridge Earthquake, $M=6.7$



4. Response Function at the Source and Receiver

If the source is shallow, the reflections from the free surface (and other structures) complicates the source wave as shown by the following figure.



A similar situation occurs near the station too. These effects are usually included as the source and receiver response functions.

5. Geometrical Spreading of Body-Wave Energy

5.1 Energy Density and Energy Flux

In an elastic medium with density ρ , the elastic energy per unit volume is given by

$$\varepsilon = \rho \dot{u}^2 \quad (22)$$

where u is the displacement and \dot{u} is the particle velocity.

Consider a plane wave propagating in x direction with velocity v . Then, the energy flux per unit area per unit time is given by

$$\phi_E = \rho \dot{u}^2 v \quad (23)$$

5.2. Radiated Energy from a Source

Consider an elastic wave radiating from a double couple source at O. Consider a small sphere with radius r around O.

Then elastic wave energy emitted per unit time from the source within a ring defined by i_h and $i_h + di_h$ is

$$E_R = 2\pi R_E \sin i_h r di_h \rho \dot{u}^2 v_h \quad (24)$$

where R_E is the radius of the Earth, and

$$u = \frac{\dot{M}}{4\pi\rho r v_c^3} R^p$$

Here the subscript h signifies the values of the variables at the source, and R^P is the radiation pattern.

5.3 Energy arriving at station P

From the figure above, the energy arriving at station P (per unit time, per unit area of wave front) is

$$\rho_0 \dot{u}_0^2 v_0 \quad (25)$$

where subscript 0 signifies the value of the variables at the station.

5.4. Geometrical Spreading Factor $g(\Delta, h) / R_E$

Since the total energy emitted in a ring defined by i_h and $i_h + di_h$ arrives in a ring defined by Δ and $\Delta + d\Delta$, we obtain from (23), (24), and (25),

$$R_E d\Delta \cos i_0 2\pi R_E \sin \Delta \rho_0 \dot{u}_0^2 v_0 = E_R \quad (26)$$

from which we obtain

$$u_0 = \frac{\dot{M}R^P}{4\pi\rho_h v_h^3} \frac{1}{R_E} \sqrt{\frac{\rho_h v_h \sin i_h}{\rho_0 v_0 \sin \Delta \cos i_0} \left| \frac{di_h}{d\Delta} \right|} = \frac{\dot{M}R^P}{4\pi\rho_h v_h^3} \frac{1}{R_E} g(\Delta, h) \quad (27)$$

where

$$g(\Delta, h) = \sqrt{\frac{\rho_h v_h \sin i_h}{\rho_0 v_0 \sin \Delta \cos i_0} \left| \frac{di_h}{d\Delta} \right|} \quad (28)$$

$g(\Delta, h) / R_E$ is called the geometrical spreading factor.

6. Effect of Anelasticity

Usually, the anelasticity of the medium is given in terms of quality factor Q . If we write the quality factor of P and S waves by Q_α and Q_β , the amplitude attenuation of P and S waves of angular frequency ω during the propagation can be given by

$$\exp\left(-\frac{\omega}{2} \int \frac{ds}{Q_\alpha \alpha}\right), \text{ and } \exp\left(-\frac{\omega}{2} \int \frac{ds}{Q_\beta \beta}\right) \quad (29)$$

where the integral is taken along the ray path. Since Q_α and Q_β are functions of depth and therefore of the path length, s , we may write these

$$\exp\left(-\frac{\omega}{2} t_\alpha^*\right), \text{ and } \exp\left(-\frac{\omega}{2} t_\beta^*\right) \quad (30)$$

where

$$t_\alpha^* = \int \frac{ds}{Q_\alpha \alpha}, \text{ and } t_\beta^* = \int \frac{ds}{Q_\beta \beta} \quad (31)$$

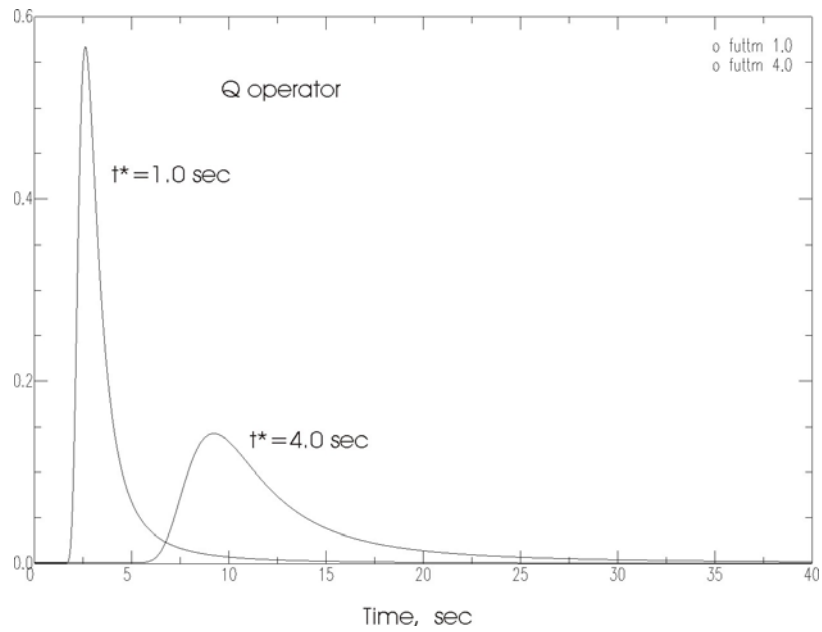
Empirically, t_α^* and t_β^* do not vary significantly with the distance, and $t_\alpha^* = 0.5$ to 1 sec and $t_\beta^* = 3$ to 4 sec for distance ranges $\Delta > 35$ degrees.

In order to maintain causality of P and S pulses, the phase spectrum needs to be modified too.

In time domain, we can represent the effect of attenuation by ‘‘Futterman Q operator’’

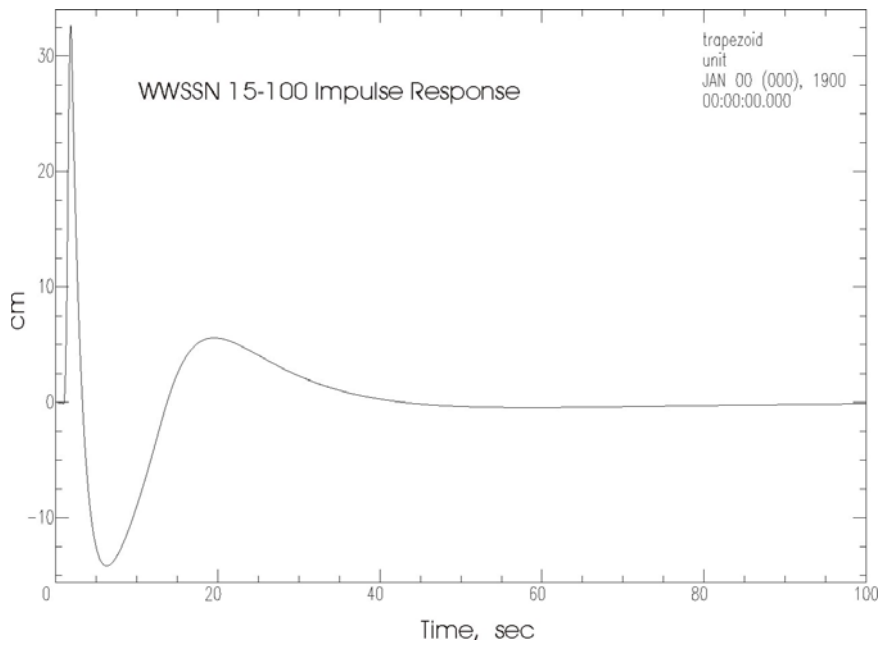
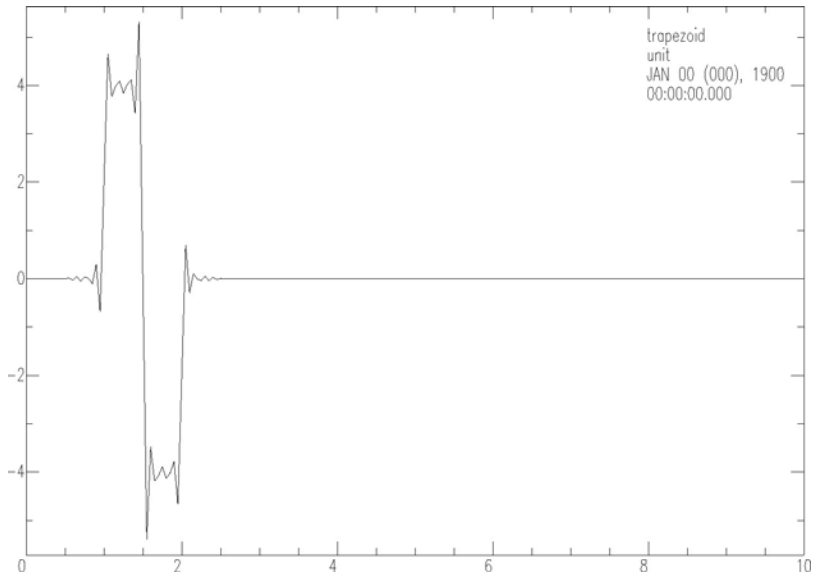
$$q(t; t_\alpha^*) \text{ and } q(t; t_\beta^*) \quad (32)$$

These functions are shown below for $t_\alpha^* = 1$ sec and $t_\beta^* = 4$ sec.



7. Instrument Response

Since seismographs have their own frequency response, they modify the waveforms. In the following, the impulse response of the VBB and WWSSN-LP instruments are shown.



8. Simplified Expressions for a Point Source

The following simplified expressions are not exact, but are useful for understanding the basic principles for retrieval of source parameters.

8.1 Retrieval of Seismic Moment M_0

We approximate a finite source by a point source with a moment rate function $\dot{M}_0(t)$. The area under $\dot{M}_0(t)$ is the seismic moment M_0 and the width of $\dot{M}_0(t)$ is approximately equal to the rupture time $\tau_0 = \tilde{L}/V$ where \tilde{L} is the length scale of the source and V is the rupture speed.

In the following, we use the vertical component of P wave for illustration purposes. We assume that the observed seismogram has been corrected for the instrument, $I(t)$, attenuation, $q(t)$, and the response of the source structure, $C_s(t)$, and the response of the receiver structure is given by a scalar C_R . Then, from the first equation in this section, we can write the vertical component of P wave, $u_p(t)$, as

$$u_p(t) = \frac{\dot{M}_0(t)R}{4\pi\rho_h\alpha_h^3} \frac{g}{R_E} C_R \quad (33)$$

From which,

$$\dot{M}_0(t) = \frac{4\pi\rho_h\alpha_h^3 R_E}{RgC_R} u_p(t) \quad (34)$$

Integrating,

$$M_0 = \frac{4\pi\rho_h\alpha_h^3 R_E}{RgC_R} \int_0^{\tau_p} u_p(t) dt \quad (35)$$

where τ_p is the duration of the P wave record.

Using (35), we can estimate M_0 from seismograms.

8.2 Determination of Radiated Energy from P waves.

Since S waves are severely attenuated during propagation to teleseismic distances, we usually use P waves to estimate the radiated energy in P waves, E_α , and then estimate the total radiated energy, E_R . If we consider a small sphere around the source, and write the P wave on the spherical surface by $U_p(t)$, the total energy radiated by P waves is given by,

$$\begin{aligned} E_\alpha &= \int_S dS \int_0^{\tau_p} \rho_h \alpha_h \dot{U}_p^2(t) dt = \int_S dS \int_0^{\tau_p} \rho_h \alpha_h \left[\frac{R}{4\pi\rho_h \alpha_h^3 r} \ddot{M}_0(t) \right]^2 dt \\ &= \rho_h \alpha_h \left[\frac{1}{4\pi\rho_h \alpha_h^3 r} \right] \int_S R^2 dS \int_0^{\tau_p} \ddot{M}_0^2(t) dt \end{aligned} \quad (36)$$

Substituting (34),

$$E_\alpha = \frac{16\pi}{15} \rho_h \alpha_h \left(\frac{R_E}{g} \right)^2 \frac{1}{R^2} \frac{1}{C_R^2} \int_0^{\tau_p} \dot{u}_p^2(t) dt \quad (37)$$

where

$$\frac{1}{4\pi r^2} \int_S R^2 dS \equiv \overline{R^2} = \frac{4}{15} \quad (38)$$

for P waves is used.

Using (37), we can estimate E_α from the observed record at a station. For a point source, we can show that

$$E_\beta = \frac{3}{2} \left(\frac{\alpha}{\beta} \right)^5 E_\alpha \approx 23E_\alpha \quad (39)$$

and

$$E_R = E_\alpha + E_\beta = 24E_\alpha \quad (40)$$

Ge 162 Problem #8 Interpretation of Far-field Body Wave

Figure 1 shows the P-wave seismograms (WWSSN long-period response) observed for the May 2, 1983 Coalinga, California, earthquake. The numbers attached to each seismogram is the amplitude.

COALINGA
Vertical P waveforms

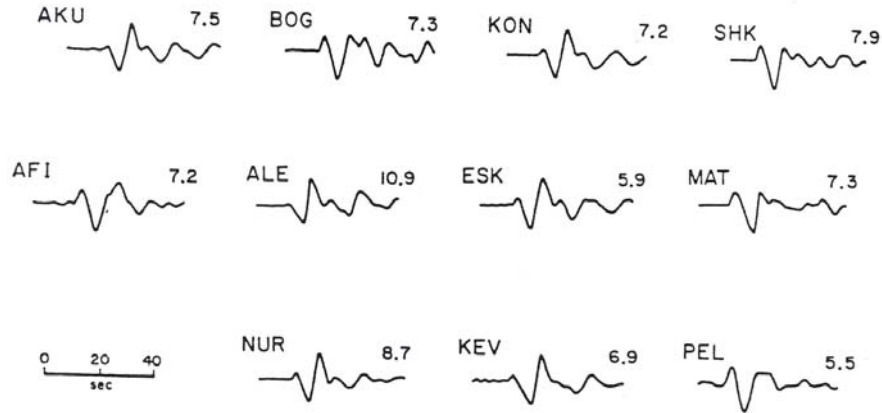


Fig. 1

In order to determine the source parameters (seismic moment, source duration), we must remove the effects of

1. Radiation pattern, R
2. Response of source and receiver structures, $C_S(t)$ and $C_R(t)$
3. Geometrical spreading, $g(\Delta, h)$
4. Attenuation (Q operator), $q(t)$
5. Instrument response, $I(t)$

Fortunately, Hartzell and Heaton (1983) have removed all of these effects, and obtained a trapezoidal displacement at point P, as shown in Figure 2.

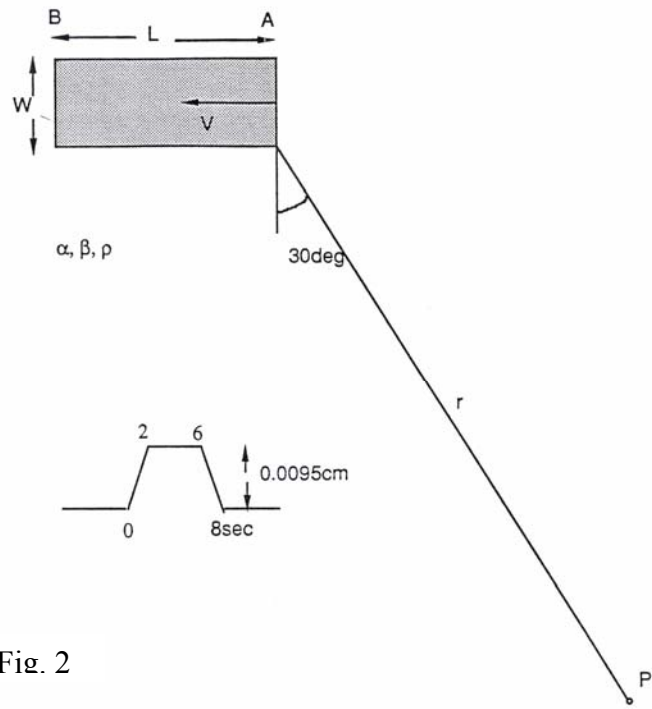


Fig. 2

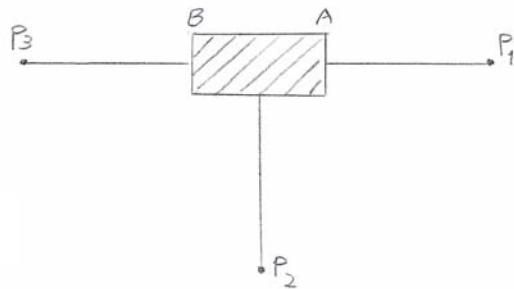


Fig. 3

As we discussed in class, the displacement $u(r, t)$ at far-field due to a Haskell type source is given by

$$u(r, \tau) = \frac{RM_0}{4\pi\rho r v_c^3} \int_{-\infty}^{+\infty} r(t_1) s(\tau - t_1) dt_1 = \frac{RM_0}{4\pi\rho r v_c^3} T(\tau; \tau_0, t_c) \quad (1)$$

where ρ is the density, v_c is P- or S-wave velocity, M_0 is the seismic moment, and $\tau = t - r/v_c$. Note that the amplitude of $T(\tau; \tau_0, t_c)$ is $1/t_c$, and the area under it is 1. t_c is given by

$$t_c = \frac{L}{V} - \frac{L \cos \Theta}{v_c}$$

where Θ is the angle between the rupture direction and the ray.

1. Check the dimension of the right-hand-side of equation (1) to make sure that it is the dimension of "length".

2. We assume that the medium is homogeneous with $\alpha = 6$ km/sec, $\beta = 3.5$ km/sec and $\rho = 2.6$ g/cm³, and the radiation pattern R is equal to 1. We also assume that the fault plane AB and P are on the same plane. The take-off angle of the ray to P is 30 degrees (note that this is different from Θ), and the distance is $r = 1000$ km. The rupture propagation is assumed to be one dimensional unilateral (A to B) with a rupture speed $V = 2.5$ km/sec.

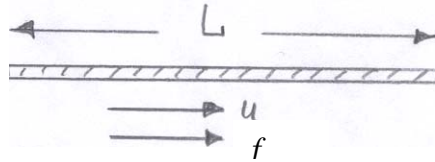
- (1) Determine the rise time τ_0 and t_c from Figure 2.
- (2) Determine the seismic moment M_0 .
- (3) Estimate the fault length L .
- (4) Assuming that the fault width $W = L/3$, estimate the average dislocation.
- (5) Estimate the particle velocity (average) of one side of the fault.
- (6) Estimate the static stress drop (use the strike-slip geometry for simplicity).
- (7) Sketch the (trapezoidal) waveform that would be observed at point P1, P2, and P3, all at a distance of 1000 km, but in three different azimuths, as shown in Figure 3.

(Note: The solution obtained by Hartzell and Heaton is slightly different from the above.)

6.2 Excitation of Surface Waves and Free Oscillations

1. One Dimensional Problem

We first consider a one-dimensional problem shown below.



$$\rho \frac{\partial^2 u}{\partial t^2} = E \frac{\partial^2 u}{\partial x^2} + \rho f \quad (1)$$

where f is the force per unit mass.

Consider a harmonic excitation $\rho f(x, t) = F(x)e^{i\omega t}$.
 Putting $u(x, t) = U(x)e^{i\omega t}$ we have

$$-\rho\omega^2 U = E \frac{d^2 U}{dx^2} + F \quad (2)$$

Let y_i , $i = 1, 2, \dots$ be the eigen functions of the homogeneous equation of (2) i.e.,

$$-\rho\omega_i^2 y_i = E \frac{d^2 y_i}{dx^2} \quad (3)$$

Then y_i 's constitute an orthogonal system. That is,

$$\int_0^L \rho y_n y_l dx = c \delta_{n,l} \quad (4)$$

Then we can expand U in y_i , i.e.,

$$U = \sum_{i=1}^{\infty} a_i y_i \quad (5)$$

where

$$a_i = \frac{1}{c} \int_0^L \rho y_i U dx \quad (6)$$

Multiplying (2) by y_n and integrating it from $x=0$ to $x=L$, we obtain

$$-c \omega^2 a_n = E \sum_l a_l \int_0^L y_l' y_n dx + \int_0^L F y_n dx$$

Using (3) and (4),

$$\begin{aligned} -c \omega^2 a_n &= -c \omega_n^2 a_n + \int_0^L F y_n dx \\ \therefore a_n &= -\frac{1}{c(\omega^2 - \omega_n^2)} \int_0^L F y_n dx \end{aligned} \quad (7)$$

$$\therefore U = \sum_{n=1}^{\infty} \left[-\frac{y_n}{c(\omega^2 - \omega_n^2)} \right] \int_0^L F y_n dx \quad (8)$$

$$\therefore u = e^{i\omega t} \sum_{n=1}^{\infty} \left[-\frac{y_n}{c(\omega^2 - \omega_n^2)} \right] \int_0^L F y_n dx \quad (9)$$

Now let us consider excitation by a step function force $H(t)$. Since

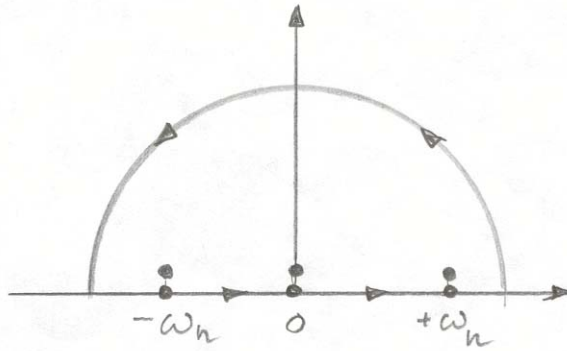
$$H(t) = \frac{1}{2\pi} \int_{-\infty}^{+\infty} \frac{1}{i\omega} e^{i\omega t} d\omega \quad (10)$$

we have from (9)

$$\therefore u(t) = \sum_{n=1}^{\infty} \left[-\frac{y_n}{c} \int_0^L F y_n dx \right] \frac{1}{2\pi} \int_{-\infty}^{+\infty} \left[-\frac{e^{i\omega t}}{i\omega(\omega^2 - \omega_n^2)} \right] d\omega \quad (11)$$

The poles are at $\omega = 0$, $\omega = \omega_n + i\varepsilon$, $\omega = -\omega_n + i\varepsilon$.

Since any physical system must have at least small attenuation, these poles are slightly above the real axis (see Morse and Feshbach, p. 1334).



Carrying out the integration along the path given above, we have, for $t > 0$,

$$u(t) = \sum_{n=1}^{\infty} \left[y_n \int_0^L F y_n dx \right] \frac{(1 - \cos \omega_n t)}{c_n \omega_n^2} \quad (12)$$

The first term

$$u(t) = \sum_{n=1}^{\infty} \left[y_n \int_0^L F y_n dx \right] \frac{1}{c_n \omega_n^2} \quad (13)$$

gives the permanent deformation, and the second term

$$u(t) = - \sum_{n=1}^{\infty} \left[y_n \int_0^L F y_n dx \right] \frac{\cos \omega_n t}{c_n \omega_n^2} \quad (14)$$

gives the free oscillation.

2. Torsional Oscillation

For torsional oscillations of a sphere, the eigen functions and the force are vectors.

$${}_n \bar{y}_l^m = y_{l,n} \begin{pmatrix} 0 \\ \frac{1}{\sin \theta} \frac{\partial Y_l^m}{\partial \phi} \\ -\frac{\partial Y_l^m}{\partial \theta} \end{pmatrix}, \quad \bar{F} = \begin{pmatrix} F_r \\ F_\theta \\ F_\phi \end{pmatrix} \quad (15)$$

The expression for step function excitation can be derived in a manner similar to the one-dimensional case.

$$\bar{u}(\bar{r}, t) = \sum_{l,m,n} \left[{}_n \bar{y}_l^m \int_V \bar{F} \cdot {}_n \bar{y}_l^m dV \right] \frac{(1 - \cos {}_n \omega_l^m t)}{{}_n c_l^m {}_n \omega_l^{m2}} \quad (16)$$

where

$${}_n c_l^m = \int_V \rho {}_n \bar{y}_l^m \cdot {}_n \bar{y}_l^m dV$$

3. Spheroidal Oscillation

$${}_n \bar{y}_l^m = y_{1,n} \begin{pmatrix} Y_l^m \\ 0 \\ 0 \end{pmatrix} + y_{3,n} \begin{pmatrix} 0 \\ \frac{\partial Y_l^m}{\partial \theta} \\ \frac{1}{\sin \theta} \frac{\partial Y_l^m}{\partial \phi} \end{pmatrix} \quad (17)$$

Then

$$\bar{u}(\bar{r}, t) = \sum_{l,m,n} \left[{}_n \bar{y}_l^m \int_V \bar{F} \cdot {}_n \bar{y}_l^m dV \right] \frac{(1 - \cos {}_n \omega_l^m t)}{{}_n c_l^m {}_n \omega_l^{m2}} \quad (18)$$

Again

$${}_n c_l^m = \int_V \rho {}_n \bar{y}_l^m \cdot {}_n \bar{y}_l^m dV \quad (19)$$

4. Displacement due to a point Moment Tensor

Displacement due to force couples can be obtained by differentiating (16) and (18) in appropriate directions. Then the displacement due to a point moment tensor M can be written as

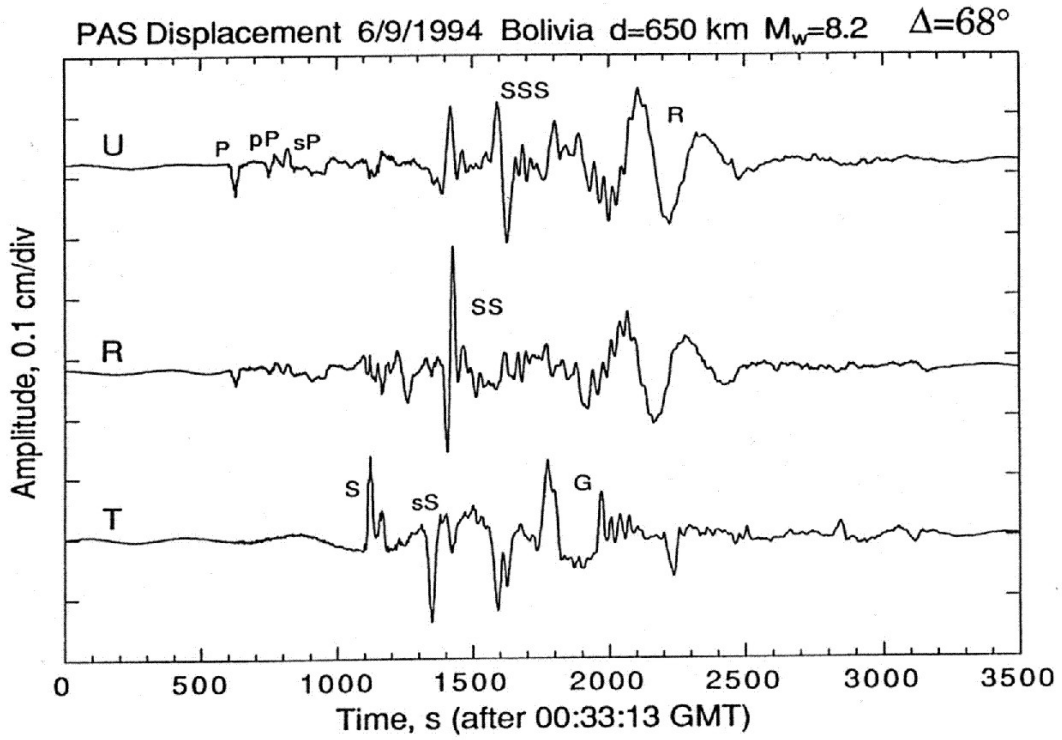
$$\bar{u}(\bar{r}, t) = \sum_{l,m,n} \left[(M : \varepsilon) {}_n \bar{y}_l^m(\bar{r}, t) \right] \frac{1 - \cos {}_n \omega_l^m t}{{}_n c_l^m {}_n \omega_l^{m2}} \quad (20)$$

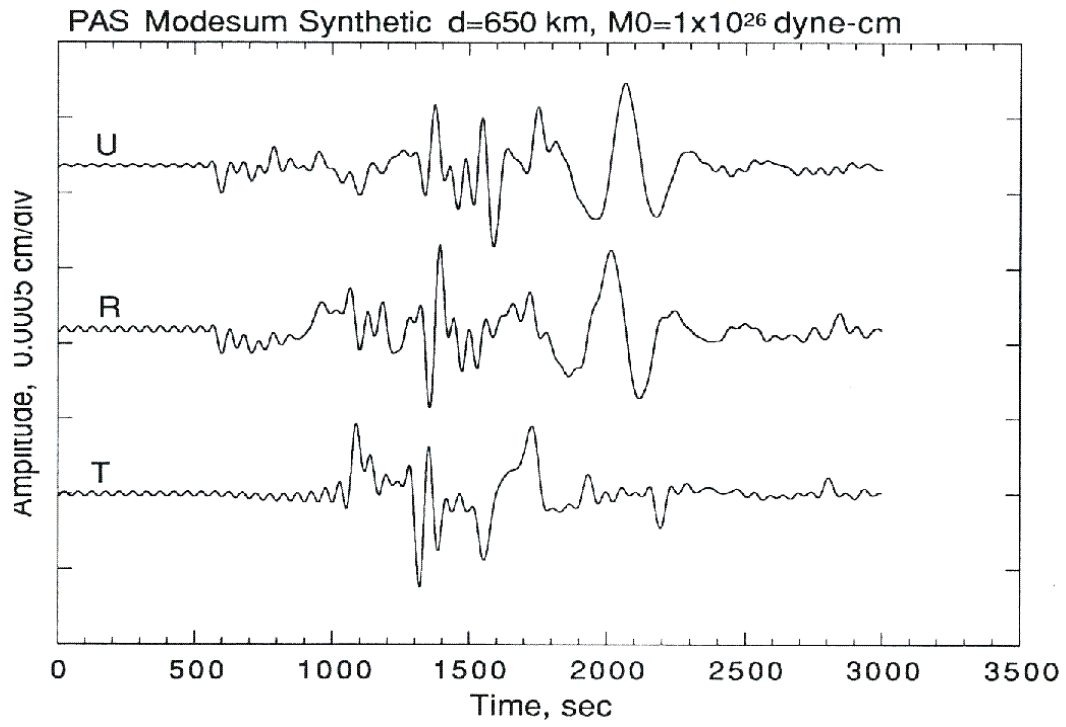
where ε is the strain tensor computed at the source for each l , m , and n .

5. Comparison with observations

Several examples are shown in the following.

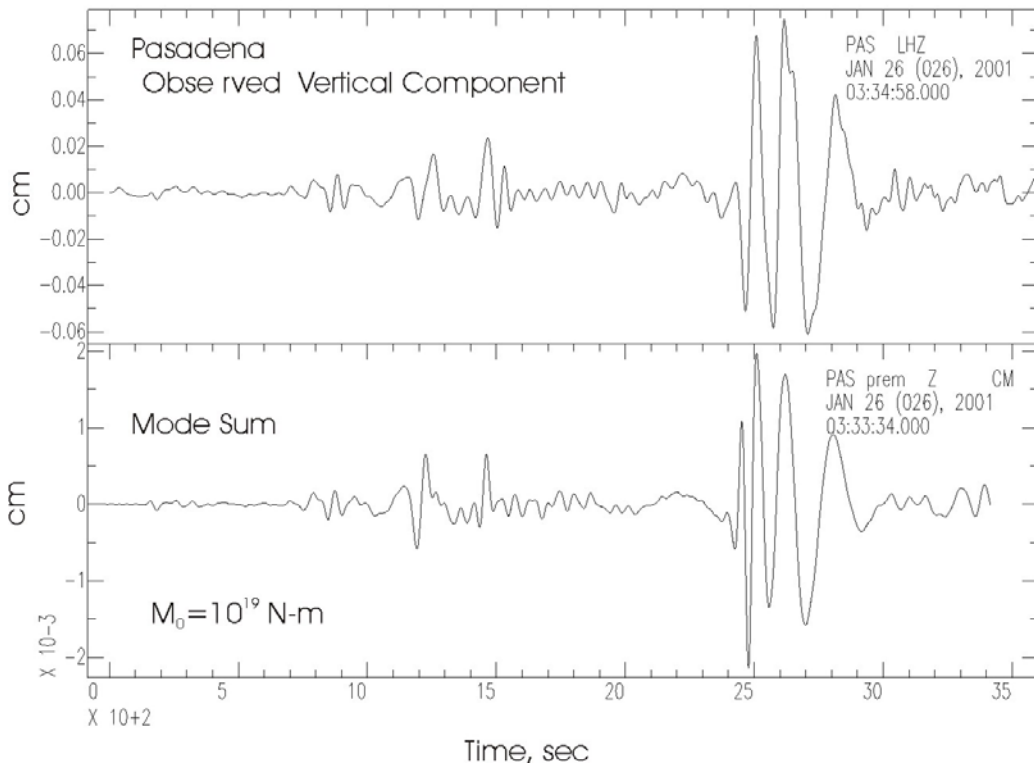
1. 1994 Bolivia Deep earthquake

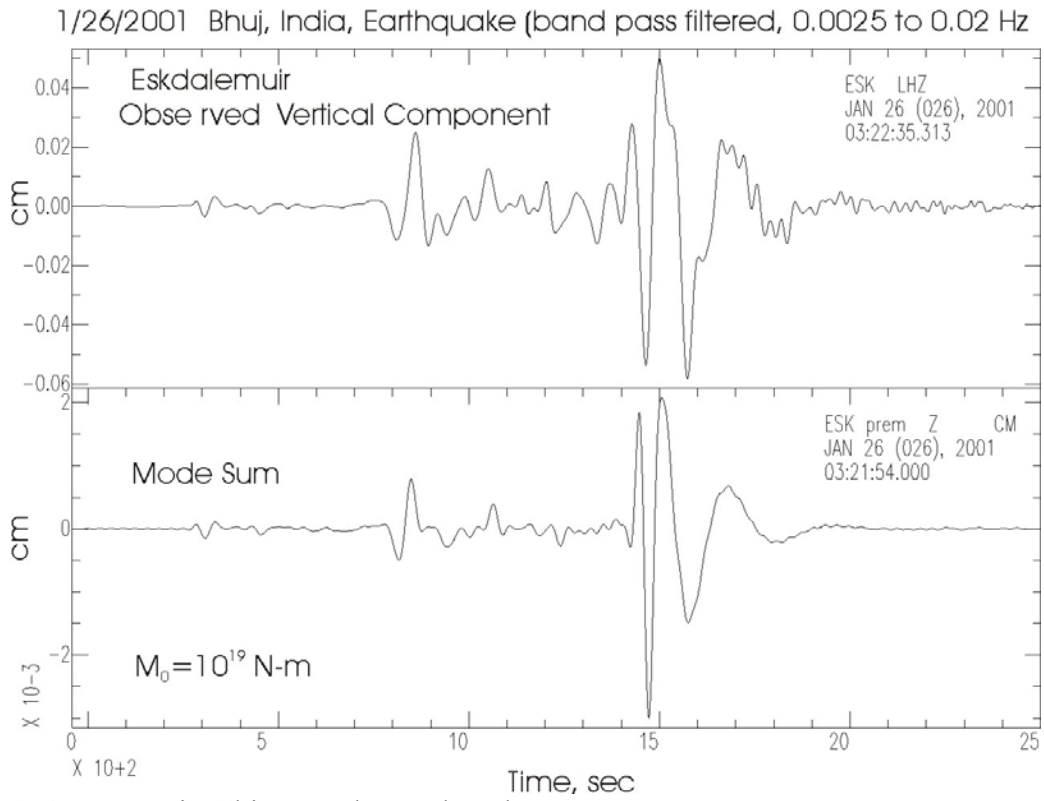




2. 2001 Bhuj India earthquake

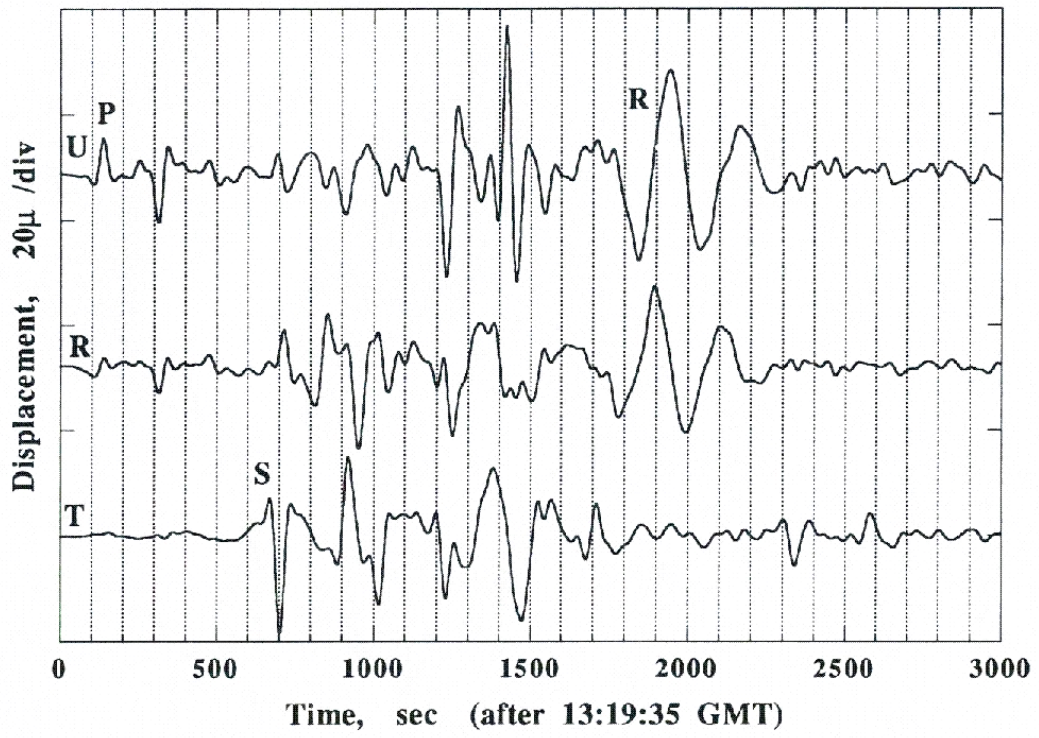
1/26/2001 Bhuj, India, Earthquake (band pass filtered, 0.0025 to 0.02 Hz)



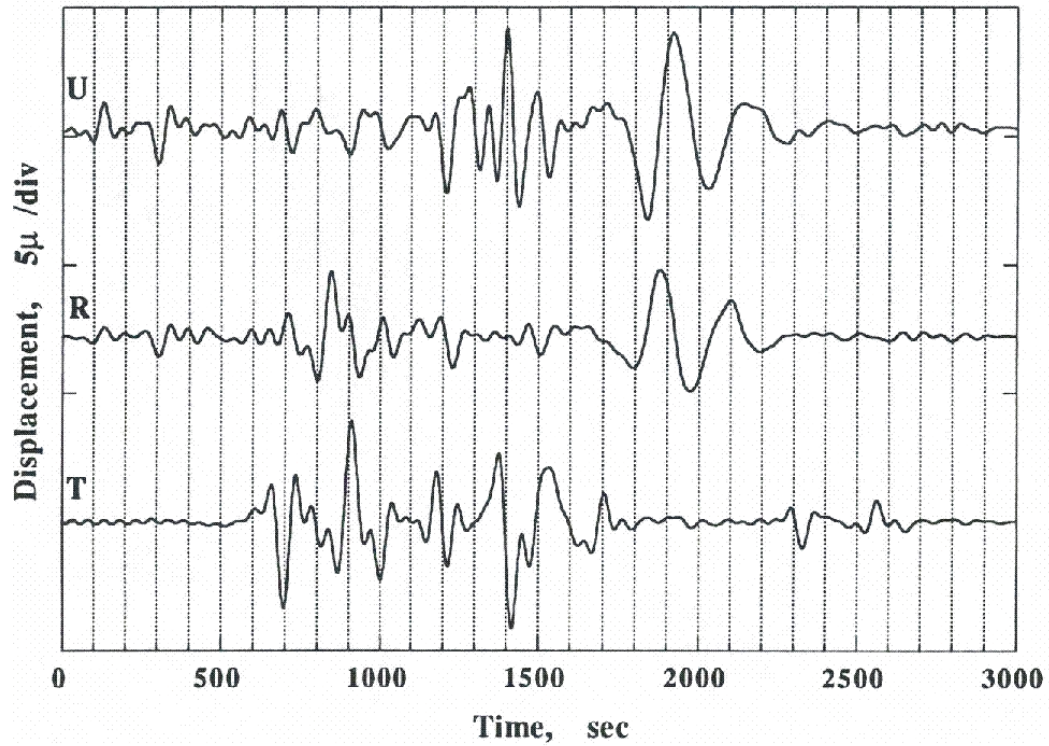


3. 1999 Russia-China Border earthquake

Russia-China Border 4/8/1999, PAS Band-Pass Filtered (0.0033 to 0.022 Hz)



Russia-China Border, PAS Synthetic (BP)



7. Summary of Seismic Source Parameters

1. Fault Geometry

Usually given by the following three parameters: ϕ_f = fault strike; δ = dip angle, λ = slip angle (rake).

2. Fault Dimension

L and W or a (radius). Area S .
($S = LW$) ($S = \pi a^2$)

3. Dislocation (Fault Offset), D

In general, $D(\vec{r}, t)$

Usually only the average \bar{D} is used

$$\bar{D} = \Delta \bar{u}$$

4. Seismic Moment (Moment)

$$M_0 = \mu S \bar{D}$$

5. Seismic Moment Tensor

$$M_{pq} = C_{ijpq} \Delta u_i v_j \Delta S \quad (\text{in general})$$

$$M = \mu \Delta S (\Delta \vec{u} : \vec{v}) \quad (\text{shear dislocation})$$

This can be related to the fault parameters (5.1.4).

6. Stresses

$$\text{Initial stress}^* \quad \sigma_0$$

$$\text{Final stress}^* \quad \sigma_1$$

$$\text{Static stress drop} \quad \Delta \sigma_s = (\sigma_0 - \sigma_1) \propto \bar{D}$$

$$\text{Frictional stress}^* \quad \sigma_f$$

$$\text{Effective tectonic stress (Dynamic stress drop)} \quad \Delta \sigma_d = \sigma_0 - \bar{\sigma}_f \propto \dot{D}$$

$$\text{Average stress}^* \quad \bar{\sigma} = (\sigma_0 + \sigma_1) / 2$$

* This cannot be determined with seismological methods

7. Energy

Radiated Energy

$$E_R \propto \rho v \int \int \dot{u}^2 dt dS$$

Potential Energy Change*

(Strain Energy + Gravitational Energy)

$$\Delta W = \bar{\sigma} \bar{D} S$$

Frictional Energy Loss*

$$E_F = \bar{\sigma}_f \bar{D} S$$

Fracture Energy*

$$E_G$$

$$\Delta W = E_R + E_F + E_G = (\text{Radiated Energy}) + (\text{Non-Radiated Energy})$$

* This cannot be determined with seismological methods

8. Rupture Mode and Rupture Speed

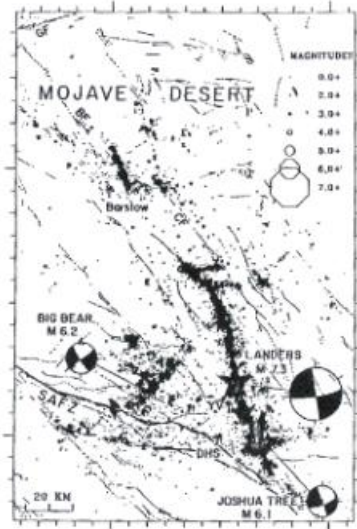
Unilateral, Bilateral, Radial, Two-Dimensional

V , usually 75 to 90% of S velocity

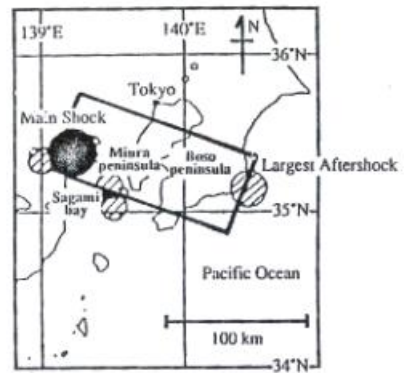
Directivity

Unilateral Faulting

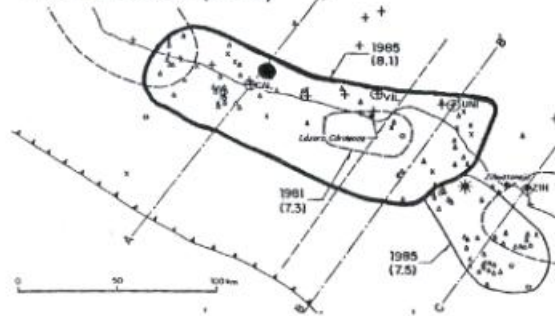
1992 Landers (M=7.3)



1923 Kanto (M=8)

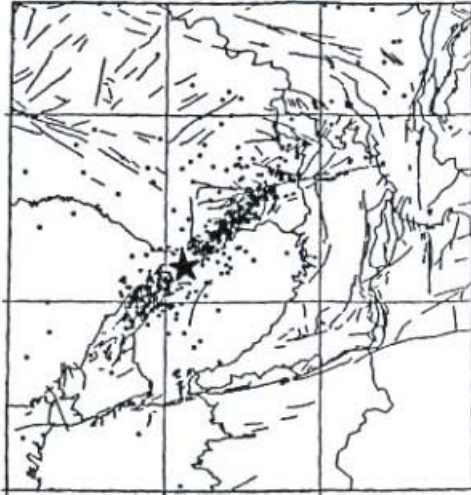


1985 Mexico (M=8)

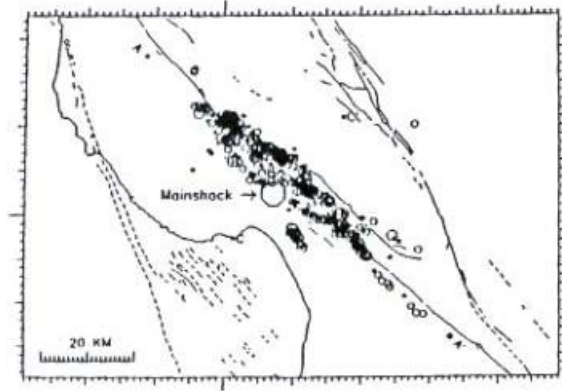


Bi-lateral Fault

1995 Kobe Earthquake



1989 Loma Prieta Earthquake

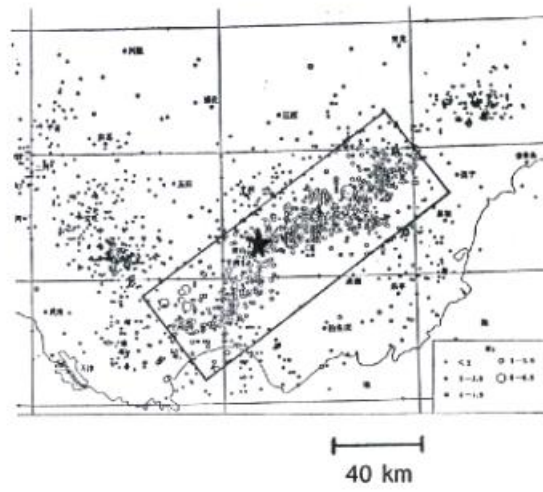


Asymmetric Bi-lateral Fault

1906 San Francisco Earthquake



1976 Tangshan Earthquake



Rupture Velocity

1992 Landers Earthquake

Wald and Heaton (1994)	Average 2.7 km/sec (75 % of "S") Range 1.0 to 4.0 km/sec
Cohee and Beroza (1994)	Average 2.5 km/sec
Dreger (1994)	2.9 km/sec (80% of "S")

1989 Loma-Prieta Earthquake

Wald et al. (1991)	2.7 km/sec
Steidl et al. (1991)	3.0 km/sec (83% of "S")
Beroza (1991)	80 % of "S"

1985 Mexico Earthquake

Mendoza and Hartzell (1989)	2.6 km/sec (70% of "S")
-----------------------------	-------------------------

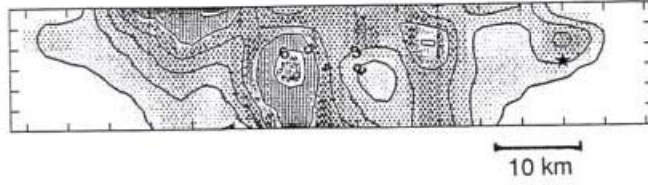
9. Complexity

Multiple Events, "Fractal" structure at short wave length?

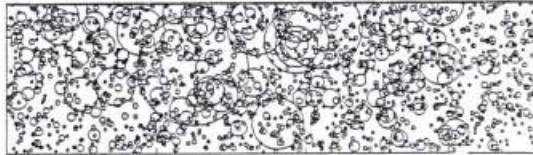
Fault Rupture Pattern

1992 Landers Earthquake

Wald and Heaton [1994]



Heterogeneous (Fractal) Model Zeng, Anderson, and Yu [1994]

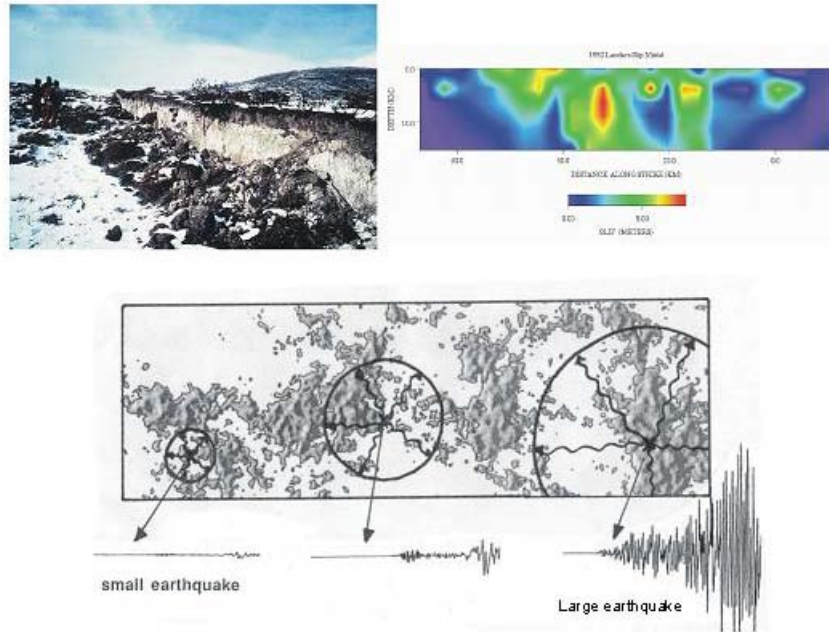


Observed



Computed

Complexity of Fault Surface and Rupture Pattern



10. Energy (or Moment) Magnitude

$$M_w = (\log M_0 - 16.1) / 1.5 \quad (M_0 \text{ in dyne-cm})$$

$$M_w = (\log M_0 - 9.1) / 1.5 \quad (M_0 \text{ in N-m})$$

From the energy budget, the radiated energy, E_R , is given by

$$E_R = \Delta W - E_F = \bar{D}S(\bar{\sigma} - \bar{\sigma}_f)$$

As mentioned above, the initial stress σ_0 , the final stress σ_1 , and the frictional stress $\bar{\sigma}_f$ cannot be determined directly with seismological methods, and E_R above cannot be determined. However, note that

$$E_R = \bar{D}S\left(\frac{\sigma_0 + \sigma_1}{2} - \bar{\sigma}_f\right) = \bar{D}S\left(\frac{\sigma_0 - \sigma_1}{2} + (\sigma_1 - \bar{\sigma}_f)\right) = \bar{D}S\left(\frac{\Delta\sigma_s}{2} + (\sigma_1 - \bar{\sigma}_f)\right)$$

If we assume that σ_1 is equal to $\bar{\sigma}_f$ (i.e., the stress on the fault plane is equal to the average frictional stress when fault motion stops), then,

$$E_R = \frac{1}{2} \bar{D} S \Delta \sigma_s = \frac{\Delta \sigma_s}{2\mu} \bar{D} S \mu = \frac{\Delta \sigma_s}{2\mu} M_0$$

For most large earthquakes, $\Delta \sigma_s / 2\mu \approx 1/(2 \times 10^4)$, and we have, approximately,

$$E_R = M_0 / (2 \times 10^4)$$

Once E_R is determined we can define a magnitude scale M_w using the Energy-Magnitude relation backward,

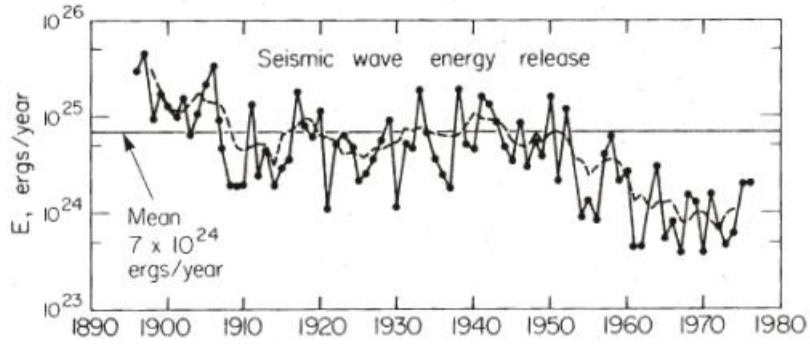
$$\log E_R = 1.5 M_w + 11.8 \quad (E_R \text{ in ergs})$$

or,

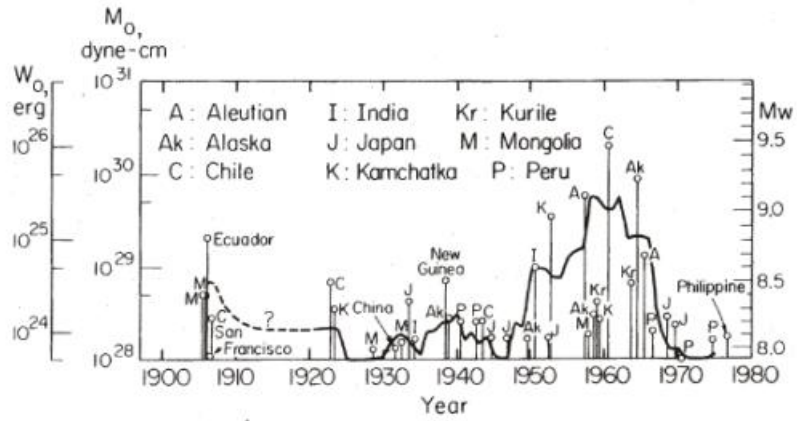
$$M_w = (\log M_0 - 16.1) / 1.5 \quad (M_0 \text{ in dyne-cm})$$

Earthquake Energy Release in the 20th Century

(old from Ms)



("New" from Mw)



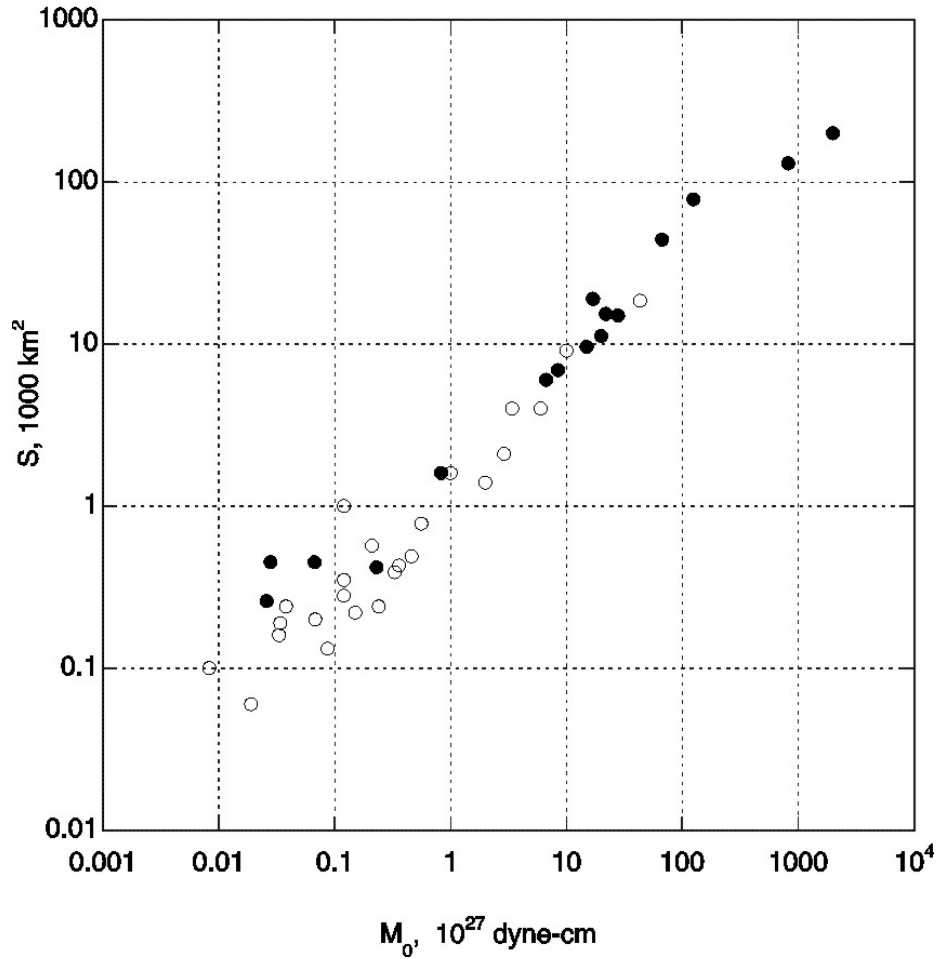
Ge 162

8. Physics of Earthquakes

8.1 Scaling Relations

For understanding the overall physics of earthquakes without going into details, it is useful to investigate scaling relations between several macroscopic source parameters.

1. Moment versus Fault Area



[closed circles: interplate, open circles: intraplate, Kanamori, H., and D. L. Anderson, Theoretical basis of some empirical relations in seismology, *Bull. Seis. Soc. Amer.*, 65 (5), 1073-1095, 1975]

By definition,

$$M_0 \propto \Delta\sigma_s a^3 \quad \text{circular}$$

$$\Delta\sigma_s w^2 L \quad \text{rectangular}$$

For a circular fault,

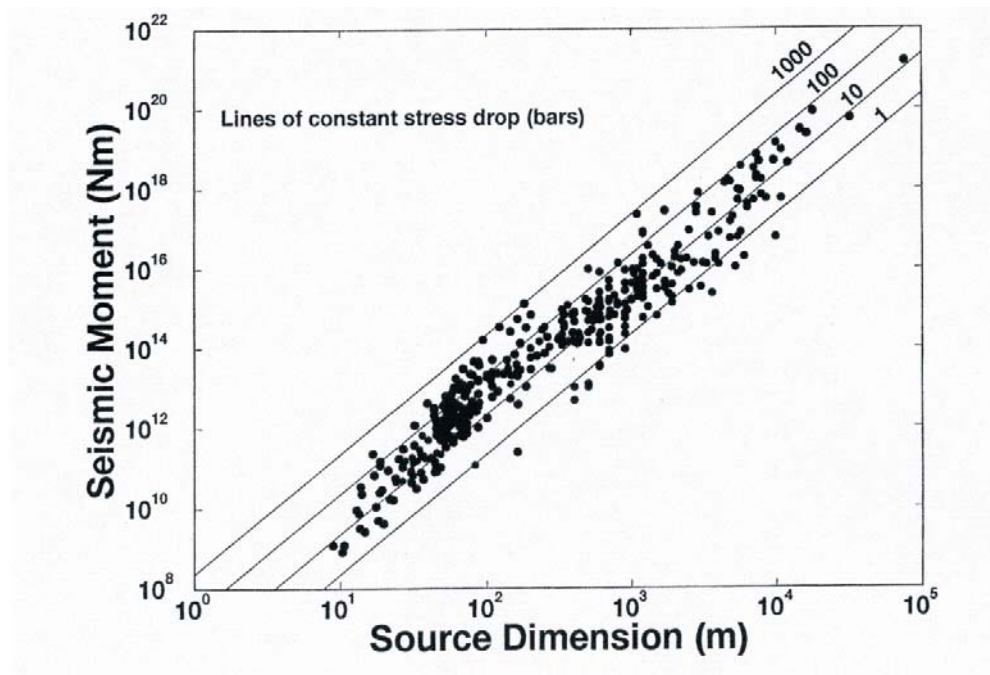
$$\log M_0 = \frac{3}{2} \log S + \log \left(\frac{16}{7} \pi^{-3/2} \Delta \sigma_s \right)$$

If $\Delta \sigma_s$ is constant, then, $\log M_0 \approx \frac{3}{2} \log S$. From the attached figure, we see,

- $\Delta \sigma_s \sim 60$ bars on the average
- $\Delta \sigma_s \sim 30$ bars interplate (plate boundary)
- $\Delta \sigma_s \sim 100$ bars intraplate

2. Seismic Moment vs. Source Dimension

The scaling relation shown above has been extended to small earthquakes as shown below.



[Modified from Abercrombie, R., and P. Leary, Source parameters of small earthquakes recorded at 2.5 km depth, Cajon Pass, Southern California: Implications for earthquake scaling, *Geophys. Res. Lett.*, 20, 1511-1514, 1993]

The $L \propto M_0^{1/3}$ scaling is seen, and this is generally interpreted as evidence for constant stress drop, but the fairly large scatter in $\Delta\sigma_s$ should be noted.

8.2 Physics of Earthquakes

The heterogeneity of properties and structures of fault planes seems to have a profound influence on dynamics of faulting. Although we cannot resolve every detail of fault zone heterogeneities, we want to interpret macroscopic seismological data in terms of the overall processes occurring on a fault plane.

8.2.1 Energy Budget

As we discussed in 5.1.5, the total potential energy (strain energy + gravitational energy) change in earthquakes is given by

$$\Delta W = \frac{1}{2}(\sigma_0 + \sigma_1)\bar{D}S \quad (1)$$

Then the energy budget can be written as

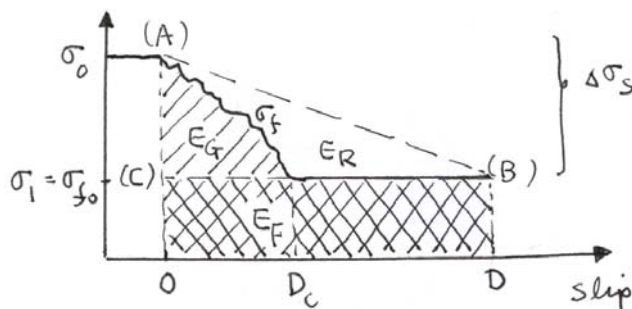
$$\Delta W = E_R + E_F + E_G \quad (2)$$

where E_R and E_G are the radiated energy and the fracture energy, respectively, and E_F

is the frictional energy. In this model, separation of E_G and E_F is somewhat arbitrary (both represent non-radiated energy, i.e., dissipation), but, E_G , and E_F are commonly defined by the hatched and cross-hatched areas shown in the figure below, respectively, i.e.,

$$E_F = \sigma_{f_0} \bar{D}S \quad (3)$$

However, here the fracture energy, E_G , is the energy dissipated during rupture over a volume surrounding the fault zone.



(In this diagram, the energies are interpreted as those per unit area.)

The radiated energy, E_R , is what we can measure from the radiated seismic waves, as shown in 6.1, but because of the practical difficulty in measuring it accurately, E_R has not been fully used in seismology for the purpose of understanding the physics of earthquakes.

Only recently, it became possible to measure E_R accurately enough so that we can investigate the physics of earthquakes in terms of energy budget.

8.2.2 The Radiation Efficiency

The ratio of the fracture energy, E_G , to the radiated energy, E_R , determines the characteristics of fracture, or an earthquake. Alternatively, the radiation efficiency defined by

$$\eta_R = E_R / (E_R + E_G) \quad (4)$$

can be used for the same purpose. Referring to the figure above,

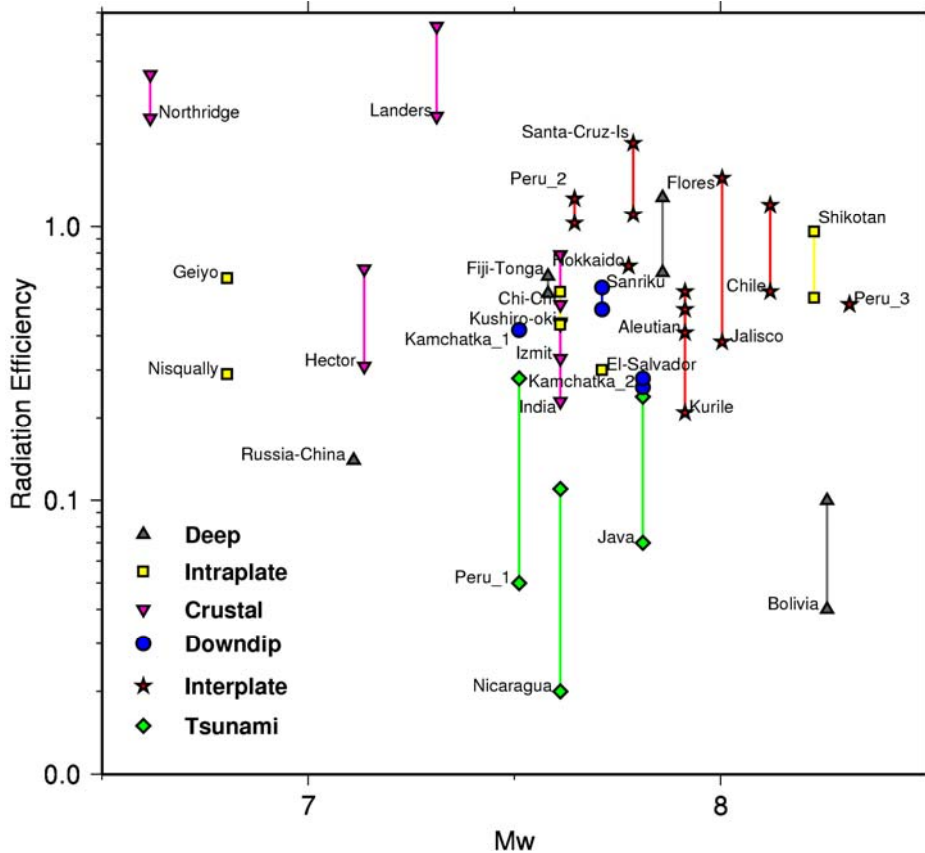
$$\eta_R = E_R / (\Delta\sigma_s \bar{D}S / 2) = E_R / (\Delta\sigma_s M_0 / 2\mu) = 2(E_R / M_0) / (\Delta\sigma_s / \mu) \quad (5)$$

Thus, we can determine η_R , from the observed macroscopic parameters, $\tilde{\epsilon} = E_R / M_0$, and the static strain drop, $\Delta\epsilon = \Delta\sigma_s / \mu$.

8.2.3 Observations

General Observation

The results for large earthquakes are summarized in the following figure.



Radiation efficiency $\eta_R = E_R / (E_R + E_G)$ as a function of M_w . The different symbols show different types of earthquakes as described in the legend. Most earthquakes have radiation efficiencies greater than 0.25, but tsunami earthquakes and two of the deep earthquakes (the Bolivia earthquake and the Russia-China earthquake) have small radiation efficiencies. (Venkataraman and Kanamori, 2004)

Except for the very large deep focus earthquake, the 1994 Bolivian earthquake, and tsunami earthquakes, the radiation efficiency, η_R , is larger than 0.25, which means that the fracture energy for most large earthquakes, regardless of their tectonic environment, are comparable or less than E_R .

Deep Focus Earthquake

It is difficult to accurately determine the size of the fault plane, S , for deep focus earthquakes. However, for the 1994 Bolivian earthquake ($M_w=8.3$, *depth*=635 km), the largest deep-focus earthquake ever recorded, the source parameters could be determined well enough to investigate the energy budget.

As we discussed in 5.1.5, we cannot determine ΔW itself, but we can estimate its lower bound,

$$\Delta W_0 = \Delta \sigma_s \bar{D} S / 2 \quad (6)$$

from $\Delta \sigma_s$, \bar{D} , and S .

The result for the 1994 Deep Bolivian earthquake ($M_w=8.3$) showed that $\Delta W_0=1.4 \times 10^{18}$ J and $E_R=5 \times 10^{16}$ J, which is only 3 % of ΔW_0 ; the difference $\Delta W_0 - E_R=1.35 \times 10^{18}$ J, was not radiated, and must have been deposited near the focal region, probably in the form of thermal energy. This energy 1.35×10^{18} J is comparable to the total thermal energy released during large volcanic eruptions such as the 1980 Mount Saint Helens eruption. The thermal energy must have been released in a relatively small focal region, about 50×50 km², within a matter of about 1 min. The mechanical part of the process, *i.e.* the earthquake observed as seismic waves, is only a small part of the whole process. Thus, the Bolivia earthquake should be more appropriately viewed as a thermal process rather than a mechanical process.

With this much of non-radiated energy, the temperature in the focal region must have risen significantly. The actual temperature rise, ΔT , depends on the thickness of the fault zone, which is not known, but if it is of the order of a few cm, the temperature could have risen to above 10,000 °C.

Shallow Earthquakes

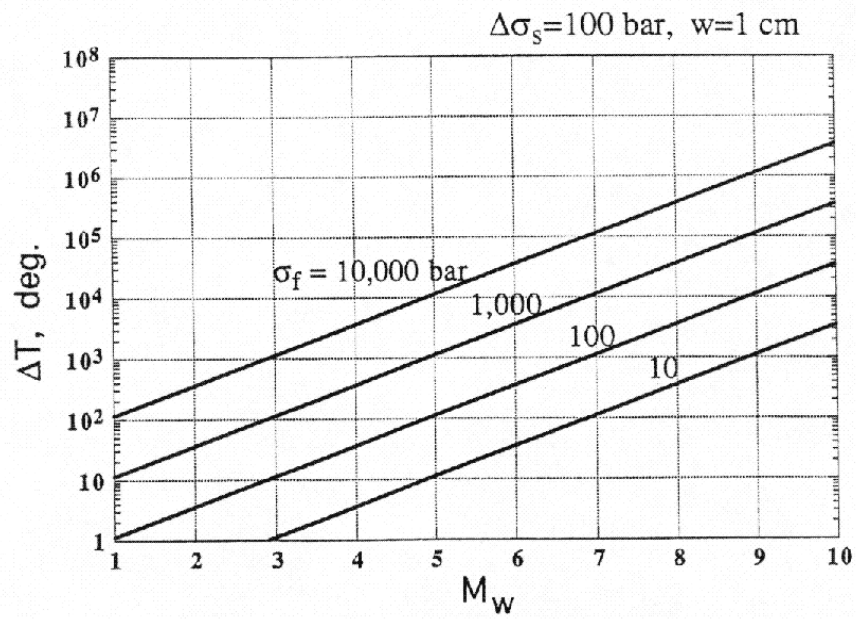
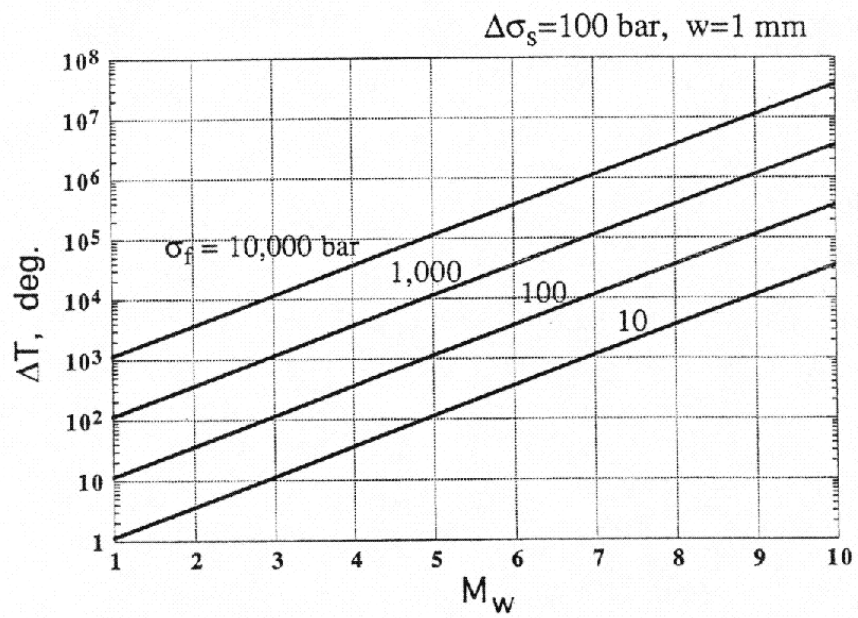
Although the situation for shallow earthquakes may be different from that for deep focus earthquakes, a simple calculation shows that if σ_f is comparable to $\Delta \sigma_s$, about 10 MPa, the effect of shear heating is significant. If the thermal energy is contained

within a few cm around the slip plane during seismic slip, the temperature can easily rise to 100 to 1000 °C.

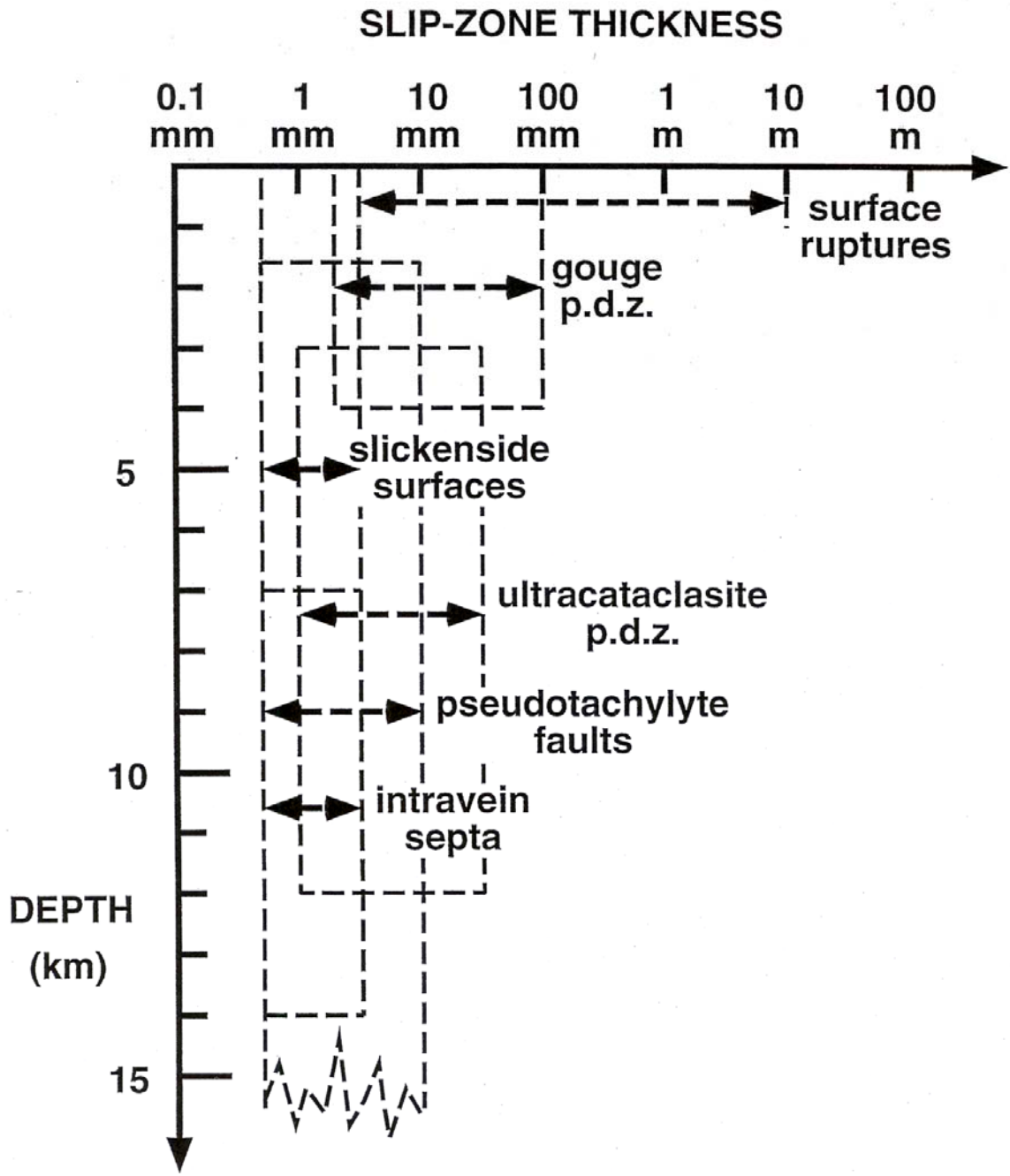
We consider a gross thermal budget during faulting under a frictional stress σ_f . Let S and D be the fault area and the displacement offset respectively. Then the total heat generated during faulting is $Q = \sigma_f DS$. If we assume that the heat is distributed during seismic faulting within a layer of thickness w around the rupture plane, the average temperature rise ΔT is given by

$$\Delta T = Q / C \rho S w = \sigma_f D / C \rho w \quad (7)$$

The figure below shows ΔT as a function of magnitude. If a fault zone is dry (no fluid), melting may occur and friction may drop. If fluids exist in a fault zone, fluid pressurization could occur.



The key question is how thick the fault slip zone is. Geologists have examined many old fault zones which were formed at depths and were brought to the surface by long-term uplift (*i.e.*, exhumed faults). Some fault zones have a very narrow (about 1 mm) distinct slip zone where fault slips seem to have occurred repeatedly. The Punchbowl fault, California, implies that earthquake ruptures were not only confined to the ultracataclasite layer, but also largely localized to a thin prominent fracture surface. They suggest that mechanisms that are consistent with extreme localization of slip, such as thermal pressurization of pore fluids, are most compatible with their observations. In other cases, several narrow slip zones were found but evidence shows that each slip zone represents a distinct slip event (*i.e.*, an earthquake). Thus, geological evidence suggests a narrow slip zone, at least for some faults, but this question will remain debatable.



(Richard Sibson, Written communication, 2000)

If a fault zone is narrow and rough, and if the material in the fault zone behaves as viscous fluid, it is also possible that elastohydrodynamic lubrication plays an important role in reducing friction for large events. An interesting consequence of this is that as the slip and slip velocity increase, the hydrodynamic pressure within a narrow zone becomes large enough to widen the gap thereby suppressing high-frequency ground motion caused by the fault asperities rubbing against each other. During the recent Chi-Chi, Taiwan, earthquake, the observed ground-motion near the northern end of the fault was extremely large (> 2.5 m/s, the largest ever recorded), but short period acceleration was not particularly strong so that the damage to ordinary structures by shaking was minor. This could be a manifestation of the high-speed lubrication effects. However, since this is the only earthquake for which such large slip and slip velocity were instrumentally observed, whether this is indeed a general behavior or not is yet to be seen.

State of Stress

The results obtained for large earthquakes suggest that the average stress level along mature faults where large earthquakes occur must be low because of the dominant thermal effects such as frictional melting and fluid pressurization, or of elastohydrodynamic lubrication. Because of melting or pressurization, a fault zone is self-organized into a low stress state. That is, even if the stress was high in the early stage of fault evolution, it would eventually settle in a low stress state after many large earthquakes. This state of stress is consistent with the generally held view that the absence of heat flow anomaly along the San Andreas fault suggests a shear strength of about 200 bars or less. The stress in the crust away from active mature faults can be high as has been shown by many in-situ measurements of stress. The stress difference is large, and a kbar type stress may be involved in small earthquakes, but the events are in general so small that it is hard to determine the stress parameters accurately. What is important, though, is that as long as the length of the fault is small, the state of stress in

the fault zone would not affect the regional stress drastically. However, as the fault grows to some length (e.g. Japanese intra-plate earthquakes like Tango, Tottori, Nobi etc), then some sort of self-organization occurs and the fault settles at a stress level somewhat higher than that on more active plate boundaries.

8.3. Earthquake as a Complex System

Large-magnitude earthquakes are rare events. To a very good approximation, the rate of occurrence of earthquakes falls exponentially as a function of magnitude, as shown in the following figure which shows the distribution of the number, N , of earthquakes equal to, or larger than, magnitude M for the world (a) and southern California (b). Approximately 1 earthquake with $M \geq 8$ occurs every year somewhere in the world, and approximately 1 earthquake with $M \geq 5.5$ occurs every year somewhere in southern California.

Magnitude-Frequency Relation (Global)

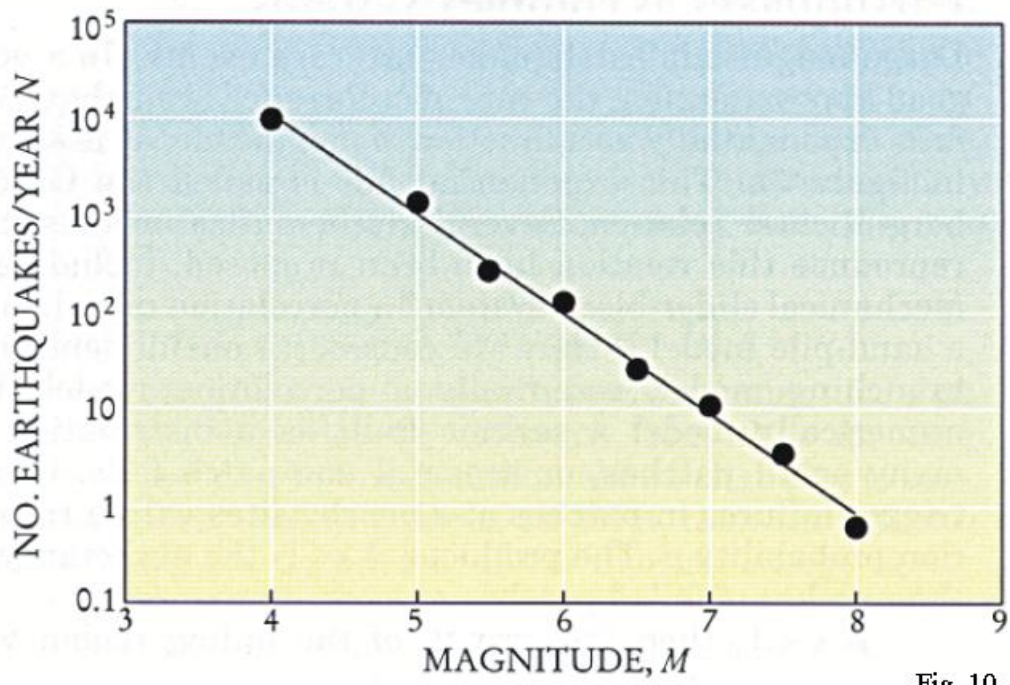
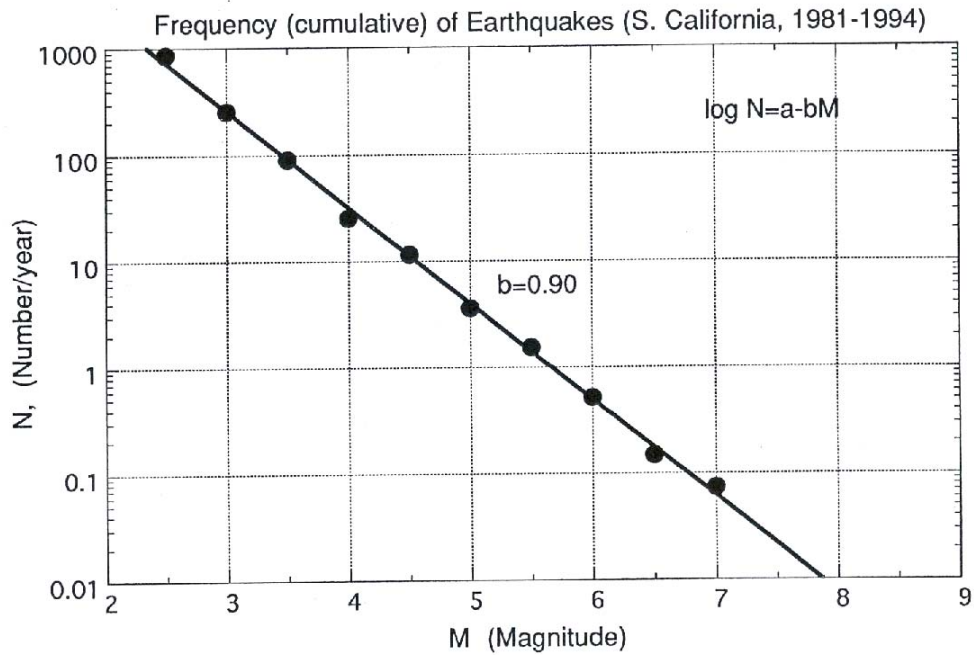


Fig. 10



In general, this distribution is expressed as

$$\log N(M)=a-bM \quad (8)$$

where a and b are constants.

The results obtained for many regions indicate that the value of b (called b value) is approximately equal to 1. This relation is called the Gutenberg-Richter relation, Ishimoto-Iida relation, or simply the magnitude-frequency relation. Since

$$M \propto \log E_R / 1.5$$

equation (1) means

$$N \propto E_R^{-b/1.5} \quad (9)$$

that is, the relation between N and E_R is given by a power law. If $b=1$ and

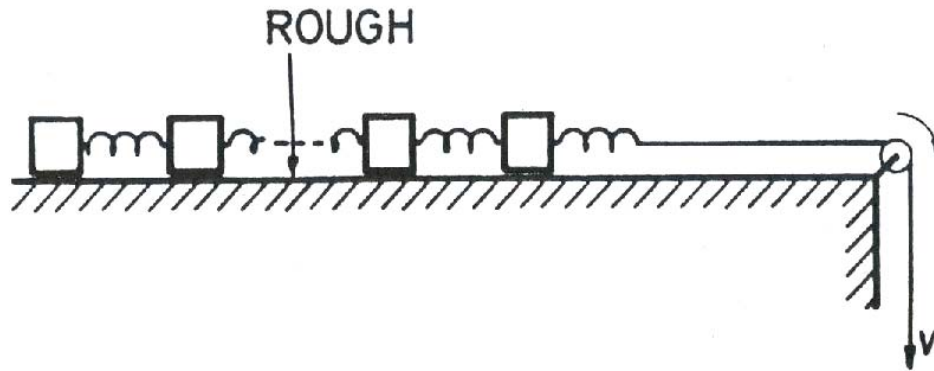
$$E_R \propto r^3 \quad (r: \text{size})$$

Then,

$$(N / N') = (r / r')^{-2} \quad (10)$$

This relation suggests "self-similarity" in 2-D.

The observation that b value is constant and close to 1 has attracted many researcher's attention. This relationship can be interpreted as a result of complex interaction between many elements in a system which has a large number of degrees of freedom. Such systems are often illustrated by a mechanical slider block model (shown below) a sand-pile model and a percolation model.



References

Fracture Mechanics and Friction

Aki, K., Characterization of barriers on an earthquake fault, *J. Geophys. Res.*, *84*, 6140-6148, 1979.

Ben-Zion, Y., and D. J. Andrews, Properties and implications of dynamic rupture along a material interface, *Bull. Seismol. Soc. Am.*, *88*, 1085-1094, 1998.

Brace, W. F., and J. D. Byerlee, Stick slip as a mechanism for earthquakes, *Science*, *153*, 990-992, 1966.

Byerlee, J. D., Friction, overpressure and fault normal compression,, *Geophysical Research Letters*, *17*, 4,741-4,750, 1990.

Dieterich, J. H., Modeling of rock friction 1. Experimental results and constitutive equations, *J. Geophys. Res.*, *84*, 2161-2168, 1979a.

Dieterich, J. H., Modeling of rock friction 2. Simulation of preseismic slip, *J. Geophys. Res.*, *84*, 2169-2175, 1979b.

- Dmowska, R., and J. R. Rice, Fracture theory and Its seismological applications, in Theories in Solid Earth Physics, edited by R. Teisseyre, pp. 187-255, PWN-Polish Publishers, Warszawa, 1986.
- Eshelby, J. D., The determination of the elastic field of an ellipsoidal inclusion and related problems, *Proceedings of the Royal Soc. London*, 241, 376-396, 1957.
- Heaton, T., Evidence for and implications of self-healing pulses of slip in earthquake rupture, *Physics of the Earth and Planetary Interiors*, 64, 1-20, 1990.
- Ida, Y., Cohesive force across the tip of a longitudinal-shear crack and Griggith's specific surface energy, *J. Geophys. Res.*, 77, 3796-3805, 1972.
- Ide, S., and M. Takeo, Determination of constitutive relations of fault slip based on seismic wave analysis, *J. Geophys. Res.*, 102, 27,379-27,391, 1997.
- Kanamori, H., Mechanics of Earthquakes, *Ann. Rev. Earth & Planetary Sciences*, 22, 207-237, 1994.
- Kostrov, B. V., Seismic moment and energy of earthquakes, and seismic flow of rock (translated to English), *Izv. Earth Physics*, 1, 23-40, 1974.
- Lachenbruch, A. H., Frictional heating, fluid pressure, and the resistance to fault motion, *J. Geophys. Res.*, 85, 6097-6112, 1980.
- Lachenbruch, A. H., and J. H. Sass, Heat flow and energetics of the San Andreas fault zone, *J. Geophys. Res.*, 85, 6185-6222, 1980.
- Lawn, B., *Fracture of Brittle Solids - Second Edition*, Cambridge University Press, Cambridge, 1-378, 1993.
- Li, V. C., Mechanics of shear rupture applied to earthquakes zones, in *Fracture Mechanics of Rock*, edited by B. Atkinson, pp. 351-428, Academic Press, London, 1987.
- Mase, C. W., and L. Smith, Pore-fluid pressures and frictional heating on a fault surface, *Pure and Applied Geophysics*, 122, 583-607, 1985.

Mase, C. W., and L. Smith, Effects of frictional heating on the thermal, hydrologic, and mechanical response of a fault, *J. Geophys. Res.*, 92, 6249-6272, 1987.

Melosh, J., Acoustic fluidization: a new geologic process?, *J. Geophys. Res.*, 84, 7513-7520, 1979.

Melosh, H. J., Dynamical weakening of faults by acoustic fluidization, *Nature*, 379, 601-606, 1996.

Rabinowicz, E., *Friction and Wear of Materials*, 2 edition, John Wiley & Sons, Inc., New York, 1-315, 1995.

Scholz, C. H., *The mechanics of earthquake faulting*, Cambridge University Press, New York, 1-438, 1990.

Weertman, J., Unstable slippage across a fault that separates elastic media of different elastic constants, *J. Geophys. Res.*, 85, 1455-1461, 1980.

Energy Budget

Brune, J. N., T. L. Henyey, and R. F. Roy, Heat flow, stress, and the rate of slip along the San Andreas fault, California, *J. Geophys. Res.*, 74, 3821-3827, 1969.

Dahlen, F. A., The balance of energy in earthquake faulting, *Geophys. J. R. astr. Soc.*, 48, 239-261, 1977.

Knopoff, L., Energy release in earthquakes, *Geophysic. Jour.*, 1, 44-52, 1958.

Kostrov, B. V., Seismic moment and energy of earthquakes, and seismic flow of rock (translated to English), *Izv. Earth Physics*, 1, 23-40, 1974.

Orowan, E., Mechanism of seismic faulting in rock deformation, *Geol. Soc. Am. Mem.*, 79, 323-345, 1960.

Savage, J. C., and J. B. Walsh, Gravitational energy and faulting, *Bull. Seismol. Soc. Am.*, 68, 1613-1622, 1978.

Melting, Fluid Pressurization, Lubrication

Brodsky, E. E., and H. Kanamori, The Elastohydrodynamic Lubrication of Faults, *J. Geophys. Res.*, *J. Geophys. Res.*, 106, 16,357-16,374

Cardwell, R. K., D. S. Chinn, G. F. Moore, and D. L. Turcotte, Frictional heating on a fault zone with finite thickness, *Geophys. J. Roy. Astron. Soc.*, 52, 525-530, 1978.

Jeffreys, H., On the mechanics of faulting, *Geol. Mag.*, 79, 291-295, 1942.

Kanamori, H., T. H. Anderson, and T. H. Heaton, Frictional melting during the rupture of the 1994 Bolivian Earthquake, *Science*, 279, 839-842, 1998.

Kanamori, H., and T. H. Heaton, Microscopic and macroscopic physics of earthquakes, AGU Monograph Series 120, "GeoComplexity and the Physics of Earthquakes", J. B. Rundle, D. L. Turcotte, and W. Klein, Eds., 147-163, American Geophysical Union, Washington D. C., 2000.

Lachenbruch, A. H., Frictional heating, fluid pressure, and the resistance to fault motion, *J. Geophys. Res.*, 85, 6097-6112, 1980.

McKenzie, D. P., and J. N. Brune, Melting on fault planes during large earthquakes, *Geophys. J. R. astr. Soc.*, 29, 65-78, 1972.

Richards, P. G., Dynamic motions near an earthquake fault: a three-dimensional solution, *Bull. Seismol. Soc. Am.*, 66, 1-32, 1976.

Sibson, R. H., Interactions between temperature and fluid pressure during earthquake faulting -- A mechanism for partial or total stress relief, *Nature*, 243, 66-68, 1973.

Sibson, R. H., Generation of pseudotachylite by ancient seismic faulting, *Geophys. J. R. astr. Soc.*, 43, 775-794, 1975.

Sibson, R. H., Kinetic shear resistance, fluid pressures and radiation efficiency during seismic faulting, *Pure and Applied Geophysics*, 115, 387-400, 1977.

Sibson, R. H., Power dissipation and stress levels on faults in the upper crust, *J. Geophys. Res.*, 85, 6239-6247, 1980.

Fault-zone Structure

Chester, F. M., and J. S. Chester, Ultracataclasite structure and friction processes of the Punchbowl fault, San Andreas system, California, *Tectonophysics*, 295, 199-221, 1998.

Others

Ando, M., Source mechanisms and tectonic significance of historical earthquakes along the Nankai trough, Japan, *Tectonophysics*, 27, 119-140, 1975.

Aviles, C. A., C. H. Scholz, and J. Boatwright, Fractal analysis applied to characteristic segments of the San Andreas fault, *J. Geophys. Res.*, 92, 331-344, 1987.

Beroza, G. C., and W. L. Ellsworth, Properties of the seismic nucleation phase, *Tectonophysics*, 261, 209-227, 1996.

Brudy, M., M. D. Zoback, K. Fuchs, F. Rumell, and J. Baumgartner, Estimation of the complete stress tensor to 8 km depth in the KTB scientific drill holes: Implications for crustal strength, *J. Geophys. Res.*, 102, 18,453-18,475, 1997.

Ellsworth, W. L., and G. C. Beroza, Seismic evidence for an earthquake nucleation phase, *Science*, 268, 851-855, 1995.

Kanamori, H., The state of stress in the Earth's lithosphere, in *Phys. Earth's Int., Course LXXVIII*, edited by A. M. Dziewonski and E. Boschi, pp. 531-554, North-Holland Pub. Co., Amsterdam, 1980.

Wesnousky, S. G., The Gutenberg-Richter or Characteristic Earthquake Distribution, Which is it?, *Bull. Seismol. Soc. Am.*, 84, 1940-1959, 1994.

Ge 162 9. Plate Motion and Great Earthquakes

Earthquakes occur in the Earth's crust and mantle due to stresses caused by global plate motion. The actual pattern of stress distribution is probably very complex, but we expect that the activities of great and large earthquakes must reflect the global plate motion.

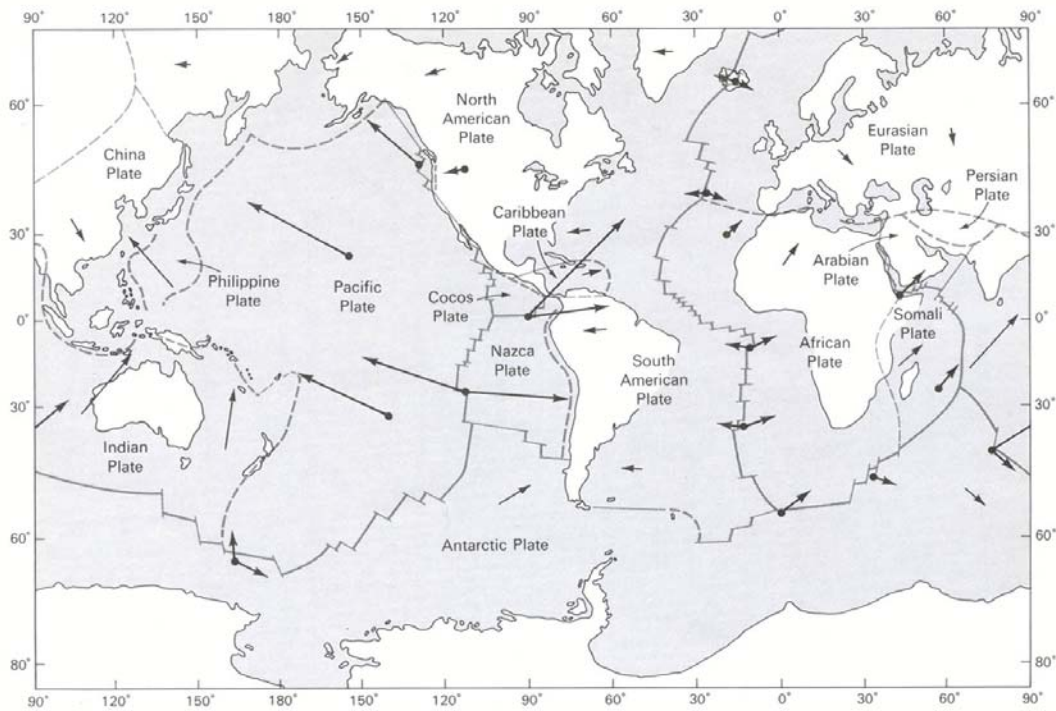
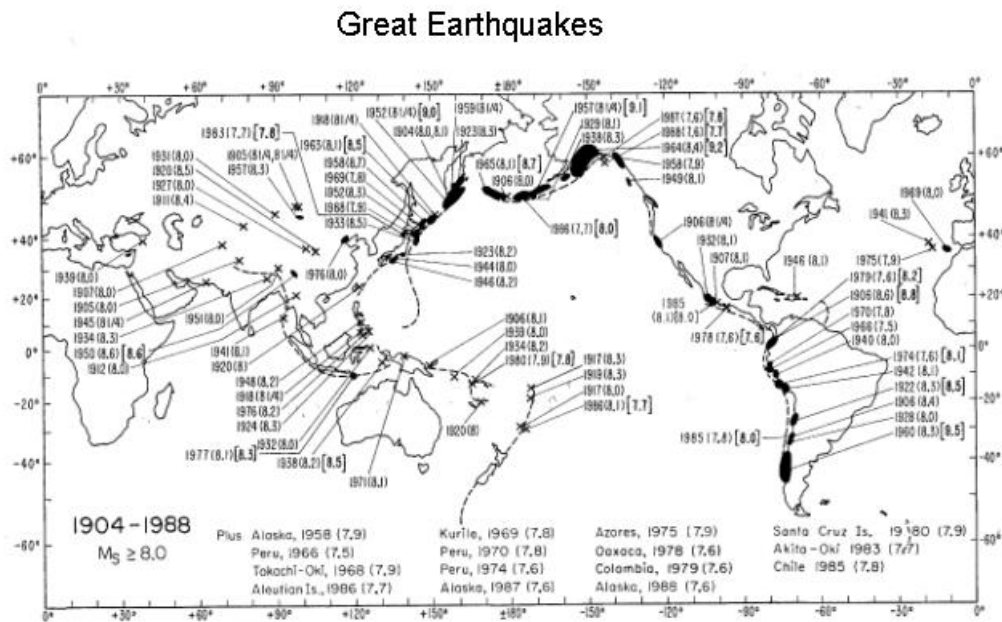


FIGURE 6-8 Present motions of plates over hot spots. The relative motions were determined from fault strikes and spreading rates on rise boundaries; with an appropriate constant rotation added, absolute motion of each plate over the mantle was determined. The lengths of arrows are proportional to the plate speed. [After J. Morgan, "Deep Mantle Convection Plumes and Plate Motions." *Amer. Assoc. Petrol. Geol. Bull.* 56, p. 203, 1972. Redrawn with permission of the author.]

The world greatest earthquakes occur at subduction zones (e.g., 1960 Chilean earthquake, and the 1964 Alaskan earthquake), but not every subduction zone has experienced a great earthquake (e.g., the Marianas, the Tonga-Kermadec). It is possible that the length of earthquake catalog is too short to be representative of long-term



seismicity. With this caveat in mind, we investigate the level of seismic activity and plate motion. Ideally, the seismic activity along a subduction zone should be defined by the energy release per unit length along the subduction zone, and unit time, i.e.,

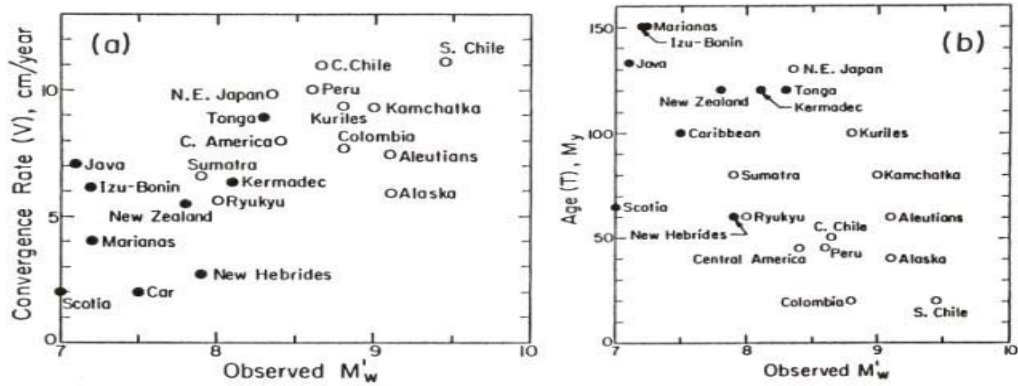
$$\bar{e} = \frac{1}{LT} \int_0^L \int_0^T E_R dldt$$

where L and T are the length of the subduction zone and the time period involved, respectively.

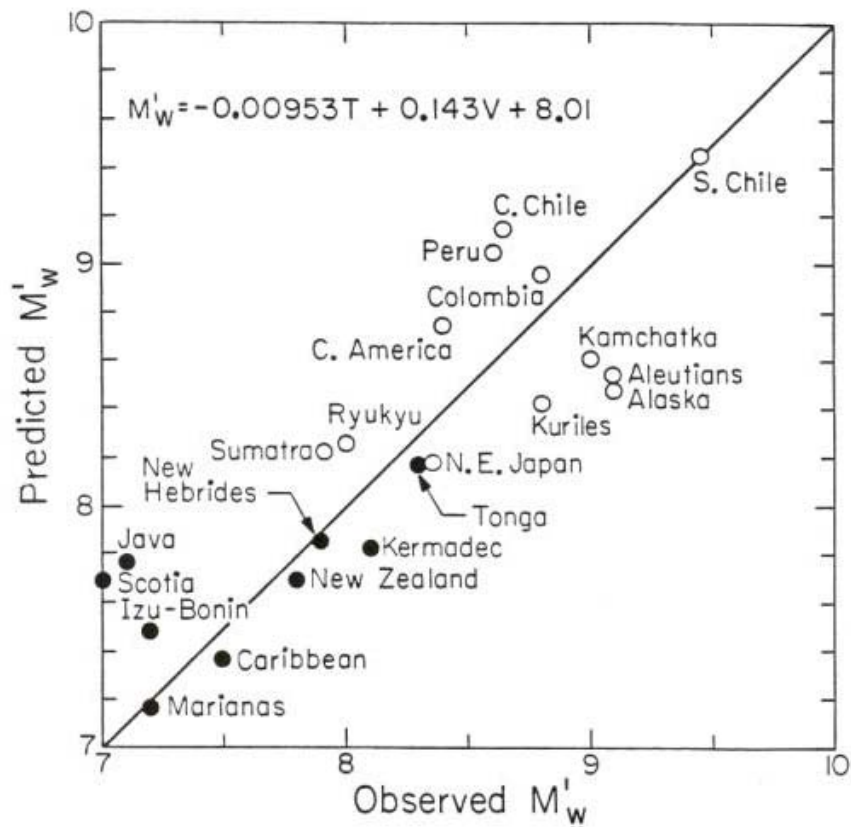
Unfortunately, the available seismic record is too short to compute this. So, we take the magnitude, M_w , of the largest earthquake that occurred in a particular subduction zone as a parameter that represents \bar{e} for that subduction zone. Then, it is reasonable to assume that

$$M_w \propto V$$

where V is the convergence rate. However, the plot of M_w versus V does not show any obvious trend. This suggests that other factors may be controlling seismicity. Another potentially relevant parameter is the age, T , of the subducting plate. However, no obvious negative correlation is seen between M_w and T .



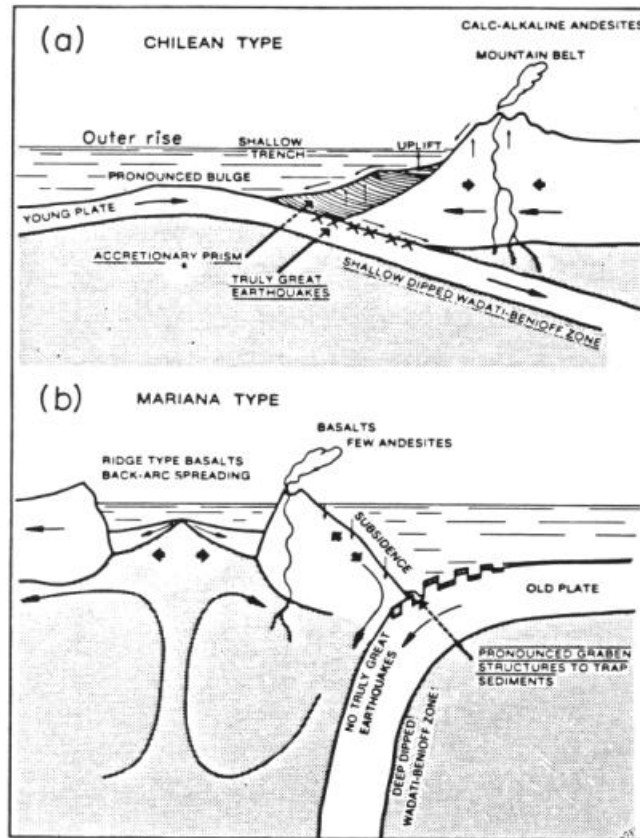
Then, we can try a 3-parameter regression between M_w , V and T . The result is shown in the following figure. The horizontal axis shows the observed M_w and the vertical axis shows M_w predicted by the regression relation.



(Ruff, L., and H. Kanamori, Seismicity and the subduction process, *Phys. Earth Planet. Inter.*, 23, 240-252, 1980)

If this regression is valid, this provides a useful method for assessing the seismic potential of subduction zones for which no great earthquake has occurred. This pattern suggests that the subduction zones where a relatively young plate is subducting at a

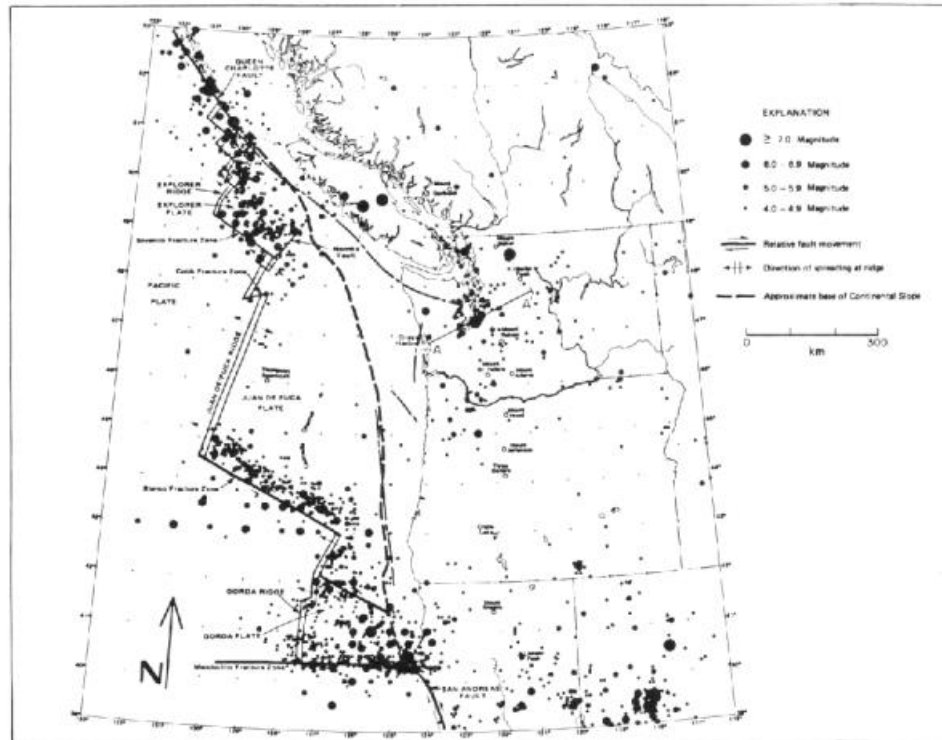
relatively fast rate are more likely to have great earthquakes, and those with an old plate subducting at a moderate rate are less likely to have great earthquakes. The end-member subduction zones are the Chilean type and the Mariana type, shown below.



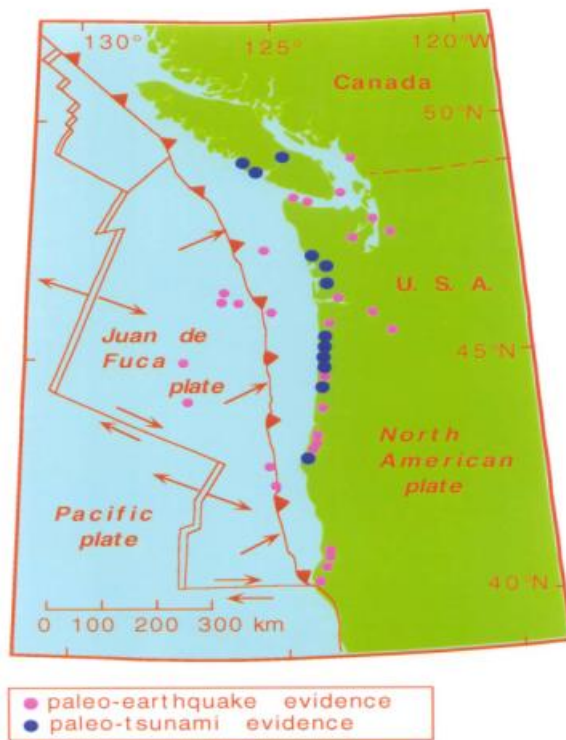
(Uyeda, S., and H. Kanamori, Back-arc opening and the mode of subduction, *J. Geophys. Res.*, 84 (B3), 1049-1061, 1979)

Another interesting implication of this correlation is the seismic potential of the Pacific Northwest (i.e., Oregon-Washington coast). The Juan de Fuca plate is subducting beneath the states of Oregon and Washington. The background seismicity there is very low, as shown below, and until mid 1980's, it was generally believed that the seismic potential in the Pacific Northwest is low (i.e., great earthquakes are unlikely). However, the age of the Juan de Fuca plate is very young, about 10 My, and it is subducting at a rate of 3 cm/year. Thus, in view of the regression relation shown above, one would expect a large, $M_w=8.5$ to 9, earthquake there. This suggestion motivated the interest of geologists who started extensive investigation for finding palaeo-seismological evidence. Geological evidence for regional submergence and evidence for large tsunami which occurred in 1700 [Satake et al., 1996] now seem to have convinced most people, which seems to have led to upgrading of building code in the area. This is a good example in which seismological study, even if it is poorly constrained, can be useful if it is followed up by investigations from different disciplines.

Seismicity in the Pacific Northwest



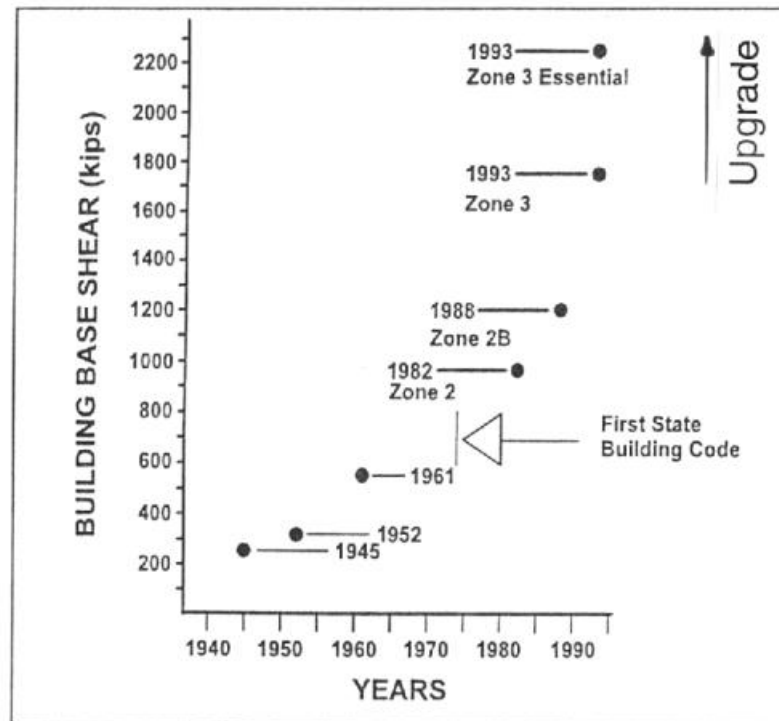
(Heaton, T., and H. Kanamori, Seismic potential associated with subduction in the northwestern United States, *Seismol. Soc. Am. Bull.*, 74 (3), 933-941, 1984)



based on Atwater et al., 1995

(see, Atwater, B. F., and others, Summary of coastal geologic evidence for past great earthquakes at the Cascadia subduction zone, Earthquake Spectra, 11, 1-18, 1995)

Change in Building Codes in Oregon



(R. S. Yeats, *Living with Earthquakes in the Pacific Northwest*, Oregon State University Press, 1998)

References

Brune, J., Seismic moment, seismicity, and rate of slip along major fault zones, *J. Geophys. Res.*, 73, 777-784, 1968.

Satake, K., Shimazaki, K., Tsuji, Y. and Ueda, K., Time and size of a giant earthquake in Cascadia inferred from Japanese tsunami records of January 1700, *Nature*, 379, 246-249, 1996.

